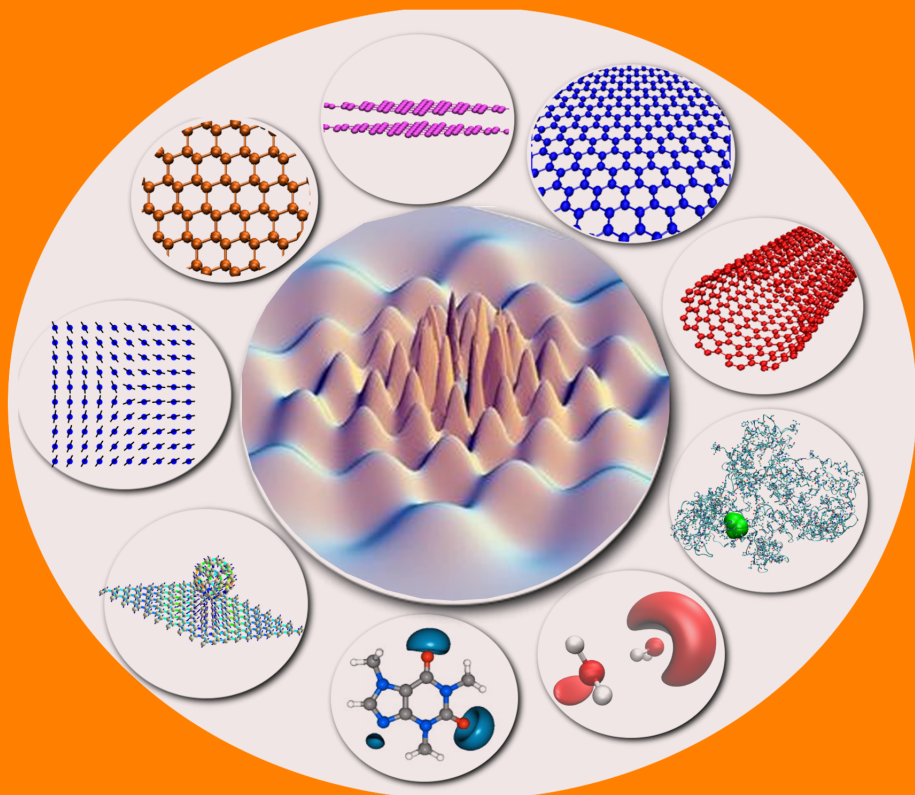
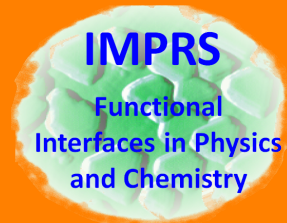


# Efficient modelling of linear electronic polarization in materials using atomic response functions



Vivekanand V. Gobre  
Fritz-Haber-institut der  
Max-Planck-Gesellschaft  
Berlin-Germany  
2016





# **Efficient modelling of linear electronic polarization in materials using atomic response functions**

vorgelegt von  
M.Sc., Physical Chemistry  
Vivekanand V. Gobre  
geb. Goa-India

Von der Fakultät II–Mathematik und Naturwissenschaften  
der Technischen Universität Berlin  
zur Erlangung des akademischen Grades

Doktor der Naturwissenschaften  
Dr. rer. nat.

genehmigte Dissertation

Promotionsausschuss:

Vorsitzende: Prof. Dr. Udo W. Pohl  
Gutachter: Prof. Dr. Alexandre Tkatchenko  
Gutachter: Prof. Dr. Eckehard Schöll

Tag der wissenschaftlichen Aussprache: 31 August 2016

Berlin–2016



# Abstract

The study of matter interacting with external fields is important to understand and design materials with desired (opto-) electronic properties. Reliable methods for the accurate and efficient calculation of the dynamic polarizability of molecules and solids are required for modeling a multitude of spectroscopic techniques, including optical absorption and refraction, Raman spectroscopy, and circular dichroism. Efficient prediction of electronic response properties is also necessary for the calculation of van der Waals (vdW) interactions, and coupling between nuclear and electronic degrees of freedom in materials. In principle, explicitly correlated wave function based first-principles techniques could be utilized to determine electronic response properties. However these methods can be only applied to rather small systems and become prohibitively expensive to study complex materials containing thousands of atoms. To address this problem, we developed an efficient non-empirical method for calculating linear response properties of non-metallic molecules and solids based on atomic response functions that describe valence atomic excitations. This is achieved by the synergistic coupling of the Tkatchenko-Scheffler (TS) method [1], which accurately treats short-range hybridization effects with the Dyson-like self-consistent screening (SCS) equation [2–6] from classical electrodynamics. The present formulation builds upon and significantly improves an earlier version of the TS+SCS approach [7], by preserving QHO invariants, satisfying the free-atom dipole oscillator strength sum rule, and using the correct spin-polarized electron densities for the free atoms. Using only the ground state electron density obtained from first-principle density functional theory calculation and accurate free-atom reference data, we obtain a performance of 3.6% for static polarizabilities and 7.6% for vdW coefficients for a large database of gas-phase molecules ( $\sim 7500$  systems). We further demonstrate the potential of the developed method for the prediction of peculiar scaling laws for vdW interactions in nanostructured materials and interfaces.



# Zusammenfassung

Die Untersuchung von Wechselwirkungen zwischen Materie und externen Feldern ist bedeutend für das Verständnis (opto-) elektronischer Materialien und das Designen ihrer gewünschter Eigenschaften. Zuverlässige Methoden, um die dynamische Polarisierbarkeit von Molekülen und Festkörpern genau und effizient zu berechnen, werden für die Modellierung verschiedenster spektroskopischer Techniken, wie z.B. optische Absorption und Brechung , Raman-Spektroskopie und Zirkulardichroismus, benötigt. Die effiziente Vorhersage der elektronischen Antwort ist ebenso für die Berechnung von van-der-Waals(vdW)-Wechselwirkungen und der Kopplung von Elektron- und Kernfreiheitsgraden notwendig. Prinzipiell kann die elektronische Antwort mit Hilfe von explizit korrelierten Wellenfunktionen aus ab-initio Methoden bestimmt werden. Jedoch ist dies nur für sehr kleine Systeme möglich und für das Studium komplexer Materialien mit mehr als 1000 Atomen unerschwinglich. Um dem Problem gerecht zu werden, berechnen wir mit einer effizienten und nicht-empirischen Methode die lineare Antwort von nicht-metallischen Molekülen und Festkörpern auf Grundlage atomarer Antwortfunktionen von Valenzatomanregungen. Dies wird durch die synergistische Kopplung der Tkatchenko-Scheffler-(TS)-Methode [1] erreicht, die akkurat die kurzreichweite Hybridisierungseffekte mit der Dyson-ähnlichen, selbkonsistenten Abschirmungs(SCS)-Gleichung [2–6] aus der klassischen Elektrodynamik nähert. Die hier dargestellte Methode baut auf einer früheren Version des TS+SCS-Ansatzes [7] auf und verbessert sie signifikant durch die Erhaltung von QHO-Invarianten, welche die Dipoloszillatorstärken-Summenregel für freie Atome erfüllt und die korrekte spinpolarisierte Elektronendichte der freien Atome verwendet. Wenn lediglich die Grundzustandselektronendichte aus einer ab-initio Dichtefunktionaltheorie-Rechnung und genaue Referenzdaten für die freien Atome verwendet werden, erhalten wir schon eine Genauigkeit von 3.6% für die statische Polarisierbarkeit und von 7.6% für die vdW-Koeffizienten in Bezug auf eine große Datenbank für Moleküle in der Gasphase ( $\sim 7500$  Systeme). Weiterhin zeigen wir das Potential der von uns entwickelten Methode für die Vorhersage der sehr verschiedenenartigen Potenzgesetze der vdW-Wechselwirkungen in nanostrukturierten Materialien und Grenzflächen.



---

## Contents

<b>1</b>	<b>Polarization in complex systems</b>	<b>1</b>
1.1	Hierarchy of methods for modeling polarization in complex materials . . . . .	3
1.2	Efficient oscillator-based approach for polarizability and van der Waals interactions . . . . .	6
<b>2</b>	<b>Theoretical background</b>	<b>11</b>
2.1	The quantum many-body problem . . . . .	11
2.1.1	Schrödinger equation . . . . .	11
2.1.2	Born–Oppenheimer approximation . . . . .	13
2.1.3	Hartree–Fock method . . . . .	15
2.1.4	Methods beyond the HF approximation . . . . .	18
2.1.5	Møller–Plesset (MP) perturbation theory . . . . .	19
2.1.6	Coupled cluster theory . . . . .	20
2.2	Fundamentals of density-functional theory . . . . .	23
2.3	Hohenberg–Kohn theorems . . . . .	23
2.4	The Kohn–Sham method . . . . .	24
2.5	The exchange–correlation approximations . . . . .	26
2.5.1	The local (spin) density approximation . . . . .	27
2.5.2	Generalized gradient approximations . . . . .	28
2.5.3	Meta-generalized gradient approximations . . . . .	28
2.5.4	Hybrid functionals . . . . .	29
2.6	Random–phase approximation for electron correlation energy . . . . .	30
2.7	van der Waals (vdW) interactions in density-functional theory . . . . .	31
2.7.1	Nonlocal vdW density functionals . . . . .	32
2.7.2	Atom pairwise dispersion corrections . . . . .	33
2.7.3	Many–body interatomic van der Waals interactions	36

<b>3</b>	<b>Approaches for computing (linear) response properties</b>	<b>41</b>
3.1	Response function . . . . .	42
3.2	The finite-field method . . . . .	42
3.3	Frequency-dependent polarizabilities . . . . .	45
3.4	Coupled-cluster response theory . . . . .	46
3.5	Time-dependent density-functional theory (TDDFT) . .	47
3.6	Linear-response formulation of TDDFT . . . . .	49
<b>4</b>	<b>Representative datasets for isotropic static polarizabilities and asymptotic van der Waals <math>C_6^{AB}</math> coefficients for molecules</b>	<b>53</b>
4.1	Experimental reference datasets . . . . .	54
4.1.1	Static polarizabilities . . . . .	54
4.1.2	vdW coefficients from dipole oscillator strength distributions . . . . .	55
4.2	Computational details . . . . .	55
4.3	Results and discussion . . . . .	56
4.3.1	Polarizabilities and vdW $C_6$ coefficients from linear response coupled cluster singles and doubles theory for atoms and molecules . . . . .	56
4.3.2	Static mean polarizabilities for a dataset of 7449 molecules . . . . .	60
4.4	Summary . . . . .	62
<b>5</b>	<b>Coarse-grained electrodynamic model of electronic polarization in materials</b>	<b>65</b>
5.1	The quantum harmonic oscillator (QHO) model . . . . .	69
5.1.1	The Hamiltonian for QHO . . . . .	69
5.1.2	Polarizabilities for the QHO model . . . . .	70
5.1.3	QHO in a uniform electric field . . . . .	72
5.1.4	Relationship between polarizability and volume of a QHO . . . . .	72
5.1.5	Dynamic polarizability of a single (QHO) oscillator	74
5.2	The electrodynamics of atomic response functions . . . .	75
5.2.1	Regularized dipole interaction tensor . . . . .	77
5.2.2	Quantum mechanically-based dipole potential . .	79
5.3	Coupled atomic response in matter (CARMA) . . . . .	81
5.4	Results and Discussion . . . . .	86
5.4.1	Dipole oscillator strength sum rule . . . . .	86
5.4.2	Static polarizability and vdW coefficients for a linear chain of H <sub>2</sub> molecules . . . . .	90
5.4.3	Performance of CARMA model for isotropic electric static polarizability and vdW coefficients of molecules . . . . .	92
5.4.4	Static polarizability and vdW coefficients in solids	93
5.5	Summary . . . . .	95

<b>6 Scaling laws for van der Waals interactions in nanostructured materials</b>	<b>97</b>
6.1 Methodology . . . . .	98
6.2 Application of CARMA model to carbon nanostructures .	99
6.2.1 Calculation of vdW coefficients . . . . .	99
6.2.2 vdW coefficients of model systems . . . . .	100
6.2.3 vdW coefficients of carbon nanostructures . . .	101
6.2.4 vdW binding between carbon nanostructures . .	103
6.3 Discussion . . . . .	105
<b>7 Towards efficient modeling of long-range interactions in nanoscale systems</b>	<b>107</b>
<b>8 Summary and Conclusions</b>	<b>109</b>
<b>Appendices</b>	<b>117</b>
<b>A Static polarizabilities and asymptotic vdW <math>C_6</math> coefficients for atoms and molecules</b>	<b>119</b>
<b>B Extra technical details</b>	<b>125</b>
B.1 Technical details about finite-difference approach . . . .	125
<b>Symbols</b>	<b>127</b>
<b>Abbreviations</b>	<b>129</b>
<b>Acknowledgements</b>	<b>131</b>
<b>Bibliography</b>	<b>133</b>



---

# 1

## Polarization in complex systems

Understanding the interaction of light with matter and techniques for studying such interactions provide an interface between physics, chemistry, and biology. Electromagnetic radiation is one of the important probes to study the structure and dynamics of matter. The absorption of ultraviolet, visible, infrared, and microwave radiation has provided detailed information about electronic, vibrational, and rotational energy levels of molecules and condensed matter, and it allows chemists and physicists to determine the structure of complex systems [8, 9]. Spectroscopic techniques have a significant impact on solid-state and molecular physics as well as inorganic and organic chemistry. An important example of such technique is X-ray diffraction experiments which have provided the details about structure of solids and biological macromolecules. When light interacts with a molecular material, photons can either lose or gain energy via transitions from the translational, rotational, vibrational, and electronic degrees of freedom of the molecular system. Moreover, the frequency spectrum of the scattered light will exhibit resonances at the frequencies corresponding to these transitions, and therefore, provides information about the energy spectra of molecular materials. Many physical properties of interest in condensed matter systems can be probed as a response of a system under study to an external perturbation (For example, the perturbation can correspond to the nuclear motion in the case of nuclear gradients or an external electric field in the case of (electronic) polarization). This is achieved experimentally for example by using spectroscopic techniques. In such cases, the response of the system is primarily of electronic nature, meaning that the electrons in the system change their quantum state(s). In such process electrons can emit or absorb photons, which in turn are measured by the experiment. From a theoretical point of view, it is possible to understand the underlying physics of the (weakly perturbed) system within the response theory [10]. The response theory allows us to calculate the variations of a given observable up to certain order in perturbation theory. Typically, the external perturbing force used in experiments is

small with respect to the internal ones in a material, so that the system is weakly perturbed. Thus, the dominant term is the linear response function. The linear-response function provides information on the ground state and the excitation spectrum, their symmetry properties, and the strength of correlations in a system.

In the present work, we are mainly interested in the response of the electronic charge densities of condensed matter systems to an arbitrary external (electric) perturbation. The main quantity of interest in this context is the linear density-density response function which directly links an external perturbing potential to the electronic density response. This quantity is crucial for prediction of the structural and electronic properties of complex systems like surfaces, polymers, hybrid organic or inorganic interfaces, nanostructures and biomolecules. The response function obtained from linear response theory provides a powerful framework to relate experiment and theory. A thorough understanding of the electronic response of condensed matter systems is a necessary first step for the design of nanoelectronics [11], chemical/bio-sensors [12, 13], electrocatalysts [14], and nanoplasmonics [15], or design materials with desired (opto)electronic properties using materials such as graphene [16] and other complex systems [17]. Since the beginning of the last century, extensive efforts have been dedicated to technological as well as fundamental research at the atomic level. To this end, the study of (linear) response functions is important because they can be directly related to properties of quantum systems. For example, dynamic polarizability is related to the optical absorption spectrum of a system.

The polarization of a bulk material is a macroscopic quantity whose relationship to the microscopic polarizabilities of the constituents atoms or molecules is very complex. The polarization properties of molecules or materials are useful especially in the description of dielectric constants, refractive indices as well as van der Waals (vdW) interaction. The macroscopic physical properties are derivatives of the polarization with respect to suitably chosen perturbations. Such properties are dielectric permittivity, piezoelectricity, effective charges, and pyroelectricity, which are phenomenologically measured as bulk material tensors [18, 19]. Moreover, ferroelectricity is a property of certain materials that have a spontaneous electric polarization that can be reversed by the application of an external electric field [18, 20].

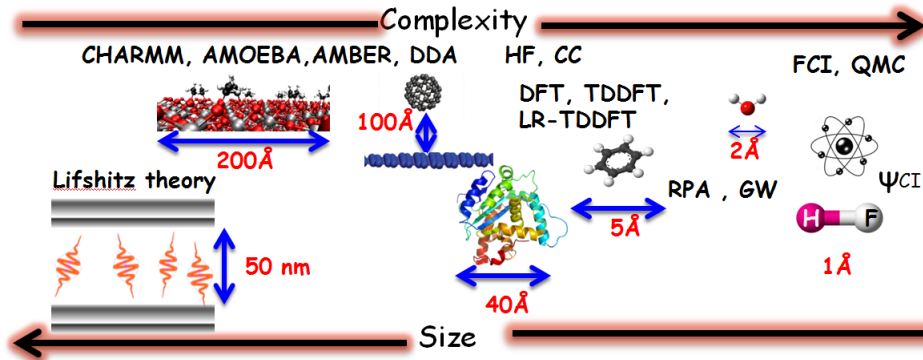
The modeling of polarization in systems like surfaces, polymers, hybrid (in)-organic interfaces, nanostructures, biomolecules can be very complex due to a multitude of intra and inter-molecular interactions which can act between neighboring atoms and molecules [21]. The intramolecular interactions can be roughly imagined as forces that keep a molecule together through different types of bonds. The intermolecular forces are those which act between molecules [22, 23]. These forces cause the modification of electronic distribution within any molecular system. In the case of a collection of molecules, the

change in the charge distribution within a molecule will modify the Coulomb forces exerted on neighboring molecules, leading to important polarization effects, which can propagate to large distances. Such forces are ubiquitous in nature, and their importance have been identified in many phenomena such as protein folding [24] and structure and properties of nanomaterials [25–27]. These forces also play a fundamental role in diverse fields, ranging from the mechanisms of anaesthesia [28], gecko [29, 30] or spider [31] adhesion and even cohesive forces between regolith grains on asteroid surfaces [32].

## 1.1 Hierarchy of methods for modeling polarization in complex materials

From the previous considerations, it is evident that we need accurate and efficient models for calculating response properties of *bio* or *nano* systems of interest. Unfortunately, the macroscale models which rely on bulk or continuum properties of materials are not often transferable to the nanoscale or lower symmetry systems, where the relevant physics can be very different. Indeed in microscopic systems, classical mechanics is not valid anymore and the principles of quantum mechanics need to be applied. Among existing models there is the

**Figure 1.1:** Schematic representation of the applicability of current theoretical tools used to calculate electronic properties for matter ranging from atoms, molecules to proteins, nanostructures, and other complex materials.



Lifshitz formulation [33], which allows calculation of the interaction free energies, torques, forces, and Hamaker coefficients for a wide range of geometries including isotropic and anisotropic plane-plane and cylinder-cylinder interactions and other complex materials [34, 35], as illustrated schematically in Figure (1.1). The Lifshitz approach is based on macroscopic quantum electrodynamics [20, 36]. However, such approach which uses the continuum approximation requires knowledge of experimental optical properties of materials for the parameterization of the model but lacks atomistic details. For simulation of materials

(e.g. proteins) polarizable force fields such as CHARMM [37], AMOEBA or AMBER [38] as well as discrete dipole approximation (DDA) [39] are largely used, but they need to be optimized using known experimental data or results from *ab initio* calculations on a particular system under study. Unfortunately, these approaches are often limited and not transferable to general materials.

Quantum-mechanical wavefunction based methods provide an accurate way for predicting ground and excited state properties. These methods rely on the Schrödinger equation [40] which is generally impossible to solve accurately for realistic many-electron systems. The Hartree-Fock (HF) method is one of the first and widely employed tools for describing many-electron systems. Moreover, the methods such as Møller-Plesset perturbation theory or configuration interaction (CI) build upon the HF approximation, are able to account for many-electron correlation effects. However, the application of these wavefunction based methods for complex systems such as nano or biostructures is still intractable due to the extremely large number of electronic degree of freedom.

Among electronic structure methods, density-functional theory (DFT) occupies an important place, as it replaces the complexity of multi-dimensional many-electron wavefunction with three-dimensional electron density. The foundation of DFT is based on the Hohenberg-Kohn theorems [41]. The practical applications of DFT to condensed matter systems is through the solution of the Kohn-Sham [42] equations. The KS equations represent a fictitious system of non-interacting electrons which generate the same density as a system of interacting electrons. DFT allows calculations of ground state properties of a large number of systems ranging from atoms and molecules to solids and surfaces. However, there are still difficulties in using DFT to properly describe intra and intermolecular interactions which are of critical importance to understanding chemical reactions, especially vdW forces, charge transfer excitations, transition states, and global potential-energy surfaces.

In recent years, the time dependent density functional theory (TDDFT) has emerged as a valuable tool for computing electronic excited state properties by extending DFT to time-dependent problems. TDDFT is based on the Runge-Gross theorem [43]. Its basic variable is the time-dependent electron density which is obtained from the solution of a fictitious system of non-interacting electrons in an effective potential. It has the big advantage of computational speed with respect to other methods that rely on wavefunctions and on the many-body Schrödinger equation. TDDFT can be viewed as a potentially exact reformulation of time-dependent quantum mechanics. However, the limitations of TDDFT is that it needs approximations for the unknown effective potential. In any case TDDFT offers a suitable compromise between accuracy and computational efficiency, allowing the description of excited electronic states. An

important concept in case of TDDFT [43, 44] is the density-density response function. This quantity is used in many methods such as symmetry adapted perturbation theory [45, 46], fluctuation-dissipation density functional theory [47–49], GW calculations [50–52], random phase approximation (RPA) [53–60] as well as beyond-RPA [61–63] methods via the adiabatic-connection fluctuation-dissipation theorem (ACFDT) [64, 65].

Response functions in TDDFT can be calculated by a variety of methods (e.g. real time-propagation, Dyson equation, Sternheimer as well as Casida method [66–68]). The time-propagation method [66] propagates a system under a given external field. The density response is obtained directly as the difference between the time-dependent density and the ground-state density. As the method is nonperturbative, all orders of response are included in the calculation, and therefore, specific orders must be numerically extracted. The Dyson equation is used to obtain directly the response functions. The Sternheimer method [67] solves for a specific order of the response for a specific field in frequency space via the variation of the wavefunctions. The Sternheimer equations form a hierachic structure, where higher-order responses can be calculated from lower-order responses. The Casida method [68] instead of finding the response, finds the poles and residues of the first-order response function, which corresponds to finding the resonant transitions of a system via an expansion in an electron-hole basis. Physically all these techniques are equivalent as they are all based on KS-DFT [42] and are simply different ways to obtain the same quantities.

The response function is in general nonlocal in space (*i.e.* it depends on coordinates  $\mathbf{r}$  and  $\mathbf{r}'$ ) and in time (or can be expressed in frequency space,  $\omega$ , by Fourier transform). The density-density response function,  $\chi(\mathbf{r}, \mathbf{r}', \omega)$ , is often derived using single particle (KS) energies and orbitals. The dimensions of  $\chi(\mathbf{r}, \mathbf{r}', \omega)$  are continuous in a basis it spans. Moreover, any real-space representation of the response function would yield matrices with dimensions too large for explicit matrix algebra. In particular, the linear density-density response tensor is a function of the inverse of the (unperturbed) Hamiltonian which in principle requires the knowledge of the entire manifold of its eigenvalues and eigenstates (*i.e.* the Kohn-Sham energies and orbitals) [43–46, 58–60]. Therefore, the evaluation of response function is a computationally demanding task and consequently restricted to small or medium-sized systems.

For a more efficient treatment of the full electronic response function  $\chi(\mathbf{r}, \mathbf{r}', \omega)$ , the (non-interacting) response function can be also derived starting from spatially partitioned coarse-grained atomic local response approximation [1, 7, 69], unlike obtained using entire set of the Kohn-Sham energies and orbitals. The interacting response is then obtained by solving a nonlocal screening equation. We initially assume that a molecular material or condensed matter, has a finite electronic gap and can be divided into effective ‘atomic’ fragments (such that the

response function  $\chi(\mathbf{r}, \mathbf{r}')$  is a sparse matrix and not dominated by highly delocalized metal like excitations) [70–72]. More generally, a system is partitioned in a electrically neutral atomic subsystems,  $\chi_{\text{atomic}}^0(\mathbf{r}, \mathbf{r}', \omega)$ , at separations larger than a few Ångström such that electron transport between the atomic subsystems is negligible. Within this assumption, we map the full nucleo-electronic system onto a set of localized atomic response functions. Within the context of present work, the nuclear degrees of freedom are kept fixed, while electronic degrees of freedom are represented by isotropically polarizable dipoles. The atomic response can be conveniently expressed in terms of multipole-multipole electronic susceptibilities. In the next section, we will present an atomic response function model for polarizability and van der Waals interactions for molecular materials based on quantum harmonic oscillators (QHOs). Moreover, such coarse-grained representation of response function allows calculation of polarizability of a molecular material having many thousands of atoms.

## 1.2 Efficient oscillator-based approach for polarizability and van der Waals interactions

The dominant contribution to the van der Waals force (fluctuating dipole-dipole) arises due to the non-zero instantaneous dipole moments of all atoms and molecules. A typical model system to illustrate the vdW interaction is a complex of two fragments of matter with non-overlapping electron densities or no permanent electrical multipoles. For instance, it can be a dimer of noble-gas atoms or 'jellium' spheres. Every quantum system with electrons has charge fluctuations that result in instantaneous polarization and hence are responsible for the vdW attraction [18, 22, 23, 33].

The non-relativistic vdW interaction energy between two small molecules or closed-shell atoms is predictable and has the asymptotic form  $r^{-6}$ , where  $r$  is the distance between two fragments of matter [73]. This is familiar long-range attraction term which describes the interactions between atoms and molecules [33, 74–76]. Whenever an atom acquires a spontaneous dipole moment  $\mu_1$ , the resulting dipole electric field ( $\mathcal{E}_1 \propto \mu_1/r^3$ ) polarizes the adjacent atom to produce an induced dipole moment  $\mu_2$ , i.e.,  $\mu_2 = \alpha \mathcal{E}_1 \propto \alpha \mu_1/r^3$ , where  $\alpha$  is the polarizability for a given atom. The potential energy of the first dipole in the field of the second dipole, i.e., the interaction energy,  $E_{\text{int}}$ , between the two dipoles, then reads  $E_{\text{int}} = -\mu_1 \mathcal{E}_2 \propto \alpha \mu_1^2/r^6$ . The magnitude of the interaction depends on the polarizability  $\alpha$  of the atoms. Basically, the polarizability is the proportionality factor between the induced electric dipole moment (of an atom) and the external polarizing field. The  $r^{-6}$  interaction energy power law between two atoms makes two

crucial approximations that are not always valid. First, the quasi-static approximation, which ignores wave retardation effects, and also possible multiple polarizing events in case of a polyatomic system. The quasi-static approximation assumes that the dipole moment  $\mu_1$  polarizes the second atom instantaneously, which is valid if  $r$  is much smaller than the typical wavelength of the fluctuating fields. However, the finite wave propagation speed of light must be taken into account when  $r$  is much larger than the typical wavelength, and this gives rise to Casimir interaction [77] energy, which asymptotically scales as  $r^{-7}$ . Generally, the interaction energy is not a simple power law between these limits, but depends instead on an integral of fluctuations at all frequencies scaled by a *frequency-dependent* polarizability of the system [33].

In case of polyatomic systems the situation is more complex because many-body polarization effects must be considered. For example, with three atoms, the initial dipole  $\mu_1$  will induce polarizations  $\mu_2$  and  $\mu_3$  in the other two atoms, but  $\mu_2$  will create its own field that further modifies  $\mu_3$ , and so on. Thus, the interaction in a many-body system is generally non-additive and simple two-body force law can not account for all interactions. These interactions can be negligible for sufficiently dilute gasses or for weak polarizabilities [33, 78]. But they become very significant for systems where many fluctuating multipoles interact in a (very) complicated way. In other words, each atom located inside a molecule or material experiences a dynamic internal electric field created by both the *local* and *non-local* fluctuations associated with the surrounding atoms. Depending on the underlying topology of the chemical environment, this fluctuating internal electric field can give rise to either polarization or depolarization effects, and is largely responsible for the anisotropy in the molecular polarizability tensor. Therefore, it is essential to include the environmental screening effects arising from both the short- and long-range in accurate first-principles calculations of the response function. Therefore, considerable research effort is being directed towards the development of density functional approximations in DFT that are capable of predicting physical and chemical properties of microscopic systems where vdw forces play an important role. Recently, Tkatchenko and co-workers [7, 56, 57] proposed a density functional method that accounts for many-body interatomic dispersion energy using the ACFDT [64, 65, 79]. In this approach, the many-body dispersion contribution is obtained from the solution of a model Hamiltonian for an arbitrary collection of localized atomic response functions (ARFs). The non-local screening is included in ARFs via a Dyson like self-consistent screening (SCS) equations [3, 5, 80]. ARFs can be constructed as functional of the electron density, obtained with DFT, to accurately capture the valence electronic response [1] in molecules and solids. These ARFs are described by spherical quantum harmonic oscillators (QHOs) coupled to each other via dipole-dipole interactions. The solution of the SCS equation for a set of localized ARFs provides microscopic non-local

polarizability for a system in the basis of ARF coordinates. Moreover, such coarse-grained representation of the response function reduces the computational cost by several orders of magnitude, unlike calculation that uses the entire manifold of Kohn-Sham energies and states.

One of the major goal achieved in my research and presented in this thesis is the construction of an efficient and accurate model for the calculation of linear polarization in materials. The formulation presented in this work builds upon and significantly improves an earlier version of the ARF model [1, 7]. The QHO invariants are preserved, the free-atom dipole oscillator strength sum rule is satisfied, and the correct spin-polarized electron densities for the free atoms are employed. We use the ground state electron density obtained from the first-principle DFT calculation and accurate free-atom quantum-mechanical reference data. The improved ARF model provides isotropic static polarizabilities with an accuracy of 3.6% for  $\sim 7500$  systems and vdW coefficients with accuracy 7.6% for a large database of gas-phase molecules (ranging from simple diatomic to polyatomic systems with functional groups including alcohol, ketone, amine and aromatic systems).

The outline of the thesis is as follows: Chapter (2) focuses on explaining the theoretical methods used to develop an efficient and accurate model for calculating linear polarization in materials. It starts with the basic ideas and methods of quantum chemistry as well as density functional theory. These methods solve the electronic many-body problem based solely on the laws of quantum mechanics. These methods give quantitative accuracy and predictive ability in a wide range of problems. Moreover, Chapter (3) introduces a hierarchy of state-of-the-art methods for computing electronic response functions. The electronic response function is of central importance for understanding many physical or chemical processes. Chapter (4) presents a brief overview of the description of electronic polarizability and asymptotic vdW coefficients of molecules using first-principles techniques, and contrasting them with experimental measurements. Chapter (5) presents an atomistic linear electrodynamics response model of polarization for molecules and materials. This approach is based on atomic response functions (ARFs). The method developed in this work is a synergistic coupling of classical electrodynamics with quantum mechanical input data and the electron density obtained using DFT calculations [7, 81]. Chapter (6) presents the application of electrodynamics response model to determine the microscopic polarizability and asymptotic vdW coefficients of a wide range of carbon-based nanomaterials, including fullerenes, carbon nanotubes, and nanoribbons, graphite, diamond, as well as single-layer and multi-layer graphene. We demonstrate that the vdW coefficients depend on the dimensionality and the atomic arrangement of carbon atoms and highlight the importance to treat vdW interactions beyond simple pairwise additivity approximation. Chapter (7) illustrates the importance of inclusion of the electrodynamic response in large-scale

atomistic simulations and potential avenues for future work.



---

# 2

## Theoretical background

This chapter focuses on explaining the theoretical methods used in this thesis for calculating linear response function for molecules and materials. It starts with the description of first-principles electronic structure methods. These methods solve the electronic many-body problem based solely on the laws of quantum mechanics, without (empirical) parameters, but with certain approximations. Practically, they have the advantage to give quantitative accuracy and predictive ability in a wide range of problems. For the interested reader, comprehensive details about the methods discussed here can be found in references [19, 82, 83].

### 2.1 The quantum many-body problem

This section introduces the basic ideas and methods of quantum chemistry. It starts with the structure of many-body Hamiltonian operator and discusses the form of many-body wavefunction. Further, we introduce the basic ideas of the Hartree-Fock approximation as well as more sophisticated techniques.

#### 2.1.1 Schrödinger equation

The single-particle time-dependent Schrödinger equation is the starting point for any electronic structure problem [40]

$$\left( -\frac{\hbar^2}{2m} \nabla^2 + V(\mathbf{r}) \right) |\psi(\mathbf{r}, t)\rangle = i\hbar \frac{d}{dt} |\psi(\mathbf{r}, t)\rangle, \quad (2.1)$$

where  $m$  is the mass of the particle,  $\psi(\mathbf{r}, t)$  is the wavefunction of the system and  $V(\mathbf{r})$  is the potential energy of the particle at the given position. The operator  $(-\frac{\hbar^2}{2m} \nabla^2 + V(\mathbf{r}))$  is called the *Hamiltonian*,  $\hat{\mathcal{H}}$ , of the system. The physical interpretation of the wavefunction is given through  $|\psi(\mathbf{r}, t)|^2$ , which is the probability density at position  $\mathbf{r}$  and time  $t$ . The probability of finding the particle in an infinitesimal volume

$\delta\mathcal{V}$  around the position  $\mathbf{r}$  at time  $t$  is then  $|\psi(\mathbf{r}, t)|^2 \delta\mathcal{V}$ . For time-independent problems the Hamiltonian operator does not explicitly depend on time,  $t$ . Assuming that the wavefunction can be written in a separable form as  $\psi(\mathbf{r}, t) = \psi(\mathbf{r})\Omega(t)$ , it can be shown by separation of variables that the time-independent Schrödinger equation is

$$\hat{\mathcal{H}}|\psi(\mathbf{r})\rangle = E|\psi(\mathbf{r})\rangle, \quad (2.2)$$

where  $E$  is the separation constant and represents an energy eigenvalue, while the time-dependent part of the equation satisfies equation

$$i\hbar \frac{d}{dt} \Omega(t) = E\Omega(t). \quad (2.3)$$

Moreover, Eq. (2.3) yields a trivial exponential solution. Therefore, Eq. (2.2) has to be solved for the particular potential. The time-independent Schrödinger equation is the one that we will be concerned with here.

Determining the properties of a material *ab initio*, that is without any empirical parameters characterising it other than its atomic structure, involves solving the Schrödinger equation for a system of many interacting particles. We start by extending Eq. (2.2) for a collection of particles. For a given system having  $P$  electrons bound to  $Q$  nuclei, the Hamiltonian in Eq. (2.2) can be written (in atomic units<sup>1</sup>) as,

$$\begin{aligned} \hat{\mathcal{H}} = & - \underbrace{\frac{1}{2} \sum_{i=1}^P \nabla_{\mathbf{r}_i}^2}_{\text{Electronic KE}} - \underbrace{\frac{1}{2M_I} \sum_{I=1}^Q \nabla_{\mathbf{R}_I}^2}_{\text{Nuclear KE}} - \underbrace{\sum_{i=1}^P \sum_{I=1}^Q \frac{Z_I}{|\mathbf{r}_i - \mathbf{R}_I|}}_{\text{Electron-Nuclear attraction energy}} \\ & + \underbrace{\sum_{i=1}^P \sum_{j>i}^P \frac{1}{|\mathbf{r}_i - \mathbf{r}_j|}}_{\text{Electron-Electron repulsion energy}} + \underbrace{\sum_{I=1}^Q \sum_{J>I}^Q \frac{Z_I Z_J}{|\mathbf{R}_I - \mathbf{R}_J|}}_{\text{Nucleus-Nucleus repulsion energy}}, \end{aligned} \quad (2.4)$$

where  $i, j$  are indices for the  $P$  electrons,  $I, J$  are indices for the  $Q$  nuclei,  $M_I$  are masses and  $Z_I$  are the charges of the nuclei. In short, this Hamiltonian can be re-written as

$$\hat{\mathcal{H}} = \hat{T}_e + \hat{T}_n + \hat{V}_{n-e} + \hat{V}_{e-e} + \hat{V}_{n-n}, \quad (2.5)$$

where  $\hat{T}_n$  and  $\hat{T}_e$  are the kinetic-energy operators related to the nuclei and the electrons, respectively, and the terms  $\hat{V}_{n-e}$ ,  $\hat{V}_{e-e}$ , and  $\hat{V}_{n-n}$  are related to the electrostatic interaction between two electrons, an electron and a nucleus, and two nuclei, respectively. Solving this Hamiltonian in a (non-relativistic, time-independent) quantum-mechanical framework means to solve the time-independent

---

<sup>1</sup>If one employs atomic units, then  $\hbar$  (Planck's constant/2π),  $m_e$  (mass of the electron), and  $|e|$  (electronic charge) are set to unity.

Schrödinger equation<sup>2</sup>

$$\hat{\mathcal{H}}\psi(\{\mathbf{r}_i\}, \{\mathbf{R}_I\}) = E\psi(\{\mathbf{r}_i\}, \{\mathbf{R}_I\}) \quad (2.6)$$

where  $E$  is the total energy of the system and the many-body wavefunction  $\psi$  is a function of all the spatial coordinates of electrons ( $\mathbf{r}_i, i = 1, 2, \dots, P$ ) and spatial coordinates of nuclei ( $\mathbf{R}_I, I = 1, 2, \dots, Q$ ). Eq. (2.6) is simple in its form but enormously complex to solve. Since each electron and each nucleus can move in the  $x$ ,  $y$  and  $z$  coordinates, solving this equation involves a problem of  $3P + 3Q$  degrees of freedom in which all particles in a system are coupled. Therefore, in practice approximations need to be made. The first important approximation is obtained by decoupling the dynamics of the electrons and the nuclei, this is known as the Born-Oppenheimer (or adiabatic) approximation [84], which will be discussed briefly in the next section.

### 2.1.2 Born–Oppenheimer approximation

The basis of the Born-Oppenheimer (BO) approximation [84] comes from the fact that the nuclei are much heavier than the electrons. Even for the lightest hydrogen nucleus, a proton has a mass that is approximately 2000 times larger than that of an electron. The ratio between electron and nucleus mass ( $m/M$ ) is very small. Therefore, in many cases the timescale of the response of the electrons is a few orders of magnitude faster than that of the nuclei, which allows the dynamics of the electrons and nuclei to be decoupled. Through this approximation, nuclei can be treated as classical particles (or point charges) and can be considered as static with respect to quantum-mechanical electrons. Mathematically, one can separate the Hamiltonian of Eq. (2.4) into an electronic part  $\hat{\mathcal{H}}_e$  consisting of

$$\hat{\mathcal{H}}_e = \hat{T}_e + \hat{V}_{n-e} + \hat{V}_{e-e}, \quad (2.7)$$

such that total Hamiltonian is given by

$$\hat{\mathcal{H}} = \hat{\mathcal{H}}_e + \hat{T}_n + \hat{V}_{n-n}. \quad (2.8)$$

One can then solve the time-independent Schrödinger equation for  $\hat{\mathcal{H}}_e$  in order to use its eigenvectors as a basis to expand the eigenstates of the full Hamiltonian as

$$\hat{\mathcal{H}}_e \phi_\nu(\mathbf{r}, \mathbf{R}) = E_\nu^e(\mathbf{R}) \phi_\nu(\mathbf{r}, \mathbf{R}), \quad (2.9)$$

where  $E_\nu^e(\mathbf{R})$  is the electronic energy for a given collection of the nuclei and the  $\phi_\nu$  are assumed to be orthonormalized. The wavefunction  $\psi$  of

---

<sup>2</sup>Here, the electron spin has been dropped for simplicity.

the many-body Hamiltonian can then be expanded as

$$\psi = \sum_{\nu} \lambda_{\nu}(\mathbf{R}) \phi_{\nu}(\mathbf{r}, \mathbf{R}), \quad (2.10)$$

where  $\lambda_{\nu}(\mathbf{R})$  is the nuclear wavefunction. If one writes  $\psi$  as Eq. (2.10) in Eq. (2.6) and multiplies by  $\langle \phi_{\mu} |$ , the expression becomes

$$\langle \phi_{\mu} | \hat{\mathcal{H}} | \phi_{\nu} \rangle = E \lambda_{\mu}, \quad (2.11)$$

such that

$$\begin{aligned} (E_{\mu}^e + \hat{T}_n + \hat{V}_{n-n}) \lambda_{\mu} + \sum_{\nu} \sum_I \frac{\hbar^2}{2M_I} & \left( \langle \phi_{\mu} | \nabla_I^2 | \phi_{\nu} \rangle \lambda_{\nu} \right. \\ & \left. + 2 \langle \phi_{\mu} | \nabla_I | \phi_{\nu} \rangle \nabla_I \lambda_{\nu} \right) = E \lambda_{\mu} \end{aligned} \quad (2.12)$$

The off-diagonal elements of the two last terms appearing in Eq. (2.12) are called non-adiabatic, referring to the fact that they involve the interaction between two different electronic states. The ones lying on the diagonal are called adiabatic (since  $\langle \phi_{\mu} | \nabla_I | \phi_{\nu} \rangle$  is anti-symmetric, its diagonal elements ( $\mu = \nu$ ) are always zero). No approximations were introduced so far. However, if one could neglect the last two terms in Eq. (2.12), by defining  $\hat{\mathcal{H}} = \hat{T}_n + \hat{V}_{n-n} + E_{\mu}^e$ , it would be possible to write  $\hat{\mathcal{H}} \lambda_{\mu} = E \lambda_{\mu}$ . To achieve this condition, approximations need to be introduced. One approximation is that it is necessary to assume an adiabatic system that is the atomic motion does not induce electronic excitations such that,  $\langle \phi_{\mu} | \nabla_I | \phi_{\nu} \rangle = \langle \phi_{\mu} | \nabla_I^2 | \phi_{\nu} \rangle = 0$  for  $\mu \neq \nu$ . The other approximation is that the diagonal elements  $\langle \phi_{\mu} | \nabla_I^2 | \phi_{\nu} \rangle$  are very small if compared to their electronic counterpart, meaning that

$$\langle \phi_{\mu} | \nabla_I^2 | \phi_{\nu} \rangle \leq \langle \phi_{\mu} | \nabla_i^2 | \phi_{\nu} \rangle. \quad (2.13)$$

It is possible to show that this is an acceptable approximation by multiplying by  $\hbar^2 / 2M_I$  each side of Eq. (2.13) and the right side by  $m_{\mu} / m_{\mu} = 1$ , arriving at

$$\frac{\hbar^2}{2M_I} \langle \phi_{\mu} | \nabla_I^2 | \phi_{\nu} \rangle \leq \frac{m_{\mu}}{M_I} \frac{\hbar^2}{2m_{\mu}} \langle \phi_{\mu} | \nabla_i^2 | \phi_{\nu} \rangle, \quad (2.14)$$

where, knowing that  $m_{\mu} / M_I$  is at least of the order of  $10^{-4}$  (electron to proton mass ratio is  $5 \times 10^{-4}$ ), the term in Eq. (2.14) can also be neglected. The total energy for some fixed configurations of the nuclei will also include the constant nuclear repulsion term leading to

$$E_{total}^{BO} = E_0^e + \hat{V}_{n-n}, \quad (2.15)$$

where  $E_0^e$  is given by Eq. (2.9). In general, under the BO approximation the electronic structure problem reduces to solving Eq. (2.9). Therefore, in general, total energies are obtained after solving Eq. (2.9) through Eq. (2.15). However, one should note that the BO approximation is not universally valid. It is well known that the BO approximation will break down when there are multiple potential energy surfaces crossing each other or close to each other in energy. Dissociative adsorption of molecules on metal surfaces is one example. Similarly, reactions involving hydrogen or proton transfer may be susceptible to breakdowns in the BO approximation [85–88]. The major difficulty in solving Eq. (2.9) is the interaction between electrons, where all the many-body quantum effects are included.

Despite the almost intractable nature of these interactions, many approximate methods have been developed to solve the Schrödinger equation by mapping the  $N$  electron Schrödinger equation into effective one-electron Schrödinger-like equations, which are easier to tackle. Some of these approximate solutions used in this thesis will be introduced in the following section. The different approximate schemes employed here can be divided into two major categories: (i) the wavefunction based methods, where the many-electron wavefunction is the key; and (ii) density-functional theory (DFT), in which electron density is the central quantity. Here, the wavefunction based methods will be introduced first.

### 2.1.3 Hartree–Fock method

The Hartree-Fock (HF) approximation is regarded as the fundamental step in quantum chemistry [89, 90]. Due to its conceptual importance, the first method discussed here used to solve the electronic Hamiltonian, defined in Eq. (2.9), is the HF method. The HF method is an improvement upon Hartree theory [89]. In Hartree theory, the wavefunction is expressed as a product of single particle orbitals  $\Psi_0^H(\mathbf{r}_N) = \phi_1(\mathbf{r}_1)\phi_2(\mathbf{r}_2) \cdots \phi_N(\mathbf{r}_N)$ . The expectation value  $\hat{\mathcal{H}}_e$  satisfies a variational principle, in the sense that it has to be bounded below by the exact energy in the BO surface. In the Hartree theory, the ansatz wavefunction ignores the Pauli principle. The Hartree wavefunction does not satisfy the antisymmetric property of the total electronic wavefunction which needs to be fulfilled since electrons are fermions. In 1930, V. Fock [90] proposed to use a Slater determinant instead of Hartree products to represent the total electronic wavefunction. It is worth pointing out here that a Slater determinant is a determinant constructed from spin orbitals. Being determinant, it obeys the antisymmetry principle by default and thus, serves as a natural choice of electronic wave function. For  $N$ -electron system, a generalized form of Slater determinant describing  $N$  electrons occupying  $N$  spin orbitals

$(\phi_1, \phi_2, \phi_3, \dots, \phi_N)$  with normalization constant can be written as

$$\Psi^{\text{HF}} = \frac{1}{\sqrt{N!}} \begin{vmatrix} \phi_1(\mathbf{r}_1) & \phi_2(\mathbf{r}_1) & \phi_3(\mathbf{r}_1) & \dots & \phi_N(\mathbf{r}_1) \\ \phi_1(\mathbf{r}_2) & \phi_2(\mathbf{r}_2) & \phi_3(\mathbf{r}_2) & \dots & \phi_N(\mathbf{r}_2) \\ \phi_1(\mathbf{r}_3) & \phi_2(\mathbf{r}_3) & \phi_3(\mathbf{r}_3) & \dots & \phi_N(\mathbf{r}_3) \\ \vdots & \vdots & \vdots & \ddots & \vdots \\ \phi_1(\mathbf{r}_N) & \phi_2(\mathbf{r}_N) & \phi_3(\mathbf{r}_N) & \dots & \phi_N(\mathbf{r}_N) \end{vmatrix} \quad (2.16)$$

where  $\phi_i(\mathbf{r}_j)$  is the single-particle wavefunction of electron  $j$  for state  $i$ . The dependency on spin component has been dropped for simplicity. The goal here is to find the best possible approximation to the ground state  $\Psi_0^{\text{HF}}$  of  $N$ -electron system described by an electronic Hamiltonian  $\hat{\mathcal{H}}_{\text{e}}$  subject to the condition that  $\langle \Psi_0^{\text{HF}} | \Psi_0^{\text{HF}} \rangle = 1$ . Thus, the electronic energy corresponding to  $\Psi_0^{\text{HF}}$  can be obtained as

$$E_0 = \langle \Psi_0^{\text{HF}} | \hat{\mathcal{H}}_{\text{e}} | \Psi_0^{\text{HF}} \rangle = \langle \Psi_0^{\text{HF}} | \hat{T}_{\text{e}} + \hat{V}_{\text{n-e}} + \hat{V}_{\text{e-e}} | \Psi_0^{\text{HF}} \rangle, \quad (2.17)$$

$E_0$  is minimized by varying the spin orbitals with a constraint that they remain orthonormal. According to the variational principle, the best spin orbitals are those which correspond to minimum electronic energy. Now using the HF wave function the electronic energy can be written as

$$\begin{aligned} \langle \Psi_0^{\text{HF}} | \hat{\mathcal{H}}_{\text{e}} | \Psi_0^{\text{HF}} \rangle &= \sum_{i=1}^N \left[ \int \phi_i^*(\mathbf{r}_i) \left( -\frac{1}{2} \nabla_i^2 + \hat{V}_{\text{n-e}} \right) \phi_i(\mathbf{r}_i) d^3 r_i \right] \\ &\quad + \underbrace{\frac{1}{2} \sum_{i=1}^N \sum_{i \neq j}^N \int \int \phi_i^*(\mathbf{r}_i) \phi_j^*(\mathbf{r}_j) \frac{1}{|\mathbf{r}_i - \mathbf{r}_j|} \phi_i(\mathbf{r}_i) \phi_j(\mathbf{r}_j) d^3 r_i d^3 r_j}_{E_{\text{Hartree}}} \\ &\quad - \underbrace{\frac{1}{2} \sum_{i=1}^N \sum_{i \neq j}^N \int \int \phi_i^*(\mathbf{r}_j) \phi_j^*(\mathbf{r}_i) \frac{1}{|\mathbf{r}_i - \mathbf{r}_j|} \phi_i(\mathbf{r}_i) \phi_j(\mathbf{r}_j) d^3 r_i d^3 r_j}_{E_{\text{x}}} \quad (2.18) \end{aligned}$$

The first two terms in braces are the kinetic energy of  $N$  independent electrons and their interaction with the external potential, respectively. The term  $E_{\text{Hartree}}$  is called the Hartree energy and the term  $E_{\text{x}}$  is called the HF exchange energy. If  $i = j$  the exchange term cancels exactly with the Hartree term such that the spurious interaction of the electron with itself is automatically removed. This exchange term only acts on electrons of the same spin<sup>3</sup>. This means that the motion of electrons of same spin in the HF approximation is correlated. The Eq. (2.18) can be

---

<sup>3</sup>Here, the spin of the electrons is not explicitly written.

written in a compact form as

$$\hat{\mathcal{F}}_i = -\frac{1}{2}\nabla_i^2 + \hat{V}_{\text{n-e}}(\mathbf{r}_i) + v^H(\mathbf{r}_i) - v^x(\mathbf{r}_i), \quad (2.19)$$

where  $\hat{\mathcal{F}}_i$  is known as the Fock operator. The expression of Eq. (2.18) allows to define the exchange potential,  $v^x$ , for the electron  $i$  as

$$v^x(\mathbf{r}_i) = \int \frac{\phi_i^*(\mathbf{r}_j)\mathcal{P}_{i,j}\phi_i(\mathbf{r}_j)}{|\mathbf{r}_i - \mathbf{r}_j|}, \quad (2.20)$$

where  $\mathcal{P}_{i,j}$  is an operator that acts on  $\phi_i(\mathbf{r}_j)$  to change  $\mathbf{r}_i$  to  $\mathbf{r}_j$ . The quantity  $v^H(\mathbf{r}_i)$  is the Hartree potential, which is the Coulomb repulsion between  $i^{\text{th}}$  electron and the electron density produced by all electrons and given by the following form

$$v^H(\mathbf{r}_i) = \int \frac{n(\mathbf{r})}{|\mathbf{r}_i - \mathbf{r}|} d^3\mathbf{r} \quad (2.21)$$

This can be considered as a classical mean-field approximation in the sense that one electron can be considered as moving in an average field given by all the other electrons present in the system. This greatly simplifies the problem as the particles are now decoupled and the problem reduces to solving a single particle Hamiltonian subject to an effective potential. Furthermore, the Hartree-Fock single particle equations can be written in the following form

$$\hat{\mathcal{F}}_i\phi_i = \epsilon_i\phi_i, \quad (2.22)$$

where  $\epsilon_i$  are the Lagrange multipliers used to constrain the normalization of the orbitals and minimize Eq. (2.18). The eigenvalues  $\epsilon_i$  that correspond to the occupied orbitals are equivalent to negative ionization potentials as shown by Koopmans' theorem [91]. This is valid within an approximation that there is no relaxation of the orbitals upon removal of electrons. Commonly  $\epsilon_i$  are just interpreted as orbital energies. However, this interpretation would only be true if electrons were really independent effective single particles.

The HF equations have to be solved self-consistently, a procedure known as the self-consistent field (SCF). Therefore, starting from an initial guess, one solves the Hamiltonian to get new orbitals, builds new potentials and solves again the HF equations. This process is repeated until the self-consistency is achieved. The exchange term appearing in Eq. (2.18) that requires the explicit calculation of four center integral. The formal scaling of HF method is of the order  $N^4$ , where  $N$  is a measure of the size of the system, e.g. electrons or basis functions.

The HF method is used extensively to study various problems, such as molecules, adsorption [92], defects in solids [93], and electronic structure of insulators [94]. A major limitation of the HF method lies in

the effective mean field treatment of the Coulomb interaction between electrons.

The difference between the ground state HF energy (in a basis set limit) and the exact ground state energy is used as a standard definition of the electron correlation energy in quantum chemistry [95]. The correlation energy is typically a small number compared to the total energy. However, it is often a very important contribution to many systems of physical and chemical interest, since the total energy difference is what matters. In the following section, we will briefly describe some of the methods which explicitly calculate the electron correlation energy.

### 2.1.4 Methods beyond the HF approximation

There is a hierarchy of methods beyond the HF approximation that aim to improve HF by including electron correlation. Most of these methods require more flexible wavefunctions than that of a HF single determinant. This is usually obtained by means of excitations of electrons from occupied to virtual orbitals. The exchange term discussed above is a form of correlation between electrons also called Pauli correlation. Now, anything missing from the Hartree-Fock energy is generally termed as correlation energy and can be expressed as

$$E_{corr}^e = E^e - E_{HF}^e \quad (2.23)$$

where  $E^e$  was defined in Eq. (2.9) calculated with the true many-body wavefunction and the term  $E_{HF}^e$  is calculated with the approximate HF wavefunction. The exact solution to the many-body problem would be the full configuration interaction (CI) [82] method.

CI is a post-Hartree–Fock linear variational method for solving the electronic many-body problem within the BO approximation. Mathematically, configurations (states) describe the linear combination of Slater determinants used for expanding the wavefunction. In terms of a specification of orbital occupation, interaction means the mixing of different electronic configurations. Such formalism is extremely computationally demanding and requires immense hardware, while the method is limited to relatively small systems. Approximating CI wavefunction by including excitations only up to a certain order causes a size-extensive problem, *i.e.* the energy in this method does not scale correctly with the number of electrons [96]. For example, let  $P$  and  $Q$  be two non-interacting systems. If a given method for the evaluation of the energy is size consistent, then the energy of the supersystem  $P + Q$ , separated by a sufficiently large distance is equal to the sum of individual fragments, *i.e.*  $E(P + Q) = E(P) + E(Q)$ . This property of size consistency is of particular importance to obtain correct dissociation curves or entire potential energy surfaces [96]. In the following section, we introduce a size-consistent method which includes correlation, so

called Møller-Plesset perturbation theory.

### 2.1.5 Møller-Plesset (MP) perturbation theory

A natural way to include electronic correlations is by adding interelectronic Coulomb interaction as a perturbation to the Hamiltonian<sup>4</sup>. A method known as Møller-Plesset perturbation theory [97] is a particular case of many-body perturbation theory where the unperturbed Hamiltonian is taken to be the Hartree-Fock one

$$\hat{\mathcal{H}}_0 = \sum_i^N \hat{\mathcal{F}}_i, \quad (2.24)$$

and the perturbation is given by the difference of the true many-body electronic Coulomb interaction and what is already included in Hartree-Fock

$$\hat{\mathcal{H}}' = \hat{\mathcal{H}}_e - \sum_i^N \hat{\mathcal{F}}_i = \sum_{i,j;i < j} \frac{1}{|\mathbf{r}_i - \mathbf{r}_j|} - \sum_i [v^H(\mathbf{r}_i) - v^X(\mathbf{r}_i)]. \quad (2.25)$$

For the Hartree-Fock Hamiltonian all single Slater-determinant wavefunctions that satisfy  $\hat{\mathcal{H}}_0 |\Psi\rangle = E^e |\Psi\rangle$  can be calculated<sup>5</sup>. These form a complete orthonormal set of functions that can be used as a starting point for perturbation theory. The difference between the ground-state determinant  $|\Psi_0\rangle$  and other possible solutions are interpreted as electronic excitations, since they differ by interchanging one or more rows of the HF determinant. If the electrons could be seen as effective single particles, this interchanging could be understood as promoting one or more electrons from an occupied state to a unoccupied one in the Hartree-Fock basis. Furthermore, the term  $|\Psi_i^a\rangle$  corresponds to a single excited electronic state,  $|\Psi_{ij}^{ab}\rangle$  to double excited electronic states and so on, where  $i, j, k, \dots$  denote occupied states and  $a, b, c, \dots$  unoccupied ones. The first order correction to the energy in this basis, with the perturbation given by Eq. (2.25) yields the HF energy itself. For the second-order perturbation term of the energy there would be matrix elements involving the ground state plus single excitations and double excitations, but not higher order excitations. The lack of contribution from higher-order excitations is due to the fact that the perturbation  $\hat{\mathcal{H}}'$  is a two-particle operator and the orbitals are orthonormal. The matrix elements of the Hamiltonian between the ground state HF wavefunction  $|\Psi_0\rangle$ , and a single excited determinant  $|\Psi_i^a\rangle$  is zero i.e.  $\langle \Psi_0 | \hat{\mathcal{H}}' | \Psi_i^a \rangle = 0$ , this is known as Brillouin's theorem [82]. This means that singly-excited states do not interact directly with the HF ground state (but can interact indirectly through

<sup>4</sup>The derivation of the first and second order corrections for the energy by using perturbation theory is can be found in the textbook of Szabo and Ostlund [82].

<sup>5</sup>Here, the HF label has been dropped for simplicity

higher order perturbation terms), therefore, any matrix element involving these two orbitals is zero. The second-order energy correction in MP2 is thus given by

$$\zeta_k^2 = \sum_{i \leq j}^{\text{occ.}} \sum_{a \leq b}^{\text{unocc.}} \frac{\langle \Psi_0 | \hat{\mathcal{H}}' | \Psi_{ij}^{ab} \rangle \langle \Psi_{ij}^{ab} | \hat{\mathcal{H}}' | \Psi_0 \rangle}{E_0^e - E_{ij}^{ab}}, \quad (2.26)$$

where  $i, j$  are occupied orbitals,  $a, b$  are empty orbitals,  $E_0^e$  is the HF ground-state energy and  $E_{ij}^{ab}$  the energy corresponding to a particular doubly excited determinant [82]. The matrix elements appearing in the numerator of Eq. (2.26) can be written as two-electron integrals over molecular orbitals  $\phi$ , and the energy difference in the denominator can be written as a difference between molecular orbital energies, since the wavefunction is a Slater determinant. The expression for the MP2 total energy is written as

$$E^{\text{MP2}} = E_{\text{HF}} + \frac{1}{4} \sum_{ijab} \frac{|\langle ij || ab \rangle|^2}{\epsilon_i + \epsilon_j - \epsilon_a - \epsilon_b}, \quad (2.27)$$

where  $\epsilon_i$  is the HF molecular orbital eigenvalue for state  $i$  and  $\langle ij || ab \rangle = \langle ij | ab \rangle - \langle ij | ba \rangle$  with

$$\langle ij | ab \rangle = \int \int \frac{\phi_i^*(\mathbf{r}) \phi_j^*(\mathbf{r}') \phi_a(\mathbf{r}) \phi_b(\mathbf{r}')}{|\mathbf{r} - \mathbf{r}'|} d^3 r d^3 r'. \quad (2.28)$$

MP2 shows improvements over HF in many respects in electronic structure calculations [98, 99]. For example, MP2 can approximately capture the weak non-covalent interactions like van der Waals (dispersion) for which HF completely fails. Also the molecular geometry obtained from MP2 shows much improvement over HF as compared with experimental measurements [100]. However, MP2 is not appropriate for metallic systems (Eq. (2.27) will be singular due to the zero gap between states) and for some molecular properties like spectroscopic constants which are not necessarily converged when going to high orders, or the convergence is slow or oscillatory [101]. Another popular method in quantum chemistry is the coupled cluster method in which the electron correlation is handled through the use of a so-called cluster operator and will be briefly introduced in the next section.

### 2.1.6 Coupled cluster theory

Coupled cluster theory was initially proposed in the context of nuclear physics [102]. It is one of the most accurate and computationally affordable methods to solve the many-body problem [103]. The

wavefunction ansatz for CC theory in quantum-chemistry is written as <sup>6</sup>

$$\Psi_{\text{CC}} = e^{\hat{T}} \Psi_0 = (1 + \hat{T} + \frac{\hat{T}^2}{2!} + \frac{\hat{T}^3}{3!} + \dots) \Psi_0, \quad (2.29)$$

where  $\Psi_0$  is the HF ground-state slater determinant and  $\hat{T}$  is a cluster operator that can be expanded in terms of single, double, triple, etc. excitations in the following way

$$\hat{T} = \hat{T}_1 + \hat{T}_2 + \hat{T}_3 + \dots \quad (2.30)$$

$$\hat{T}_1 \Psi_0 = \sum_i^{\text{occ. unocc.}} \sum_a t_i^a \Psi_i^a \quad (2.31)$$

$$\hat{T}_2 \Psi_0 = \sum_{ij}^{\text{occ. unocc.}} \sum_{ab} t_{ij}^{ab} \Psi_{ij}^{ab} \quad (2.32)$$

$$\hat{T}_3 \Psi_0 = \sum_{ijk}^{\text{occ. unocc.}} \sum_{abc} t_{ijk}^{abc} \Psi_{ijk}^{abc} \quad (2.33)$$

⋮

$$(2.34)$$

where  $t_i^a$ ,  $t_{ij}^{ab}$ ,  $t_{ijk}^{abc}$  are the excitation amplitudes. Due to nonlinear terms in the exponential expansion in Eq. (2.29), we have additional higher order excitations terms like,  $\hat{T}^2$ ,  $\hat{T}_1 \hat{T}_2$  etc. The exponential operator  $e^{\hat{T}}$  (by grouping the expansion by excitation order) can be written as

$$\begin{aligned} e^{\hat{T}} = 1 &+ \hat{T}_1 + \left( \hat{T}_2 + \frac{\hat{T}_1^2}{2} \right) + \left( \hat{T}_3 + \hat{T}_1 \hat{T}_2 + \frac{\hat{T}_1^3}{6} \right) + \\ &\left( \hat{T}_4 + \hat{T}_3 \hat{T}_1 + \frac{\hat{T}_2^2}{2} + \frac{\hat{T}_2 \hat{T}_1^2}{2} + \frac{\hat{T}_1^4}{48} \right) + \dots, \end{aligned} \quad (2.35)$$

where the first term on the right corresponds to the Hartree-Fock system, the second term produces all single excitations, the third all double excitations, etc. The coupled-cluster energy is then obtained by minimizing, as a function of the amplitudes, the following expression

$$E^{\text{CC}} = \langle \Psi_0 | e^{-\hat{T}} \hat{\mathcal{H}} e^{\hat{T}} | \Psi_0 \rangle. \quad (2.36)$$

Up to this step, everything is exact. The expansion of the cluster operator  $\hat{T}$  up to  $\hat{T}_N$  would mean all possible excited determinants are included and the coupled cluster results from Eq. (2.36) would equal those obtained from full CI calculations. Therefore, in practice a truncation of  $\hat{T}$  must be performed. The coupled cluster singles and doubles (CCSD) theory is the one obtained when  $e^{\hat{T}}$  is written as

---

<sup>6</sup>For detailed formulas of the energy and wavefunction of CCSD the reader is referred to Refs. [82, 103].

$\hat{T}_1 + \hat{T}_2$  yielding all possible single and double excitations and their corresponding correlation (see Eq. (2.35)) as well as contributions of higher orders ( $\hat{T}_1\hat{T}_2, \hat{T}_2^2$ , etc.). The scaling of CCSD is already of  $N^6$ , where  $N$  is the size of the system, like number of electrons or basis-functions). Coupled cluster singles, doubles and triples (CCSDT) theory would consider  $\hat{T} = \hat{T}_1 + \hat{T}_2 + \hat{T}_3$ , but that is already extremely computationally expensive.

The sampling of correlated many electron wavefunction for realistic systems, such as bio-molecules and complex nanostructures is prohibitively expensive, so alternative approaches are required. Density functional theory (DFT) [41] provides a successful approach. DFT is an exact reformulation of the quantum many-body problem in terms of the ground-state density, rather than the ground-state wavefunction. Nowadays DFT is one of the most widely used quantum-mechanical methods in condensed-matter physics and chemistry [104–108]. In the next section the basic formulation of DFT will be discussed.

## 2.2 Fundamentals of density-functional theory

The term density-functional theory (DFT) refers to methods that express the ground-state energy as a *functional* of the electronic density. A *functional* is a mathematical construction that maps functions onto numbers. In quantum chemistry, the orbital functional takes the electron orbitals of a system and returns an energy value. DFT reduces the complexity of the many-body problem by substituting the  $3N$  dimensional many-electron wavefunction,  $\Psi(\mathbf{r}_1, \mathbf{r}_2, \dots, \mathbf{r}_N)$ , by its ground-state electronic density,  $n_0(\mathbf{r})$ . It incorporates ideas from the previous work of L. Thomas and E. Fermi in the 1920's [109, 110], including also the work of J. Slater [111]. DFT has been successful in predicting molecular geometries, lattice constants and properties for a wide range of materials.

## 2.3 Hohenberg–Kohn theorems

The foundation of DFT is based on the pioneering work by Hohenberg and Kohn, who formulated two theorems [41].

1. The ground state electron density  $n_0(\mathbf{r})$  of an  $N$ -electron system determines uniquely the external potential  $v_{\text{ext}}(\mathbf{r})$ . Therefore, the Hamiltonian and consequently all other properties including the energy of the system can be expressed as a *functional* of the ground state electron density of that system.
2. For an  $N$ -electron system with external potential  $v_{\text{ext}}(\mathbf{r})$ , the energy corresponding to any  $N$ -electron trial density  $n(\mathbf{r})$  is always greater than or equal to the exact ground state energy,  $E_0$ , of that system, *i.e.*  $E_0 \equiv E[n_0(\mathbf{r})] < E[n(\mathbf{r})]$ . Importantly, the equality is achieved *if and only if*  $n(\mathbf{r})$  is the ground state electron density of that system.

These theorems imply that the ground-state energy can be variationally expressed as a functional of the ground-state electron density of the  $N$ -electron system. In DFT, the electronic energy functional is composed of contributions from the kinetic energy, the Hartree energy, the external potential and the electronic exchange-correlation term [83, 112]. The energy functional can be written as

$$E[n(\mathbf{r})] = F_{HK}[n(\mathbf{r})] + E_{\text{ext}}[n(\mathbf{r})] \quad (2.37)$$

$$= F_{HK}[n(\mathbf{r})] + \int v_{\text{ext}}(\mathbf{r}) n(\mathbf{r}) d\mathbf{r}. \quad (2.38)$$

The term  $F_{HK}[n(\mathbf{r})]$  is the universal (Hohenberg-Kohn) functional of the electron density and it does not depend upon the physical system

under investigation.  $E_{\text{ext}}[n(\mathbf{r})]$  is the energy due to the external potential. The HK functional is defined as the sum of the kinetic energy functional,  $T[n(\mathbf{r})]$  and the electron-electron interaction energy functional,  $E_{\text{e-e}}[n(\mathbf{r})]$ ,

$$F_{\text{HK}}[n(\mathbf{r})] = T[n(\mathbf{r})] + E_{\text{e-e}}[n(\mathbf{r})]. \quad (2.39)$$

HK theorems assure the existence of the energy functional  $E[n(\mathbf{r})]$  which reaches its minimum when the true ground state electron density is obtained. However, these theorems do not explicitly state how to construct the crucial functional  $F_{\text{HK}}[n(\mathbf{r})]$ .

In addition, M. Levy in 1979 found an elegant proof for the HK theorems which generalizes them also for degenerate ground-state(s) [113–115]. This means that no matter how one gets the electronic density, it is theoretically possible to use it to (re-)construct the corresponding external potential, under specific constraints. In any case this approach does not provide a practical numerical way to solve the problem and therefore to obtain the electronic densities required to reconstruct the external potential. In 1965, W. Kohn and L. Sham proposed a method to practically perform DFT calculations which is now called the Kohn-Sham method [42].

## 2.4 The Kohn–Sham method

In the Kohn-Sham (KS) approach [42], the interacting many-electron system with electron density,  $n(\mathbf{r})$ , is mapped onto a system of fictitious non-interacting particles with density,  $n^{\text{KS}}(\mathbf{r})$ , which is constrained to have exactly the same density  $n(\mathbf{r})$  of the interacting system

$$n(\mathbf{r}) = n^{\text{KS}}(\mathbf{r}) = \sum_i^N |\psi_i|^2, \quad (2.40)$$

where  $\psi_i$  are orthonormal orbitals or so-called single-particle KS orbitals. Further, the kinetic-energy operator appearing in Eq. (2.39) is written in two parts

$$T[n(\mathbf{r})] = T_s[n(\mathbf{r})] + T_c[n(\mathbf{r})]. \quad (2.41)$$

$T_s[n(\mathbf{r})]$  belongs to a system of non-interacting electrons and  $T_c[n(\mathbf{r})]$  corresponds to the remaining part that accounts for the many-electron correlation contributions to the kinetic energy. Then, the kinetic energy operator of a non-interacting system can be calculated from the KS orbitals as

$$T_s = -\frac{1}{2} \sum_i^N \langle \psi_i | \nabla^2 | \psi_i \rangle. \quad (2.42)$$

Also, the potential energy corresponding to the electron-electron interaction (second term in Eq. (2.39)) is partitioned as follows,

$$E_{\text{e-e}}[n(\mathbf{r})] = E_{\text{H}}[n(\mathbf{r})] + E_{\text{xc}}[n(\mathbf{r})] \quad (2.43)$$

where  $E_{\text{H}}[n(\mathbf{r})]$  is the Hartree or classical electrostatic energy corresponding to the Coulomb interaction. The term  $E_{\text{xc}}[n(\mathbf{r})]$  is exchange and correlation energy between the interacting electrons which contains all the remaining contributions (quantum-mechanical many-body effects) to the total electronic energy expression. This also includes the residual part of the true kinetic energy  $T_c$  which is not accounted for by  $T_s$ . The available approximations for the exchange-correlation functional will be discussed in Section (2.5).

For a charge distribution  $n(\mathbf{r})$  the Hartree energy can be written as,

$$E_{\text{H}}[n(\mathbf{r})] = \int v_{\text{H}}(\mathbf{r}) n(\mathbf{r}) d\mathbf{r}, \quad (2.44)$$

with the Hartree potential,  $v_{\text{H}}$ , given by

$$v_{\text{H}}(\mathbf{r}) = \int \frac{n(\mathbf{r}')}{|\mathbf{r} - \mathbf{r}'|} d\mathbf{r}'. \quad (2.45)$$

In this fashion the KS total energy functional is written as

$$E_{\text{KS}} = T_s[n(\mathbf{r})] + E_{\text{H}}[n(\mathbf{r})] + E_{\text{xc}}[n(\mathbf{r})] + E_{\text{ext}}[n(\mathbf{r})]. \quad (2.46)$$

The ground-state energy is obtained by minimizing Eq. (2.46) with respect to the density of a system, with constraints such that  $\int n(\mathbf{r}) d\mathbf{r} = N$ , one obtains,

$$\frac{\delta}{\delta n(\mathbf{r})} \left( E_{\text{KS}}[n(\mathbf{r})] - \mu \left[ \int n(\mathbf{r}) d\mathbf{r} - N \right] \right) = 0 \quad (2.47)$$

$$\frac{\delta E_{\text{KS}}[n(\mathbf{r})]}{\delta n(\mathbf{r})} = \mu \quad (2.48)$$

$$\frac{\delta T_s[n(\mathbf{r})]}{\delta n(\mathbf{r})} + v_{\text{H}}(\mathbf{r}) + v_{\text{ext}}(\mathbf{r}) + \frac{\delta E_{\text{xc}}[n(\mathbf{r})]}{\delta n(\mathbf{r})} = \mu \quad (2.49)$$

where  $\mu$  is the Lagrange multiplier for the number of electrons and the term,  $\frac{\delta E_{\text{xc}}[n(\mathbf{r})]}{\delta n(\mathbf{r})}$ , is called the exchange-correlation  $v_{\text{xc}}(\mathbf{r})$  potential.

Unfortunately, the dependence of  $v_{\text{xc}}$  on the electron density is unknown and must be approximated and will be discussed in Section (2.5). The last three terms in Eq. (2.49) define the local effective potential,  $v_{\text{eff}}(\mathbf{r})$ , which describes the non-interacting fictitious electronic system moving in an overall effective field given by

$$v_{\text{eff}}(\mathbf{r}) = v_{\text{H}}(\mathbf{r}) + v_{\text{ext}}(\mathbf{r}) + v_{\text{xc}}(\mathbf{r}). \quad (2.50)$$

From Eq. (2.49) and Eq. (2.50), we obtain

$$\frac{\delta T_s[n(\mathbf{r})]}{\delta n(\mathbf{r})} + v_{\text{eff}}(\mathbf{r}) = \mu. \quad (2.51)$$

Now, the initial interacting many-body problem reduces to a set of coupled one-particle KS orbital equations. In this procedure it is necessary to solve the following set of  $N$  one-electron Schrödinger-like equations

$$\left( -\frac{1}{2}\nabla^2 + v_{\text{eff}} \right) \psi_i = \epsilon_i \psi_i, \quad (2.52)$$

where  $\psi_i$  are the KS orbitals and  $\epsilon_i$  are the corresponding eigenenergies. The effective potential,  $v_{\text{eff}}$ , depends on the electron density evaluated using KS orbitals via

$$n^{\text{KS}}(\mathbf{r}) = \sum_{i=1}^N |\psi_i|^2. \quad (2.53)$$

In order to find the density of the interacting system, the Kohn-Sham equations Eq. (2.50), Eq. (2.52), and Eq. (2.53) must be solved self-consistently. The general procedure is to start with an initial guess for the electron density  $n(\mathbf{r})$  (for example, the superposition of free atom electron densities), construct the effective potential,  $v_{\text{eff}}$ , and then solve Eq. (2.52) to obtain the Kohn-Sham orbitals. Now based on these orbitals, a new density is obtained and the process continues until convergence is achieved.

Finally, the total ground state energy is given by the following expression

$$E_{\text{KS}}[n] = \sum_{i=1}^N \epsilon_i - \frac{1}{2} \int v_{\text{H}}(\mathbf{r}) n(\mathbf{r}) d\mathbf{r} - \int v_{\text{ext}}(\mathbf{r}) n(\mathbf{r}) d\mathbf{r} + E_{\text{xc}}[n]. \quad (2.54)$$

If each term in the Kohn-Sham energy functional was known, we would be able to obtain the exact ground state electron density and the total energy of a system. Unfortunately, the functional form of  $E_{\text{xc}}[n]$  is unknown in general. This includes the non-classical part of the electron-electron interaction along with the component  $T_c[n]$  of the kinetic energy of the real system. Therefore, it is necessary to approximate  $E_{\text{xc}}$  and this issue will be discussed in detail in the next section.

## 2.5 The exchange–correlation approximations

For practical use of the Kohn-Sham equations to study the electronic structure of atoms, molecules or materials, we must know the functional form of the exchange-correlation energy *a priori*. The performance of DFT calculations clearly depends on the approximation for the exchange-correlation functional. However, the exact form of  $E_{\text{xc}}$  is unknown and may never be known in a closed mathematical

form. The most popular exchange-correlation functional forms are categorized with varying levels of complexity often known as "Jacob's ladder", a classification proposed by John Perdew [116]. The "Jacob's ladder" starts with the Hartree approximation (where  $E_{xc}[n] = 0$ ) or independent electron approximation to the exact non-local exchange-correlation functional.

Numerous approximations to  $v_{xc}[n] = \frac{\delta E_{xc}[n(\mathbf{r})]}{\delta n(\mathbf{r})}$  were proposed over the years (See Ref. [117] for an extensive list of available approximations). In the local-density approximation (LDA) the exchange-correlation functional is expressed in terms of the (local) electron density [42, 118]. The next level is categorized by generalized gradient approximations (GGAs). In GGA-type approximations,  $E_{xc}$  is expressed in terms of the density and gradients of the density [119]. Furthermore, meta-generalized gradient (meta-GGA) approximations also introduce a dependence of the exchange-correlation functional on the second derivatives of the density or the Laplacians [120]. A class of functionals called hybrid functionals on the other hand, can be obtained from any functional by replacing a fraction of (local) exchange with HF exact exchange [121].

All (semi)-local functionals suffer from the so called self-interaction error. The self-interaction corrected functionals aim to eliminate self-interaction error by introducing non-local corrections [122]. Finally, optimized effective potentials (OEP) based exchange correlation potentials indicate a class of local potentials derived from non-local, orbital-dependent terms for the exchange-correlation energy [123].

### 2.5.1 The local (spin) density approximation

The simplest approximation for  $E_{xc}$  is called the local (spin) density approximation (LSDA or LDA). Here, the functional for the exchange-correlation potential  $v_{xc}$  is derived from a homogeneous electron gas (HEG) model [42]. The exchange-correlation energy functional has the form<sup>7</sup>

$$E_{xc}^{LDA} = \int n(\mathbf{r}) \epsilon_{xc}^{HEG}[n(\mathbf{r})] d\mathbf{r} \quad (2.55)$$

where  $\epsilon_{xc}^{HEG}$  is the exchange-correlation energy per particle of an electron gas with uniform (spin) density. The analytical expression for the exchange energy of the HEG model is known and given by [104]

$$E_x^{LDA} = -\frac{3}{2} \left( \frac{3}{4\pi} \right)^{1/3} \int n^{4/3}(\mathbf{r}) d\mathbf{r} \quad (2.56)$$

However, the exact expression for the correlation energy component  $E_c$  of the HEG is not known in general, but only known for high or low density limits [124]. Calculations for intermediate densities of

---

<sup>7</sup>If we introduce the spin densities  $n_\uparrow$  and  $n_\downarrow$ , then the exchange-correlation energy per particle can be written  $\epsilon_{xc}[n_\uparrow(\mathbf{r}), n_\downarrow(\mathbf{r})]$ .

$\epsilon_c^{HEG}$  have been performed using the Quantum Monte Carlo (QMC) method [125]. There are several variants of fits to  $\epsilon_c^{HEG}$  which give similar results [118, 126, 127]. The LDA approximation is homogeneous in nature and valid for systems with slowly varying densities and can be inaccurate in situations with strong density inhomogeneity, for example in atoms or molecules. In general, LDA predicts too strong binding, large cohesive energies and underestimates lattice constants in solids [128, 129]. To overcome these limitations, generalized gradient approximations have been developed wherein the exchange-correlation energy depends on the gradient of the electron density.

### 2.5.2 Generalized gradient approximations

In GGAs, the exchange-correlation potential contains also the contribution from the gradient  $\nabla n(\mathbf{r})$  of the electron density. The form of the xc energy functional for GGA is given by

$$E_{xc}^{GGA} = \int n(\mathbf{r}) \epsilon_{xc}^{GGA}[n(\mathbf{r}), \nabla n(\mathbf{r})] d\mathbf{r}. \quad (2.57)$$

For GGA functionals  $\epsilon_{xc}^{GGA}[n(\mathbf{r}), \nabla n(\mathbf{r})]$  is often written in terms of an enhancement factor  $F_{xc}$  multiplied by the exchange-energy density of the homogeneous electron gas

$$E_{xc}^{GGA} = \int \epsilon_x^{HEG} F_{xc}(n(\mathbf{r}), \nabla n(\mathbf{r})) d\mathbf{r}. \quad (2.58)$$

The GGA type functional approximations typically perform better when compared to LDA, especially for geometries and ground-state energies of molecules [130–132]. There is another class of GGA approximations containing one or more fitting parameter which are obtained by fitting parameters in  $F_x$  to reproduce the total energies from the data of atoms and molecules, e.g. revPBE [133, 134] and PBEsol [135]. This sometimes provides better description of the electronic structure of solids and surfaces. Becke and coworkers proposed an exchange functional that was based on fitting of two parameters to bond and dissociation energies of a set of diatomic molecules [136, 137]. The functionals including Becke exchange approximation are popular in the chemistry community, due to their fairly good description of atoms and molecules e.g. BLYP [138].

### 2.5.3 Meta-generalized gradient approximations

A meta-GGA (mGGA) DFT functional in its original form includes the second derivative of the electron density (the Laplacian). This is a natural development after the GGA , that includes only the density and its first derivative in the exchange-correlation potential [139–

[141]. Nowadays a mGGA functional is referred more typically to one that includes a dependence on the kinetic energy density, *i.e.* on the Laplacian of the orbitals. The general form of a ( $\tau$ -dependent) mGGA functional is

$$E_{\text{xc}}^{\text{mGGA}} = \int n(\mathbf{r}) \epsilon_{\text{xc}}^{\text{mGGA}}[n(\mathbf{r}), \nabla n(\mathbf{r}), \nabla^2 n(\mathbf{r})] d\mathbf{r}. \quad (2.59)$$

Here the kinetic-energy density is obtained using Kohn-Sham orbitals and indirectly depends on the density. The kinetic energy density in mGGA can approximately include exact exchange non-locality, that it partially cures electron self-interaction error in semi-local GGAs. The kinetic energy density using KS orbitals is given by [142]

$$\tau(\mathbf{r}) = \frac{1}{2} \sum_i |\nabla \psi_i|^2 \quad (2.60)$$

where  $\psi_i$  are the Kohn-Sham orbitals. Moreover the following relation for  $\tau(\mathbf{r})$  holds

$$\tau(\mathbf{r}) = \frac{1}{4} \nabla^2 n(\mathbf{r}) - \frac{1}{2} \sum_i \psi_i^* \nabla^2 \psi_i. \quad (2.61)$$

Most mGGA functionals use only  $\tau$  because it is strictly positive and thus avoids the divergence of the Laplacian near the nuclei. Perdew and coworkers argued [143] that  $\nabla^2 n$  or  $\tau(\mathbf{r})$  essentially contains the same information beyond what is contained in  $n$  and  $\nabla n$ . But the use of  $\tau(\mathbf{r})$  requires the evaluation of an additional functional derivative, namely

$$\frac{\delta \tau(\mathbf{r})}{\delta n(\mathbf{r})} \quad (2.62)$$

This term is hard to evaluate since  $\tau$  is not an explicit functional of  $n(\mathbf{r})$ . The majority of meta-GGAs do not evaluate the functional derivative with respect to the density but with respect to the KS orbitals [144]. There are many mGGA functionals which have been developed so far, for example, PKZB [145] and TPSS [139] functionals. And there are also mGGA which include a fraction of the exact exchange: M05 [146], M06 [147, 148], and M08 [149] suite of functionals devised by Zhao and Truhlar. These functionals can have many parameters fitted to barrier heights of chemical reactions and non-covalent interactions.

## 2.5.4 Hybrid functionals

Hybrid functionals are a class of approximations to the  $E_{\text{xc}}$  energy functional in DFT. These functionals include a fraction of exact exchange from the Hartree-Fock exchange energy using KS orbitals.

The exact exchange energy functional can be expressed as

$$E_x^{EXX} = -\frac{1}{2} \sum_{pq} \int \int \frac{\psi_p^*(\mathbf{r})\psi_p(\mathbf{r}')\psi_q^*(\mathbf{r}')\psi_q(\mathbf{r})}{|\mathbf{r} - \mathbf{r}'|} d\mathbf{r} d\mathbf{r}' \quad (2.63)$$

This type of functionals reduce the self-interaction error present in local LDA, semi-local GGAs and mGGAs functionals. In this approach one needs to evaluate the non-local exchange operator which in turn increases the computational cost [150]. The functional called PBE0 [151, 152], which has the form

$$E_{xc}^{PBE0} = a_0 E_x^{EXX} + (1 - a_0) E_x^{PBE} + E_c^{PBE} \quad (2.64)$$

mixes 25% ( $a_0 = 1/4$ ) of exact exchange ( $E_x^{EXX}$ ) with 75% exchange energy from the PBE functional. The value 1/4 was chosen based on considerations from fourth order many-body perturbation theory [121, 153]. Another important hybrid functional is B3LYP [154]. It has the following form

$$E_{xc}^{B3LYP} = a_0 E_x^{EXX} + (1 - a_0) E_x^{LDA} + a_1 \Delta E_x^B + (1 - a_2) E_c^{VWN} + a_2 E_c^{LYP} \quad (2.65)$$

where  $\Delta E_x^B$  corresponds to only the gradient correction to the exchange energy given by Becke [137],  $E_x^{LDA}$  is the LDA exchange functional,  $E_c^{VWN}$  is the LDA correlation functional of Vosko, Wilk, and Nusair (VWN) [127], and  $E_c^{LYP}$  the GGA correlation functional of Lee, Yang, and Parr. The functional contains three empirical parameters,  $a_0 = 0.20$ ,  $a_1 = 0.72$ , and  $a_2 = 0.81$  fitted to reproduce atomization energies, ionization potentials, and proton affinities of molecules. This functional was first implemented in the Gaussian code 03 [155]. This functional is one of the most popular in the quantum-chemistry community due to its good description of molecules and their vibrational frequencies.

All functionals discussed up to this point do not treat long-range electron correlation and thus, fails to describe van der Waals interactions. We now proceed to discuss methods for long range electron correlation energy.

## 2.6 Random-phase approximation for electron correlation energy

The random-phase approximation (RPA) was originally proposed by Bohm and Pines [156–158] for the electron gas, but recently it has also been applied to periodic solids [159–161] and finite systems [47, 58, 162]. This approximation is used for computing the ground-state correlation energy of many-electron systems and intrinsically treats long-range correlation and thus also accounts for van der Waals interactions. This method has shown significant

improvements over semi-local density functionals for description of non-covalent interactions. RPA correlation energy in density functional theory is most often calculated in a post-processing or in non-self-consistent framework. Within this approach, the XC energy (in RPA) is obtained by the contribution of the exact exchange energy and the RPA correlation energy  $E_c^{RPA}$  [163–165]

$$E_{xc}^{RPA} = E_c^{RPA} + E_x^{EXX}. \quad (2.66)$$

The functional form of the RPA correlation energy  $E_c^{RPA}$  can be formulated based on the adiabatic-connection fluctuation-dissipation theorem (ACFDT) [65, 79]. In this case the correlation energy can be written as

$$E_c^{RPA} = -\frac{1}{2\pi} \int_0^\infty d\omega \mathbf{Tr}[\ln(1 - \chi^0(i\omega)v) + \chi^0(i\omega)v] \quad (2.67)$$

where  $\omega$  is the frequency,  $v$  is the bare Coulomb interaction and  $\chi^0$  is Kohn-Sham density-density response function. The reference bare response function  $\chi^0$  computed using the set of single-particle occupied and virtual orbitals  $\psi_p(\mathbf{r})$  with corresponding energies  $\epsilon_p$  and occupation numbers  $f_p$  determined from semi-local DFT, Hartree-Fock or hybrid self-consistent field calculations such that [166, 167],

$$\chi^0(\mathbf{r}, \mathbf{r}', i\omega) = \sum_{pq} (f_p - f_q) \frac{\psi_p^*(\mathbf{r}) \psi_p(\mathbf{r}') \psi_q^*(\mathbf{r}') \psi_q(\mathbf{r})}{\epsilon_p - \epsilon_q + i\omega}. \quad (2.68)$$

The exchange part for the RPA,  $E_x^{EXX}$  is evaluated as the exact exchange energy (See Eq. (2.63)). The molecular orbitals and energies appearing in Eq. (2.68) are obtained after solving KS equations self-consistently. Using DFT orbitals while evaluating  $E_{xc}^{RPA}$  has been shown to work very well for extended systems including metallic ones, providing very good lattice constants, bulk moduli, heats of formation, adsorption energies and surface energies [128]. However, RPA shows poor performance for short-range correlation. This limitation can be removed through incorporating a local field factor [168, 169] into RPA-like equations, or can be added on via an explicit density functional.

## 2.7 van der Waals (vdW) interactions in density-functional theory

Van der Waals (vdW) or dispersion interactions are ubiquitous in nature. They arise from quantum-mechanical fluctuations in the electron density, which lead to instantaneous dipole moments and higher-order multipole moments. The instantaneous multipole moments on one atom induce multipole moments on the second atom in turn. The

interaction of these multipoles results in an attractive force, known as London dispersion forces [170]. The term vdW not only refers to the dispersion interactions, but may also include permanent multipole-multipole interactions and permanent multipole-induced multipole interactions. Here, we use the term "vdW" to refer to dispersion energy. The local (LDA) and semi-local (GGAs) functionals of DFT take into consideration only the electronic density at point  $\mathbf{r}$  and in its immediate neighborhood. Therefore, the density and its gradient expansion have no information of fluctuations in the density which arise beyond few Ångström away from the point where they are evaluated and fail to capture correlations beyond this scale. For example, in the LDA and GGA functionals, the asymptotic interaction between two neutral atoms decreases exponentially, instead of the expected characteristic  $1/R^6$  tail [171]. Intense efforts have been directed towards the development of efficient DFT functionals which include vdW interactions. This section provides a brief overview of the available approaches to include vdW interactions in density-functional theory.

### 2.7.1 Nonlocal vdW density functionals

The vdW density functionals (vdW-DF) are nonlocal in nature and explicitly depend on the electron density. These functionals model dispersion based on coupled local oscillators having a frequency determined by the local density and its gradient. The coupling responsible for dispersion interactions is introduced through a double integration and the chosen form ensures the standard  $1/R^6$  asymptote, but does not account for more intricate non-additive many-body effects. In the general vdW-DF framework, the XC energy takes the form

$$E_{\text{xc}} = E_{\text{x}}^0 + E_{\text{c}}^0 + E_{\text{c}}^{\text{nl}} \quad (2.69)$$

where  $E_{\text{x}}^0$  and  $E_{\text{c}}^0$  are the exchange and correlation terms from local functional respectively and  $E_{\text{c}}^{\text{nl}}$  is the nonlocal part accounting for long-range vdW interactions. The simplest form for the nonlocal correlation energy is given by

$$E_{\text{c}}^{\text{nl}} = \int \int n(\mathbf{r}) \phi(\mathbf{r}, \mathbf{r}') n(\mathbf{r}') d^3\mathbf{r} d^3\mathbf{r}' \quad (2.70)$$

where the correlation kernel  $\phi(\mathbf{r}, \mathbf{r}')$  depends upon  $|\mathbf{r} - \mathbf{r}'|$ , and the charge density and density gradients at  $\mathbf{r}$  and  $\mathbf{r}'$ . The interaction kernel  $\phi(\mathbf{r}, \mathbf{r}')$  is governed by two properties: at what separation the interaction appears and the difference in electron density at interacting points. Depending on the kernel function used four main flavors have been developed are vdW-DF [54] and vdW-DF2 [172] from Chalmers-Rutgers collaboration, and the somewhat more heuristic VV09 [173] and VV10 [174] functionals from Vydrov and van Voorhis. The nonlocal vdW-DF functional has been applied to a broad range of molecules

and materials [175] and has already provided useful predictions for weakly interacting systems, such as molecular complexes, polymer crystals, and molecules adsorbed on surfaces. Recent studies for bulk crystals [176, 177] suggest that many challenges still remain, particularly in more complex materials including extended solids.

### 2.7.2 Atom pairwise dispersion corrections

The long-range vdW energy between two non overlapping fragments  $A$  and  $B$  of the physical system under study can be expressed as a multipolar expansion

$$E_{\text{disp}}^{AB} = -\frac{C_6^{AB}}{R^6} - \frac{C_8^{AB}}{R^8} - \frac{C_{10}^{AB}}{R^{10}} \dots \quad (2.71)$$

where  $C_n^{AB}$  are the multipolar vdW coefficients. A widespread approach to include long-range vdW interactions in DFT is to truncate above expression to the dipole-dipole order and keep only the leading  $C_6^{AB}/R^6$  term. Now, the dipole-dipole  $C_6^{AB}$  vdW coefficient can be expressed in terms of the so-called Casimir-Polder integral [77]

$$C_6^{AB} = \frac{3}{\pi} \int_0^\infty \alpha_A(i\omega) \alpha_B(i\omega) d\omega \quad (2.72)$$

where  $\alpha_{A/B}(i\omega)$  is frequency-dependent polarizability of  $A$  and  $B$  evaluated at imaginary frequency. The heteronuclear  $C_6^{AB}$  vdW coefficient of two fragments  $A$  and  $B$  can be expressed as [178],

$$C_6^{AB} = \frac{2C_6^{AA}C_6^{BB}}{\frac{\alpha_0^B}{\alpha_0^A}C_6^{AA} + \frac{\alpha_0^A}{\alpha_0^B}C_6^{BB}} \quad (2.73)$$

in terms of the homonuclear coefficients  $C_6^{AA}$  and  $C_6^{BB}$  and their static ( $\alpha_0^A$  and  $\alpha_0^B$ ) polarizabilities. In semi-empirical corrections the  $C_6$  coefficients of Eq. (2.73) are evaluated, and the term  $-\sum_A \sum_{B>A} C_6^{AB}/R^6$  is added to the exchange-correlation energy in DFT, with a suitable damping function which avoids singularity when  $R \rightarrow 0$  and couples to the underlying DFT functional. The general form of this type of correction to the DFT energy is

$$E_{\text{DFT+vdW}} = E_{\text{DFT}} + f_{\text{damp}}(R_{AB}) \frac{C_6^{AB}}{R_{AB}^6} \quad (2.74)$$

where  $f_{\text{damp}}$  is the damping function which may contain one or more empirical parameters. There are several methods which are based on Eq. (2.74) and differ in the way  $C_6$  coefficients are determined or the damping function is defined [179–188]. Among these DFT+vdW approaches, the ones proposed by Grimme (DFT-D) [183, 184], Becke

and Johnson (XDM) [187, 189] and Tkatchenko and Scheffler (TS) [1] are the most popular.

In DFT-D methods, the computation of dispersion coefficients is based on calculated atomic ionization potentials and static polarizabilities. This approach employs purely empirical pairwise corrections with fixed  $C_6$  coefficients irrespective of the environment of the atoms [183, 184]. However, the environment of an atom crucially influences its polarizability. The  $C_6$  coefficient for carbon for instance can vary by as much as about 20% for different hybridization states  $sp$ ,  $sp^2$ , and  $sp^3$  [181]. Therefore, the dispersion coefficients do depend on the electronic structure. In general, vdW coefficients strongly depend on the molecular environment of each atom [190, 191]. This issue is somewhat overcome by DFT-D3 method wherein  $C_6$  coefficient are coordination number (geometry) dependent [192].

Becke and Johnson proposed an environment-dependent dispersion correction called exchange-dipole moment (XDM) model [189]. The XDM model stipulates that the dispersion attraction between two molecules is due to the dipole moment of the instant exchange hole of one molecule and the induced dipole moment of the second molecule. This model is conceptually simple and yet has been shown to yield fairly accurate dispersion coefficients without empirical fitting parameters. Furthermore, it can be applied to both intermolecular and intramolecular interactions with a simple density-partitioning scheme and with one or two fitting parameters. The XDM model is especially appealing because it can be made to depend only on the electron spin densities and their gradients, which are the same list of variables as most of the local or semi-local functionals. The first one is the change given by scaling the polarizabilities of atoms in molecules from their reference values according to their effective atomic volumes. The second is through the changes of the exchange hole, which are a response to the chemical environment, but are also difficult to quantify in a precise manner.

The alternative TS method [1] determines polarizabilities and vdW  $C_6^{AB}$  coefficients as a functional of the electron density. Based on Eq. (2.73), heteroatomic  $C_6^{AB}$  coefficients can be calculated from the knowledge of their homoatomic counterparts. The TS method uses the Hirshfeld partitioning scheme [193] to define “atom in molecule” vdW  $C_{6AA}^{\text{eff}}$  coefficients. The effective coefficients  $C_6^{\text{eff},AB}$  in a atom specific environment are calculated based on the values for the neutral free atoms  $C_6^{\text{eff},AA}$  and defined as

$$\begin{aligned} C_6^{\text{eff},AA} &= \left( \frac{\eta^{\text{eff},A}}{\eta^{\text{free},A}} \right) \left( \frac{\kappa^{\text{free},A}}{\kappa^{\text{eff},A}} \right)^2 \left( \frac{V^{\text{eff},A}}{V^{\text{free},A}} \right)^2 C_6^{\text{free},AA} \\ &= \left( \frac{\eta^{\text{eff},A}}{\eta^{\text{free},A}} \right) \left( \frac{\kappa^{\text{free},A}}{\kappa^{\text{eff},A}} \right)^2 \left( \frac{\int r^3 n^{\text{eff},A}(\mathbf{r}) d^3\mathbf{r}}{\int r^3 n^{\text{free},A}(\mathbf{r}) d^3\mathbf{r}} \right)^2 C_6^{\text{free},AA} \quad (2.75) \end{aligned}$$

where  $V^{\text{eff},A}/V^{\text{free},A}$  will be termed as Hirshfeld volume ratio. The proportionality constant

$$\left(\frac{\eta^{\text{eff},A}}{\eta^{\text{free},A}}\right)\left(\frac{\kappa^{\text{free},A}}{\kappa^{\text{eff},A}}\right)^2 = 1 \quad (2.76)$$

is assumed and this approximation is valid for a large variety of molecular materials [1]. In general  $\frac{\kappa^{\text{free},A}}{\kappa^{\text{eff},A}} \neq 1$ , since the static polarizability of a molecule cannot be expressed as a sum over atomic polarizabilities or in a case where the concept of atoms-in-molecules cannot be applied. Such assumption to represent polarizability can fail qualitatively for metallic or low-dimensional systems [194]. The TS method allows the definition of effective static atomic polarizabilities in a material as a functional of electron density and can be expressed as

$$\alpha^{\text{eff},A} = \left(\frac{V^{\text{eff},A}}{V^{\text{free},A}}\right)\alpha^{\text{free},A}. \quad (2.77)$$

The reference values for free atom isotropic static polarizability  $\alpha^{\text{free},A}$  and vdW  $C_6^{\text{free},AA}$  coefficients are taken from self-interaction corrected time-dependent DFT calculations [195]. The effective density  $n^{\text{eff},A}(\mathbf{r})$  is obtained through Hirshfeld partitioning [193]

$$n^{\text{eff},A}(\mathbf{r}) = n(\mathbf{r}) \frac{n^{\text{free},A}(\mathbf{r})}{\sum_B n^{\text{free},B}(\mathbf{r})}, \quad (2.78)$$

where  $n(\mathbf{r})$  is the electronic density of the complete system,  $n^{\text{free},A}(\mathbf{r})$  is the density of the free atom, and the index  $B$  runs over all atoms of the molecule, taken as free atoms, but in the position they would be actually found in the molecule. The vdW energy in the TS method has the following form [1]

$$E_{\text{TS}} = - \sum_{A,B} f_{\text{damp}}(R_{AB}, R_{AB}^0) \frac{C_6^{AB}}{R_{AB}}. \quad (2.79)$$

The damping function employed takes the form

$$f_{\text{damp}}(R_{AB}, R_{\text{vdW}}^{\text{eff},AB}) = \left(1 + \exp\left[-d\left(\frac{R_{AB}}{s_R R_{\text{vdW}}^{\text{eff},AB}} - 1\right)\right]\right)^{-1}. \quad (2.80)$$

The term  $R_{\text{vdW}}^{\text{eff},AB} = R_{\text{vdW}}^{\text{eff},A} + R_{\text{vdW}}^{\text{eff},B}$  in Eq. (2.80) is the sum of effective van der Waals radii [1]. The effective vdW radius of an atom  $A$  in a molecule can be obtained from its free-atom vdW radius via

$$R_{\text{vdW}}^{\text{eff},A} = \left(\frac{V^{\text{eff},A}}{V^{\text{free},A}}\right)^{1/3} R_{\text{vdW}}^{\text{free},A}. \quad (2.81)$$

Here, the vdW radius,  $R_{\text{vdW}}^{\text{free},A}$ , corresponds to half the distance between two atoms where the Pauli repulsion balances the London dispersion attraction [196]. The  $R_{\text{vdW}}^{\text{free},A}$  for neutral atoms can be obtained from electron density at the minimum of potential energy for rare gas systems. In practice, noting the value of electron density contour at the equilibrium separation for rare gas dimers, the value for  $R_{\text{vdW}}^{\text{free},A}$  for other elements in the same row of the periodic table (See Table (A.1)) can be derived (where the electron density is obtained using accurate wavefunction. *e.g.* CCSD method).

The parameter  $d$  in Eq. (2.80) which controls the steepness of damping function was set to 20 as it was found to have only a minor influence on the results in the range between 12 and 45. The parameter  $s_R$  controls the distance,  $R_{AB}$ , at which the damping function approaches zero, and hence defines the onset of the dispersion correction. The best value of  $s_R$  thus depends on the functional that is employed. It was determined for several exchange-correlation functionals using the S22 database [197]. The latter contains accurate binding energies of 22 non-covalently bonded dimers based on CCSD(T) calculations extrapolated to the complete basis set limit. The 22 dimers are sorted into groups with predominant vdW-bonded character, predominant H-bonded character and mixed complexes. Recently, Marom et al. [198] assessed the performance of several representative XC functionals for the S22 database, a dimer of NiPc molecules and the layered solid hexagonal boron nitride, with and without including vdW interactions based on the TS scheme. For all functionals tested, the inclusion of vdW interactions improved the description of binding energies. However, a many-body description of vdW interactions is essential for extended molecules and molecular solids. In the following section, we introduce a method which includes many-body interatomic vdW interactions within the DFT framework [7].

### 2.7.3 Many-body interatomic van der Waals interactions

Interatomic pairwise dispersion approaches based on the standard  $C_6/R^6$  summation formula were popularized by Grimme [179] and are now among the most widely used methods [188, 190, 199] for including the dispersion energy in DFT. Despite their simplicity, these pairwise-additive models provide remarkable accuracy when applied to small molecular systems, especially when accurate dispersion coefficients ( $C_6$ ) are employed for the atoms in molecules [1, 198]. Only recently have efforts been focused on going beyond the pairwise treatment of vdW contributions, for example, the importance of the non-additive three-body interatomic Axilrod–Teller–Muto term [192, 200, 201] was assessed, as well as the role of non-local screening in solids [202] and molecules adsorbed on surfaces [203].

Furthermore, an efficient and accurate interatomic many-body

dispersion (MBD) approach has recently been proposed [7], which demonstrated that a many-body description of vdW interactions is essential for extended molecules and molecular solids, and that the influence of many-body vdW interactions can already become significant when considering the binding between relatively small organic molecules [7, 204]. As mentioned earlier, the influence of the local environment on the polarizabilities is taken into account in the TS scheme by involving the ground-state electronic density through Hirshfeld partitioning. However, the polarizability of an atom is also influenced by the fluctuating dipoles originating at atomic sites located at larger distances (electrostatic screening). Recently, Tkatchenko and co-workers [7, 57] proposed a method, here referred to as MBD@rsSCS, that accounts for both many-body dispersion contributions and screening effects. This is achieved by modelling the atoms in the molecule as a collection of spherical quantum harmonic oscillators (QHOs), which are coupled to each other via dipole-dipole potential (which is based on coupled fluctuating-dipole model (CFDM) [205]). The Hamiltonian for this model system reads [7]

$$\hat{\mathcal{H}}_{\text{MBD}} = -\frac{1}{2} \sum_{p=1}^N \nabla_{\chi_p}^2 + \frac{1}{2} \sum_{p=1}^N \omega_p^2 \chi_p^2 + \sum_{p>q}^N \omega_p \omega_q \sqrt{\alpha_p \alpha_q} \chi_p \mathcal{T}_{pq} \chi_q, \quad (2.82)$$

where  $\chi_p = \sqrt{m_p} \xi_p$  with  $\xi_p$  describing the displacement of the QHO  $p$  from equilibrium and  $m_p = 1/(\alpha_p \omega_p^2)$ . The key ingredients are the characteristic excitation frequencies  $\omega_p$ , the polarizabilities  $\alpha_p$ , and  $\mathcal{T}_{pq}$ , a dipole-dipole interaction tensor, which we will address in more detail below. After diagonalizing the Hamiltonian, the many-body dispersion (MBD) energy can be obtained via

$$E_{\text{MBD}} = \frac{1}{2} \sum_{i=1}^N \sqrt{\lambda_i} - \frac{3}{2} \sum_{p=1}^N \omega_p \quad (2.83)$$

where  $\lambda_i$  denotes the eigenvalues of the Hamiltonian. The general form of this type of correction to the DFT energy is

$$E_{\text{DFT+MBD}} = E_{\text{DFT}} + E_{\text{MBD}} \quad (2.84)$$

where the  $E_{\text{DFT}}$  self-consistent energy is obtained using local or semi-local functionals.

As mentioned earlier in this chapter, the adiabatic-connection fluctuation-dissipation (ACFD) theorem [64, 65, 79, 206, 207] gives an exact expression for the exchange-correlation energy. One of the most popular approximations to evaluate the correlation energy in this framework is the random-phase approximation (RPA) [163]. In fact, it can be shown that for the model system of QHOs coupled via a dipole-dipole potential the correlation energy of ACFD-RPA corresponds to the energy expression in Eq. (2.83) [56]. From this, we

can see that the Hamiltonian in Eq. (2.82) captures screening effects as well as many-body energy contributions. Local or semi-local DFT exchange-correlation functionals already efficiently account for short-range correlation. In order not to double count short-range correlation, in the MBD@rsSCS method a range-separation approach is used. This is realized by range-separating the dipole-dipole interaction tensor  $\mathcal{T}$  into a long-range part  $\mathcal{T}_{LR}$  and a short-range part  $\mathcal{T}_{SR}$ , where in the many-body Hamiltonian (Eq. (2.82)) only the long-range part is employed. In this way, the many-body Hamiltonian will include long-range screening, but will lack short-range screening effects. To account also for short-range screening effects, short-range screened polarizabilities  $\alpha_p^{rsSCS}$  (and characteristic excitation frequencies) are obtained, which are then used as input in the many-body Hamiltonian. This is done again by modelling each atom in the molecule as a spherical QHO and employing the self-consistent screening (SCS) equations from classical electrodynamics [3, 5, 80]

$$\alpha_p^{rsSCS}(\mathbf{r}, i\omega) = \alpha_p^{TS}(\mathbf{r}, i\omega) + \alpha_p^{TS}(\mathbf{r}, i\omega) \sum_{p \neq q}^N \mathcal{T}_{SR} \alpha_q^{rsSCS}(\mathbf{r}, i\omega) \quad (2.85)$$

where  $\alpha_p^{TS}(i\omega)$  denotes the frequency-dependent polarizability obtained from the TS scheme, which already accounts for hybridization effects [1]. The positions of the atoms (QHOs) are denoted by  $\mathbf{r}_p$  and  $\mathbf{r}_q$  with  $\mathbf{r}_{pq} = |\mathbf{r}_p - \mathbf{r}_q|$ . By employing a short-range only dipole-dipole interaction tensor  $\mathcal{T}_{SR}$ , the polarizabilities  $\alpha_p^{rsSCS}(i\omega)$  capture only short-range screening. The characteristic excitation frequencies  $\omega_p^{rsSCS}(i\omega)$  are also obtained from the SCS equations described above. In more detail, the self-consistently screened characteristic excitation frequencies are calculated from the  $C_6^{rsSCS}$  coefficients, which are obtained by integrating the Casimir-Polder integral (see Eq. (2.72)) using  $\alpha^{rsSCS}$  (see Refs. [1, 7]). The short-range part of the dipole-dipole interaction tensor is given by

$$\mathcal{T}_{SR,pq} = (1 - f(\mathbf{r}_{pq})) \mathcal{T}_{pq} \quad (2.86)$$

where the dipole-dipole interaction tensor is defined as  $\mathcal{T}_{pq} = \nabla_{\mathbf{r}_p} \otimes \nabla_{\mathbf{r}_q} V(\mathbf{r}_{pq})$ .

$$V(\mathbf{r}_{pq}) = \frac{\text{erf}[\mathbf{r}_{pq}/\sqrt{2}\sigma]}{\mathbf{r}_{pq}} \quad (2.87)$$

is the Coulomb potential for the interaction of two spherical Gaussian charge distributions at distance  $\mathbf{r}_{pq}$ , where  $\sigma = \sqrt{\sigma_p^2 + \sigma_q^2}$  with  $\sigma_p = (\sqrt{2/\pi} \alpha_p^{TS}(i\omega))^{1/3}$  being the width of the Gaussian function. The function  $f(\mathbf{r}_{pq})$  is the Fermi-type damping function as used also in the TS approach (see Eq. (2.80)). The parameter  $d$  in Eq. (2.80) is fixed to 6, while  $s_R$  is determined separately for each exchange-correlation

functional by minimizing energy differences with respect to the S66×8 database [32]. In principle,  $\mathcal{T}_{\text{LR}}$  is defined as  $\mathcal{T}_{\text{LR}} = \mathcal{T} - \mathcal{T}_{\text{SR}}$ . However,  $\mathcal{T}$  is frequency dependent, which is not computationally efficient. The interaction potential is a function of the Gaussian width  $\sigma$ , which depends on the polarizability, which is in turn frequency dependent. As only the long range is described here, one can approximate  $\mathcal{T}_{\text{LR}}$  as the product of the damping function and the dipole-dipole interaction tensor of two point dipoles

$$\begin{aligned}\mathcal{T}_{\text{LR}} &= f(\mathbf{r}_{pq}) \nabla_{\mathbf{r}_p} \otimes \nabla_{\mathbf{r}_q} \frac{1}{\mathbf{r}_{pq}} \\ &= f(\mathbf{r}_{pq}) \frac{-3r_{pq}^i r_{pq}^j + r_{pq}^2 \delta_{ij}}{r_{pq}^5}\end{aligned}\quad (2.88)$$

where the indices  $i$  and  $j$  denote the Cartesian components of  $\mathbf{r}_{pq}$ . The evaluation of the MBD@rsSCS long-range correlation energy can now be summarized in three steps. In the first step, the polarizabilities are obtained in the TS scheme. Then, the short-range (SR) range-separated self-consistently screened polarizabilities  $\alpha^{\text{rsSCS}}$  are obtained using the SCS procedure defined in Eq. (2.85). Using  $\alpha^{\text{rsSCS}}$ ,  $\omega^{\text{rsSCS}}$  and the long-range dipole-dipole interaction tensor  $\mathcal{T}_{\text{LR}}$  one can then evaluate the many-body long-range correlation energy using Eq. (2.83). The performance of the MBD@rsSCS method coupled with the PBE and PBE0 exchange-correlation functionals was recently benchmarked. This model has provided improved qualitative and quantitative agreement with both experimental results and wavefunction-based benchmarks [204]. Interestingly, MBD correctly predicts the experimentally known relative stabilities of the molecular crystal polymorphs of glycine [208] and aspirin [209], for which pairwise corrections fail. Recent reviews provide perspectives on the role of non-additive dispersion effects in molecular materials and the key successes of the MBD model [81, 210].



---

# 3

## Approaches for computing (linear) response properties

This chapter introduces different methods for computing electronic response functions for molecular systems. The interaction of electrons in molecules with external electric or optical fields is characterized by induced electric multipole moments. For example, the induced dipole moment is related to the electric field through the dipole polarizability. The static electric dipole polarizability can be defined as a measure of the distortion of the electronic density under the effect of a static external electric field. The electronic response function is of central importance for understanding many physical or chemical processes. The linear response theory provides a powerful technique for relating theory and experiments. A central quantity in this context is the frequency dependent density-density response function which is a crucial ingredient to many theoretical calculations. This quantity is related to many methods such as time-dependent density functional theory (TDDFT) [43, 44], symmetry adapted perturbation theory (SAPT) [45, 46], fluctuation-dissipation density functional theory [47–49], GW calculations [50–52], van der Waals interactions [53–57] or random phase approximation (RPA) [58–60] as well as beyond-RPA [61–63] methods via the adiabatic-connection fluctuation-dissipation theorem [64, 65]. This chapter is organized as follows: Initially, we introduce general properties of a response function that maps an external field to a physical observable. Then, the finite field approximation is discussed for computing the static electric response. Finally, we discuss the state-of-the-art linear response coupled cluster singles and doubles (LR-CCSD) method for computing static and dynamic response function molecules and materials. In the following section, we will discuss how a specific response function is connected to a specific physical property.

### 3.1 Response function

In spectroscopic experiments, an external field  $\mathcal{E}(\mathbf{r}, t)$  is applied to a sample. The sample, which is a fully interacting many-electron system from the theoretical point of view, responds to the external field. Then the response can be measured for some physical observable  $\mathcal{P}$

$$\Delta\mathcal{P} = \Delta\mathcal{P}[\mathcal{E}]. \quad (3.1)$$

In general, the dependence of the functional  $\Delta\mathcal{P}[\mathcal{E}]$  on  $\mathcal{E}$  is very complex, as it must reproduce the response for a field of any strength and shape. However, if the external field is weak, the response can be expanded as a power series with respect to the field strength [211, 212]. The first-order response, also called the linear response of the observable

$$\delta\mathcal{P}^{(1)}(\mathbf{r}, t) = \int \int \chi^{(1)}(\mathbf{r}, \mathbf{r}', t, t') \delta\mathcal{E}^{(1)}(\mathbf{r}', t') d\mathbf{r}' dt' \quad (3.2)$$

is a convolution of the linear response function  $\chi^{(1)}(\mathbf{r}, \mathbf{r}', t, t')$ , and the field  $\delta\mathcal{E}^{(1)}(\mathbf{r}', t')$ , expanded to first order in the field strength. The linear response function is nonlocal in space and in time, but the above time convolution simplifies to a product in frequency space

$$\delta\mathcal{P}^{(1)}(\mathbf{r}, \omega) = \chi^{(1)}(\mathbf{r}, \mathbf{r}', \omega) \delta\mathcal{E}^{(1)}(\mathbf{r}', \omega) \quad (3.3)$$

The linear response function  $\chi^{(1)}(\mathbf{r}, \mathbf{r}', \omega)$  depends only on a single frequency  $\omega$ , which is a consequence of the homogeneity of time. At every order in the field strength, each observable/field pair has its own response function that is connected to a specific physical property. For example, the first-order response of the dipole moment to a dipole electric field in first order is the polarizability. The second-order response of the same pair provides the hyperpolarizability, and the first-order response of the magnetic moment to a homogeneous magnetic field is the magnetic susceptibility.

### 3.2 The finite-field method

Molecular response property calculations require energy derivatives, which can be symbolically represented by  $\frac{dE}{d\lambda}$  where  $\lambda$  is a parameter that defines the electronic Hamiltonian  $\hat{\mathcal{H}}(\lambda)$ . For example,  $\lambda$  can correspond to the nuclear coordinate in the case of nuclear derivatives or an external electric field in the case of polarization. The static dipole polarizability tensor,  $\alpha_{ij}$ , of a molecule is expressed as

$$\mu_i = \alpha_{ij}\mathcal{E}_j \quad (3.4)$$

where  $\mu_i$  is the induced dipole moment,  $\mathcal{E}_j$  is the magnitude of the electric field, and  $i,j$  label Cartesian components [21]. Alternatively, the static dipole polarizability can be written as partial derivatives with respect to components of the electric field (in the limit  $\mathcal{E} \rightarrow 0$ ),

$$\alpha_{ij} = -\left(\frac{\partial E}{\partial \mathcal{E}_i \partial \mathcal{E}_j}\right)_{\mathcal{E} \rightarrow 0} \quad (3.5)$$

where  $E$  denotes the total energy of a system. Using the Hellmann-Feynman theorem [213, 214] Eq. (3.5) for the dipole polarizability, it can be written as,

$$\frac{\partial E}{\partial \lambda} = \left\langle \frac{\partial \hat{\mathcal{H}}}{\partial \lambda} \right\rangle. \quad (3.6)$$

The Hellmann-Feynman theorem describes how the energy  $E$  of a system changes as the Hamiltonian of the system varies with respect to the interacting parameter  $\lambda$ . In the present case, the total Hamiltonian,  $\hat{\mathcal{H}}$  is the sum of the unperturbed Hamiltonian,  $\hat{\mathcal{H}}^0$  and the perturbed Hamiltonian,  $\hat{\mathcal{H}}^1$  and the interacting parameter is the electric field strength,  $\mathcal{E}_i$ . The perturbation caused by an electric field  $\mathcal{E}$  is expressed as<sup>1</sup>

$$\hat{\mathcal{H}} = \hat{\mathcal{H}}^0 + \hat{\mathcal{H}}^1 \quad (3.7)$$

$$\hat{\mathcal{H}}^1 = -\boldsymbol{\mu} \cdot \boldsymbol{\mathcal{E}} \quad (3.8)$$

$$\boldsymbol{\mu} = \sum_i q_i \mathbf{r}_i \quad (3.9)$$

where  $q_i$  is the charge of the particle  $i$  at the location  $\mathbf{r}_i$ . Since the unperturbed Hamiltonian  $\hat{\mathcal{H}}^0$  is independent of the electric field it follows from Eq. (3.5) and Eq. (3.6) that

$$\frac{\partial E}{\partial \mathcal{E}_i} = \left\langle \frac{\partial \hat{\mathcal{H}}}{\partial \mathcal{E}_i} \right\rangle = \left\langle \frac{\partial \hat{\mathcal{H}}^1}{\partial \mathcal{E}_i} \right\rangle = \langle \mu_i \rangle \quad (3.10)$$

The static response properties of a molecule can be also defined by expanding the field dependent energy  $E(\mathcal{E})$  in a Taylor expansion

$$E = E(0) + \left(\frac{\partial E}{\partial \mathcal{E}_i}\right)_0 \mathcal{E}_i + \frac{1}{2!} \left(\frac{\partial^2 E}{\partial \mathcal{E}_i \partial \mathcal{E}_j}\right)_0 \mathcal{E}_i \mathcal{E}_j + \frac{1}{3!} \left(\frac{\partial^3 E}{\partial \mathcal{E}_i \partial \mathcal{E}_j \partial \mathcal{E}_k}\right)_0 \mathcal{E}_i \mathcal{E}_j \mathcal{E}_k + \dots \quad (3.11)$$

Differentiation of above Eq. (3.11) with respect to electric field  $\mathcal{E}_i$  yields

$$\frac{\partial E}{\partial \mathcal{E}_i} = \left(\frac{\partial E}{\partial \mathcal{E}_i}\right)_0 + \frac{1}{2!} \left(\frac{\partial^2 E}{\partial \mathcal{E}_i \partial \mathcal{E}_j}\right)_0 \mathcal{E}_j + \frac{1}{3!} \left(\frac{\partial^3 E}{\partial \mathcal{E}_i \partial \mathcal{E}_j \partial \mathcal{E}_k}\right)_0 \mathcal{E}_j \mathcal{E}_k + \dots, \quad (3.12)$$

The expectation value of the dipole moment in the presence of the electric field is the sum of the permanent dipole moment and the

---

<sup>1</sup> $\mathcal{E} \in \{\mathcal{E}_i, \mathcal{E}_j, \mathcal{E}_k\}$  are Cartesian components of the electric field

contribution induced by the field

$$\langle \mu_i \rangle = \mu_i^0 + \alpha_{ij} \mathcal{E}_j + \beta_{ijk} \mathcal{E}_j \mathcal{E}_k + \gamma_{ijkl} \mathcal{E}_j \mathcal{E}_k \mathcal{E}_l \dots \quad (3.13)$$

where  $\alpha_{ij}$  is the dipole polarizability,  $\beta_{ijk}$  is the first hyperpolarizability and  $\gamma_{ijkl}$  is the second hyperpolarizability tensors. For a spherically symmetric system the principle components of dipole polarizability are equal *i.e.*  $\alpha_{xx} = \alpha_{yy} = \alpha_{zz}$ . For clusters or molecular systems, the polarizability can be formulated as the second derivative of the energy or first derivative of the induced dipole moment with respect to external perturbing field (See Eq. (3.12) and Eq. (3.13)), using an accurate wavefunction.

In order to evaluate the dipole moment the finite-field method described by Cohen and Roothaan [215] can be employed. In this method the dipole moment is calculated by taking the first derivative of the energy  $E(\mathcal{E}_i)$  (See Eq. (3.12)) by the external field  $\mathcal{E}_i$  using finite differences [216] (the central approximation). As a result we get the following 2-point expression for the dipole moment components

$$\mu_i = \frac{E(\mathcal{E}_i) - E(-\mathcal{E}_i)}{2\mathcal{E}_i}. \quad (3.14)$$

Similarly, the polarizability is the second derivative of the interaction energy by the external field  $\mathcal{E}_i$ . The 3-point finite-difference approximation (with errors of order  $\mathcal{E}_i^2$ ) gives

$$\alpha_{ij} = -\frac{E(\mathcal{E}_i, \mathcal{E}_j) - E(\mathcal{E}_i, -\mathcal{E}_j) + E(-\mathcal{E}_i, \mathcal{E}_j) + E(-\mathcal{E}_i, -\mathcal{E}_j)}{4\mathcal{E}_i \mathcal{E}_j} \quad (3.15)$$

$$\alpha_{ii} = -\frac{E(\mathcal{E}_i) - 2E(0) + E(-\mathcal{E}_i)}{\mathcal{E}_i^2}. \quad (3.16)$$

The energy values  $E$  can be obtained using any total energy method described earlier by applying finite electric field, that include wavefunction based methods such as HF (Section (2.1.3)), MP2 (Section (2.1.5)), CCSD (Section (2.1.6)) or using any density functional approximation (Section (2.5)).

The choice of the applied homogeneous field should be done very carefully. For this purpose, one should carry out a series of calculations with different amplitudes of the external field  $\mathcal{E}$ . From these calculations, we can find out the range of the amplitudes of the field where the property under the investigation does not change significantly with the change of the amplitude  $\mathcal{E}$ . The field from this range only can be used for the further calculation of the dipole moment. Sometimes for different properties different amplitudes of the external field should be applied. In general, the method described above can be only applied to compute the static polarizability.

### 3.3 Frequency-dependent polarizabilities

The response of molecules to static and dynamic (time- or frequency-dependent) perturbations, e.g. external electric fields, is of great importance for a variety of fields. For example, the frequency-dependent polarizability, describing the linear response to an electric field, determines optical properties such as refractive indices, dielectric constants, Verdet constants, and Raman intensities, as well as vdW dispersion coefficients of long-range intermolecular interaction [217]. In particular the expression for the dipole expectation value can be used to define the permanent dipole moment and the polarizability and hyperpolarizabilities as discussed in Eq. (3.13). The notation can be established by writing the formulas for the first three molecular response functions [217]

$$\mu_i^1 = \alpha_{ij}(-\omega, \omega) \mathcal{E}_j \quad (3.17)$$

$$\mu_i^2 = \beta_{ijk}(-\omega_3; \omega_1, \omega_2) \mathcal{E}_j \mathcal{E}_k \quad (3.18)$$

$$\mu_i^3 = \gamma_{ijkl}(-\omega_4; \omega_1, \omega_2, \omega_3) \mathcal{E}_j \mathcal{E}_k \mathcal{E}_l \quad (3.19)$$

The time-dependent field components are here taken to be the complex forms which combine in the nonlinear interaction to give an induced dipole component at the sum frequency,  $\sum \omega_i$ . The negative sign indicates an output frequency. The most direct approach to the calculation of the time-dependent polarizabilities is to apply standard time-dependent perturbation theory to the evolution of the wavefunction in the time-dependent Schrödinger equation. The wavefunction is formally expanded in terms of the complete set of molecular eigenfunctions (ground  $\Psi_0$  and excited states  $\Psi_n$ ) and the solutions are obtained in terms of matrix elements of the perturbation between these states and the corresponding eigenvalues [217]. For example, the dipole polarizability is a linear response function to an oscillating electric field  $\mathcal{E}_i \exp(-i\omega t)$  and is defined by the following expression

$$\alpha_{ij}(\omega) = \sum_{n \neq 0} \left( \frac{\langle \Psi_0 | \mu_i | \Psi_n \rangle \langle \Psi_n | \mu_j | \Psi_0 \rangle}{\omega - \omega_n + i\eta} \right) - \sum_{n \neq 0} \left( \frac{\langle \Psi_0 | \mu_j | \Psi_n \rangle \langle \Psi_n | \mu_i | \Psi_0 \rangle}{\omega + \omega_n - i\eta} \right) \quad (3.20)$$

where the summation is over all discrete and continuous spectra (the sum-over-states method). The main task here is to find a set of excitation energies  $\omega_n$  and matrix elements  $\langle \Psi_0 | \mu_i | \Psi_n \rangle$ . The frequencies  $\omega$  should be far from any absorption frequencies.

We are often interested only in the spherical average (or isotropic component) of the polarizability tensor  $\bar{\alpha}(\omega) = (1/3)\alpha_{ii}(\omega)$ , which can

be written as (disregarding the infinitesimal shifts  $\pm\eta$ )

$$\bar{\alpha}(\omega) = \sum_{n \neq 0} \frac{f_n}{\omega^2 - \omega_n^2} \quad (3.21)$$

where  $f_n$  are the oscillator strengths

$$f_n = \frac{2}{3} \omega_n \sum_i |\langle \Psi_0 | \mu_i | \Psi_n \rangle|^2 \quad (3.22)$$

The oscillator strength  $f_n$  gives the intensity in the absorption or emission spectrum of the electronic transition from state  $|\Psi_0\rangle$  to state  $|\Psi_n\rangle$  corresponding to the excitation energy  $\omega_n$ . The knowledge of the dynamic polarizability  $\bar{\alpha}(\omega)$  thus gives access to the full absorption or emission spectrum of the system.

## 3.4 Coupled-cluster response theory

The coupled cluster (CC) response theory is the state-of-the-art method for computing molecular response properties. CC theory has been introduced in Section (2.1.6). The linear response coupled cluster method (LRCC) have been used for calculations of static and frequency-dependent first (hyper)-polarizabilities and described extensively in literature [218–224]. Here, we present only basic features of this LRCC method. The polarizability can be obtained as the second derivative of the coupled-cluster energy functional from the original energy formula Eq. (2.36). In this thesis we are concerned with the LRCC method which compute dynamic polarizability at imaginary frequency. In the next subsection, we present in brief derivation of linear response function for complex frequency (for comprehensive details Ref. [225–227]).

### Response function for a complex frequency

The linear response function for a coupled-cluster wavefunction is

$$\langle\langle A; B \rangle\rangle_\omega = \frac{1}{2} \hat{C}^{\pm\omega} \hat{P}_{A,B} \langle \Phi | (1 + \Lambda) \left\{ \left[ \overline{A}, \hat{T}_{B,\omega}^{(1)} \right] + \left[ \left[ \overline{H}, \hat{T}_{A,\omega}^{(1)} \right], \hat{T}_{B,-\omega}^{(1)} \right] \right\} | \Phi \rangle \quad (3.23)$$

where  $\hat{C}$  enforces time-reversal symmetry and  $\hat{P}$  permutes  $A$  and  $B$ . Evaluating this quantity requires, in addition to the cluster amplitudes  $\hat{T}$ , the evaluation of the  $\Lambda$  amplitudes of gradient theory and the first-order response with respect to operators  $A$  and  $B$  at both positive and negative frequency [225–227]. For a purely imaginary frequency ( $\omega_R = 0$ ), the linear response function can be reduced to the following contributions from the real and imaginary components of the response

amplitudes,

$$\langle\langle A; B \rangle\rangle_{\omega_I} = \langle\langle A; B \rangle\rangle_R + \langle\langle A; B \rangle\rangle_I \quad (3.24)$$

$$\begin{aligned} \langle\langle A; B \rangle\rangle_R &= \hat{P}_{A,B}\langle\Phi|(1+\Lambda)\left[\overline{A}, \hat{T}_{B,R}^{(1)}\right]|\Phi\rangle \\ &\quad + \langle\Phi|(1+\Lambda)\left[\left[\overline{H}, \hat{T}_{A,R}^{(1)}\right], \hat{T}_{B,R}^{(1)}\right]|\Phi\rangle \end{aligned} \quad (3.25)$$

$$\langle\langle A; B \rangle\rangle_I = \hat{C}^{\pm\omega_I}\langle\Phi|(1+\Lambda)\left[\left[\overline{H}, \hat{T}_{A,I}^{(1)}\right], \hat{T}_{B,-I}^{(1)}\right]|\Phi\rangle \quad (3.26)$$

where  $\hat{T}_{O,R}^{(1)}$  is the real component of the response amplitudes with respect to operator  $O$  at static frequency and  $\hat{T}_{O,\pm I}^{(1)}$  are the imaginary components of the response amplitudes with respect to operator  $O$  at frequency  $\pm\omega_I$ . The operator  $\hat{C}^{\pm\omega_I}$  symmetrizes with respect to  $\omega_I$  to preserve time-reversal symmetry, while  $\hat{P}_{A,B}$  is the interchange operator for property operators  $A$  and  $B$ . In the case of dipole polarizabilities,  $A$  and  $B$  are both dipole moment operators, and the polarizability is given by

$$\alpha_{ij}(i\omega_I) = -\langle\langle \mu_i; \mu_j \rangle\rangle_{\omega_I}. \quad (3.27)$$

The equations to compute imaginary-frequency response and dynamic polarizabilities were implemented in NWChem by Jeff Hammond [228]. The connection between imaginary-frequency dynamic polarizabilities and  $C_6$  coefficients can be derived using perturbation theory for long-range intermolecular forces. To obtain  $C_6$  coefficients, the Casimir-Polder integral must be evaluated numerically. The coupled cluster response theory is an accurate way to obtain dynamical response of the system. However, this method is very expensive and can be applied efficiently to system with less than a few dozen atoms.

## 3.5 Time-dependent density-functional theory (TDDFT)

Time Dependent Density Functional Theory (TDDFT) extends DFT to model time dependent phenomena. Many excited states properties can be obtained by directly solving the TDDFT equations given an initial condition and a time-dependent external potential (which is usually fixed for a system). TDDFT is an exact reformulation of the time-dependent Schrödinger equation and can be applied to describe in general time-dependent phenomena [229, 230]. TDDFT is based on the Runge-Gross (RG) theorem [43]. It states that there is a one-to-one correspondence between time-dependent density and time-dependent external potential,  $v_{\text{eff}}^{\text{RG}}(\mathbf{r}, t)$ ,

$$v_{\text{eff}}^{\text{RG}}(\mathbf{r}, t) = v_{\text{H}}(\mathbf{r}, t) + v_{\text{xc}}(\mathbf{r}, t) + v_{\text{ext}}(\mathbf{r}, t) \quad (3.28)$$

which is extension of the effective single-particle potential Eq. (2.50) and the time-dependent density,  $n(\mathbf{r}, t)$ ,

$$n(\mathbf{r}, t) = \sum_i |\Psi_i(\mathbf{r}, t)|^2. \quad (3.29)$$

The time-dependent KS equations are written as follows,

$$\left( -\frac{1}{2}\nabla^2 + v_{\text{eff}}^{\text{RG}}(\mathbf{r}, t) \right) \Psi_i(\mathbf{r}, t) = i \frac{d}{dt} \Psi_i(\mathbf{r}, t). \quad (3.30)$$

Solutions of above Eq. (3.30) for an electronic system yields the time-dependent KS orbitals and time-dependent density,  $n(\mathbf{r}, t)$ . The exact functional form of the time-dependent exchange-correlation potential,

$$v_{\text{xc}}(\mathbf{r}, t) = \frac{\delta E_{\text{xc}}[n(\mathbf{r}, t)]}{\delta n(\mathbf{r}, t)} \quad (3.31)$$

is unknown, therefore in practice it needs to be approximated. In real-time TDDFT the key quantity for electric response is the time-dependent dipole that can be calculated directly from the electronic density and the atomic charges,  $Z_A$ , and positions,  $R_A$

$$\mu(t) = \int \mathbf{r} n(\mathbf{r}, t) d\mathbf{r} - \sum_A Z_A R_A \quad (3.32)$$

In this approach, to obtain the absorption spectrum one first excites the system from its ground state by applying a uniform electric field of the form  $\mathcal{E}_{\text{ext}}(\mathbf{r}, t) = \delta(t)\mathcal{E}$ . The constant coefficient  $\mathcal{E}$  should be small enough for the system to remain in the linear regime. In practice, it is more precise to apply the kick as a phase in the initial conditions  $\Psi(t = 0^+) = \Psi(t = 0^-)e^{-i\mathcal{E}t}$ . The Kohn-Sham equations are then propagated forward in real time, and the time-dependent density  $n(\mathbf{r}, t)$  is readily computed. The polarizability is obtained by doing the propagation for three perturbations, one along each axis, and then obtaining the time-dependent dipole moment for each one of them, hence building the  $\mu_{ij}(t)$  tensor, the first index indicates the components of the dipole and the second the direction of the perturbation. The complex polarizability tensor as a function of frequency  $\omega$ , is then calculated as a Fourier transform

$$\alpha_{ij}(\omega) = \frac{1}{\mathcal{E}} \int e^{-i\omega t} \cdot [\mu_{ij}(t) - \delta_{ij}\mu_i(0)] dt \quad (3.33)$$

This approach has been used for a large variety of systems: metal and semi-conducting clusters [231–234], aromatic hydrocarbons [235–237], or protein chromophores [238, 239]. The advantage of real time-propagation TDDFT is that non-linear response can be computed as well. However, real-time TDDFT calculations can become rather expensive for realistic systems. In the following section, we introduce linear-response extension of TDDFT.

## 3.6 Linear-response formulation of TDDFT

Many applications of TDDFT involve the calculation of optical absorption spectra in the linear regime using the dipole approximation. The results of such calculations can be compared with the findings of spectroscopic experiments in case when the external perturbing field is small. Despite the local nature of the effective single-particle potential  $v_{\text{KS}}$ , the full solution of the time-dependent Kohn-Sham (TDKS) equations can be quite demanding for very large systems. On the other hand, the calculation of physical observables like excitation energies or polarizabilities of atomic and molecular systems requires only the knowledge of the linear density response of the system. A much simpler perturbative solution of the TDKS equations therefore seems desirable. Linear response theory is a reformulation of the time-dependent Schrödinger equation in a perturbative treatment. Following Ref. [240], consider a small perturbation  $v_1(\mathbf{r}, t)$  which is applied at time  $t_0$  to a many-electron system in its ground state

$$v_{\text{ext}}(\mathbf{r}, t) = \begin{cases} v_0(\mathbf{r}) & \text{if } t \leq t_0 \\ v_0(\mathbf{r}) + v_1(\mathbf{r}, t) & \text{if } t > t_0 \end{cases}$$

The system reacts to this perturbation with a time-dependent density response which can be written as a functional Taylor series expansion

$$n(\mathbf{r}, t) - n_0(\mathbf{r}) = n_1(\mathbf{r}, t) + n_2(\mathbf{r}, t) + n_3(\mathbf{r}, t) + \dots \quad (3.34)$$

Here,  $n_0(\mathbf{r})$  denotes the ground-state density of the unperturbed system at  $t \leq t_0$  and a lower index is used to indicate the order in the external perturbation, such that, the first order perturbation is indicated by  $v_1$ . The exact first order density response  $n_1(\mathbf{r}, t)$  can be expressed according to

$$n_1(\mathbf{r}, t) = \int \int \chi(\mathbf{r}, \mathbf{r}', t, t') v_1(\mathbf{r}', t') d\mathbf{r}' dt', \quad (3.35)$$

where  $\chi(\mathbf{r}, \mathbf{r}', t, t')$  denotes the density-density response function of the interacting system

$$\chi(\mathbf{r}, \mathbf{r}', t, t') = \left. \frac{\delta n[v_{\text{ext}}](\mathbf{r}, t)}{\delta v_{\text{ext}}(\mathbf{r}', t')} \right|_{v_0} \quad (3.36)$$

Making use of the functional chain rule the interacting response function can also be written as

$$\chi(\mathbf{r}, \mathbf{r}', t, t') = \int \int \frac{\delta n(\mathbf{r}, t)}{\delta v_{\text{KS}}(\mathbf{r}_1, t_1)} \frac{\delta v_{\text{KS}}(\mathbf{r}_1, t_1)}{\delta v_{\text{ext}}(\mathbf{r}', t')} \Bigg|_{v_0} d\mathbf{r}_1 dt_1 \quad (3.37)$$

Next, we take the functional derivative of Eq. (2.50) with respect to the external potential

$$\begin{aligned} \frac{\delta v_{\text{KS}}(\mathbf{r}, t)}{\delta v_{\text{ext}}(\mathbf{r}', t')} &= \delta(\mathbf{r} - \mathbf{r}') \delta(t - t') + \\ &\int \int \left( \frac{\delta(t - t_1)}{|\mathbf{r} - \mathbf{r}_1|} + \frac{\delta v_{\text{xc}}(\mathbf{r}, t)}{\delta n(\mathbf{r}_1, t_1)} \right) \frac{\delta n(\mathbf{r}_1, t_1)}{\delta v_{\text{ext}}(\mathbf{r}', t')} d\mathbf{r}_1 dt_1. \end{aligned} \quad (3.38)$$

Inserting Eq. (3.38) into Eq. (3.37) we arrive at

$$\begin{aligned} \chi(\mathbf{r}, \mathbf{r}', t, t') &= \chi_{\text{KS}}(\mathbf{r}, \mathbf{r}', t, t') + \int d\mathbf{r}_1 \int dt_1 \int d\mathbf{r}_2 \int dt_2 \chi_{\text{KS}}(\mathbf{r}, \mathbf{r}_1, t, t_1) \\ &\times \left( \frac{\delta(t_1 - t_2)}{|\mathbf{r}_1 - \mathbf{r}_2|} + f_{\text{xc}}[n_0](\mathbf{r}_1, \mathbf{r}_2, t_1 - t_2) \right) \chi(\mathbf{r}_2, \mathbf{r}', t_2, t'), \end{aligned} \quad (3.39)$$

where we have introduced the Kohn-Sham response function

$$\chi_{\text{KS}}(\mathbf{r}, \mathbf{r}', t, t') = \left. \frac{\delta n[v_{\text{KS}}](\mathbf{r}, t)}{\delta v_{\text{KS}}(\mathbf{r}', t')} \right|_{v_{\text{KS}}[n_0]}, \quad (3.40)$$

and the so-called exchange-correlation kernel

$$f_{\text{xc}}[n_0](\mathbf{r}, \mathbf{r}', t, t') = \left. \frac{\delta v_{\text{xc}}[n](\mathbf{r}, t)}{\delta n(\mathbf{r}', t')} \right|_{n_0}, \quad (3.41)$$

Eq. (3.39) is the central result of the TDDFT response formalism. It is a Dyson-type equation which relates the interacting and the Kohn-Sham response functions. Inserting the response Eq. (3.39) back into Eq. (3.35) leads to the time-dependent Kohn-Sham equation for the linear density response

$$n_1(\mathbf{r}, t) = \int \int \chi_{\text{KS}}(\mathbf{r}, \mathbf{r}', t, t') v_{\text{KS},1}(\mathbf{r}', t') d\mathbf{r}' dt'. \quad (3.42)$$

The effective potential

$$v_{\text{KS},1}(\mathbf{r}, t) = v_1(\mathbf{r}, t) + \int \frac{n_1(\mathbf{r}', t)}{|\mathbf{r} - \mathbf{r}'|} d\mathbf{r}' + \int \int f_{\text{xc}}[n_0](\mathbf{r}, \mathbf{r}', t, t') n_1(\mathbf{r}', t') d\mathbf{r}' dt', \quad (3.43)$$

contains the external perturbation  $v_1$ , as well as the Hartree and exchange-correlation contributions up to first order in the perturbing potential  $v_1$ . The result in Eq. (3.42), Eq. (3.43) shows, that the exact linear density response  $n_1(\mathbf{r}, t)$  of an interacting system can be written as the linear density response of a non-interacting system to the effective perturbation  $v_{\text{KS},1}(\mathbf{r}, t)$ . For the treatment of excitation energies and polarizabilities it is useful to consider the linearized Kohn-

Sham Eq. (3.42) in frequency space. Inserting Eq. (3.43) in Eq. (3.42) and performing a Fourier transform, the frequency-dependent linear density response can be written as

$$\begin{aligned} n_1(\mathbf{r}, \omega) &= \int \chi_{\text{KS}}(\mathbf{r}, \mathbf{r}_1; \omega) v_1(\mathbf{r}_1, \omega) d\mathbf{r}_1 \\ &+ \int \int \chi_{\text{KS}}(\mathbf{r}, \mathbf{r}_1; \omega) \left( \frac{1}{|\mathbf{r}_1 - \mathbf{r}_2|} + f_{\text{xc}}[n_0](\mathbf{r}_1, \mathbf{r}_2; \omega) \right) n_1(\mathbf{r}_2, \omega) d\mathbf{r}_1 d\mathbf{r}_2. \end{aligned} \quad (3.44)$$

The Kohn-Sham response function  $\chi_{\text{KS}}$  can be directly expressed in terms of the static unperturbed Kohn-Sham orbitals  $\psi_k(\mathbf{r}) = \psi_k(\mathbf{r}, t_0)$ , their occupation numbers  $f_k$  (with values 0 or 1), and their orbital energies  $\epsilon_k$

$$\chi_{\text{KS}}(\mathbf{r}, \mathbf{r}'; \omega) = \sum_{j,k} (f_k - f_j) \frac{\psi_j(\mathbf{r}) \psi_k^*(\mathbf{r}) \psi_j^*(\mathbf{r}') \psi_k(\mathbf{r}')}{\omega - (\epsilon_j - \epsilon_k) + i\eta}. \quad (3.45)$$

The summation extends over both occupied and unoccupied orbitals and includes also the continuum states. We stress here that some functional derivatives that have been considered in the present section rely on the inverse mappings,  $v_{\text{ext}}(\mathbf{r}, t) = v_{\text{ext}}[n](\mathbf{r}, t)$ ,  $v_{\text{KS}}(\mathbf{r}, t) = v_{\text{KS}}[n](\mathbf{r}, t)$ . The existence and uniqueness of these mappings are guaranteed by the Runge-Gross [43] and van Leeuwen's theorem [241] so that all functional derivatives are well defined. From the relation Eq. (3.41) it can be seen that approximations for the exchange-correlation kernel  $f_{\text{xc}}$  can be obtained by evaluating the functional derivative of approximate time-dependent Kohn-Sham potentials with respect to the density. The most commonly used approximations for the kernel  $f_{\text{xc}}$  include the adiabatic LDA (ALDA) and the so-called PGG (Petersilka, Gossmann, Gross) kernel [242]. The ALDA is based on the functional form of the static LDA and given by

$$f_{\text{xc}}^{\text{ALDA}}[n_0](\mathbf{r}, \mathbf{r}'; \omega) = \delta(\mathbf{r} - \mathbf{r}') \frac{d^2}{dn^2} \left( n \epsilon_{\text{xc}}^{\text{HEG}}(n) \right) \Bigg|_{n=n_0(\mathbf{r})} \quad (3.46)$$

where  $\epsilon_{\text{xc}}^{\text{HEG}}(n)$  is the energy density of the homogeneous electron gas with density  $n$ . The PGG kernel reads

$$f_{\text{xc}}^{\text{PGG}}[n_0](\mathbf{r}, \mathbf{r}'; \omega) = - \frac{2 |\sum_k f_k \psi_k(\mathbf{r}) \psi_k^*(\mathbf{r}')|^2}{|\mathbf{r} - \mathbf{r}'| n_0(\mathbf{r}) n_0(\mathbf{r}')} \quad (3.47)$$

and is derived from the exchange-only limit of the time-dependent Kohn-Sham potential within the optimized effective potential theory of TDDFT [240]. Both approximations are frequency independent which has implications for the calculation of excitation energies within TDDFT.

Important applications of the TDDFT response formalism include: The calculation of excitation energies. Optical absorption spectra of atoms and molecules which are accessible from the frequency-dependent polarizability

$$\alpha_{ij}(\omega) = -\frac{2}{\mathcal{E}} \int n_1^{(i)}(\mathbf{r}, \omega) r_j d\mathbf{r}, \quad i, j = x, y, z \quad (3.48)$$

that emerges as response to a monochromatic perturbing potential  $v_1^{(i)} = \mathcal{E} r_i \cos(\omega t)$ . In general, the photoabsorption cross section tensor  $\sigma_{ij}(\omega)$  is related to the tensor of the frequency-dependent polarizability according to

$$\sigma_{ij}(\omega) = \frac{4\pi\omega}{c} \text{Im}[\alpha_{ij}(\omega)]. \quad (3.49)$$

The calculation of van der Waals  $C_6^{\text{AB}}$  dispersion coefficients between two molecules  $A$  and  $B$ , which can be computed using the Casimir-Polder formula.

$$C_6^{\text{AB}} = \frac{3}{\pi} \int_0^\infty \alpha^A(i\omega) \alpha^B(i\omega) d\omega. \quad (3.50)$$

The response properties of a system can be calculated from a direct propagation of the full TDKS equations in real-time with a weak perturbing potential.

A key property of the TDDFT response formalism is that all involved quantities are solely functionals of the ground-state density so that only a much cheaper KS ground-state calculation has to be performed to compute the induced density response. In general, the construction of the bare response function,  $\chi_{\text{KS}}(\mathbf{r}, \mathbf{r}', \omega)$  in Eq. (3.45), from single-particle KS orbitals is one of the major computationally demanding tasks.

---

# 4

## Representative datasets for isotropic static polarizabilities and asymptotic van der Waals $C_6^{AB}$ coefficients for molecules

The molecular polarizability is an essential quantity for the description of many physical and chemical processes, such as the scattering of light by molecules, and intermolecular interactions. The theoretically derived polarizabilities have been used in the verification of experimentally determined values and, in the prediction of properties as well as the design of new materials. Therefore, an accuracy of a few percent in the calculated values is necessary for this purpose. The present chapter provides a brief overview of the description of electronic polarizability and van der Waals  $C_6$  coefficients of molecules using first-principles techniques, and contrasting them with experimental measurements. There are various methods for the calculation of molecular response properties (as discussed extensively in Chapter (3)). Several *ab initio* methods have become available for the accurate determination of frequency-dependent polarizabilities. In particular, time-dependent Hartree-Fock (TDHF) [243], time-dependent MP2 [244–247], and coupled-cluster response theory [222, 248, 249] which have been also used for the calculation of (hyper)polarizabilities. On the other hand, time-dependent density-functional theory (TDDFT) provides an efficient framework for calculating molecular response functions; this includes real-time propagation as well as linear response methods. The advantage of real time-propagation TDDFT is that all order responses can be computed as well. This approach has been used for a large variety of systems: aromatic hydrocarbons [235–237], metal and semi-conducting clusters [231–234], and protein chromophores [238, 239].

A direct comparison of calculated and experimental polarizabilities also requires the ability to calculate frequency-dependent polarizabilities since experiments are mostly performed at nonzero frequencies. In this work, calculations of static and dynamic molecular polarizabilities are presented using various methods. Also, the underlying motivation of this study is to explore the accuracy of commonly used electronic

structure methods to calculate static dipole polarizability as well as asymptotic vdW  $C_6$  coefficients for molecules. The static polarizability calculations have been carried out using finite field method (as discussed in Section (3.2) in Chapter (3)) using total electronic energy using wavefunction based methods as well as using semi-local and hybrid functionals in DFT. The dynamic polarizabilities are calculated using the linear response coupled-cluster singles and doubles (LRCCSD) method. Accurate experimental data for molecular polarizabilities and vdW coefficients are considered as a reference for selecting the most accurate electronic structure method. This chapter is organized as follows: First, we introduce the experimental representative datasets for static molecular polarizabilities and asymptotic vdW coefficients. Then, we present the computational details for the calculations performed for the present study. Moreover, we discuss the results by comparing them with experimental measurements. Finally, we present benchmark sets of electric static dipole polarizabilities of  $\approx 7.5k$  molecules and a large database ( $\approx 1.2k$  systems) of inter-molecular  $C_6^{AB}$  coefficients. The following section provides details about an extensive dataset of experimental molecular polarizabilities and a set of vdW  $C_6$  coefficients obtained from experimental (pseudo) dipole oscillator strength distributions data.

## 4.1 Experimental reference datasets

### 4.1.1 Static polarizabilities

A straightforward technique for measuring polarizabilities is to deflect the atoms in an inhomogeneous electric field. There are many reviews of polarizability data, including experimental details [250]. The experimental polarizabilities are mostly determined by measurements of a dielectric constant or refractive index which can be very accurate to  $\approx 0.5\%$ . However, the polarizabilities should be analyzed with some caution as some of the results may contain contributions from the optical frequencies [250]. The CRC Handbook of Chemistry and Physics provides an annually updated list of polarizability values for atoms and molecules [250]. Here, we have compiled a set of 238 small (organic) molecules ranging from simple diatomic to polyatomic systems. The experimental values for isotropic molecular polarizability are available for this dataset [250] (See Table (A.4)).

In many cases, the polarizability is well approximated by a single scalar value. However, the polarizability is a tensorial property and in Cartesian reference frame it is a rank 2 tensor. The isotropic polarizability  $\alpha_{iso}$  is defined as an average of principal components of the polarizability tensor. To perform a rigorous analysis of components of the polarizability tensor, we refer to data as compiled by Thole [5] for various molecular systems. This data set contains

small (organic) molecules ranging from simple diatomics ( $\text{H}_2$ , CO etc.) to polyatomic systems like cyclohexane. Importantly, for these molecules, experimental data for the principal components of molecular polarizability tensor are available as compiled in Ref. [5].

#### 4.1.2 vdW coefficients from dipole oscillator strength distributions

A variety of important properties of molecules can be evaluated using the dipole oscillator strength distributions (DOSDs) data. The DOSDs for an atom or a molecule is defined using (differential) dipole oscillator strengths,  $\partial f / \partial \omega$ , as a function of excitation energy  $\omega$ , from the electronic absorption threshold  $\omega_0$  up to high energies. The DOSDs is usually derived using the molecular photo-absorption and fast electron inelastic scattering data [251–264]. These distributions were constructed from extensive experimental information, including discrete oscillator strength, photoabsorption, and high energy inelastic scattering data, and were constrained to satisfy the Thomas-Reiche-Kuhn sum rule and to reproduce available accurate refractivity and dispersion measurements data for the dilute gases. As such, these distributions represent a collection of the best information on the dipole oscillator strength distributions available.

The DOSDs have been used to evaluate a variety of properties for the atoms and molecules of interest including dipole-dipole dispersion coefficients. In present work, we have assembled a dataset of vdW  $C_6$  coefficients which are derived from DOSD information (See Table (A.3)) [251–264]. This dataset contains  $C_6^{AB}$  coefficients for 1225 pairs of species that include atom-atom, atom-molecule and molecule-molecule interactions. The DOSDs and the derived  $C_6$  coefficients are based on experimental results with an estimated accuracy of  $\approx 2\%$  [252, 253]. In the following section, we discuss the computational methodology used to perform calculations in the present work.

## 4.2 Computational details

All DFT calculations were carried out with the FHI-aims package [265], which implements full-potential, all-electron electronic-structure theory with numeric atom-centered (NAO) basis functions. The FHI-aims all-electron code offers accurate and efficient implementation of DFT with (semi-)local, hybrid functionals and beyond DFT methods to obtain ground-state properties of periodic and cluster systems, up to systems with thousands of atoms. Furthermore, the molecular polarizabilities have been determined via a finite field (FF) approach (as discussed in Section (3.2)), by using positive and negative perturbing fields and then calculating the polarizability from the changes in the induced dipole moment (*i.e.* two-point finite differences). The polarizability

can be obtained using methods described in Chapter (3) by applying a finite electric field, that include wavefunction based methods or using any density functional approximation (Section (2.5)). The choice of the applied homogeneous field has been made very carefully. For this purpose, one should carry out a series of calculations with different amplitudes of the external field  $\mathcal{E}$ . From these calculations, we can find out the range of the amplitudes of the field where the property under the investigation does not change significantly with the change of the amplitude  $\mathcal{E}$ . The field from this range only can be used for the further calculation of the dipole moment.

A usual way of obtaining  $C_6$  coefficients is Cauchy series. In this procedure the dynamic polarizability is fitted to Cauchy polynomial and expansion coefficients of this series are related to vdW coefficients. The method used in present work evaluate dynamic polarizability on imaginary frequency argument. We have calculated the frequency-dependent polarizability for atoms and small molecules using the linear-response coupled-cluster method (LR-CCSD), as implemented in the NWChem code [225–227]. The dynamic dipole polarizability tensor for an atom and a molecule is obtained as function of frequency argument  $i\omega$ , by solving linear response equations based on the converged coupled cluster wave function including single and double excitations, as discussed in Section (3.4). The vdW  $C_6^{AB}$  coefficients, for system  $A$  and  $B$  determines the attractive dipole-dipole vdW interaction. The  $C_6^{AB}$  coefficients are calculated using the Casimir-Polder formula as an integral over imaginary frequency-dependent polarizability,  $\alpha(i\omega)$ . The integral over dynamic polarizability on the imaginary axis was evaluated by numerical quadrature scheme to obtain the  $C_6^{AB}$  coefficient. Here, we used a 20 point Gaussian-Legendre quadrature rule to determine the vdW  $C_6^{AB}$  coefficient. Due to the increasing computational cost of correlated calculations with the number of electrons and basis functions, the basis set limit could not be explored in all cases. Therefore, the augmented d-aug-cc-pVDZ basis set been used for all  $p$  block elements which allows us to obtain dynamic response for a molecule as large as linear heptane. In following section, we compare experimental and calculated polarizabilities and vdW  $C_6$  coefficients.

## 4.3 Results and discussion

### 4.3.1 Polarizabilities and vdW $C_6$ coefficients from linear response coupled cluster singles and doubles theory for atoms and molecules

The electronic response of an atom or a molecule to time-varying electric fields is more complex than the static behavior. Hence a more sophisticated description of the polarizability is needed here than in the static case. In particular, the antisymmetric part of the tensor

polarizability can be nonzero. A system can absorb and emit photons so the polarizability tensor consists of two parts: a dispersive part and an absorptive part and they are related to one another by a Kramers-Kronig transformation [266, 267]. The polarizability depends on the frequency of the light inducing the dipole moment. However, as the frequency increases to extremely high values, eventually the charges are unable to follow the changing field and the polarizability then drops to zero. The polarizability  $\alpha(i\omega)$  is well-defined on the whole imaginary axis. The dispersion of  $\alpha(i\omega)$  is smooth and monotonic. Here, we first discuss static polarizabilities calculated using accurate linear-response coupled-cluster single double (LRCCSD) method.

The Table (4.1) provides isotropic and principal components of the polarizability tensor for benzene calculated using the LRCCSD method using a few basis sets. The relative principal components of

**Table 4.1:** The isotropic polarizability  $\alpha_{iso}$ , along with its three components  $\alpha_{xx}$ ,  $\alpha_{yy}$  and  $\alpha_{zz}$  (in bohr<sup>3</sup>) for benzene molecule calculated using LR-CCSD method (in bohr<sup>3</sup>).

Basis set	$\alpha_{iso}$	$\alpha_{xx} = \alpha_{yy}$	$\alpha_{zz}$	Time <sup>1</sup> (s)
6-31G	51.2	67.7	18.3	1016
6-31+ +G**	64.9	77.0	40.9	6266
aug-cc-pVDZ	69.6	81.7	45.4	10064
d-aug-cc-pVDZ	69.9	82.1	45.5	18384
aug-cc-pVTZ	69.5	81.3	44.9	68723
Experiment [268–271]	$71.28 \pm 0.89$	$82.36 \pm 0.79$	$49.13 \pm 1.09$	

<sup>1</sup> 800 cpu for single response calculation at  $\omega = 0$ .

polarizability tensor obtained using the LRCCSD method correlate well with those obtained using experiment. The LRCCSD method correctly captures anisotropy in molecular polarizability tensor of benzene. It can be noticed that using Dunning's correlation consistent basis sets which include polarization functions by definition provide accurate scalar and tensor polarizabilities. For benzene, Dunning's basis sets greatly outperform Pople basis sets of similar size for polarizability calculations at the CCSD level of theory. However, the component of polarizability tensor perpendicular to benzene plane is underestimated as compared with experiment and would require more denser basis set to converge to this limit. The LRCCSD calculations are difficult to converge especially in the static case. Since LRCCSD calculations are computationally demanding here we use the d-aug-cc-pVDZ basis set for all subsequent calculations for molecules. This basis set can be augmented with core functions for geometric or nuclear property calculations, and with diffuse functions for electronic excited-state calculations, electric response property calculations, and long-range interactions, such as vdW forces. The Table (4.2) shows the three components of the molecular static polarizability  $\alpha_{xx}$ ,  $\alpha_{yy}$  and  $\alpha_{zz}$ , along with the isotropic

**Table 4.2:** The isotropic polarizability  $\alpha_{iso}$ , along with its three components  $\alpha_{xx}$ ,  $\alpha_{yy}$  and  $\alpha_{zz}$  (in bohr<sup>3</sup>) for a database of molecules calculated using LR-CCSD method along with experimental reference data taken from Ref. [5, 269].

molecule	Experiment					LRCCSD				
	$\alpha_{iso}$	$\alpha_{xx}$	$\alpha_{yy}$	$\alpha_{zz}$	$\Delta\alpha$	$\alpha_{iso}$	$\alpha_{xx}$	$\alpha_{yy}$	$\alpha_{zz}$	$\Delta\alpha$
H <sub>2</sub>	5.3	4.9	4.9	6.3	1.4	5.2	4.5	4.5	6.6	2.1
N <sub>2</sub>	11.9	9.8	9.8	16.1	6.3	11.8	10.2	10.2	14.9	4.6
O <sub>2</sub>	10.8	8.2	8.2	15.9	7.7	10.3	8.0	8.9	14.2	5.8
CO	13.2	11.0	11.0	17.6	6.6	13.3	11.9	11.9	16.1	4.1
Ethane	30.2	26.9	26.9	37.1	10.2	28.7	27.5	27.5	31.1	3.6
Propane	43.1	38.7	38.7	51.7	13.0	40.8	37.7	39.8	44.8	6.3
Cyclopentane	61.7	56.7	61.9	66.7	8.6	59.7	54.1	62.4	62.5	8.4
Cyclohexane	74.2	63.3	79.7	79.7	16.4	71.3	65.0	74.5	74.5	9.5
Dimethylether	35.4	29.6	33.3	43.1	12.0	34.0	31.1	31.8	39.2	7.8
P-dioxane	58.0	47.2	63.4	63.4	16.2	57.5	52.6	55.2	64.6	10.9
Methanol	22.4	17.9	21.8	27.6	8.5	21.6	20.3	20.7	23.7	3.2
Ethanol	34.3	30.4	33.6	38.9	7.4	33.7	31.4	33.6	36.2	4.2
Formaldehyde	16.5	12.4	18.6	18.6	6.3	18.1	13.1	18.3	23.0	8.5
Acetone	43.1	29.8	49.7	49.7	19.9	42.5	34.5	45.7	47.4	12.2
Acetonitrile	30.2	26.0	26.0	38.7	12.8	29.4	24.4	24.4	39.3	14.8
(CH <sub>3</sub> ) <sub>3</sub> CCN	64.7	60.9	60.9	72.3	11.3	65.6	61.6	61.6	73.6	12.0
Methane	17.7	17.7	17.7	17.7	0.0	16.8	16.8	16.8	16.8	0.0
Benzene	69.7	45.1	82.0	82.0	36.9	69.7	45.4	81.8	81.8	36.4

static polarizability,  $\alpha_{iso}$ , and polarizability anisotropy<sup>1</sup>  $\Delta\alpha$  for a set of 18 molecules calculated using LRCCSD theory compared with experimental data [5]. The polarizabilities calculated using LRCCSD linear response correctly reproduce relative principal components of polarizability tensor as compared with experiments. For this set of 18 molecules LRCCSD theory predicts isotropic static polarizabilities with accuracy of 3.1%. The mean average relative error<sup>2</sup> (MARE) between experimental polarizability anisotropy  $\Delta\alpha$  to that obtained using LRCCSD method is 31.7%. The source of such error on polarizability anisotropy  $\Delta\alpha$  could be due to larger errors in relative values of the principal components of the tensor. Discrepancies between theory and experiment for the principal components of polarizability are of the order of 10%. Therefore, errors of 10% in the principal components imply errors larger than 50% in differences between components. In general to define the polarizability tensor for a chiral material essentially requires (at the most) six components of tensor. Also, the mean unsigned error on  $\Delta\alpha$  is -19.6% with respect to experiments. The experimental studies did not distinguish between  $\alpha_{xx}$  and  $\alpha_{yy}$  for propane molecule or between

<sup>1</sup>The anisotropic polarizability  $\Delta\alpha$  for any polyatomic molecule can be expressed as,

$$\Delta\alpha = \sqrt{\frac{1}{2}((\alpha_{xx} - \alpha_{yy})^2 + (\alpha_{xx} - \alpha_{zz})^2 + (\alpha_{yy} - \alpha_{zz})^2)}.$$

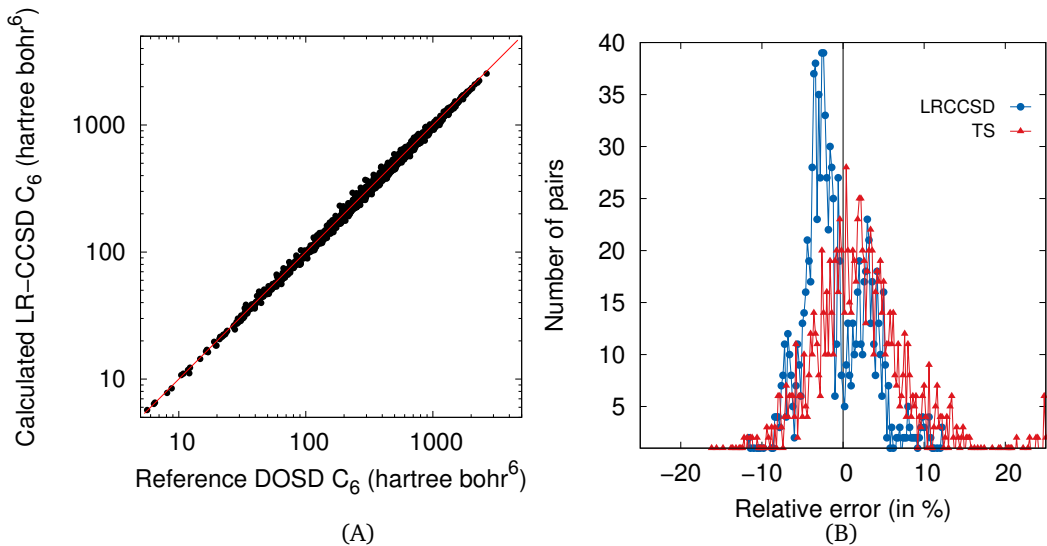
<sup>2</sup>Here,  $\{a_i\}$  are the set of  $N$  reference values and by  $\{f_i\}$  the corresponding  $N$  calculated values. The individual errors with respect to the actual values are given by:

$$\text{MARE} = \frac{100}{N} \sum_{i=1}^N |\frac{f_i - a_i}{f_i}| ; \quad \text{MRE} = \frac{100}{N} \sum_{i=1}^N \frac{(f_i - a_i)}{f_i}.$$

$\alpha_{yy}$  and  $\alpha_{zz}$  for P-dioxane, formaldehyde and acetone, while electronic structure calculation lead to visible difference in these components of the polarizability [5].

So far we have analysed the static polarizabilities determined using the LRCCSD method. Now, we discuss the dynamic polarizability evaluated on the imaginary axis. We have selected a set of atoms and molecules (See Table (A.1) and A.3). For these systems, accurate values for vdW  $C_6$  coefficients are available from experimental dipole oscillator strength distributions (DOSD) data [251–264]. The Figure (4.1)–

**Figure 4.1:** A) Correlation plots for van der Waals  $C_6$  coefficients computed using LR-CCSD method with respect to accurate DOSD results from the experiments for 1128 pairs of inter-molecular,  $C_6^{AB}$  coefficient. B) The relative error for  $C_6$  coefficients derived using LR-CCSD theory with respect to DOSD values for 1128 pairs (including atom-atom, atom-molecule and molecule-molecule interaction).



A shows the correlation plot for  $C_6^{AB}$  coefficients for 1128 pairs of species that include atom-atom, atom-molecule and molecule-molecule interaction calculated using LRCCSD method compared with  $C_6^{AB}$  coefficients derived from DOSD information [1, 252–264]. The MARE for 40 pairs of homo-molecular,  $C_6^{AB}$  coefficients is 6.3% with respect to experiments. The LRCCSD method predicts vdW coefficients with an accuracy of 4.9% for 1128 pairs including atom-atom, atom-molecule and molecule-molecule interaction with respect to DOSD data.

The calculated polarizabilities at imaginary frequency  $i\omega$  behave correctly at large frequencies. Furthermore, the relative error distribution between experimental and calculated vdW coefficients using LRCCSD are shown Figure (4.1)–B. It can be observed that there is a systematic underestimation of  $C_6$  coefficients with respect to those derived using DOSD data. These errors are most likely due to the omission of higher-excited amplitudes and smaller basis set. The only outliers for LRCCSD method are cases involving the N<sub>2</sub>O and SO<sub>2</sub>

molecule (10–25% deviation), where DOSD values [263] are smaller than those derived using LRCCSD theory. Furthermore, the source of such errors is the incorrect description of static limit  $\omega \approx 0$ . Such error in  $C_6$  coefficients can be eliminated by using accurate static polarizability value in Eq. (2.73) for atoms and molecules. The MARE for static polarizabilities calculated using LR-CCSD with respect to experimental values [250] for 39 molecules is 4.9% (see Table (A.3)). The accuracy of isotropic static dipole polarizabilities and vdW  $C_6$  coefficients for neutral free atoms in gas phase computed at LR-CCSD level of theory with respect to self-interaction corrected TDDFT values from the database of Chu and Dalgarno [195], is 3% and 5%, respectively, for  $\alpha(0)$ , and  $C_6$  coefficients (See Table (A.1)). Moreover, using accurate experimental static polarizability vdW  $C_6$  coefficients for all 1128 pairs can be corrected using Eq. (2.73). This approach provides a way to correct  $C_6$  coefficients derived using LRCCSD theory and yields vdW coefficients with an accuracy of 3.4%. The Figure (4.1)-B also shows the relative error distribution between DOSD reference vdW coefficients and those calculated with TS method. The TS method provides vdW coefficients with an accuracy of 5%. Therefore, the LRCCSD theory provides static polarizabilities and vdW coefficients accurate to few percent when compared with reliable experimental values.

### 4.3.2 Static mean polarizabilities for a dataset of 7449 molecules

In the present section, we introduce a representative benchmark set of electric static dipole polarizabilities of  $\approx 7.5K$  molecules. Initially, we discuss the static polarizability results obtained using different electronic structure methods by comparing them with the experimental dataset of 238 molecules. Finally, we present a dataset of 7211 small organic molecules containing up to 7 heavy atoms including C, N, O, S, and Cl obtained from GDB-13 database [272]. GDB-13 is the largest freely available small molecule database. The most accurate electronic structure method is then used to compute electric static dipole polarizabilities of resulting dataset of  $\approx 7.5K$  molecular systems.

In Section (4.1.1), we have presented a set of 238 small (organic) molecules. The experimental values for isotropic molecular polarizability are available [250] for this dataset. The geometries for these molecules were initially obtained using molecular modeling software ArgusLab [273] with molecular mechanics force field. This database contains molecules ranging from simple diatomic ( $H_2$ ,  $N_2$ ,  $CO$  etc.) to polyatomic systems with functional groups including alcohol, ketone, amine and aromatic systems. The geometries of molecules have been optimized with the PBE+TS functional using NAO *tier2* basis set, as implemented in the FHI-aims package. The induced dipole moments were obtained using electronic structure methods such as

Hartree-Fock (HF) theory, semi-local and hybrid functionals such as LDA, PBE, PBE0 as well as Tkatchenko-Scheffler (TS) method in DFT, employing NAO *tier2* basis function with the additional diffuse functions from d-aug-cc-pVQZ gaussian basis set. A field strength of 0.0002 a.u. has been used. The above basis set and field strength for induced dipole moment calculations were selected based on a convergence test for static polarizabilities for H<sub>2</sub>, N<sub>2</sub>, HCl and CO molecules (See Appendices B.1). Furthermore, the molecular polarizabilities for 238 molecules were determined via a finite field (FF) approach (as discussed in Section (3.2)), by using positive and negative perturbing fields and then calculating the polarizability from the changes in the induced dipole moment (*i.e.* two-point finite differences). The calculated isotropic static polarizabilities for a set of 238 molecules are given in Table (A.4). Most of the experimental data can be found in the compilation of T. Miller [250].

**Figure 4.2:** A. Correlation plot for isotropic static molecular polarizability for 238 organic molecules from experiments compared with HF, LDA, PBE, PBE0 and TS method. B) The distribution relative errors (x-axis) for all molecules using HF, LDA, PBE, PBE0 and TS method with respect to experimental polarizabilities. The y-axis indicates corresponding polarizabilities of all molecules normalized to unity with respect to isotropic polarizability of the largest molecule.

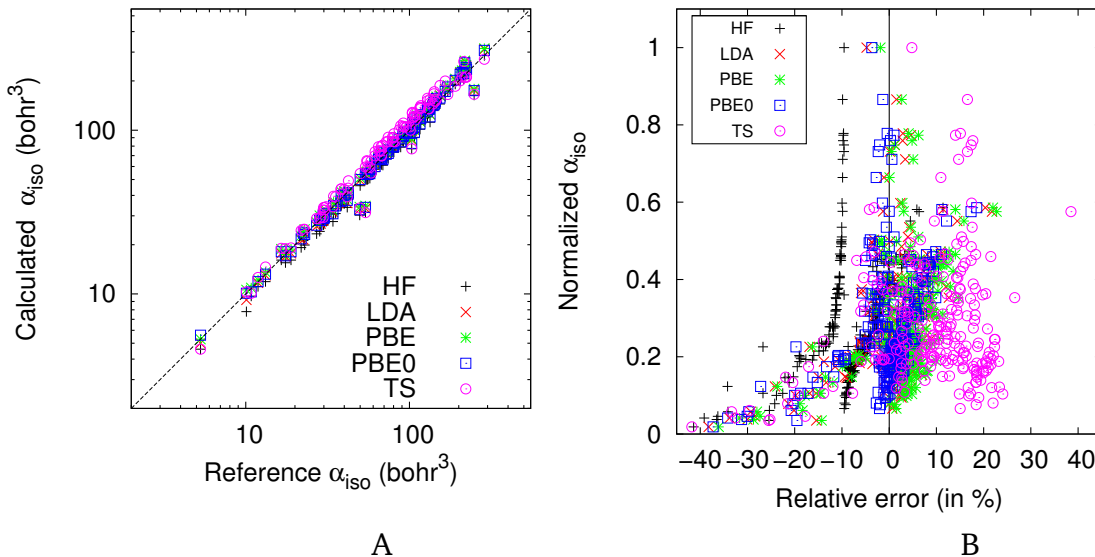


Figure (4.2)-A shows the comparison between experimental isotropic static polarizability  $\alpha_{\text{iso}}$  and those calculated with HF, LDA, PBE, PBE0 and TS methods (See Table (A.4) for more details). The HF method yields mean absolute relative error (MARE) of 9.0% on experimental values for isotropic polarizabilities and it systematically underestimates polarizabilities. In contrast, LDA and PBE functionals provide MARE of 5.3% and 6.1%, respectively, predicting polarizabilities which are slightly overestimated.

The distribution of relative errors for different methods is shown in Figure (4.2) B. The HF method predicts smaller polarizabilities which can be noticed from the mean relative error (MRE) of -8.5%. It is interesting to note that LDA and PBE functional yields MRE of 0.8% and 2.7%, respectively. The result reported in Table (A.4) for the hybrid functional PBE0 agrees better with the experimental data for 238 molecules with an accuracy of 4.6%. The high accuracy of the PBE0 functional for static polarizabilities has been noted previously [274]. The Figure (4.2) also shows isotropic static polarizabilities using TS method. As discussed in Section (2.7.2) using atomic polarizabilities in Eq. (2.77), the molecular polarizability can be obtained as sum over atomic polarizabilities. Such simple approximation yields isotropic polarizabilities for molecules with an accuracy of 12%, but overestimates polarizabilities in most cases.

Furthermore, we have gathered geometries of 7211 molecules containing up to 7 heavy atoms including C, N, O, S, and Cl from GDB-13 database [272] derived using SMILES string representation [275, 276]. The equilibrium geometries for these systems are obtained via optimization using PBE+TS functional [1, 277]. As discussed above, the hybrid PBE0 functional provides isotropic static polarizabilities with an accuracy of 4.6%. Therefore, we consider PBE0 functional as a reference to obtain static polarizabilities of 7211 molecules. We perform hybrid PBE0 calculation [152] to obtain induced dipole moments with NAO tier 2 basis set including diffuse functions from d-aug-cc-pVQZ gaussian basis set. The polarizability tensors for these systems are obtained via numerical difference. Finally, we have the benchmark database of electric static dipole polarizabilities of resulting dataset of 7449 molecular systems, which we will use to assess a coarse-grained electrodynamic model developed in the next Chapter.

## 4.4 Summary

In conclusion, we have analyzed the performance of electronic structure methods including HF, LRCCSD response theory and different exchange-correlation functionals in DFT, including LDA, PBE, PBE0 and TS in predicting electronic static polarizability with respect to a database of experimental isotropic polarizabilities for organic molecules. We have calculated accurate polarizabilities and vdW coefficients using LRCCSD theory for molecules. The LRCCSD method yields homomolecular  $C_6^{AA}$  coefficients (for 40 pairs) with the accuracy of 6.3% with respect to DOSD data. The MARE for 1128 pairs inter-molecular  $C_6^{AB}$  coefficients is 4.9% which reduces to 3.4% when vdW coefficients are corrected using accurate static polarizability values for atoms and molecules. Therefore, LRCCSD method can be considered accurate and feasible method for computing dynamic polarizabilities and vdW  $C_6$  coefficients for small molecules. The hybrid functional PBE0 in

DFT yields precise results for mean polarizabilities with an accuracy 4.6%, but still tends to slightly overestimate. The semi-local functionals such as LDA and PBE provide MARE of 5.3% and 6.1%, respectively, predicting polarizabilities which are slightly overestimated. Finally, we have presented representative benchmark sets of electric static dipole polarizabilities of  $\approx 7.5K$  molecules and a large database of intermolecular  $C_6^{AB}$  coefficients. These datasets will be useful in comparing static polarizabilities and vdW coefficients obtained using polarizability model developed in present work and will be discussed in Chapter (5).



## Coarse-grained electrodynamic model of electronic polarization in materials

The effective treatment of complex processes of chemical and biological relevance imposes practical choices in the construction of the rigorous theoretical models. Accurate modeling of many-body polarization and dispersion interactions is thus required to understand novel phenomena in complex systems. These interactions often determine the structure and properties of materials. The availability of efficient and accurate methods for the calculation of intermolecular interactions is the prerequisite for a successful molecular simulation of liquids, mesophases [278], crystals [279], composites and nanostructures [280]. Correct treatment of these interactions is also necessary for the understanding of the dynamics of relative phase stabilities, phase transitions and cohesion in multi-molecular systems. A thorough knowledge of the electronic properties of condensed matter systems is a first step required for the design of novel opto-electronic [281], electrocatalysts [14], chemical/bio-sensors [12, 13], nanoelectronics [11], nanoplasmonics [15], and other complex systems [16, 17].

Currently, (semi)-empirical forcefield schemes (based on pairwise approximation) are available for large-scale atomistic simulation of condensed phase systems which allows calculations of dynamics or cohesive energies for time scales of the order of seconds. In general, forcefields need to be optimized using known experimental data or results from *ab initio* calculations on a particular system under study. Unfortunately, this approach is often limited and not transferable to general materials. Quantum chemical wavefunction methods are available which are fully *ab initio*. The main advantage of these methods is that they do not use any empirical parameters. There is a hierarchy of *ab initio* methods of varying complexity and predictive ability for a system under study. However, these approaches are computationally intensive and do not (yet) open a path to large-scale atomistic simulation.

The density-functional theory (DFT) is a widely used method to predict structure and dynamics of matter. In DFT, the primary equations are cast in terms of the electron density rather than the many-electron wave functions. The ground state energy of a many-electron system is determined up to an additive constant by the electron density. The DFT is an exact ground-state theory, in practice only approximated forms of the DFT are known. The majority of DFT applications to condensed matter systems use the Kohn-Sham (KS) [42] formalism. This approach provides the energy of a system as a functional of a noninteracting wave function, which is a functional of the density. However, the exact form of (exchange-correlation) energy functional is not known. In particular, KS-DFT lacks in the correct treatment of the non-local exchange-correlation term. Numerous approximations to the exchange-correlation functional are available for the calculation of the electronic structure properties of condensed phase systems [117] (as discussed extensively in Section (2.5)).

Among various available methods for the calculation of ground and excited properties of condensed matter systems, the time-dependent density functional theory (TDDFT) [43, 44], symmetry adapted perturbation theory [45, 46], fluctuation-dissipation density functional theory [47–49], GW calculations [50–52], random phase approximation (RPA) [53–60] as well as beyond-RPA [61–63] methods are widely used. The key quantity required among these methods is the linear density-density response function,  $\chi(\mathbf{r}, \mathbf{r}', \omega)$ .

The response function is of paramount importance. This quantity is crucial for accurate prediction of the structural and electronic properties of complex systems like surfaces, polymers, hybrid (in)-organic interfaces, nanostructures, and biomolecules. The frequency dependent density-density response function is usually obtained using the Dyson equation [282, 283]. The response function is non-local and a function of (continuous) single particle basis functions. In general, the real-space representation of response function yields matrices too large for explicit matrix algebra. Therefore, the evaluation of response function is a computationally expensive task.

In this chapter, we introduce an atomistic electrodynamics response model for molecules and materials. The present approach is based on atomic response functions (ARFs) which model linear polarization for a system that naturally incorporate the effects of the local chemical environment and non-local screening. The ARF approach has been successfully applied to study model systems (*e.g.* hydrogen-chain, nanoribbons etc.) [205, 284–287]. The ARF method augments the standard set of coordinates by a set of atomic dipoles which are intended to represent the electronic degrees of freedom. In the spirit of the BO approximation, the electrodynamics response is obtained via the electronic degrees of freedom represented by the dipoles, while nuclear degrees of freedom are kept fixed. Recently, ARF idea has been extended in DFT framework to calculate non-local vdW interactions in complex

materials [7, 81].

Many polarization models such as the Drude oscillator [288], fluctuating charges [289], and induced dipoles [5] have been developed and are mainly based on point dipole approximation. These models are quite appealing as they reproduce mean polarizabilities satisfactorily but overestimate the anisotropy of the polarizability [5]. However, such methods have severe limitations as the parameters of the model need to be optimized using known experimental or *ab initio* data and also leads to a phenomenon known as ‘polarization catastrophe’ [3, 5]. This occurs when polarizability of two mutually interacting inducible dipoles diverge (or tends to infinity) at a (critical) finite distance [5, 290] due to collective effects [291]. To avoid such unphysical effects, Thole [5] has suggested various damping functions such as linear or exponential of the Coulomb interaction affecting the corresponding interaction tensor.

In present work, ARFs are described using quantum harmonic oscillators (QHOs) having spherical spatial charge distributions. The ARF model mimics the coarse-grained (linear) electronic response of an atom by replacing the actual set of electrons and protons with a single negatively charged ‘quasiparticle’ harmonically bound to a positively charged heavy ‘quasi nucleus’. The ground state density of a QHO has *s* type symmetry and the density of the first excited state has *p* type symmetry. Furthermore, the response function for an ARF (within dipole approximation) can be modeled as a single dipole oscillator with single excitation (resonant) frequency (*s*→*p* transition). The simplest approximation is the one-term formula which is equivalent to the two-point zeroth-order Padé approximant [1, 292].

The ARFs can be constructed as functional of the electron density obtained using ground state DFT calculation to accurately capture the response of valence electrons [1] for each atomic element. Thus, each atom *i* in a material is associated with a single dipole oscillator with a frequency-dependent polarizability [7, 81]. The effective polarizability of an atom in a material is then defined through Hirshfeld partitioning [193] of the electron density. Within this approach an ARF includes hybridization, local exchange-correlation, and static charge transfer effects [1]. Then, an ARF  $\chi_{0,i}$  for an atom *i* can be represented by considering the response of the valence electrons into a single atom-centered dipole oscillator at position  $R_p$  using

$$\chi_{0,i}(\mathbf{r}, \mathbf{r}', i\omega) = \alpha_i(\mathbf{r}, i\omega) \nabla_{\mathbf{r}} \delta^3(\mathbf{r} - R_p) \otimes \nabla_{\mathbf{r}'} \delta^3(\mathbf{r}' - R_p) \quad (5.1)$$

The bare response function  $\chi_0(\mathbf{r}, \mathbf{r}', i\omega)$  for a system of *N* ARFs, follows as the direct sum over the individual ARFs,

$$\begin{aligned} \chi_0(\mathbf{r}, \mathbf{r}', i\omega) &= \chi_{0,i}(\mathbf{r}, \mathbf{r}', i\omega) \oplus \chi_{0,j}(\mathbf{r}, \mathbf{r}', i\omega) \oplus \chi_{0,k}(\mathbf{r}, \mathbf{r}', i\omega) \oplus \dots \\ &\quad \dots \oplus \chi_{0,N}(\mathbf{r}, \mathbf{r}', i\omega) \end{aligned} \quad (5.2)$$

Thus, such an approach allows the definition of a bare response function  $\chi_0[n(\mathbf{r})]$  as functional of electron density obtained with DFT rather than explicitly derived using single particle orbitals. Interestingly, such additive approximation for the response function utilizing the electron density of a molecule and high-level reference data for the free atoms already provide isotropic polarizabilities with an accuracy [81] of  $\approx 12\%$  and asymptotic vdW  $C_6$  coefficients with an accuracy [1] of  $\approx 5\%$ . However, this additive ansatz for the response function fails to capture intrinsic anisotropy and the screening effects which stem from long-range electrodynamic fluctuations.

The collective (dynamic) many-body polarization which can arise in a system can be obtained from the solution of the Dyson-like self-consistent screening (SCS) equation of classical electrodynamics (using normalized propagators or dipole tensor) [3, 5, 6, 80, 293]. The method developed in this work is a synergistic coupling of classical electrodynamics with quantum mechanical input data and the electron density obtained using DFT calculation (which includes (local) electron exchange-correction effects in an ARF) [7, 81]. The formulation presented in this chapter builds upon and significantly improves an earlier version of the ARF model [7], by preserving QHO invariants, satisfying the dipole oscillator strength sum rule, and using the correct spin-polarized electron densities for the free atoms to construct promolecular density which maps valence electronic response to a set of ARFs. As it will be shown, the proposed parameter-free method which computes polarizability of finite gap materials as a functional of ground-state electron density represents an accurate and efficient way of calculating response properties of complex materials. This method provides isotropic static polarizability with an accuracy of 3.6% for  $\approx 7500$  molecules and 7.6% for vdW  $C_6$  coefficients for an extensive database of gas-phase molecules when compared with accurate reference data. The coarse-grained representation of the response function in terms of ARFs reduces the computational cost by several orders of magnitude compared to full electronic calculation. This chapter is organized as follows: First we introduce the necessary properties (*i.e.* wavefunction, density, polarizability, Coulomb potential) of a QHO which will be useful to define the input required for the ARF model. Then, we introduce a method to compute the interacting (linear) response for a collection of ARFs. Furthermore, we describe a procedure to construct bare response function as functional of electron density obtained using DFT that maps atoms in a given (molecular) system of interest to the model system of ARFs. Finally, we discuss the results obtained using the ARF model applied to molecules and non-metallic solids.

## 5.1 The quantum harmonic oscillator (QHO) model

The quantum harmonic oscillator model is one of the most important system in quantum mechanics. The harmonic oscillator can be used to describe vibrations in molecules as well as the phonons in solids. The QHO can be characterized by three parameters, mass, frequency, and charge. In QHO model, a quasi-particle (with charge  $-q$ ) having mass  $m$  and attached to a center at  $\mathbf{R}$  (or a pseudo centre with background charge  $+q$ ) by a harmonic potential. The Schrödinger equation of a spherically-symmetric three-dimensional harmonic oscillator can be solved explicitly by separation of variables to obtain the eigenfunctions and eigenvalues. The basics of the quantum harmonic oscillator model will be discussed in the next section.

### 5.1.1 The Hamiltonian for QHO

The Hamiltonian for a spherically-symmetric three-dimensional harmonic oscillator (in spherical polar coordinates centered at  $\mathbf{R}$ ) is given by [294]

$$\hat{\mathcal{H}} = -\frac{1}{2m_a} \nabla_{\mathbf{r}}^2 + \frac{1}{2} m_a \omega^2 \mathbf{r}^2 \quad (5.3)$$

$\mathbf{r}$  is the position coordinate of the particle, mass  $m_a$  and frequency  $\omega$ . The Schrödinger equation can be solved explicitly by the separation of variables to obtain the eigenvectors and eigenvalues. The general formula for the normalized wavefunctions can be written as

$$\psi_{klm}(r, \theta, \phi) = N_{kl} r^l L_k^{(l+\frac{1}{2})} \left( m_a \omega r^2 \right) \exp \left( -\frac{m_a \omega}{2} r^2 \right) Y_{l,m}(\theta, \phi) \quad (5.4)$$

where

$$N_{kl} = \left( \frac{m_a^3 \omega^3}{4\pi} \right)^{1/4} \left( \frac{2^{k+2l+3} k! (\frac{m_a \omega}{2})^l}{(2k+2l+1)!!} \right)^{1/2} \quad (5.5)$$

is a normalization constant,  $Y_{l,m}(\theta, \phi)$  is a spherical harmonic function,  $L_k^{(l+\frac{1}{2})} \left( m_a \omega r^2 \right)$  are generalized Laguerre polynomials;  $k$ ,  $l$  and  $m$  are the quantum numbers and the energy eigenvalues

$$E_{klm} = \left( 2k + l + \frac{3}{2} \right) \omega, \quad (5.6)$$

respectively. The ground-state wavefunction of a QHO is

$$\psi_0(\mathbf{r}) = \left( \frac{m_a \omega}{\pi} \right)^{3/4} \exp \left( -\frac{m_a \omega}{2} r^2 \right). \quad (5.7)$$

Therefore, the ground-state charge density of a QHO has the following form

$$n_0(\mathbf{r}) = \left( \frac{m_a \omega}{\pi} \right)^{3/2} \exp \left( - m_a \omega r^2 \right). \quad (5.8)$$

The term

$$\sigma = \sqrt{\frac{1}{2m_a \omega}} \quad (5.9)$$

is the spatial variance or spread of a QHO. Using this relation, a more convenient expression for the QHO density distribution can be written as

$$n_0(\mathbf{r}) = \left( \frac{1}{(2\pi)^{3/2} \sigma^3} \right) \exp \left( - \frac{r^2}{2\sigma^2} \right) \quad (5.10)$$

The  $\sigma$  determines the width of the Gaussian. In general, this term is called the standard deviation, and the square of it,  $\sigma^2$ , the variance. The  $\sigma$  can only take positive values,  $\sigma > 0$ . Such QHO representation is isotropic. In the following section, we discuss in brief polarizabilities for the QHO model derived using perturbation theory.

### 5.1.2 Polarizabilities for the QHO model

The polarizability of QHO model can be derived starting from the second order perturbation theory. The following derivation can also be found in Ref. [295, 296]. The frequency-dependent polarizabilities using sum-over-states expression can be defined as

$$\alpha_{\ell m, \ell' m'}(\omega) = \sum_n \frac{\langle 0 | \hat{Q}_{\ell m} | n \rangle \langle n | \hat{Q}_{\ell' m'}^\dagger | 0 \rangle}{E_n - E_0 + \omega} + \frac{\langle 0 | \hat{Q}_{\ell m}^\dagger | n \rangle \langle n | \hat{Q}_{\ell' m'} | 0 \rangle}{E_n - E_0 - \omega} \quad (5.11)$$

where  $\hat{Q}_{\ell m}$  is the multipole-tensor operator in the spherical tensor representation [295, 296]. The multipole-tensor operator is defined as

$$\begin{aligned} \hat{Q}_{\ell m}(\mathbf{r}) &= q R_{\ell m}(\mathbf{r}) \\ &= q r^\ell C_{\ell m}(\theta, \phi) = q r^\ell \left( \frac{4\pi}{2\ell+1} \right)^{1/2} Y_{\ell m}(\theta, \phi), \end{aligned}$$

and  $n$  represents the eigenstates  $(k, \ell'', m'')$ , with  $E_n - E_0 = (2k + \ell)\omega_{n0}$ . The matrix elements using QHO wavefunctions can be expressed as

$$\begin{aligned} \langle 0 | \hat{Q}_{\ell m} | n \rangle &\equiv \langle 000 | \hat{Q}_{\ell m} | k \ell'' m'' \rangle \\ &= \int_r \int_\Omega \mathcal{R}_{00} \mathcal{Y}_{00} \left[ qr^\ell \left( \frac{4\pi}{2\ell+1} \right)^{1/2} Y_{\ell m} \right] \mathcal{R}_{k\ell''} \mathcal{Y}_{\ell'' m''}. \end{aligned}$$

This simplifies because  $\mathcal{Y}_{00} = 1/\sqrt{4\pi}$ , and  $\int_{\Omega} \mathcal{Y}_{\ell m} \mathcal{Y}_{\ell'' m''} = \delta_{\ell, \ell''} \delta_{m, -m''}$ , using the Kronecker  $\delta$ .

$$\langle 000 | \hat{Q}_{\ell m} | k \ell'' m'' \rangle = \sqrt{\frac{q^2}{2\ell+1}} \delta_{\ell, \ell''} \delta_{m, -m''} \int_r r^\ell \mathcal{R}_{00} \mathcal{R}_{k\ell} .$$

where the full 3-quantum number representation is given explicitly. There is a property unique to the  $k = 0$  state which allows further simplification, in that  $\mathcal{R}_{0\ell} \propto r^\ell R_{00}$ , and hence differ only by a normalization factor,

$$\left[ \frac{\mathcal{R}_{0\ell}}{N_{0\ell}} \right] = r^\ell \left[ \frac{\mathcal{R}_{00}}{N_{00}} \right] \implies r^\ell \mathcal{R}_{00} = C_\ell \mathcal{R}_{0\ell},$$

where

$$C_\ell^2 = \left[ \frac{N_{00}}{N_{0\ell}} \right]^2 = (2\ell + 1)!! \left( \frac{1}{2m_a \omega_{n0}} \right)^\ell, \quad (5.12)$$

$$\begin{aligned} \langle 000 | \hat{Q}_{\ell m} | k \ell'' m'' \rangle &= \sqrt{\frac{q^2}{2\ell+1}} \delta_{\ell, \ell''} \delta_{m, -m''} \int_r C_\ell \mathcal{R}_{0\ell} \mathcal{R}_{k\ell} \\ &= C_\ell \sqrt{\frac{1}{2\ell+1}} \delta_{0k} \delta_{\ell, \ell''} \delta_{m, -m''}. \end{aligned} \quad (5.13)$$

Substituting this identity into (5.11) yields (here we drop dependence on the angular frequency  $\omega$  for simplicity),

$$\alpha_{\ell m, \ell' m'} \equiv 2 \frac{q^2 C_\ell^2 / (2\ell + 1)}{(0 + \ell) \omega_{n0}} \delta_{\ell\ell'} \delta_{mm'},$$

which can be simplified and expressed as isotropic polarizabilities  $\alpha_\ell$ ,

$$\alpha_{\ell m, \ell' m'} = \alpha_\ell \delta_{\ell\ell'} \delta_{mm'},$$

where

$$\alpha_\ell = \left[ \frac{q^2}{m_a \omega_{n0}^2} \right] \left[ \frac{(2\ell - 1)!!}{\ell} \right] \left[ \frac{1}{2m_a \omega_{n0}} \right]^{\ell-1}.$$

In the case of dipole polarizability where  $\ell = 1$ , the above equation reduces to

$$\alpha = \frac{q^2}{m_a \omega_{n0}^2} \quad (5.14)$$

Consequently, substituting Eq. (5.9) (i.e. spread of a QHO), the dipole polarizability of a QHO can be expressed in term of its spatial variance

$$\alpha = 4m_a q^2 \sigma^4 \quad (5.15)$$

Therefore, the Eq. (5.15) relates polarizability to the charge, mass and the variance of a QHO. In the following subsection we discuss the

ground state energy and wave function of a QHO in an uniform electric field and the relationship between various QHO invariants.

### 5.1.3 QHO in a uniform electric field

The ground state energy and wave function of a QHO model atom in an uniform electric field,  $\mathcal{E}$ , along the  $z$ -axis, are given by [295, 296]

$$E_0 = \frac{3}{2}\omega - \frac{1}{2}\alpha\mathcal{E}^2 \quad (5.16)$$

$$\psi_{0,\mathcal{E}}(\mathbf{r}) = \left(\frac{1}{2\pi\sigma^2}\right)^{3/4} \exp\left(-\frac{(\mathbf{r}-\mathbf{R})^2}{4\sigma^2}\right). \quad (5.17)$$

where  $\mathbf{R}$  is the QHO position ( $\mathbf{R} = \frac{\alpha\mathcal{E}}{q}\hat{z}$ ),  $q$  and  $\alpha$  is the (effective) charge and the polarizability of a QHO, respectively. It can be shown that there exist non-vanishing induced (spherical) multipole moments of the QHO model in a uniform field which are given by

$$\hat{Q}_{l0} = q\left(\frac{\alpha\mathcal{E}}{q}\right)^l - q\delta_{l,0} \quad (5.18)$$

Thus, the QHO model reduces to the dipole limit ( $l \rightarrow 1$ ) for the uniform field case and higher order responses such as hyperpolarizability, in principle which can originate from a spherical distribution perturbed by a uniform field are absent in the QHO model due to the lack of on-site "anharmonic" terms.

The term  $\sigma$  is related to the (dipole) wave function  $\psi_{0,\mathcal{E}}(\mathbf{r})$  and the corresponding charge density of the QHO. Therefore, the variance  $\sigma$  can be used to define the (dipole) density distribution of a QHO model atom (which will be discussed in the Section (5.3)). The QHO has a spatial charge distribution and occupies certain "effective volume". Another important quantity we require is the effective "volume" occupied by a QHO and will be discussed in the next subsection.

### 5.1.4 Relationship between polarizability and volume of a QHO

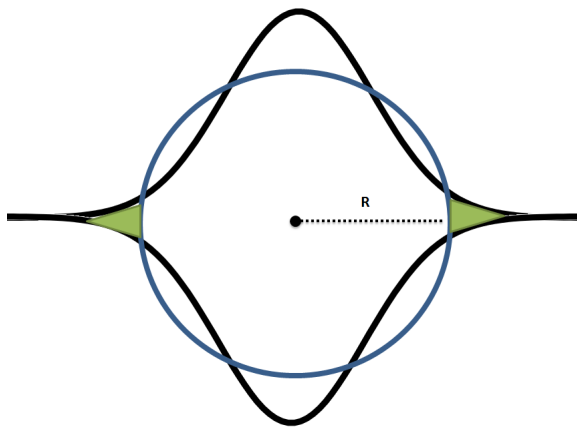
Classical models of the polarizability, such as the conducting sphere model or the homogeneous electron gas model yield a polarizability proportional to  $R^3$  where  $R$  is the radius of the sphere [19, 297]. This implies that the polarizability can be expressed in terms of the volume,  $V$ , of the sphere, *i.e.*  $\alpha \approx \frac{4\pi}{3}R^3$ . In case of molecules, the correlations between polarizability and volume have been empirically demonstrated by Politzer and co-workers [298, 299]. The effective volume of a QHO can be derived as spatial density-weighted integration over QHO charge density. The volume occupied by the charge density,  $n_0(\mathbf{r})$ , can be

defined using the following analytic integration

$$V^{\text{QHO}} = \int r^3 n_0(\mathbf{r}) d^3\mathbf{r} = \left(\frac{128}{\pi}\right)^{1/2} \sigma^3 \quad (5.19)$$

The above relation states that the volume of a QHO can be expressed in terms of its spread. Therefore, the Eq. (5.19) can be used to relate the polarizability and the volume of a QHO. Substituting Eq. (5.19) in

**Figure 5.1:** Schematic representation of the density distribution of conducting sphere model having uniform density within radius  $R$  (blue circle) and one dimensional representation of charge density of a QHO (black curve). The shaded green region indicate the density of QHO outside certain radius  $R$  due to continuous charge distribution.



Eq. (5.15), the relation between polarizability and the effective volume of a QHO can be written as

$$\alpha = 4\left(\frac{\pi}{128}\right)^{4/3} m_a q^2 V^{4/3} \quad (5.20)$$

Eq. (5.20) indicates that the polarizability  $\alpha$  of a QHO is proportional to  $V^{4/3}$ , unlike  $\alpha \propto \frac{4\pi}{3}R^3 \propto V$  for a sphere of radius  $R$ . The non-linear relationship between the polarizability and the volume of QHO is due to its quantum property. Therefore, the exponent 4/3 is a result of QHO charge distribution which has a Gaussian form which decays monotonically whereas the sphere model assumes that the polarizability is strictly zero outside radius  $R$ , as illustrated schematically in Figure (5.1). Therefore, such smoothly decaying charge density of a single QHO is ideal to model coarse-grained electron density of atoms. The Eq. (5.20) will be useful later when we will define the effective polarizability of an atom embedded in a material and will be discussed in the Section (5.3)). In the next subsection, we introduce the dynamic polarizability for a single (dipole) oscillator.

### 5.1.5 Dynamic polarizability of a single (QHO) oscillator

The expression for the frequency dependent polarizability for a single oscillator  $p$  can be written as [1, 7, 178]

$$\alpha_p(i\omega) = \frac{\alpha_p^0 \omega_p^2}{\omega_p^2 + \omega^2} \quad (5.21)$$

where the  $\alpha_p^0$  is the static dipole polarizability, and  $\omega_p$  is an effective excitation frequency of an oscillator. There are many approximate formulae for dynamic polarizability  $\alpha(\omega)$  while Eq. (5.21) allows to define bounds on vdW two-body  $C^{pq}$  coefficients. If the two-body isotropic coefficients of the homoatomic interactions are accurately known, the crossing point of  $\alpha_p(i\omega)$  and  $\alpha(i\omega)$  can be so chosen such that  $\alpha_p(i\omega)$  overestimates  $\alpha(i\omega)$  in certain ranges of  $\omega$  and underestimates  $\alpha(i\omega)$  in other parts of the spectrum. The net result that  $\alpha(i\omega)$  when calculated using Casimir-Polder integral should yield the correct value  $C_6^{pp}$ .

The Eq. (5.21) is expressed in imaginary frequency argument and therefore it is a monotonically decreasing function. The numerator  $\alpha_p^0 \omega_p^2$  in Eq. (5.21) is the oscillator strength  $f_p$  which can be related to the effective charge (or electrons in valence region) in an atom

$$f_p = \alpha_p^0 \omega_p^2 \quad (5.22)$$

The oscillator strength  $f_p$  is a quantity that expresses the probability of absorption or emission of radiation in transitions between energy levels of a system. This is known as the Thomas–Reiche–Kuhn sum rule or dipole oscillator strength sum rule [300].

The isotropic  $C_6$  term describing the vdW interaction between two non-overlapping fragments  $p$  and  $q$  (in vacuum) is given by Casimir-Polder intergral

$$C_6^{pq} = \frac{3}{\pi} \int_0^\infty \alpha_p(i\omega) \alpha_q(i\omega) d\omega \quad (5.23)$$

where  $\alpha(i\omega)$  is the frequency-dependent polarizability of  $p$  or  $q$  evaluated at imaginary frequencies. In case of identical oscillators  $p = q$ , integrating Eq. (5.23) using dynamic polarizability in Eq. (5.21) yields

$$C_6^{pp} = \frac{3}{4} (\alpha_p^0)^2 \omega_p \quad (5.24)$$

such that

$$\omega_p = \frac{4}{3} \frac{C_6^{pp}}{(\alpha_p^0)^2} \quad (5.25)$$

Secondly, the oscillator strength sum in Eq. (5.22) turns out to be

$$f_p = \frac{9}{16} \frac{(C_6^{pp})^2}{(\alpha_p^0)^3}. \quad (5.26)$$

In order to define the dynamic polarizability in using Eq. (5.21) for an atom or an atomic response function (ARF) in vacuum, we just need the knowledge of accurate free atom static polarizability  $\alpha_p^0$  and homo-atomic vdW  $C_6^{pp}$  coefficient (See Figure (5.4)). So far we have discussed necessary properties and relationships of QHO model. In the next section, we describe a method to compute the interacting (linear) response for a collection of ARFs.

## 5.2 The electrodynamics of atomic response functions

Our system is composed of an assembly of atomic response functions (ARFs). Each ARF consist of associated charge density distribution which is described by a QHO. We assume that initially such distribution does not overlap with density distribution of other ARFs. This 'assumption' is necessary for the validity of the multipole expansions of the potentials of the charge distribution at a point  $p$  in space. The center of the region of unit  $p$  is located at  $\mathbf{r}_p$ . The  $n$ th rank (or  $n$ th order) electric multipole moment [3, 6, 293] of unit  $p$  can be written as

$$\mu_p^{(n)} = (n!)^{-1} \oint n(\mathbf{r})(\mathbf{r} - \mathbf{r}_p)^n d\mathbf{r} \quad (5.27)$$

where  $n(\mathbf{r})$  is the charge density at point  $\mathbf{r}$ , the expression  $(\mathbf{r} - \mathbf{r}_p)^n$  indicate the direct or polyadic product of the  $n$  factors  $\mathbf{r} - \mathbf{r}_p$  and the integration is over the charge density. The multipole moment polytensor of unit  $p$  is the vector  $(\mu_p^{(1)}, \mu_p^{(2)}, \mu_p^{(3)}, \dots)$  where each tensor  $\mu_p^{(n)}$  is arranged as an array of its components in standard order. Formally, such polytensors are infinite arrays, though they are truncated at some desired tensor rank for practical applications (e.g.  $n = 1$  in case of dipole moment).

The collective (dynamic) many-body polarization which can arise in a system or for a collection of ARFs can be obtained from the solution of the Dyson-like self-consistent screening (SCS) equation of classical electrodynamics [3–6, 80]. In present approach atoms in a system are considered as an arrangement of polarizable dipoles. According to classical electrodynamics, the induced dipole in such a system satisfies the equation

$$\mu(\mathbf{r}) = \bar{\alpha}(\mathbf{r})\mathcal{E} + \bar{\alpha}(\mathbf{r}) \int \bar{\mathcal{T}}(\mathbf{r}, \mathbf{r}') \mu(\mathbf{r}') d\mathbf{r}' \quad (5.28)$$

where  $\bar{\alpha}(\mathbf{r})$  is the local polarizability,  $\mathcal{E}$  is an (external) uniform electric field, and  $\bar{\mathcal{T}}$  is the dipole-dipole interaction tensor. For a collection of  $N$  atoms, the induced dipole moment in a basis of atomic position,  $\mu_p$  at atom  $p$  is given in terms of the external polarizing field and the field generated by neighboring dipoles which leads to following set of linear response equations

$$\mu_p = \bar{\alpha}_p [\mathcal{E}_p + \sum_{p \neq q}^N \bar{\mathcal{T}}_{pq} \mu_q] \quad (5.29)$$

where  $\bar{\alpha}_p$  is the atomic polarizability tensor of atom  $p$  and  $\bar{\mathcal{T}}_{pq}$  provides dipole-dipole field connecting atoms  $p$  and  $q$ . The Eq. (5.29) can be casted in a matrix representation as

$$\begin{bmatrix} (\bar{\alpha}_1)^{-1} & \bar{\mathcal{T}}_{12} & \dots & \bar{\mathcal{T}}_{1N} \\ \bar{\mathcal{T}}_{21} & (\bar{\alpha}_2)^{-1} & \dots & \bar{\mathcal{T}}_{2N} \\ \vdots & \ddots & \ddots & \vdots \\ \vdots & \ddots & \ddots & \vdots \\ \bar{\mathcal{T}}_{N1} & \bar{\mathcal{T}}_{N2} & \dots & (\bar{\alpha}_N)^{-1} \end{bmatrix} \begin{bmatrix} \mu_1 \\ \mu_2 \\ \vdots \\ \vdots \\ \mu_N \end{bmatrix} = \begin{bmatrix} \mathcal{E}_1 \\ \mathcal{E}_2 \\ \vdots \\ \vdots \\ \mathcal{E}_N \end{bmatrix} \quad (5.30)$$

or as

$$\mathcal{P}\mu = \mathcal{E} \quad (5.31)$$

with

$$\mathcal{P}_{pq} = \begin{cases} (\bar{\alpha}_p)^{-1} & \text{if } p = q \\ \bar{\mathcal{T}}_{pq} & \text{if } p \neq q \end{cases} \quad (5.32)$$

where  $\mathcal{P}$  is a  $3N \times 3N$  matrix containing the inverse of the atomic polarizability tensors  $(\bar{\alpha}_p)^{-1}$  along the  $3 \times 3$  diagonals and the non-diagonal components correspond to the dipole interaction tensors. The matrix  $\mathcal{P}$  depends only on the atomic polarizabilities and on their arrangement in space as described by the interaction tensors and not on the external field. The inversion of matrix  $\mathcal{P}$  produces  $\mathcal{Q}$ , a generalized polarizability matrix<sup>1</sup>. Consequently, the induced dipole moment can be rewritten as  $\mu = \mathcal{Q}\mathcal{E}$ . Within this formulation solving Eq. (5.29) will give rise to the interacting non-local polarizability tensor for a system.

For a molecule, the molecular polarizability,  $\bar{\alpha}_{mol}$ , is just the response to an uniform field. Therefore, the molecular polarizability tensor can be obtained as a sum over all  $3 \times 3$  submatrices  $\mathcal{Q}_{pq}$

$$\mu_{mol} = \left[ \sum_p^N \sum_q^N \mathcal{Q}_{pq} \right] \mathcal{E} = \bar{\alpha}_{mol} \mathcal{E} \quad (5.33)$$

which after contraction yields a  $3 \times 3$  matrix corresponding to the polarizability tensor. Finally, the averaged molecular polarizability can

---

<sup>1</sup> $\mathcal{Q} = \mathcal{P}^{-1} = (\alpha^{-1} + \sum \mathcal{T})^{-1}$

be determined by taking the trace of the tensor  $\bar{\alpha}_{mol}$ .

The point-dipole approximation in Eq. (5.29) provides a reasonably simple and straightforward formalism for treating a system as an assembly of polarizable atoms at large interacting distances. In the original point-induced dipole model by Applequist [301], the tensor  $\bar{\mathcal{T}}$  is defined using the bare Coulomb potential, *i.e.*  $\phi = \frac{1}{r}$ . This model reproduced mean polarizabilities satisfactorily but overestimated the anisotropy of the polarizability [5]. Furthermore, at short distances the interaction of the induced dipoles becomes too strong leading to even shorter distances and consequently stronger interactions. This is known as “polarization catastrophe” which also manifests in the ill-condition of the interaction matrix  $\mathcal{Q}$ . For small distances  $r$ , the values of the  $\bar{\mathcal{T}}$  are in the same order of magnitude as the inverse values of the polarizability. As a result, the inverse of the interaction matrix may not be positive definite anymore leading to negative eigenvalues, *i.e.*, induced dipoles pointing in the opposite direction of the underlying electric field [5]. In order to avoid such unphysical effects, Thole has suggested many damping functions (such as linear and exponential) of the Coulomb interaction affecting the corresponding dipole-dipole tensor  $\bar{\mathcal{T}}$ . In reality, atoms should be characterized by dipole-density distributions that lead to finite molecular polarizabilities and stem from Pauli exchange-repulsion at short inter-atomic distances. Therefore, the tensor  $\bar{\mathcal{T}}$  must be regularized (or damped) and this procedure will be discussed in the following section.

### 5.2.1 Regularized dipole interaction tensor

The dipole-dipole tensor  $\bar{\mathcal{T}}$  is the central quantity which describes coupling between induced dipole moments. It is defined as negative double-gradient of the Coulomb potential. For a pair of electrical point charges  $p$  and  $q$ , the dipole-dipole interaction tensor can be obtained using the Coulomb potential and is given by the expression

$$\mathcal{T}_{ij}^{pq} \equiv -\nabla_{R_p} \otimes \nabla_{R_q} \left( \frac{1}{\mathbf{R}^{pq}} \right) \quad (5.34)$$

$$= -\frac{3\mathbf{R}_p \cdot \mathbf{R}_q}{R^5} - \frac{\delta_{ij}}{R^3}. \quad (5.35)$$

The problem when considering point charges is that the term  $\mathcal{T}_{ij}$  diverges as  $|\mathbf{R}^{pq}| \rightarrow 0$ . Therefore, we need to renormalize the bare Coulomb potential ( $1/R$ ). In real systems, the electronic distributions are also affected by Pauli exchange-repulsion effect at short interatomic distances which needs to be modelled accurately. Since we are modelling atoms using QHOs, the charge distribution of a QHO has a Gaussian form as described in Section (5.1.1). The Coulomb electrostatic energy between two Gaussian charge distributions can be

evaluated by following integral equation [302]

$$\phi^{\text{QHO}}(R_{pq}) = \int \int \frac{n(R_p - \mathbf{r}_1)n(R_q - \mathbf{r}_2)}{|\mathbf{r}_{12}|} d\mathbf{r}_1 d\mathbf{r}_2 \quad (5.36)$$

where  $R_{pq}$  is distance between two charge distributions. Each of these distribution is normalized to have unit charge such that  $\int n_p^{\text{QHO}}(\mathbf{r})d\mathbf{r} = \int n_q^{\text{QHO}}(\mathbf{r})d\mathbf{r} = 1$ . For large separations Eq. (5.36) reduces to the expression for the point charges. The integral in Eq. (5.36) cannot be factorized in the Cartesian direction due to the presence of the inverse operator  $\mathbf{r}_{12}^{-1}$ . The idea here is to re-express inverse operator in terms of a one dimensional integral over a Gaussian function which is separable in the Cartesian directions<sup>2</sup>. Furthermore, using suitable coordinate transformation the integral in Eq. (5.36) can be written in simple form (the detailed proof is given in Ref [302])

$$\phi^{\text{QHO}}(R_{pq}) = \frac{\text{erf}(R_{pq}/\sigma_{pq})}{R_{pq}} \quad (5.37)$$

$$= \frac{1}{R_{pq}} \frac{2}{\sqrt{\pi}} \int_0^{R_{pq}/\sigma_{pq}} \exp^{-x^2} dx \quad (5.38)$$

where erf is called the Gauss error function and  $\sigma_{pq}$  is the effective spread (variance) of the Gaussian centered between two charge distributions. Initially, we assumed that the QHOs were well separated by a sufficiently large distance, allowing us to use the bare dipole-dipole interaction potential to describe the inter-oscillator couplings. Now considering the general case which involves shorter inter-atomic distance, for any material with overlapping atomic wavefunctions. The dipole-dipole interaction potential between oscillators  $p$  and  $q$  is straightforwardly obtained from the regularized Coulomb potential ,

$$\mathcal{T}^{pq} = \begin{cases} \nabla_{R_p} \otimes \nabla_{R_q} \phi^{\text{QHO}} & \text{if } p \neq q \\ 0 & \text{if } p = q, \end{cases}$$

and is therefore a  $3 \times 3$  second-rank tensor with components given by

$$\mathcal{T}_{ij}^{pq} = \left( \frac{3R_i \cdot R_j - R_{pq}^2 \delta_{ij}}{R_{pq}^5} \left[ \text{erf}\left(\frac{R_{pq}}{\sigma_{pq}}\right) - \frac{2}{\sqrt{\pi}} \frac{R_{pq}}{\sigma_{pq}} \exp\left(-\frac{R_{pq}^2}{\sigma_{pq}^2}\right) \right] - \frac{4}{\sqrt{\pi}} \frac{R_i \cdot R_j}{\sigma_{pq}^3 R_{pq}^2} \exp\left(-\frac{R_{pq}^2}{\sigma_{pq}^2}\right) \right), \quad (5.39)$$

in which  $i$  and  $j$  represent the coordinates  $x, y, z$  in the Cartesian reference frame,  $R_i$  and  $R_j$  are the respective components of the interoscillator distance  $R_{pq}$  , and  $\delta_{ij}$  is the standard Kronecker delta.

---

<sup>2</sup>The Coulomb operator is expressed as  $\frac{1}{|\mathbf{r}_{12}|} = \frac{1}{\sqrt{\pi}} \int_{-\infty}^{+\infty} \exp(-|\mathbf{r}_{12}|^2 x^2) dx$

The advantage of this approach is that the above expression for the dipole-dipole interaction potential attenuates the interaction between oscillators at short distances converging to a finite value even in the zero-distance limit. Furthermore, it becomes equivalent to the point dipole-dipole interaction potential for large interoscillator distances.

The term  $\sigma_{pq} = \sqrt{\sigma_p^2 + \sigma_q^2}$ , is an effective width obtained from the Gaussian widths of oscillators  $p$  and  $q$ , that essentially determines the correlation length of this interaction potential. The  $\sigma$  parameter physically correspond to the spatial spread of the local dipole moment distribution centered on a given oscillator. In classical electrodynamics, the Gaussian width (variance) is directly related to the polarizability and can be derived from the dipole self-energy. In the zero-distance limit of the dipole-dipole interaction potential derived above in Eq. (5.39), the spread of a QHO is related to polarizability and can be written as [6]

$$\sigma_p = \left( \sqrt{\frac{2}{\pi}} \frac{\alpha_p^{\text{iso}}}{3} \right)^{1/3}. \quad (5.40)$$

The idea in present work is to model  $\sigma$ , the variance QHOs, by the position dependent dipole moment distribution for atoms in a system. Conceptually, such dipole moment distribution could be derived using quantum mechanical electronic density for neutral free atoms. The details of this procedure will be discussed in the following section.

### 5.2.2 Quantum mechanically-based dipole potential

The fundamental quantity of the QHO model developed in this work is the position dependent dipole moment density. The dipole polarizability relates the response of a dipole moment to an external electric field. Therefore, the term  $\sigma$  in Eq. (5.15) describes the spatial extent of the local dipole density distribution centered on a given QHO. The dipole density can be defined using the expectation value of the squared dipole moment operator [189, 303–305]

$$\langle \mu^2 \rangle = \left( \sum_i q_i \mathbf{r}_i \right)^2, \quad (5.41)$$

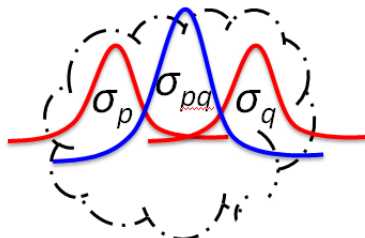
where  $q_i$  are charges in a system. For a spherically symmetric system or atom, the dipole density may be written as

$$\langle \mu^2 \rangle = \int r^2 n(\mathbf{r}) d\mathbf{r}, \quad (5.42)$$

where  $n(\mathbf{r})$  is electron density of an atom. In present work we are modelling (linear polarization) charge density of atoms with isotropic QHOs. The dipole potential  $\nabla_{\mathbf{r}_i} \otimes \nabla_{\mathbf{r}_j} |\mathbf{r}_i - \mathbf{r}_j|^{-1}$  between two point charges decays as  $r^{-3}$ , where  $r$  distance between two point charges. Therefore, dipole potential in present ARF model should

decay asymptotically as  $r^{-3}$  at long-range or at very large inter-atomic distances. As discussed in Section (5.2.1), the term  $\sigma_{pq}$ , is an effective width obtained from the Gaussian widths of oscillators  $p$  and  $q$ , that essentially determines the correlation length of the dipole interaction potential. The  $\sigma_{p/q}$  parameter physically correspond to the spatial spread of the local dipole moment distribution centered on a given oscillator (as shown schematically in Figure (5.2)). To accurately

**Figure 5.2:** Schematic illustration of two interacting ARFs in a material having Gaussian variance  $\sigma_p$  and  $\sigma_q$ . The effective dipole correlation length at short distances is given by Gaussian having variance  $\sigma_{pq} = \sqrt{\sigma_p^2 + \sigma_q^2}$  centered between QHOs  $p$  and  $q$ . In the limit  $\sigma_{pq} \rightarrow 0$  tends to point dipole approximation.



model dipole potential due to a QHO charge density,  $\phi^{\text{QHO}}(\mathbf{R} - \mathbf{r}) = \text{erf}(|\mathbf{R} - \mathbf{r}|/2\sigma)/|\mathbf{R} - \mathbf{r}|$ , to that of neutral free atom we just need variance  $\sigma$  of a QHO. The  $\sigma$  value can be derived using electron densities obtained using an accurate electronic structure calculation for atoms and the resulting dipole potential should decay as  $r^{-3}$  asymptotically. In present work, we first obtain electron density  $n(\mathbf{r})$  for neutral atoms using accurate wavefunction obtained using coupled-cluster (CC) theory including single and double excitation (CCSD). The solution of the Poisson equation

$$\nabla^2 \phi^{(2)}(\mathbf{r}) = -4\pi r^2 n(\mathbf{r}), \quad (5.43)$$

for electronic dipole density distribution for free atoms results in dipole potential,  $\phi^{(2)}$ . The radial Poisson equation is solved numerically for spherically symmetric atomic density using the Numerov method. We ensure first that the Coulomb potential resulting from these accurate atomic densities has correct  $r^{-1}$  asymptote and the integral over atomic electron density provides correct number of electrons. Further we fit this accurate dipole potential to the potential of a QHO charge density distribution [6]. Note that, large for  $r$ , the erf function approaches unity and the potential  $\phi(r)$  approaches the point potential  $\phi(r) \approx \frac{1}{r}$  as shown in Figure (5.3). Therefore, the value for  $\sigma^{\text{free}}$  are extracted from the fit for the Gaussian potential in the region larger than 1 bohr from the center of nuclei where  $\text{erf} \rightarrow 1$ . The variances for few neutral free atoms are provided in Table (5.1). In the Section (5.1), we have discussed necessary properties of the QHO response model. The Section (5.2) introduces a method to compute

**Figure 5.3:** The potential from the spherical Gaussian distribution of unit charge with exponent  $\sigma = 1$  (dashed red curve),  $\text{erf}(r)/r$ , plotted as function of the distance from the center of the charge distribution and compared with the corresponding potential from a point charge  $1/r$  (thick black curve) along with the  $\text{erf}(r)$  error function (dashed blue curve).

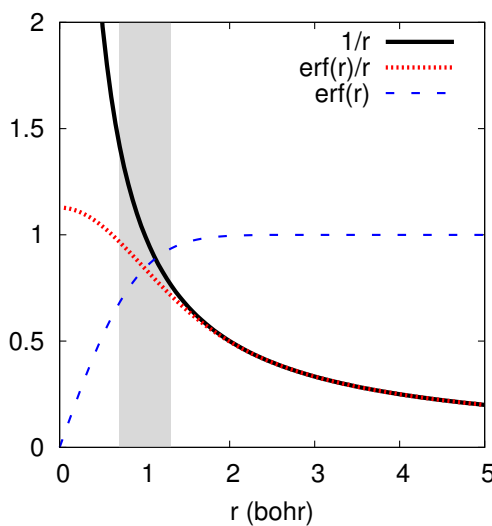


**Table 5.1:** The value of variance of dipole density distribution  $\sigma^{\text{free}}$  for few neutral free atoms (in bohr).

	$\sigma^{\text{free}}$		$\sigma^{\text{free}}$
H	1.518	Zn	1.792
He	1.065	Ga	2.058
Li	3.164	Ge	1.915
B	1.824	As	1.756
C	1.509	Se	1.640
N	1.347	Br	1.540
O	1.266	Kr	1.309
F	1.118	Cd	1.733
Ne	1.012	In	1.972
Al	2.258	Sn	1.918
Si	1.978	Sb	1.813
P	1.735	Te	1.752
S	1.634	I	1.668
Cl	1.459	Xe	1.430
Ar	1.317		

interacting polarizability for a collection of ARFs. In the following section, we introduce a method called coupled atomic response in matter (CARMA). This approach calculates interacting polarizability for a system of ARFs and represents a synergistic coupling of classical electrodynamics with quantum mechanical input data and the density functional theory [7, 81].

### 5.3 Coupled atomic response in matter (CARMA)

The solution of the self-consistent screening equation for a set of localized ARFs provides microscopic non-local polarizability for a system. The (interacting) polarizability tensor based on the SCS equation for an ARF can be written as

$$\alpha_p^{\text{SCS}}(\mathbf{r}, i\omega) = \alpha_p^0(\mathbf{r}, i\omega) + \alpha_p^0(\mathbf{r}, i\omega) \sum_{p \neq q}^N \mathcal{T}_{pq}(\mathbf{r}, \mathbf{r}', i\omega) \alpha_q^{\text{SCS}}(\mathbf{r}, i\omega), \quad (5.44)$$

where  $\alpha_p^{\text{SCS}}(i\omega)$  is the fully screened atomic polarizability tensor for a given frequency of the electric field, which can be derived after solving

the SCS equation.

The central quantities required to solve Eq. (5.44) are the polarizability  $\alpha_p^0(\mathbf{r}, i\omega)$  and the dipole-dipole field tensor  $\mathcal{T}_{pq}(\mathbf{r}, \mathbf{r}', i\omega)$  which connects (polarizing) fields at position  $p$  and  $q$ . The polarizability tensor for a molecular system can be expressed in terms of  $3N \times 3N$  matrix in the basis of ARF coordinates. The frequency dependent polarizability tensor for an ARF can be written as

$$\alpha_p^0(i\omega) = \left( \frac{\alpha_p^0[n(\mathbf{r})]\omega_p^2[n(\mathbf{r})]}{\omega_p^2[n(\mathbf{r})] + \omega^2} \right) \delta_{ij}, \quad (5.45)$$

where the static polarizability  $\alpha_p^0$ , the effective excitation frequency,  $\omega_p$ , are defined as functional of ground-state electron density and Kronecker delta function  $\delta_{ij}$  (with  $i, j = 1, 2, 3$ . tensor components). Now we proceed to map the atoms in a given (molecular) system of interest to the model system of ARFs. Each atom  $p$  in the molecular system will be represented by a single ARF characterized by a Cartesian position vector  $\mathbf{R}_p$  and a corresponding frequency-dependent dipole polarizability given by Eq. (5.45). We assume that the system which can be an individual molecule or even condensed matter has a finite electronic gap and can therefore be divided into effective atomic fragments. Here we use Hirshfeld [193] partitioning scheme to divide an integral over the entire molecular volume into a sum of atomic integrals. Each atomic integral is evaluated on a spherical grid using numerical techniques. Prior to the application of this partitioning scheme one must setup a set of spherically averaged atomic densities for all elements that are present in the molecular system of interest. For consistency, this needs to be carried out with the same level of theory that is used for the molecular calculations [193, 306–309]. The Hirshfeld partitioning of the total electron density,  $n(\mathbf{r})$ , into atomic fragment electron densities,  $n_p(\mathbf{r})$ , is utilized to obtain the effective volume of atom in a material and is defined by

$$V_p^{\text{rel}}[n(\mathbf{r})] = \frac{V_p^{\text{eff}}}{V_p^{\text{free}}} = \frac{\int r^3 w_p(\mathbf{r}) n(\mathbf{r}) d^3 r}{\int r^3 n_p^{\text{spin,free}}(\mathbf{r}) d^3 r}, \quad (5.46)$$

where  $n(\mathbf{r})$  is the total electronic density and  $n_p^{\text{spin,free}}(\mathbf{r})$  is the density of the free atom. The Hirshfeld atomic partitioning weight for a given atom  $p$  is given by

$$w_p(\mathbf{r}) = \frac{n_p^{\text{spin,free}}(\mathbf{r})}{\sum_q^n n_q^{\text{spin,free}}(\mathbf{r})}, \quad (5.47)$$

where  $\mathbf{r}$  is the distance from the nucleus of atom  $p$ , and the sum over  $q$  runs over all atoms of the system. The electron density for neutral free atoms calculated using spin-unrestricted calculations. Both  $n(\mathbf{r})$

and  $n_p^{\text{spin,free}}(\mathbf{r})$  are obtained using the FHI-aims package [265], which implements all-electron electronic-structure theory with numeric atom-centered basis functions. The Hirshfeld weighing function  $w_p(\mathbf{r})$  can be derived using spin-restricted and spin-unrestricted calculation for neutral free atoms. The spin-unrestricted calculation for free atoms correctly provides the integer orbital occupation numbers for valence orbitals unlike spin-restricted calculation.

We have outlined the details regarding the partitioning of the electron density of a molecular system into 'atomic' regions. Now we processed to assign parameters in the ARF model as functional of electron density. The central ingredient in the ARF model is the static polarizability. The polarizability is often expressed in terms of the volume,  $V$ . Classical models such as the homogeneous electron gas model or the conducting sphere model yield a polarizability proportional to  $R^3$ , where  $R$  is the radius of the sphere [19, 297]. The methods (such as Becke and Johnson XDM model or Tkatchenko-Scheffler method) which are based on a Hirshfeld scheme to partition molecular polarizabilities in terms of atomic contributions assumes that the polarizability is directly proportional to atomic 'volume' [1, 187, 189, 310, 311], *i.e.*  $\alpha \propto V = \frac{4\pi}{3}R^3$ . These methods define the effective static polarizability of an atom in a material by scaling (accurate) static polarizability of that atom with Hirshfeld volume ratio,  $V_p^{\text{rel}}$ . In the Section (5.1.4)), we have discussed the relationship between the polarizability and the volume of a QHO, *i.e.*  $\alpha \propto V^{4/3}$ . Therefore, using this relationship which is a consistent property of QHO, the effective static polarizability for an ARF in a material as functional of electron density can be defined as

$$\frac{(\alpha_p^0)^{\text{eff}}}{\alpha_p^{\text{free}}} = \left( \frac{V_p^{\text{eff}}}{V_p^{\text{free}}} \right)^{4/3},$$

or as

$$\alpha_p^0[n(\mathbf{r})] = (V_p^{\text{rel}}[n(\mathbf{r})])^{4/3} \alpha_p^{\text{free}}, \quad (5.48)$$

where  $V_p^{\text{rel}}$  is relative volume ratio obtained using the Hirshfeld [193, 307–309] partitioning scheme of electron density,  $\alpha_p^{\text{free}}$  is the reference free-atom static dipole polarizability which can be taken from either experimental data or high-level quantum chemical calculations [195](See Table (A.1)). The term  $V_p^{\text{rel}}$  depends on the self-consistent electron density obtained using (semi-)local DFT functional (in the current case using PBE [277] functional) and accounts for the effect of the local charge distribution. Therefore, the Eq. (5.48) includes hybridization, local exchange-correlation, and static charge transfer effects [1]. This short-range information is an important ingredient in the ARF model.

Furthermore, the ARF (within dipole approximation) can be modeled as a single dipole oscillator with a single excitation frequency

$\omega_p$  (for  $s \rightarrow p$  resonant transition for a QHO model atom) [1, 7]. Therefore, the excitation frequency  $\omega_p$  for an ARF can be defined using accurate free atom static polarizability and homo-atomic vdW coefficient (See Eq. (5.25) in Section (5.1.5)). The ARF model in present work is developed to satisfy neutral free atom valence electron sum rule. This is accomplished by defining the excitation frequency  $\omega_p$  as a functional of electron density. The 'effective' excitation frequency then can be defined as

$$\omega_p[n(\mathbf{r})] = \frac{4}{3} \frac{C_6^{\text{free}}}{(\alpha^{\text{free}})^2} \left( \frac{1}{V_p^{\text{rel}}[n(\mathbf{r})]} \right)^{2/3}. \quad (5.49)$$

The Eq. (5.49) is consistent with the fact that excitation frequency for QHO model is inversely proportional to effective volume of a QHO (*i.e.*  $\omega_p^{\text{QHO}} \propto V^{-2/3}$ ). The relationship (or scale factors) between local atomic fragment volume with polarizability and excitation frequency conserve sum rule (for effective charge) in a given ARF. In many cases, the polarizability of system is dominated by the contributions from valence electrons. Moreover, the oscillator strength of a given ARF is given by Eq. (5.22) and its value depends only on input neutral free atom parameters.

The final ingredient required to solve Eq. (5.44) is the dipole-dipole tensor. The (regularized) dipole-dipole interaction tensor for ARF model (see Eq. (5.39)),  $\mathcal{T}_{pq}$ , requires only effective variance of local (dipole) density distribution. The effective variance is defined as  $\sigma_{pq} = \sqrt{\sigma_p^2 + \sigma_q^2}$  with respect to a Gaussian centered between ARF  $p$  and  $q$ . The dipole-dipole propagator  $\mathcal{T}_{pq}$  instantaneously connects polarizing field at  $\mathbf{r}$  and  $\mathbf{r}'$  and assumes quasi-static approximation. The (dipole) wave function for a QHO in field for frequency  $\omega$  can written as

$$\psi_{0,\omega}(\mathbf{R} - \mathbf{r}) = \left( \frac{1}{2\pi\sigma^2} \right)^{3/4} \exp \left( - \frac{(\mathbf{r} - \mathbf{R})^2}{4\sigma^2} \right), \quad (5.50)$$

where the vector  $\mathbf{r}$  is defined with respect to center ( $\mathbf{R} = \frac{\alpha\omega}{q}\hat{z}$ ) of a QHO (as discussed in the Section (5.1.3)). Therefore, the term  $\sigma$  can be viewed as variance or expectation value of local (dipole) moment distribution. In Section (5.2.2), we have discussed a method to accurately model the variance  $\sigma$  of a QHO to that of neutral free atom in vaccum. Using the relationship between volume and variance of a QHO (see Eq. (5.19)), *i.e.*  $\sigma \propto V^{1/3}$ . The dipole moment distribution for an atom in a material can be defined as

$$\sigma_p(\mathbf{r}) = \left( V_p^{\text{rel}}[n(\mathbf{r})] \right)^{1/3} \sigma_p^{\text{free}}, \quad (5.51)$$

such that interaction potential also depends on electron density. The dependence of  $\sigma_p$  on frequency argument  $i\omega$  or in complex plane can

be very distinct. Here, we simply define a monotonically decreasing frequency dependent dipole density for each ARF  $p$  is defined as

$$\sigma_p(\mathbf{r}, i\omega) = \left( \frac{\alpha_p^0(i\omega)}{\alpha_p^0(0)} \right)^{1/4} \left( V_p^{\text{rel}}[n(\mathbf{r})] \right)^{1/3} \sigma_p^{\text{free}}. \quad (5.52)$$

The CARMA method combines above ingredients to include short-range overlap hybridization effects in polarizability, as well as long range electrodynamic screening through SCS equation. For a system containing  $N$  atoms, the response function or the polarizability matrix  $\mathcal{P}$  can be constructed such that the diagonal contains the inverse of isotropic polarizability tensor via Eq. (5.45) and non diagonal term include  $\mathcal{T}_{pq}$ , the dipole tensor which connects atoms  $p$  and  $q$  ( $p, q = 1, 2, \dots, N$ ) with coupling term  $\sigma_{pq} = \sqrt{\sigma_p^2 + \sigma_q^2}$  where  $\sigma_p$  or  $\sigma_q$  is defined by Eq. (5.52) for each frequency ( $i\omega$ ). For an extended system, the matrix  $\mathcal{P}$  includes additional terms corresponding to the dipole field due to periodic boundary conditions. Therefore, the Eq. (5.30) becomes

$$\mathcal{P} = \begin{bmatrix} \alpha_1^{-1} + \sum \mathcal{T}_{11'} & \mathcal{T}_{12} + \sum \mathcal{T}_{12'} & \dots & \mathcal{T}_{1N} + \sum \mathcal{T}_{1N'} \\ \mathcal{T}_{21} + \sum \mathcal{T}_{21'} & \alpha_2^{-1} + \sum \mathcal{T}_{22'} & \dots & \mathcal{T}_{2N} + \sum \mathcal{T}_{2N'} \\ \vdots & \vdots & \ddots & \vdots \\ \vdots & \vdots & \ddots & \vdots \\ \mathcal{T}_{N1} + \sum \mathcal{T}_{N1'} & \dots & \dots & \alpha_N^{-1} + \sum \mathcal{T}_{NN'} \end{bmatrix} \quad (5.53)$$

where  $p'$  and  $q'$  denote the atoms from the image cell ( $p, q = 1, 2, \dots, N$ ). The interactions of an atom with its own images are contained in the diagonals and those with the images of other atoms are located in the non-diagonal parts. The dipole field due to periodic images need to included using a real space spherical radius  $\mathcal{R}$  with respect to the unit cell.

Furthermore, the inversion of matrix  $\mathcal{P}$  yields a fully interacting non-local polarizability tensor (matrix  $\mathcal{Q}$ ) of a system in the basis of QHO position. The  $\alpha_{\text{system}}^{\text{SCS}}$  tensor is obtained as a summation of atomic subblocks of matrix  $\mathcal{Q}_{pq}$ . After diagonalization of the  $\alpha_{\text{system}}^{\text{SCS}}$  tensor, one can obtain the three principal components of the total polarization matrix for a molecule or a crystal, and the average value corresponds to the average of the trace as given by  $\alpha_{\text{system}}^{\text{iso}} = (\alpha_{xx} + \alpha_{yy} + \alpha_{zz})/3$ . Furthermore, this procedure can be followed to derive the full polarizability  $\alpha_{\text{system}}$  spectrum as a function of the imaginary frequency argument ( $i\omega$ ) which is a monotonically decreasing function. Consequently, the vdW coefficients of the system can be calculated by integrating the polarizability over  $i\omega$  frequency. The Gauss-Legendre integral approach can be used to evaluate  $C_6$  coefficients and a converged integral can be obtained by using finite (a

20 point) numerical frequency grid. Thus, the resulting polarizability  $\alpha_{\text{system}}^{\text{SCS}}(i\omega)$  now contains coupled atomic response accounted via short-range and long-range electrodynamic screening [1, 3, 5–7, 293]. Therefore, the developed ARF model can be used to compute dynamic polarizability efficiently of molecules as well as periodic (finite gap) materials. The proposed polarizability model will be termed as coupled atomic response in matter or CARMA. To assess the accuracy and applicability of CARMA model, calculations are performed for a wide variety of molecular system and will be described in the next section.

## 5.4 Results and Discussion

In this section, we discuss the results obtained using the CARMA model applied to molecules and non-metallic solids. We use our scheme for the calculation of static polarizabilities, vdW  $C_6$  coefficients, effective oscillator strengths and oscillator strength sums. The CARMA model has been applied to calculate static polarizabilities of an extensive database of molecules ( $\approx 7500$  systems) and vdW  $C_6$  coefficients for 1225 pairs that included atom-atom, atom-molecule and molecule-molecule interactions (as discussed in the Chapter (4)). Comparison with values from the available experimental data as well as results from the *ab initio* calculations leads to the conclusion that our results from the CARMA approach are accurate. In the following section, we first discuss the bounds on dipole oscillator strength distribution as well as the relationship between dipole polarizability and electronic sum rule for CARMA model.

### 5.4.1 Dipole oscillator strength sum rule

Certain moments of the dipole oscillator distribution of atoms and molecules can be calculated from the theory using sum rules or deduced from the experimental data. The oscillator strength sums or Cauchy moments are important for the description of a variety of molecular properties, for example, dynamic polarizabilities at real and imaginary frequencies [253], inelastic scattering cross sections [312], Verdet constants of atoms [313], vdW coefficients between atoms or molecules and the paramagnetic contribution to the Cotton-Mouton constants of atoms [314].

In response theory, the Cauchy moments are usually defined by the sum-over-states formula which provides bounds on dipole oscillator distribution. The first Cauchy moment of any dynamic property is the static response property e.g. static dipole polarizability. The expressions for the dynamic properties at imaginary frequency are also obtained from the Cauchy moments. For example, the distribution of the transition dipole strength function  $S(\omega)$  provides an estimate of the static electric dipole polarizability [315–317] for a system and can be

expressed as

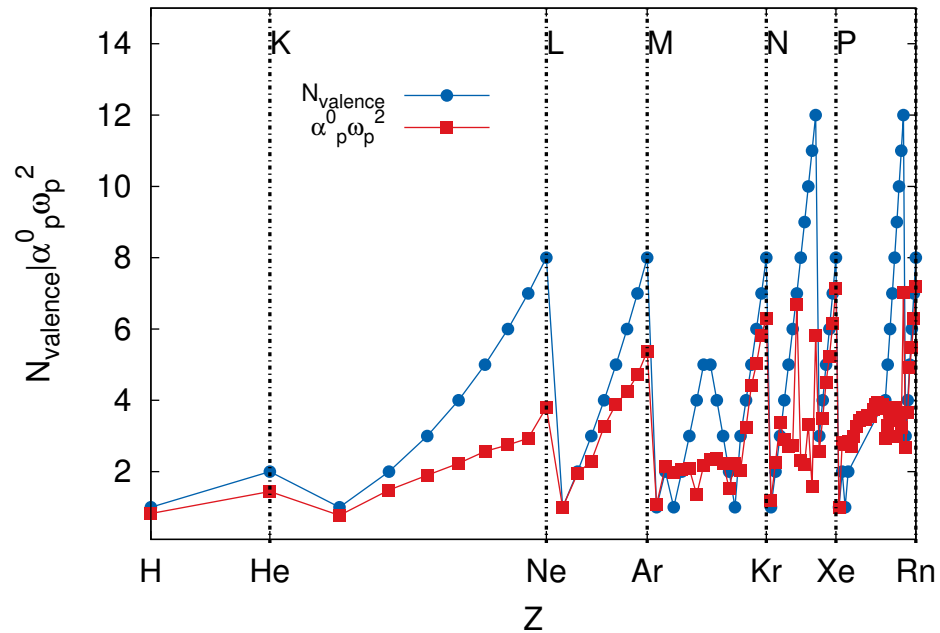
$$\alpha = \int \frac{S(\omega)}{\omega^2} d\omega. \quad (5.54)$$

The electronic  $f$ -sum rule also known as Thomas-Reiche-Kuhn (TRK) sum rule [300, 316] reads

$$\mathcal{N}_e = \int S(\omega) d\omega. \quad (5.55)$$

This sum rule can be obtained as integral over the frequency dependent response function or the electric-dipole strength distribution function of a system. Since we are mapping valence electronic response to a set of ARFs, therefore, polarizability resulting from CARMA model should satisfy the valence  $f$ -sum rule. The effective number of electrons in an ARF is given by  $f_p = \alpha_p^0 \omega_p^2$  (as discussed in Section (5.1.5)). The Figure (5.4) shows the oscillator strength  $f_p$  defined for elements in the periodic table as function of atomic number  $Z$ . The  $f_p$  values are tabulated using accurate neutral free atom static polarizability and homo-atomic vdW  $C_6$  coefficients (See Table (A.1)). Since the free atom parameter are derived using accurate many body calculations which leads to shell-structure effect in the oscillator strength spectra for neutral free atoms. Moreover, for a collection of  $N$  atoms, the net

**Figure 5.4:** The x-label indicate atomic number  $Z$ , while the y-axis shows the effective valence electron  $\mathcal{N}_{valence}$  in an atomic species (excluding core electrons) and the oscillator strength  $f_p$  defined in Eq. (5.22) derived using accurate free atom reference parameters (see Table (A.1))



charge in a system can be derived as sum over oscillator strength,  $f_p$ ,

as,

$$\mathcal{N}_e = \sum_p^N f_p = \sum_p^N \alpha_p^0 \omega_p^2 = \frac{9}{16} \sum_p^N \frac{(C_6^{pp})^2}{(\alpha_p^0)^3}. \quad (5.56)$$

In case of CARMA model, the value of  $f_p$  simply depends upon the input static dipole polarizability  $\alpha$  and the homo atomic vdW  $C_6$  coefficient for neutral free atoms (See Figure (5.4) and Table (A.1)). In order to compare accuracy of sum rule defined for CARMA model, we first calculate reference electronic sum rule using (linear) optical absorption spectrum for small organic molecules using TDDFT calculations. To obtain the linear optical absorption spectrum of the system, we follow the method proposed by Yabana and Bertsch [315], and excite all frequencies of the system by giving some small momentum  $\mathcal{K}$  to the electrons. This is performed by transforming the ground-state wavefunctions according to  $\Psi_i(\mathbf{r}, \delta t) = e^{i\mathcal{K}\hat{z}}\Psi_i(\mathbf{r}, 0)$  and then propagating them for some (finite) time. The spectrum can then be obtained from the expression for the dipole strength function  $\mathcal{S}(\omega)$

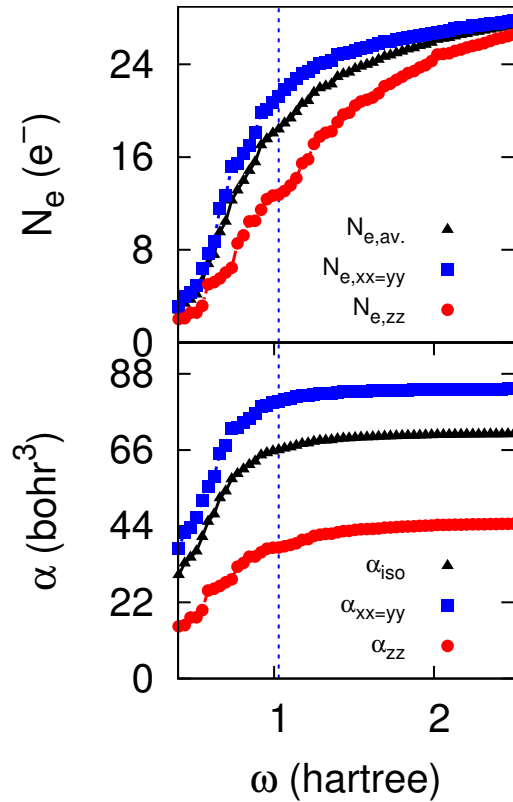
$$\mathcal{S}(\omega) = \frac{2\omega}{\pi} \text{Im} \alpha(\omega), \quad (5.57)$$

where the dynamical polarizability,  $\alpha(\omega)$ , is essentially the Fourier transform of the dipole moment of the system  $\mu(t)$

$$\alpha(\omega) = \frac{1}{\mathcal{K}} \int dt e^{i\omega t} [\mu(t) - \mu(0)]. \quad (5.58)$$

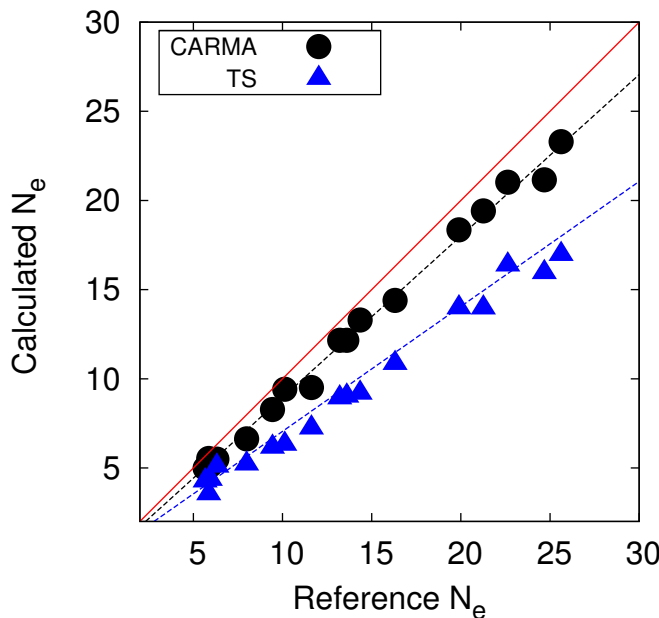
Within this definition, the TRK  $f$ -sum rule for the number of electrons,  $\mathcal{N}_e$ , is given by the integral in Eq. (5.55). These sum rules can be used to check the quality of the calculations. The procedure to calculate the dipole strength function is as follows. We perform time-dependent DFT calculations using the Octopus code [318]. The ion-electron interaction was modeled with norm-conserving Troullier-Martins pseudopotentials [319]. The time-dependent dipole moments  $\mu(t)$  for small organic molecules (See Table (4.2)) are obtained by propagating Perdew-Burke-Ernzerhof (PBE) Kohn-Sham wavefunctions for finite time. The dynamic polarizability generally related to optical absorption and in its most general form, a  $3 \times 3$  tensor. This means that to obtain the entire dynamic polarizability tensor of the molecule we usually need to apply 3 different perturbations along  $x$ ,  $y$ ,  $z$  axis. Furthermore, the dynamical polarizability,  $\alpha(\omega)$ , is then calculated by the Fourier transform of the time-dependent dipole moment of a system  $\mu(t)$  which gives the strength function  $\mathcal{S}(\omega)$ . The completeness of spectrum is checked by partially integrating the dipole strength function. The Figure (5.5) shows the components of static polarizability tensor and effective number of electrons  $\mathcal{N}_e$  for benzene molecule obtained using TDPBE calculation as a function of energy. The experimental value of static polarizability for benzene molecule is 69.7 bohr<sup>3</sup>. While,

**Figure 5.5:** The plot shows the convergence of static polarizability and  $\mathcal{N}_e$  sum rule for benzene obtained using dipole strength function. Each point in curve is integral in Eq. (5.55) and Eq. (5.54) up to energy  $\omega$ .



TDPBE calculation provides slightly overestimated static polarizability sum rule which is 70.6 bohr<sup>3</sup>. The number of 'effective' valence electrons in the benzene molecule is 18 (excluding filled core shell electrons in atoms). Furthermore, for benzene molecule, the value for  $\mathcal{N}_e$  sum rule using TDPBE calculation can be determined using energy  $\omega$  value corresponding to the converged static polarizability (dashed vertical line Figure (5.5)). Partially integrating Eq. (5.55) till the energy corresponding to the converged static polarizability for benzene provide  $\mathcal{N}_e$  sum rule of 17.5 this value is consistent with available valence electrons in the benzene. The correlation between the electronic  $\mathcal{N}_e$  sum rule derived using TDPBE calculations and the CARMA model along with the TS method for a set of 18 molecules is shown in Figure (5.6). In Section (5.3), we have introduced a procedure which defines ARFs as a functional electron density. Using expression Eq. (5.48) and Eq. (5.49) for single oscillator polarizability, the dependence of electron density on oscillator strength cancel out. Therefore, the effective charge in a system simply dependent upon input free atom parameters *i.e.* the static polarizability and homo-atomic vdW  $C_6$  coefficient. The accuracy of  $\mathcal{N}_e$  sum rule for CARMA model with respect to TDPBE calculations is 10.5% (see Figure (5.6)) whereas using the TS method yields a mean average relative error of 33%. The TS method includes the effect of volume scaling in the effective static polarizability for a given ARF.

**Figure 5.6:** Correlation of electronic  $f$ -sum rules obtained from TDDFT calculation compared with CARMA model (black circle) and TS method (blue triangle).



However, using the definition for static polarizability from Eq. (5.48) and excitation frequency Eq. (5.49) in Eq. (5.21) conserve oscillator strength  $f_p$  in the case of CARMA model. Therefore, the sum rule obtained using the CARMA model better correlates with the reference TDPBE calculations. In the following subsection, we discuss the CARMA model applied to determine static and dynamical polarizabilities for diverse sets of molecules ranging from simple diatomic ( $\text{H}_2$ ,  $\text{N}_2$ , CO etc.) to polyatomic systems with functional groups including alcohol, ketone, amine and aromatic systems.

#### 5.4.2 Static polarizability and vdW coefficients for a linear chain of $\text{H}_2$ molecules

For many molecules with near spherical symmetry, the polarizability is well approximated by a single scalar constant. The isotropic polarizability ( $\alpha_{\text{iso}} = (\alpha_{xx} + \alpha_{yy} + \alpha_{zz})/3$ ) is defined as average of the principal components of the polarizability tensor. In general, the redistribution of electronic charge for a molecular system under influence of an external electric field cannot be characterized by a single scalar value. This can be most clearly observed by considering a simple diatomic molecule like  $\text{H}_2$ . The  $\text{H}_2$  molecule has no permanent dipole moment, but the charge distribution along the internuclear axis is large compared to the distribution perpendicular to this axis. Therefore, we

expect the charge separation induced by an external field to be greater along the internuclear axis than along a perpendicular axis. Here, we apply CARMA model developed in present work to calculate the static polarizability tensor and vdW coefficient of the linear  $(H_2)_3$  chain. The linear  $(H_2)_3$  chain consists of three  $H_2$  dimers with alternating bond lengths (bond length of 2 Bohr inside the dimer and 3 Bohr between the dimers). An accurate calculation of the polarizability of such hydrogen dimer chains is considered to be a significant challenge for electronic structure theory [286]. We have also calculated the reference frequency-dependent polarizability for  $(H_2)_3$  using the linear response coupled-cluster method (LR-CCSD). The LR-CCSD method is a state-of-the-art approach for computing static and frequency dependent molecular polarizabilities, and it yields results that agree to  $\approx 3\%$  when compared to reliable experimental values (as discussed in Chapter (4)). The results for the isotropic and anisotropic  $C_6$  coefficients for this chain at the TS, CARMA, and LR-CCSD levels of theory are shown in Table (5.2). In TS method, the molecular polarizability is expressed

**Table 5.2:** The isotropic static polarizability and vdW  $C_6$  coefficients for the linear  $(H_2)_3$  chain calculated using the TS, CARMA and LR-CCSD levels of theory. The  $\alpha_{\perp}$  and  $\alpha_{\parallel}$  components of polarizability are defined with respect to the principal axis of the linear  $(H_2)_3$  chain. The static polarizabilities are defined in Bohr<sup>3</sup> and the vdW coefficients are defined in Hartree·Bohr<sup>6</sup>.

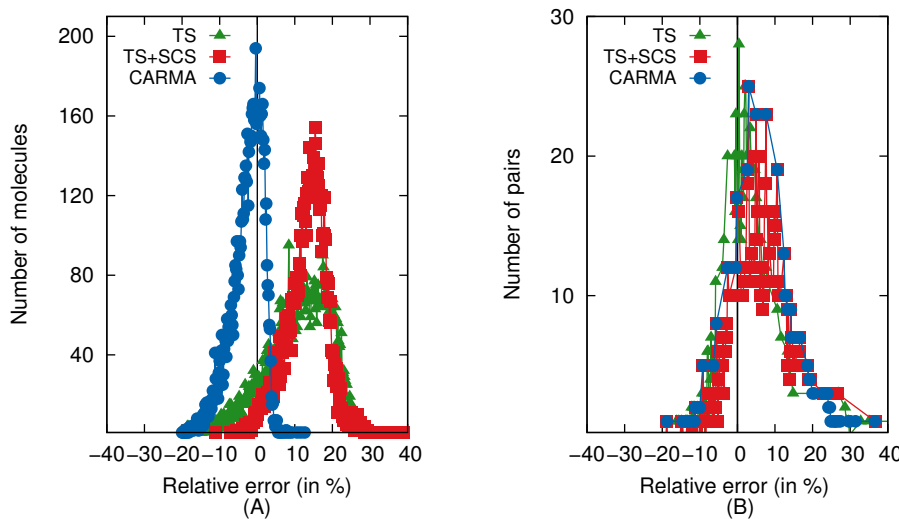
	$\alpha_{\text{iso}}$	$\alpha_{\perp}$	$\alpha_{\parallel}$	$C_{6,\text{iso}}$	$C_{6,\perp}$	$C_{6,\parallel}$
TS	18.1	-	-	105.6	-	-
CARMA	25.2	14.6	46.2	209.1	91.1	604.3
LR-CCSD	28.8	17.0	52.4	238.0	114.7	638.8

as sum over atomic polarizability and does not capture anisotropy in molecular polarizability. After solving SCS equation the CARMA model correctly captures the dipole alignment (polarization) along the  $(H_2)_3$  chain, leading to a significant anisotropy that is in good agreement with the reference LR-CCSD values. Moreover, the solution of SCS procedure yields the full polarizability  $\alpha_{\text{system}}(i\omega)$  tensor of a system as a function of the imaginary frequency argument. Therefore, the isotropic and the anisotropic components vdW coefficients ( $C_{6,\perp}$  and  $C_{6,\parallel}$ ) can be calculated using the Casimir-Polder integral. The Table (5.2) also shows the isotropic  $C_{6,\text{iso}}$  and anisotropic ( $C_{6,\perp}$  and  $C_{6,\parallel}$ ) vdW coefficients for  $(H_2)_3$  chain at the TS, CARMA, and LR-CCSD levels of theory. The parallel and perpendicular components of vdW coefficients ( $C_{6,\perp}$  and  $C_{6,\parallel}$ ) for  $(H_2)_3$  chain are in good agreement with respect to those obtained using LR-CCSD calculations. The isotropic  $C_6$  coefficient is also noticeably improved when using the CARMA approach in comparison to TS method. In the following section, we apply CARMA model to calculate electric static polarizabilities and vdW coefficients of benchmark datasets of molecules as discussed in Chapter (4).

### 5.4.3 Performance of CARMA model for isotropic electric static polarizability and vdW coefficients of molecules

In the Chapter (4), we have introduced representative benchmark sets of electric static dipole polarizabilities for 7449 molecules and vdW  $C_6^{AB}$  coefficients for 1225 pairs of species that include atom-atom, atom-molecule and molecule-molecule interaction. Here, we use these datasets to assess the performance of CARMA model in predicting static polarizability and asymptotic vdW  $C_6^{AB}$  coefficients. Therefore, the electric static polarizabilities and asymptotic vdW coefficients are then calculated for this diverse set of molecules. The distributions of relative errors for Tkatchenko–Scheffler (TS) method [1], TS+SCS [7] and CARMA model with respect to the reference PBE0 polarizabilities for  $\approx 7.5k$  molecules are in shown Figure (5.7)–(A). In TS polarizability

**Figure 5.7:** A) The plot shows the distribution of relative errors for isotropic static polarizability of 7449 molecules calculated using TS (green-triangles), TS+SCS (red-squares) and CARMA model (blue-circles) on the reference PBE0 polarizabilities. B) The plot shows distribution of relative error for  $C_6^{AB}$  coefficients of 1225 pairs of atoms and molecules calculated using TS, TS+SCS and CARMA model on experimentally derived vdW coefficients.



model, the molecular polarizability is expressed as a sum over electron density dependent atom hybridized polarizabilities. The TS method provides isotropic molecular polarizabilities with an accuracy of 12.2% on the benchmark set of electric static dipole polarizabilities for 7449 molecules and systematically overestimates polarizabilities. The atomic response function model in present work relies on the definition that the atomic polarizability of each atom in a system is defined as functional of electron density,  $\alpha[n(\mathbf{r})]$ . Moreover, the key quantities required to obtain the polarizability tensor of a system (after solving the SCS

equation) are effective static polarizability  $\alpha_p$  and the variance  $\sigma_p$  for each atom in a system which are defined as functional of electron density [1]. The TS+SCS model [7] uses definition of input  $\alpha_p$  and  $\sigma_p$  given by Eq. (2.77) and Eq. (5.40), while for the CARMA model inputs are defined by Eq. (5.48) and Eq. (5.51), respectively. Both TS and TS+SCS method predicts isotropic polarizabilities within 12% relative to those obtained using PBE0 functional. The TS method shows a broad distribution of relative errors for static polarizabilities while TS+SCS model has small standard deviation but still systematically overestimates polarizabilities. The CARMA model predicts isotropic static polarizabilities with an accuracy of 3.6% and this can be clearly observed from the distribution of relative errors shown in Figure (5.7)–(A). Furthermore, the mean average relative error on the principal components of the polarizability tensor in comparison with PBE0 functional is 4.3%, 9.7% and 10.5%, for  $\alpha_{xx}, \alpha_{yy}, \alpha_{zz}$  respectively.

Similarly, the distributions of relative errors for 1225 pairs of vdW coefficients obtained using TS method [1], TS+SCS [7] and CARMA model with respect to the  $C_6$  coefficients derived using experimental DOSD data are shown in Figure (5.7)(B). The TS method already provides the vdW coefficients with an accuracy of 5.1% [1]. Moreover, the TS+SCS model predicts slightly overestimated  $C_6$  coefficients with an error bar of 6.3%. The CARMA model provides static polarizability with good accuracy as compared with earlier TS+SCS model [7]. Therefore, the CARMA model yields  $C_6$  coefficients with an accuracy of 7.6% on the 1225 pairs of vdW coefficients which is clearly observed from Figure (5.7)(B). The CARMA model provides an accurate and efficient framework for calculating dynamic polarizability tensor for molecules. In the following section, we analyse the dynamic polarizabilities and vdW coefficients calculated using CARMA model for 23 cubic extended solids.

#### 5.4.4 Static polarizability and vdW coefficients in solids

The electronic excitation spectrum of a material is generally described in terms of a frequency dependent complex electronic dielectric function  $\epsilon(\omega) = \epsilon_1(\omega) + i\epsilon_2(\omega)$ . The real part or the imaginary part contains all the desired response information since the causality argument relate the real and imaginary parts via the Kramers-Kronig transformation and can be written as

$$\epsilon_1(\omega) - 1 = n^2(\omega) - 1 = \frac{2}{\pi} P \int_0^\infty \frac{\omega' \epsilon_2(\omega')}{\omega'^2 - \omega^2} d\omega', \forall \omega < \omega_0 \quad (5.59)$$

where  $\omega_0$  is the threshold frequency and  $n$  is the refractive index. The frequency  $\omega$  is assumed to be higher than vibrational modes therefore only electronic excitations are being considered. A simple approximate

formula for Eq. (5.59) for inter band transitions by individual oscillators and recognize that each valence electron contributes one such oscillator may be approximated by

$$\epsilon_2 - 1 = \sum_n \frac{f_n}{\omega_n^2 - \omega^2} \quad (5.60)$$

which is Kramers–Heisenberg dispersion formula for an assembly of weakly interacting atoms. In Eq. (5.60),  $f_n$  is the electric-dipole oscillator strength associated with transitions at frequency  $\omega_n$ . Therefore, the usefulness of Eq. (5.60) depends on whether real solids obey the single oscillator approximation with reasonable accuracy or the experimentally observed values of the parameters  $f_n$  and  $\omega_n$ . The SO model has been applied to many different types of condensed-matter systems. This method provides a simple connection between the refractive index  $n(\omega)$  and two SO parameters ( $E_0$  and  $E_d$ ) as

$$n^2(\omega) - 1 = \frac{E_0 E_d}{E_0^2 - \omega^2} \quad (5.61)$$

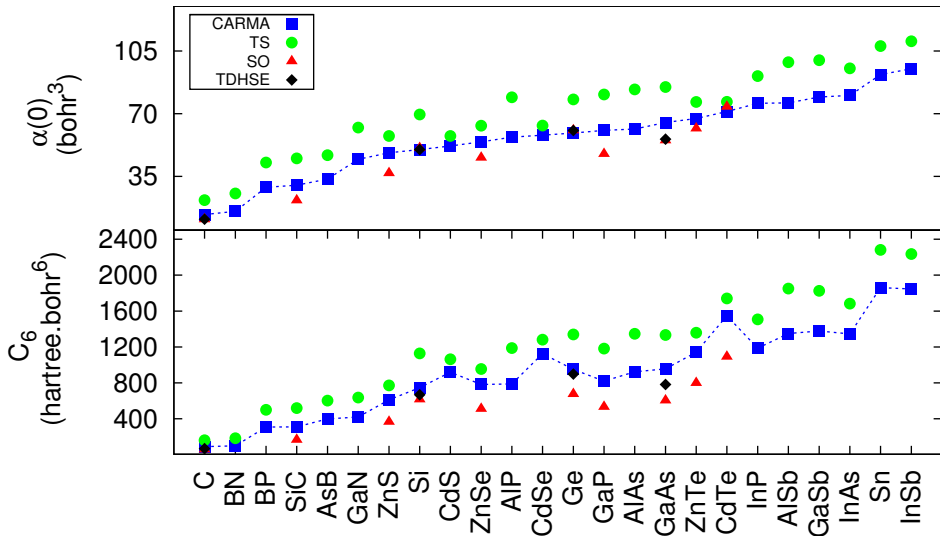
where  $\omega$  is the photon energy,  $E_0$  is the single oscillator energy, and  $E_d$  is the dispersion energy, which is a measure of the strength of interband optical transitions [320]. The SO parameters have fundamental physical meaning the refer to  $E_0$  effective energy gap related to the direct band gap, and  $E_d$  is an interband strength parameter, which is closely related to the chemical-bonding nature of a molecular material. It is clear that the accuracy of the SO model depends greatly upon the accuracy of experimental optical spectra. In reality, reliable optical-spectrum measurement is a difficult task, as a large enough spectral energy range must be measured, which is rarely done. In this section we discuss CARMA model applied to compute the dynamic polarizabilities for 23 non-metallic periodic crystal with cubic symmetry.

Figure (5.8) shows the static polarizabilities and van der Waals  $C_6$  coefficient per unit cell for 23 IIIA–VA group solids (as compiled in Ref. [202] and corresponding values are shown in Table (A.2)). The reference values for static polarizabilities and van der Waals  $C_6$  coefficients per unit cell are obtained using experimental refractive index data [202, 320]. Using the Clausius-Mossotti relation<sup>3</sup>, static polarizabilities and  $C_6$  coefficients per unit cell were then obtained using the single oscillator (SO) approximation [320]. The static polarizabilities and dispersion coefficients have been compared using four approaches: the SO model, the DFT-based CARMA model and the TS method, together with the TD-HSE benchmark, which is only available for the diamond- type solids and GaAs, as shown in Figure (5.8). The TS and CARMA model overestimate static

---

<sup>3</sup> $\alpha_{\text{unitcell}} = \frac{3}{4\pi} V \frac{\epsilon - 1}{\epsilon + 2}$ , Clausius-Mossotti formula which relates the dielectric function  $\epsilon$  to the polarizability, where  $V$  is volume of the cell.

**Figure 5.8:** Calculated static polarizabilities (bohr<sup>3</sup>) and  $C_6$  dispersion coefficients (hartree·bohr<sup>6</sup>) per unit cell for 23 IIIA–VA group solids using the CARMA method, along with TS method and SO model [320]. The TDDFT values are obtained from TDHSE dielectric function [202, 321]. All values are calculated at the experimental unit-cell volumes (as compiled in Ref. [321] and provided in Table (A.2)).



polarizabilities and  $C_6$  coefficients per unit cell with respect to values obtained using SO model which are available for 10 solids. The mean average relative error for static polarizability for 10 solids obtained using the TS method and CARMA model with respect to experimental reference is  $\approx 50\%$  and  $\approx 17\%$ , respectively. The TD-HSE values are accurate, but have a high computational cost. The SO model yields a good prediction for the static polarizability, however,  $C_6$  dispersion coefficients are underestimated due to the limited spectral range of experimental measurements. The TS approach is found to overestimate both the polarizability and dispersion coefficients, in line with its neglect of the electrodynamic screening. Finally, the CARMA model yields good results at a rather low computational cost: the vdW parameters are considerably reduced with respect to the TS results due to the inclusion of the long-range electrodynamic response, resulting in much better agreement with the available TDDFT benchmark data.

## 5.5 Summary

Reliable methods for efficient calculation of the dynamic polarizability of molecules and solids are required for modeling a multitude of spectroscopic techniques, including optical absorption and refraction, Raman spectroscopy, and circular dichroism. Efficient prediction of electronic response properties is also necessary for the calculation of screened exact exchange, van der Waals (vdW) interactions, and coupling between nuclear and electronic degrees of freedom in

materials. In principle, explicit excited-state first-principles techniques could be utilized to determine electronic response properties. However, these methods can be only applied to rather small systems and become prohibitively expensive to study complex materials containing thousands of atoms. To address this problem, we developed an efficient non-empirical method (CARMA) for calculating response properties of non-metallic molecules and solids based on coupled quantum harmonic oscillators (QHO) that describe valence atomic excitations. This is achieved by the synergistic coupling of the Tkatchenko-Scheffler type polarizability for treating short-range hybridization effects with the self-consistent Dyson-like screening (SCS) equation from classical electrodynamics. The present formulation builds upon and significantly improves an earlier version of the TS+SCS approach, by preserving QHO invariants, satisfying the free-atom Thomas-Reiche-Kuhn sum rule, and using the correct spin-polarized electron densities for the free atoms. Using only the ground state electron density obtained from first-principle density functional theory calculation and accurate free-atom reference data, we obtain a performance of 3.6% for static polarizabilities and 7.6% for vdW coefficients for a large database of gas-phase molecules ( $\sim 7500$  systems).

---

# 6

## Scaling laws for van der Waals interactions in nanostructured materials

The discovery and the ensuing burst of applications of carbon-based nanomaterials, including fullerenes [322], carbon nanotubes [323], single-layer and multilayer graphene (MLG) [324], have undoubtedly revolutionized materials science, revealing bright prospects in nanotechnology and other related fields. Low-dimensional nanostructures have been demonstrated to possess previously unexpected electronic [16], optical [325], cohesive [194, 326] and thermal [327] properties. The self-assembly of such nanostructures is often governed by the ubiquitous van der Waals (vdW) interactions, the description of which requires the usage of quantum electrodynamics [33, 55]. Despite this well-known fact, most of the widely employed atomistic models for vdW interactions in nanomaterials are based on a simple pairwise interacting ‘atoms-in-molecules’ picture, ignoring the rather strong electrodynamic response effects, which stem from long-range fluctuations in matter. For example, recent work by Ruzsinszky et al. [326] showed that electrodynamic effects can dramatically influence the vdW interaction between large fullerene molecules.

Here we determine the microscopic polarizability and vdW coefficients of molecules and materials, including electrodynamic response effects, by utilizing a recently developed parameter-free method based on a system of coupled quantum harmonic oscillators (QHO) [7]. This method is applied to a wide range of carbon-based nanomaterials, including fullerenes, carbon nanotubes and nanoribbons, graphite, diamond, as well as single-layer and MLG. Our microscopic calculations, valid at close and far ( $<10\text{ nm}$ ) separations between nanostructures, reveal that vdW interactions act at distances greater than typically assumed and show unusual behaviour depending on the dimensionality of the system. The peculiar vdW scaling laws lead to a decreasing binding energy for a fullerene molecule adsorbed on MLG as a function of the number of graphene layers, contrary to conventional expectations.

## 6.1 Methodology

We represent the  $N$  atoms in a given material as a collection of  $N$  QHO, each of which is characterized initially by an isotropic frequency-dependent dipole polarizability. To account for the local chemical environment, we utilize the Tkatchenko-Scheffler prescription [1], in which the static polarizability,  $\alpha_i^{TS}[n(\mathbf{r})]$ , and the excitation frequency  $\omega_i^{TS}[n(\mathbf{r})]$  for every  $i$ -th QHO are defined as functionals of the ground-state electron density,  $n(\mathbf{r})$ , obtained from a self-consistent quantum mechanical calculation using DFT. We require that the response of the material is not dominated by delocalized excitations and can therefore be initially divided into effective atomic fragments. The Hirshfeld [193] partitioning of the electron density is then utilized to account for the local chemical environment surrounding each atom. As both parameters ( $\alpha_i[n(\mathbf{r})]$  and  $\omega_i[n(\mathbf{r})]$ ) are referenced to highly accurate free-atom reference data, short-range quantum mechanical exchange-correlation effects are accounted for in these quantities by construction. In fact, the frequency-dependent polarizabilities defined in this manner yield  $C_6$  coefficients that are accurate to 5.5% when compared with reference experimental values for an extensive database of atoms and small molecules [1].

To accurately capture the long-range electrodynamic response screening and anisotropy effects beyond the local chemical environment, we self-consistently solve the Dyson-like screening equation (SCS), see equations (2)-(4), in Ref. [7]. In short, we solve the following equation to determine the non-local (interacting) polarizability tensor  $\alpha_{pq}^{SCS}(\mathbf{r}, \mathbf{r}'; i\omega)$ , where  $p$  and  $q$  indicate the Cartesian components of polarizability tensor.

$$\alpha^{SCS}(\mathbf{r}, i\omega) = \alpha^{TS}(\mathbf{r}, i\omega) - \alpha^{TS}(\mathbf{r}, i\omega) \times \int \mathcal{T}_{pq}(\mathbf{r}, \mathbf{r}', i\omega) \alpha^{SCS}(\mathbf{r}, i\omega) d\mathbf{r}', \quad (6.1)$$

where  $\mathcal{T}_{pq}(\mathbf{r}, \mathbf{r}', i\omega)$  is the dipole-dipole interaction tensor. Eq. (6.1) can be written as a system of algebraic equations on the basis of QHO positions. The interacting polarizability tensor  $\alpha_{pq}^{SCS}(\mathbf{r}, \mathbf{r}'; i\omega)$  is obtained upon solving this system of algebraic equations, and in practice amounts to an inversion of a  $3N \times 3N$  matrix at every frequency of interest. The charge density distribution of each QHO required for the calculation of  $\mathcal{T}_{pq}(\mathbf{r}, \mathbf{r}', i\omega)$  is defined as

$$n_0^{\text{QHO}}(\mathbf{r}) = |\psi_0^{\text{QHO}}(\mathbf{r})|^2 = \frac{\exp[-r^2/2\sigma^2(i\omega)]}{(2\pi)^{3/2}\sigma^3(i\omega)}, \quad (6.2)$$

where  $\sigma$  represents the width of the Gaussian. An improvement of the TS+SCS method published in Ref. [7] is used for all the results reported in this paper. The  $\sigma_i^{\text{free}}$  parameter corresponding to every free atom  $i$  is obtained from the electron density computed with the coupled-cluster

singles and doubles (CCSD) method, by fitting the dipole potential resulting from this accurate electron density to a model QHO potential. This allows us to reliably model interactions for interatomic distances beyond  $\sim 0.5$  Å. For an atom in a material, and for each frequency of the electric field, the  $\sigma(i\omega)$  parameter is defined by the aforementioned TS prescription as [328]

$$\sigma_i(i\omega) = \left( \frac{\alpha_i^{\text{TS}}(i\omega)}{\alpha_i^{\text{TS}}(0)} \right)^{1/3} (V_{\text{rel}}^{\text{Hirshfeld}})^{1/3} \sigma_i^{\text{free}}, \quad (6.3)$$

where  $V_{\text{rel}}^{\text{Hirshfeld}}$  is the Hirshfeld volume ratio between an atom-in-a-material and the free atom. This straightforward modification of the TS+SCS method leads to an improved performance for molecular static polarizabilities (7% mean absolute error on more than 7000 organic molecules). The values of the employed parameters were obtained from CCSD calculations for the free carbon atom and DFT electron density calculations for all materials, and they are  $\sigma_C^{\text{free}}=1.514$  bohr,  $V_{\text{rel}}^{\text{Hirshfeld}}=0.911$  for the carbon atom in diamond,  $V_{\text{rel}}^{\text{Hirshfeld}}=0.884$  for graphite, and  $V_{\text{rel}}^{\text{Hirshfeld}}=0.863$  for  $sp^2$ -bonded carbon in all the other materials (slight variations of this value are observed in different nanostructures, but these variations have negligible effect on the final results). All DFT calculations have been performed using the full-potential all-electron real-space code FHI-aims [265]. We employed the PBE functional [277] for all DFT calculations. Special care has been taken to use sufficiently large supercells to eliminate any possible interactions with artificial periodic images for low-dimensional systems. Typically, vacuum sizes of 500 Å were used for this purpose. Such large unit cells do not substantially increase the computational cost in real-space DFT codes. For molecular systems (fullerenes, GNRs), no periodic boundary conditions were employed.

## 6.2 Application of CARMA model to carbon nanostructures

### 6.2.1 Calculation of vdW coefficients

Here only the salient features of our method are described. We refer the reader to ref. [7] and the Methods section for additional details of our approach. We map a given molecule or material to a system of QHO, with a single QHO assigned to every atom. The QHO parameters are determined as functionals of the ground-state electron density, obtained from density-functional theory (DFT) calculation of the self-consistent electronic structure, using the Tkatchenko–Scheffler (TS) method [1]. The QHOs are subsequently coupled through the dipole–dipole potential, and the response of the fully interacting many-

atom system is determined upon solving the self-consistent Dyson-like screening equation [3, 5, 80]. The solution of the self-consistent screening (SCS) equation yields the interacting frequency-dependent polarizability for the system of interest, thus going beyond the standard pairwise approximation. The fundamental equations of the employed method are equivalent to ref. [7], with an improved mapping of the interactions present in the full electronic system to the QHO model. This simple yet effective modification leads to a noticeable improvement in the description of the static polarizability for molecules and solids.

### 6.2.2 vdW coefficients of model systems

Before applying our method to carbon nanostructures, we investigated its performance for fundamental carbon-based model systems: benzene,  $C_{60}$  fullerene, graphite and diamond. For the polarizability and vdW  $C_6$  coefficients of small molecules, such as benzene, the conventional ‘atoms-in-molecules’ picture can be successfully employed. For example, the TS method [1] leads to accurate values of  $\alpha=74.4 \text{ bohr}^3$  and  $C_6=1,783 \text{ hartree}\cdot\text{bohr}^6$  for benzene, compared with reference experimental values of  $\alpha=71.3 \text{ bohr}^3$  and  $C_6=1,723 \text{ a.u.}$  [250, 329] (here and in what follows, the notation ‘a.u.’ is used to denote Hartree atomic units). However, the TS method does not capture the anisotropy in the polarizability [1], which arises mainly from the interaction between the dipoles. Upon including the electrodynamic response by solving the SCS equation, the anisotropy in the static polarizability is significantly improved, whereas the isotropic vdW  $C_6$  coefficient is still accurately determined (1,697 a.u.). Predicting accurate polarizability and  $C_6$  coefficient for the  $C_{60}$  fullerene is a more demanding task because of the coupling between localized  $sp^2$  bonds and excitations delocalized over the  $C_{60}$  molecule. The experimental estimate for the static polarizability of  $C_{60}$  is  $8.6 \pm 0.9 \text{ a.u. per atom}$  [330]. The SCS method somewhat underestimates the static polarizability and yields 7.5 a.u. per atom. This is consistent with the fact that the inclusion of excitations delocalized over the whole molecule will increase the static polarizability of the  $C_{60}$  molecule. However, here our focus lies on the  $C_6$  coefficients, which are obtained upon integration over the imaginary frequency. The ‘metal-like’ delocalized excitations become important only at rather low imaginary frequencies, and their inclusion is not expected to appreciably change our conclusions. In fact, the computed carbon–carbon  $C_6$  coefficient of 24.2 a.u. inside  $C_{60}$  is only slightly lower than the time-dependent hybrid DFT (TDDFT) estimate of 28.3 a.u. [331, 332]. Similarly accurate results are obtained for solids, including graphite and diamond. For graphite, we determine the  $C_6$  coefficient of 28 a.u., which is in good agreement with the estimate done using the experimentally measured dielectric function (24 a.u.) [333]. For diamond, the computed value of 22 a.u. agrees rather well with the value of 17 a.u. determined from the experimental

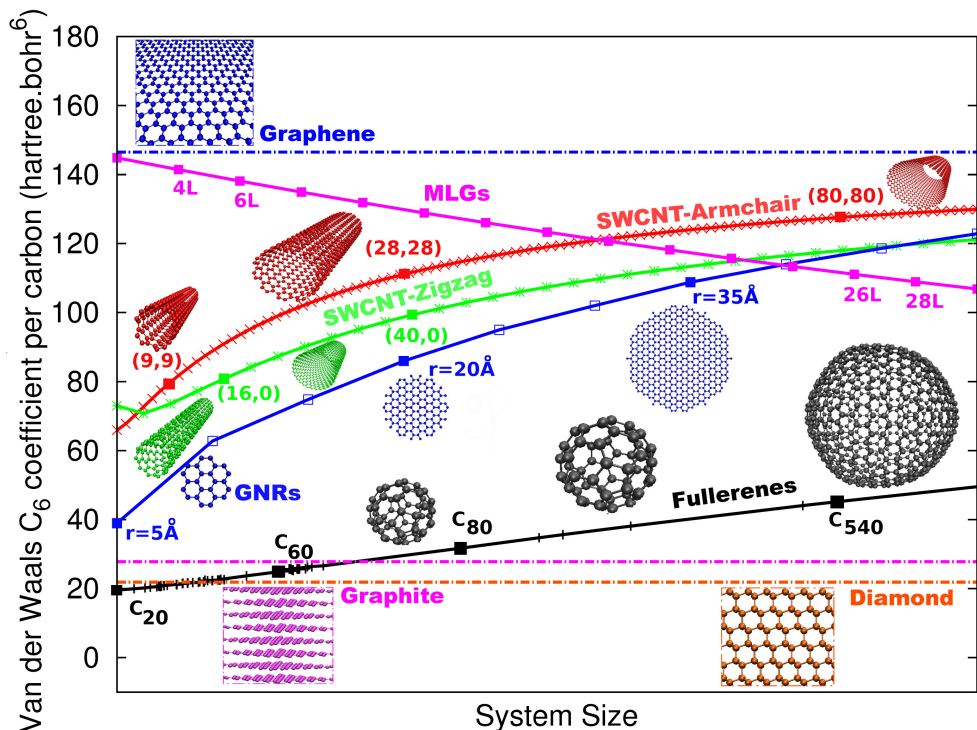
dielectric function [202]. We conclude that our method is capable of accurately describing the frequency-dependent polarization and the resulting vdW  $C_6$  coefficients for a wide range of molecules and solids. We proceed to study the vdW  $C_6$  coefficients for carbon nanostructures of different dimensionality.

### 6.2.3 vdW coefficients of carbon nanostructures

The main results are summarized in Figure (6.1), where we present the  $C_6$  coefficient per carbon atom (see definition in the Methods section) for nanostructures of different dimensionality, including zero-dimensional fullerenes, one-dimensional single-wall carbon nanotubes, two-dimensional single-layer and MLG, and three-dimensional graphite and diamond. The  $C_6$  coefficient per carbon atom varies by almost an order of magnitude among the different nanostructures, with the lowest value found for small fullerenes and the largest for graphene. These findings demonstrate that the conventional approximation of fixed carbon–carbon  $C_6$  coefficient fails dramatically when modelling vdW interactions between nanostructures. The pairwise approximation is especially problematic when the interaction between different nanostructures is studied, for example, binding between fullerenes/nanotubes with graphene layers or graphite surface (see below).

We proceed to analyse the  $C_6$  per carbon atom as a function of system size for different classes of nanostructures. For the fullerene family, the system size is defined by the fullerene radius. Therefore, as shown in Figure (6.1), the  $C_6$  coefficient increases linearly as a function of the fullerene radius. This leads to the following fitted scaling power law as a function of the number of carbon atoms  $n$ ,  $C_6^{C-C} \approx n^{2.35}$ . In contrast, a simple pairwise approximation predicts  $C_6^{C-C} \approx n^2$ . The faster growth of  $C_6$  coefficients upon including electrodynamic response can be explained by the polarization (depolarization) inside the fullerene (vacuum) when increasing the fullerene radius. In fact, in the limit of giant fullerenes, the  $C_6$  per carbon should approach that of a carbon atom in a graphene layer. However, local curvature effects clearly reduce the polarizability even for quite large fullerenes. The rapid increase of  $C_6$  is in qualitative agreement with recent calculations based on a representation of a fullerene as a hollow metallic sphere, in which it was found that in the asymptotic regime of giant fullerenes,  $C_6^{C-C}$  grows as  $n^{2.75}$  (ref. [326]). The smaller exponent found in our work stems from a fit to smaller fullerene sizes and from the fact that every carbon atom is modelled as a QHO. We consider this atomistic representation as more realistic compared with modeling fullerenes as hollow metallic spheres. In fact, recent TDDFT calculations suggest a scaling power law of  $n^{2.2}$  for of fullerenes from  $C_{60}$  to  $C_{84}$  (ref. [332]). Our model yields a very good agreement with TDDFT for these small fullerenes, predicting a scaling of  $n^{2.25}$ . In conclusion, three different

**Figure 6.1:** vdW  $C_6$  coefficients per carbon atom (the  $C_6$  of the full system divided by  $N_C^2$ , where  $N_C$  is the number of carbon atoms) for nanostructures of different dimensionality, as calculated by the electrodynamic response model of ref. [7]. The size ranges for different systems are as follows: (1) the radius of fullerenes is varied from 2 to 12 Å; (2) the radius of single-wall carbon nanotubes (SWCNT)-Armchair( $n,n$ ) and SWCNT-Zigzag( $n,0$ ) vary between 2 and 60 Å; (3) the graphene nanoribbons (GNRs) vary in radius from 5 to 50 Å; (4) the number of layers in multilayer graphene (MLG) varies from 2 to 30, where each point on the plot corresponds to an increase of two layers



methods unambiguously demonstrate that the coefficient grows much faster in fullerenes than a simple pairwise model would suggest.

For graphene nanoribbons (GNRs), the system size is defined by the radius of the circle enclosing the GNR. In contrast to fullerenes, the  $C_6$  coefficients of GNRs increase superlinearly as a function of the GNR radius. There are significant edge-polarization effects in GNRs, which lead to larger polarizability density as one goes away from the centre of the GNR towards the edges. This behaviour is explained by stronger polarization of ‘less constrained’ edge atoms. As expected, the  $C_6$  coefficients of GNRs tend to that of single-layer graphene as the GNR size grows.

Similar to the case of GNRs, the  $C_6$  coefficients of single-walled carbon nanotubes (SWCNTs) grow superlinearly as a function of the SWCNT radius. The vdW coefficients also depend on the chirality of the SWCNTs, in general increasing faster for armchair nanotubes than for zigzag ones. The superlinear increase of the  $C_6$  coefficient for SWCNTs stems from the remarkable axial polarization that arises

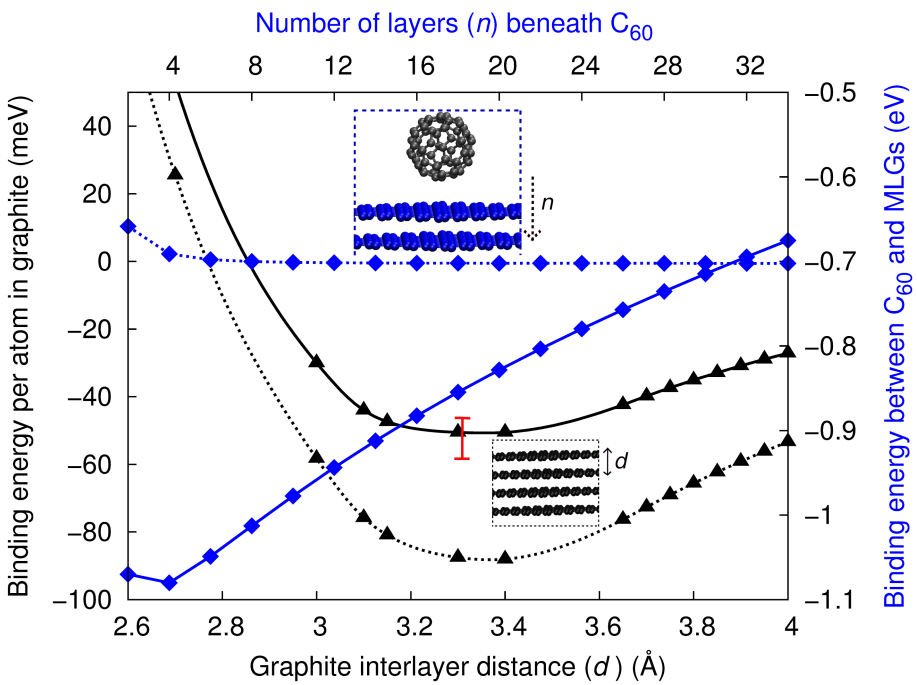
from the favourable alignment of the dipoles along the SWCNT axis. In contrast, we find depolarization in the direction perpendicular to the SWCNT. Both of these findings are in agreement with DFT calculations [334]. However, our method is significantly more efficient and allows the calculation of the microscopic polarization tensor even for very large nanostructure assemblies containing many thousands of atoms. Not unexpectedly, even more remarkable behaviour is noticeable for single-layer graphene and MLG nanostructures. The carbon–carbon  $C_6$  coefficient of 147 a.u. in two-dimensional graphene is 5.3 times larger than that of three-dimensional graphite. This can be rationalized by a substantial in-plane polarization in graphene on the expense of depolarization in the direction perpendicular to the graphene layer. In contrast, the interplay of interlayer and intralayer polarization leads to a smaller  $C_6$  coefficient for carbon in graphite. Notably, the convergence of the  $C_6$  coefficient from the graphene limit to the graphite limit is exceedingly slow as a function of the number of graphene layers for MLGs. We observe a linear behaviour for up to 30 stacked graphene layers, and a naive linear extrapolation suggests that at least 90 graphene layers would be required to converge the carbon–carbon  $C_6$  coefficient to the graphite limit. From the geometry point of view, such an unusually slow convergence stems from noticeable surface polarization effects for MLGs. Physically, this behaviour can be explained by the self-consistent nature of electrodynamic response equations that effectively couple all the interacting QHOs, leading to effects that propagate much further beyond the decay of the standard dipole–dipole  $\sim R_{AB}^{-3}$  interaction law, where  $R_{AB}$  is the distance between two QHOs.

#### 6.2.4 vdW binding between carbon nanostructures

Having presented the peculiar scaling laws for vdW coefficients in different carbon nanostructures, we now study the impact of our findings for the interlayer-binding energy in graphite and the  $C_{60}$  fullerene interacting with MLGs. The interlayer-binding energy of graphite has been a subject of intense investigation over the last decade. Experimental measurements yield values from  $31 \pm 2$  meV (ref. [335]) to  $52 \pm 5$  meV (ref. [336]) per carbon atom. State-of-the-art theoretical calculations using the random-phase approximation (utilizing Perdew–Burke–Ernzerhof (PBE) [277] wavefunctions) to the electron correlation energy predicts a value of 48 meV per atom [337], whereas quantum Monte Carlo calculations yield a larger value of 56 meV per atom [338]. The interlayer binding in graphite has been frequently approximated as a sum of pairwise potentials with vdW  $C_6$  coefficients obtained using the experimental dielectric function of graphite (24 a.u.) or explicitly fitted to experimental measurements. Such a simple approximation assumes that the carbon–carbon  $C_6$  coefficient is the same in graphene and graphite, and this result is

far from reality as clearly illustrated in Figure (6.1) Electrodynamic response effects lead to radically different polarization behaviour in two-dimensional graphene and three-dimensional graphite. In Fig. 6.2, the

**Figure 6.2:** Graphite interlayer-binding energy as a function of the interlayer distance  $d$  using the PBE functional with TS pairwise vdW energy (PBE-TS, dotted black line, triangles) and PBE with self-consistently screened (SCS) vdW energy (PBE-TS+SCS, solid black line, triangles). The measured experimental-binding energy from ref. 25 is marked in red. Binding energy of  $C_{60}$  fullerene on multilayered graphene as a function of number of graphene layers, using PBE-TS (dotted blue line, diamonds) and PBE-TS+SCS (solid blue line, diamonds) methods. The centre of the  $C_{60}$  molecule is located 7.5 Å away from the closest graphene sheet.



interlayer-binding energy of graphite is presented as a function of the distance between the layers. The pairwise approximation using the PBE-TS method overestimates the binding considerably, by at least 30 meV per atom. Accurate inclusion of electrodynamic response screening in the PBE-TS+SCS method leads to interlayer-binding energy that agrees exceptionally well with the measurements of Zacharia et al. [336], as well as random-phase approximation [337] and quantum Monte Carlo [338] calculations. The important improvement of the binding energy in the PBE-TS+SCS method stems from a much larger  $C_6$  coefficient of graphene when compared with graphite. This results in an increased vdW energy contribution for a carbon atom inside graphene and a concomitantly smaller interlayer-binding energy.

Finally, we illustrate how the peculiar scaling laws for vdW coefficients in nanomaterials can lead to unusual binding behaviour between nanostructures of different dimensionality. The binding energy of a fullerene on MLGs is shown in Fig. 6.2 as a function of number

( $n$ ) of graphene layers beneath the fullerene. Conventionally, one would expect the binding energy to increase with  $n$ , as shown by the dotted blue curve in Fig. 6.2, as there are more atoms to interact with (presumably equal to more polarization). In addition, a simple pairwise model would lead to a quick convergence of the binding energy with respect to  $n$  because of a rather quick  $R_{AB}^{-6}$  decay of the pairwise vdW energy for two atoms A and B. This simple view is, however, deceptive. In fact, as  $n$  increases, the polarizability and  $C_6$  per carbon atom in MLGs decrease (see Fig. 6.1). This leads to overall depolarization of the fullerene/MLG complex, and shows a decreasing binding energy with increasing  $n$ . As the convergence of the  $C_6$  coefficient with  $n$  is rather slow, the binding energy also converges slowly. We remark that a fully anisotropic treatment of the vdW interactions is probable to decrease the slope of the binding energy curve for  $C_{60}$  on MLGs. However, it is noteworthy that the pairwise and the fully screened vdW energy converge to different values of the binding energy, with the latter yielding somewhat weaker binding. This is consistent with our observations for the graphite interlayer-binding energy. We are not aware of direct experimental measurements for the binding energy of fullerene with graphite; however, we expect similar findings as for the graphite interlayer binding, where the PBE-TS+SCS method yields more accurate results than a simple pairwise approximation to the vdW energy. The rather unconventional behaviour of the binding energy for adsorption on MLGs with the number of layers  $n$  is a general phenomenon for a variety of adsorbates, ranging from small molecules to larger objects.

### 6.3 Discussion

To place our findings in the broader context of current understanding of vdW interactions, we note that it is widely accepted that these interactions are inherently non-additive (many-body) phenomena, corresponding to correlations between fluctuating multipoles in matter [33]. Interested readers are referred to the previous papers by Axilrod and Teller [339], Bade [284] and Zwanzig [340] for the analysis and explanations of many-body contributions to vdW interactions. The seminal ideas proposed in this previous work to treat vdW interactions beyond simple pairwise additivity have been utilized more recently to study model systems, characterized by point polarizabilities, see for example, the analysis by Cole [285], Donchev [205] and Dobson [286] among others. The crucial idea of our method is to extend the description from point-polarizable fluctuating dipoles to QHO extended in space and described by dipole density distributions (see Methods and ref. [6]). All the necessary parameters are determined from the self-consistent electron density using state-of-the-art electronic structure calculations, apart from the available high-level reference data for

atomic polarizabilities [7]. The efficiency and accuracy of our methods make it possible to carry out calculations on a broad variety of real materials. Recently, our methods have been implemented in the widely used VASP code [341] and benchmarked for a set of pristine three-dimensional solids. In this work, we significantly extend previous observations on the importance of electrodynamic response effects to more general nanostructures of lower dimensionality, including the interaction between different nanostructures. The coupled QHO model assumes that the material can be initially partitioned into well-defined atomic fragments. Thus, the possibility of hopping of electrons over long distances is neglected. The coupling of screening and such delocalized electrons can lead to other types of non-additivity not addressed in this work. For example, Dobson et al. [194] and Misquitta et al. [342] have identified peculiar asymptotic power laws for the interaction between low-dimensional materials. Subsequently, it has been found that these effects contribute very little at equilibrium separations between nanostructures [337]. The incorporation of delocalized electrons into the coupled QHO model will be a subject of future work. In conclusion, we have identified an unusual behaviour caused by electrodynamic response in vdW interactions for nanostructured materials. Depending on the dimensionality and the atomic arrangement of carbon atoms, the vdW coefficients per carbon atom exhibit peculiar scaling laws that can be exploited for controlling the self-assembly of complex nanostructures, as recently suggested by experimental measurements [343, 344].

## Towards efficient modeling of long-range interactions in nanoscale systems

Efficient and accurate treatment of polarization has remained a theoretical challenge. The polarization properties of molecules or materials are useful in the description of various physical properties as well as van der Waals (vdW) interactions. The first challenge we encountered was exploring computational tools that should be affordable for the calculation of vdW interactions in complex materials. An important concept in the description of vdW interactions is the density-density response function. The correlation energy of many-body system can be obtained using the response function via the adiabatic-connection fluctuation-dissipation theorem (ACFDT) [64, 65]. The response function is usually calculated from the Kohn-Sham energies and orbitals. However, this is computationally expensive, therefore more efficient alternative approaches are required.

In Chapter (5), we have introduced a coarse-grained (CG) electrodynamic model (CARMA) of electronic polarization in materials. In this approach, the (interacting) response function,  $\chi^{\text{CG}}(\mathbf{r}, \mathbf{r}', i\omega)$ , is derived starting from spatially partitioned atomic response functions as functional of the electron density. The accuracy and efficiency of CARMA model has been demonstrated by calculating the polarizability and vdW coefficients of a wide range of systems including molecules and non-metallic solids compared with accurate reference data. Moreover in Chapter (6), we have applied CARMA model to determine the microscopic polarizability and asymptotic van der Waals (vdW)  $C_6$  coefficients of a wide range of carbon-based nanomaterials, including fullerenes, carbon nanotubes and nanoribbons, graphite, diamond, as well as single-layer and multi-layer graphene. Furthermore, we have identified unique scaling laws in vdW interactions for nanostructured materials. The vdW coefficients depend on the dimensionality and the atomic arrangement of carbon atoms and demonstrate the importance of treating vdW interactions beyond simple pairwise additivity approximation.

Here we briefly discuss the possible improvements for the electrodynamic response model, which would extend it to an even wider range of important materials at the nanoscale.

The CARMA model discussed in Chapter (5) yields the full non-local interacting response matrix as a function of quantum harmonic oscillators (QHOs) positions. The QHO model possesses a response to infinite order in the multipole expansion. The current model restricts the response to the dipole approximation, effectively allowing excitations only to the first excited state for every QHO due to the dipole selection rule. In principle, the full response function can be computed for a system of QHOs up to an arbitrary energy cutoff for the excited states. This would allow us to treat multipole responses higher than dipole (quadrupole, octupole, etc.). The CARMA model can also be extended to represent every atom by several QHOs. The primary challenge we encounter in calculating dynamic polarizability of complex solid-state materials (with many thousands of atoms) is the computational bottleneck of matrix inversion. The matrix inversion problem can be cast in term of a generalized eigenvalue problem. Moreover, the linear algebra library such as eigenvalue solvers for petaflop-applications ELPA [345] coupled with CARMA model allows calculating polarizability tensor for systems with many thousands of atoms on modern computational hardware. Furthermore, the present coarse-grained representation of the response function can be extended to include oscillators which mimic charge hopping between atomic sites (metallic excitations) [70–72].

---

# 8

## Summary and Conclusions

Understanding the physical mechanism that connects polarization properties of *bio* or *nano* structures is an ongoing and interdisciplinary challenge. In principle, explicit excited-state first-principles techniques could be utilized to determine electronic polarization properties of materials. However, these methods are computationally expensive. In the present work, we have developed an efficient scheme for modeling linear electronic polarization using atomic response functions. This model is a (synergistic) coupling of classical electrodynamics with quantum mechanical input data and the electron density obtained using density functional theory calculations. The accuracy of results obtained using this model has been verified by comparing them with experimental as well as theoretically derived spectroscopic constants, such as electric static polarizability and asymptotic dipole-dipole van der Waals coefficients. Moreover, the electrodynamic response model has been applied to wide range of Carbon based materials depending on the dimensionality and the atomic arrangement of Carbon atoms at the nanoscale, yielding important insights into the capabilities and limitations of current theoretical tools in predicting polarization properties of materials. The present coarse-grained can be also extended for modeling various spectroscopic techniques, including optical absorption and refraction, Raman spectroscopy, and circular dichroism. Efficient prediction of electronic response function is also necessary for the calculation of screened exact exchange, van der Waals (vdW) interactions, and coupling between nuclear and electronic degrees of freedom in materials.



---

## List of Figures

1.1	Schematic representation of the applicability of current theoretical tools used to calculate electronic properties for matter ranging from atoms, molecules to proteins, nanostructures, and other complex materials. . . . .	3
4.1	A) Correlation plots for van der Waals $C_6$ coefficients computed using LR-CCSD method with respect to accurate DOSD results from the experiments for 1128 pairs of inter-molecular, $C_6^{AB}$ coefficient. B) The relative error for $C_6$ coefficients derived using LR-CCSD theory with respect to DOSD values for 1128 pairs (including atom-atom, atom-molecule and molecule-molecule interaction). . . . .	59
4.2	A. Correlation plot for isotropic static molecular polarizability for 238 organic molecules from experiments compared with HF, LDA, PBE, PBE0 and TS method. B) The distribution relative errors (x-axis) for all molecules using HF, LDA, PBE, PBE0 and TS method with respect to experimental polarizabilities. The y-axis indicates corresponding polarizabilities of all molecules normalized to unity with respect to isotropic polarizability of the largest molecule. . . . .	61
5.1	Schematic representation of the density distribution of conducting sphere model having uniform density within radius $R$ (blue circle) and one dimensional representation of charge density of a QHO (black curve). The shaded green region indicate the density of QHO outside certain radius $R$ due to continuous charge distribution. . . . .	73

- 5.2 Schematic illustration of two interacting ARFs in a material having Gaussian variance  $\sigma_p$  and  $\sigma_q$ . The effective dipole correlation length at short distances is given by Gaussian having variance  $\sigma_{pq} = \sqrt{\sigma_p^2 + \sigma_q^2}$  centered between QHOs  $p$  and  $q$ . In the limit  $\sigma_{pq} \rightarrow 0$  tends to point dipole approximation. . . . . 80
- 5.3 The potential from the spherical Gaussian distribution of unit charge with exponent  $\sigma = 1$  (dashed red curve),  $\text{erf}(r)/r$ , plotted as function of the distance from the center of the charge distribution and compared with the corresponding potential from a point charge  $1/r$  (thick black curve) along with the  $\text{erf}(r)$  error function (dashed blue curve). . . . . 81
- 5.4 The x-label indicate atomic number  $Z$ , while the y-axis shows the effective valence electron  $\mathcal{N}_{\text{valence}}$  in an atomic species (excluding core electrons) and the oscillator strength  $f_p$  defined in Eq. (5.22) derived using accurate free atom reference parameters (see Table (A.1)) . . . . . 87
- 5.5 The plot shows the convergence of static polarizability and  $\mathcal{N}_e$  sum rule for benzene obtained using dipole strength function. Each point in curve is integral in Eq. (5.55) and Eq. (5.54) up to energy  $\omega$ . . . . . 89
- 5.6 Correlation of electronic  $f$ -sum rules obtained from TDDFT calculation compared with CARMA model (black circle) and TS method (blue triangle). . . . . 90
- 5.7 A) The plot shows the distribution of relative errors for isotropic static polarizability of 7449 molecules calculated using TS (green-triangles), TS+SCS (red-squares) and CARMA model (blue-circles) on the reference PBE0 polarizabilities. B) The plot shows distribution of relative error for  $C_6^{AB}$  coefficients of 1225 pairs of atoms and molecules calculated using TS, TS+SCS and CARMA model on experimentally derived vdW coefficients. . . . . 92
- 5.8 Calculated static polarizabilities ( $\text{bohr}^3$ ) and  $C_6$  dispersion coefficients (hartree· $\text{bohr}^3$ ) per unit cell for 23 IIIA–VA group solids using the CARMA method, along with TS method and SO model [320]. The TDDFT values are obtained from TDHSE dielectric function [202, 321]. All values are calculated at the experimental unit-cell volumes (as compiled in Ref. [321] and provided in Table (A.2)). . . . . 95

- 6.1 vdW  $C_6$  coefficients per carbon atom (the  $C_6$  of the full system divided by  $N_C^2$ , where  $N_C$  is the number of carbon atoms) for nanostructures of different dimensionality, as calculated by the electrodynamic response model of ref. [7]. The size ranges for different systems are as follows: (1) the radius of fullerenes is varied from 2 to 12 Å; (2) the radius of single-wall carbon nanotubes (SWCNT)-Armchair( $n,n$ ) and SWCNT-Zigzag( $n,0$ ) vary between 2 and 60 Å; (3) the graphene nanoribbons (GNRs) vary in radius from 5 to 50 Å; (4) the number of layers in multilayer graphene (MLG) varies from 2 to 30, where each point on the plot corresponds to an increase of two layers . . . . . 102
- 6.2 Graphite interlayer-binding energy as a function of the interlayer distance  $d$  using the PBE functional with TS pairwise vdW energy (PBE-TS, dotted black line, triangles) and PBE with self-consistently screened (SCS) vdW energy (PBE-TS+SCS, solid black line, triangles). The measured experimental-binding energy from ref. 25 is marked in red. Binding energy of  $C_{60}$  fullerene on multilayered graphene as a function of number of graphene layers, using PBE-TS (dotted blue line, diamonds) and PBE-TS+SCS (solid blue line, diamonds) methods. The centre of the  $C_{60}$  molecule is located 7.5 Å away from the closest graphene sheet. . . . . 104
- B.1 Convergence of the (isotropic) static polarizability (y-axis) for  $H_2$ ,  $N_2$ ,  $HCl$  and  $CO$  molecules calculated based on finite-differences with varying external perturbing field (x-axis). The prefix "E" in legends indicate finite-differences derivative with the total electronic energy and "D" with the induce dipole moment. Whereas, *tier1* and *tier2* are NAO basis functions and "d" indicate diffuse function from d-aug-cc-pVQZ basis set. The experimental values for isotropic polarizabilities are taken from Ref. [250]. . . . . 126



---

## List of Tables

4.1	The isotropic polarizability $\alpha_{\text{iso}}$ , along with its three components $\alpha_{xx}$ , $\alpha_{yy}$ and $\alpha_{zz}$ (in bohr <sup>3</sup> ) for benzene molecule calculated using LR-CCSD method (in bohr <sup>3</sup> ) . . . . .	57
4.2	The isotropic polarizability $\alpha_{\text{iso}}$ , along with its three components $\alpha_{xx}$ , $\alpha_{yy}$ and $\alpha_{zz}$ (in bohr <sup>3</sup> ) for a database of molecules calculated using LR-CCSD method along with experimental reference data taken from Ref. [5, 269]. . . . .	58
5.1	The value of variance of dipole density distribution $\sigma^{\text{free}}$ for few neutral free atoms (in bohr) . . . . .	81
5.2	The isotropic static polarizability and vdW $C_6$ coefficients for the linear (H <sub>2</sub> ) <sub>3</sub> chain calculated using the TS, CARMA and LR-CCSD levels of theory. The $\alpha_{\perp}$ and $\alpha_{\parallel}$ components of polarizability are defined with respect to the principal axis of the linear (H <sub>2</sub> ) <sub>3</sub> chain. The static polarizabilities are defined in Bohr <sup>3</sup> and the vdW coefficients are defined in Hartree·Bohr <sup>6</sup> . . . . .	91
A.1	The recommended values for isotropic static polarizability, $\alpha^{\text{free},A}$ (in bohr <sup>3</sup> ), the homo-atomic van der Waals coefficient, $C_6^{\text{free},AA}$ (in hartree · bohr <sup>6</sup> ), and vdW Radii, $R_{\text{vdW}}^{\text{free},A}$ (in bohr) for neutral free atoms. The vdW Radii, $R_{\text{vdW}}^{\text{free},A}$ for respective elements are defined as discussed in Ref. [1] . . . . .	120
A.2	The isotropic static polarizability $\alpha(0)$ (in bohr <sup>3</sup> ) and van der Waals $C_6$ coefficients (in hartree · bohr <sup>6</sup> ) calculated using the CARMA method for 23 semiconductor solids (per primitive unit cell containing two atoms). The lattice constants are taken from the references cited in the table. . . . .	121

A.3 The isotropic static polarizability, $\alpha(0)$ (in bohr <sup>3</sup> ), and van der Waals $C_6$ coefficient (in hartree·bohr <sup>6</sup> ) for molecules calculated using linear response CCSD method. The experimental values for isotropic static polarizabilities are taken from Ref. [250]. The values for $C_6^{\text{DOSD}}$ coefficient are taken from experimental dipole oscillator strength distributions (DOSD) data. [252–264]	121
A.4 The isotropic polarizability $\alpha_{\text{iso}}$ for a dataset of 238 molecule calculated using various methods (in bohr <sup>3</sup> ). The experimental values for isotropic static polarizabilities are taken from Ref. [250]. . . . .	122

## **Appendices**



---

A

**Static polarizabilities and asymptotic vdW  
 $C_6$  coefficients for atoms and molecules**

**Table A.1:** The recommended values for isotropic static polarizability,  $\alpha^{\text{free,A}}$  (in bohr<sup>3</sup>), the homo-atomic van der Waals coefficient,  $C_6^{\text{free,AA}}$  (in hartree · bohr<sup>6</sup>), and vdW Radii,  $R_{\text{vdW}}^{\text{free,A}}$  (in bohr) for neutral free atoms. The vdW Radii,  $R_{\text{vdW}}^{\text{free,A}}$  for respective elements are defined as discussed in Ref. [1].

Element	$C_6^{\text{free,AA}}$	$\alpha^{\text{free,A}}$	$R_{\text{vdW}}^{\text{free,A}}$	Ref.	Element	$C_6^{\text{free,AA}}$	$\alpha^{\text{free,A}}$	$R_{\text{vdW}}^{\text{free,A}}$	Ref.
H	6.50	4.50	3.10	[195]	Te	396.00	37.65	4.22	a
He	1.46	1.38	2.65	[195]	I	385.00	35.00	4.17	a
Li	1387.00	164.20	4.16	[346]	Xe	285.90	27.30	4.08	a
Be	214.00	38.00	4.17	[195]	Cs	6582.08	427.12	3.78	[346]
B	99.50	21.00	3.89	[195]	Ba	5727.00	275.00	4.77	a
C	46.60	12.00	3.59	[195]	La	3884.50	213.70	3.14	b
N	24.20	7.40	3.34	[195]	Ce	3708.33	204.70	3.26	b
O	15.60	5.40	3.19	[195]	Pr	3911.84	215.80	3.28	b
F	9.52	3.80	3.04	[195]	Nd	3908.75	208.40	3.30	b
Ne	6.38	2.67	2.91	[195]	Pm	3847.68	200.20	3.27	b
Na	1556.00	162.70	3.73	[346]	Sm	3708.69	192.10	3.32	b
Mg	627.00	71.00	4.27	[195]	Eu	3511.71	184.20	3.40	b
Al	528.00	60.00	4.33	[195]	Gd	2781.53	158.30	3.62	b
Si	305.00	37.00	4.20	[195]	Tb	3124.41	169.50	3.42	b
P	185.00	25.00	4.01	[195]	Dy	2984.29	164.64	3.26	b
S	134.00	19.60	3.86	[195]	Ho	2839.95	156.30	3.24	b
Cl	94.60	15.00	3.71	[195]	Er	2724.12	150.20	3.30	b
Ar	64.30	11.10	3.55	[195]	Tm	2576.78	144.30	3.26	b
K	3897.00	292.90	3.71	[346]	Yb	2387.53	138.90	3.22	b
Ca	2221.00	160.00	4.65	[195]	Lu	2371.80	137.20	3.20	b
Sc	1383.00	120.00	4.59	[195]	Hf	1274.80	99.52	4.21	a
Ti	1044.00	98.00	4.51	[195]	Ta	1019.92	82.53	4.15	a
V	832.00	84.00	4.44	[195]	W	847.93	71.04	4.08	a
Cr	602.00	78.00	3.99	[195]	Re	710.20	63.04	4.02	a
Mn	552.00	63.00	3.97	[195]	Os	596.67	55.06	3.84	a
Fe	482.00	56.00	4.23	[195]	Ir	359.10	42.51	4.00	a
Co	408.00	50.00	4.18	[195]	Pt	347.10	39.68	3.92	a
Ni	373.00	48.00	3.82	[195]	Au	298.00	36.50	3.86	a
Cu	253.00	42.00	3.76	[195]	Hg	392.00	33.90	3.98	a
Zn	284.00	40.00	4.02	[195]	Tl	717.44	69.92	3.91	a
Ga	498.00	60.00	4.19	[195]	Pb	697.00	61.80	4.31	a
Ge	354.00	41.00	4.20	[195]	Bi	571.00	49.02	4.32	a
As	246.00	29.00	4.11	[195]	Po	530.92	45.01	4.10	a
Se	210.00	25.00	4.04	[195]	At	457.53	38.93	4.07	a
Br	162.00	20.00	3.93	[195]	Rn	390.63	33.54	4.23	a
Kr	129.60	16.80	3.82	[195]	Fr	4224.44	317.80	3.90	a
Rb	4691.00	319.20	3.72	[346]	Ra	4851.32	246.20	4.98	a
Sr	3170.00	199.00	4.54	[195]	Ac	3604.41	203.30	2.75	b
Y	1968.58	126.74	4.82	a	Th	4047.54	217.00	2.85	b
Zr	1677.91	119.97	4.53	a	Pa	2367.42	154.40	2.71	b
Nb	1263.61	101.60	4.24	a	U	1877.10	127.80	3.00	b
Mo	1028.73	88.42	4.10	a	Np	2507.88	150.50	3.28	b
Tc	1390.87	80.08	4.08	a	Pu	2117.27	132.20	3.45	b
Ru	609.75	65.89	4.00	a	Am	2110.98	131.20	3.51	b
Rh	469.00	56.10	3.95	a	Cm	2403.22	143.60	3.47	b
Pd	157.50	23.68	3.66	a	Bk	1985.82	125.30	3.56	b
Ag	339.00	50.60	3.82	a	Cf	1891.92	121.50	3.55	b
Cd	452.00	39.70	3.99	a	Es	1851.10	117.50	3.76	b
In	707.05	70.22	4.23	a	Fm	1787.07	113.40	3.89	b
Sn	587.42	55.95	4.30	a	Md	1701.00	109.40	3.93	b
Sb	459.32	43.67	4.28	a	No	1578.18	105.40	3.78	b

<sup>a</sup>Present work linear response coupled cluster singles and doubles (LR-CCSD).

<sup>b</sup>For lanthanides and actinide, the  $C_6^{\text{free,AA}}$  coefficients are constructed to satisfy valence electronic sum rule using the static polarizabilities from Ref [347].

**Table A.2:** The isotropic static polarizability  $\alpha(0)$  (in bohr<sup>3</sup>) and van der Waals  $C_6$  coefficients (in hartree · bohr<sup>6</sup>) calculated using the CARMA method for 23 semiconductor solids (per primitive unit cell containing two atoms). The lattice constants are taken from the references cited in the table.

	$\alpha(0)$						$C_6$					
	TS	SO [320]	TDHSE [202]	RPA@PBE	TS+SCS	CARMA	TS	SO [320]	TDHSE [202]	RPA@PBE	TS+SCS	CARMA
C [348]	21.8	11.0	11.1	11.0	14.1	13.7	160.4	58.0	66.9	63.1	89.5	86.7
BN [349]	25.5	-	-	9.9	16.1	15.3	183.4	-	-	54.2	99.0	93.8
BP [350]	42.7	-	-	27.1	28.6	28.8	499.7	-	-	246.6	292.1	299.1
SIC [351]	45.0	21.6	-	21.6	28.6	29.9	518.8	164.9	-	174.2	280.8	298.9
AsB [352]	46.8	-	-	32.1	32.5	33.4	602.4	-	-	329.3	370.6	388.4
GaN [351]	62.3	-	-	22.2	35.0	44.2	637.2	-	-	162.6	309.6	405.2
ZnS [353]	57.6	36.8	-	-	44.0	48.2	771.8	365.7	-	-	535.9	603.0
Si [354]	69.5	50.8	50.0	50.8	47.7	49.8	1128.4	615.9	667.9	639.1	676.1	726.7
Cds [355]	57.6	-	-	-	48.0	51.9	1063.3	-	-	-	819.8	912.0
ZnSe [356]	63.3	45.4	-	48.2	48.9	54.4	955.3	509.8	-	616.0	673.6	773.8
AlP [357]	79.2	-	-	44.8	52.8	56.7	1187.4	-	-	523.0	689.8	765.2
CdSe [355]	63.3	-	-	62.7	52.7	58.0	1282.2	-	-	875.0	986.7	1118.1
Ge [354]	77.9	60.7	60.6	68.1	53.6	59.0	1339.5	675.6	897.9	926.9	805.9	928.7
GaP [357]	80.7	47.5	-	48.0	53.0	60.5	1182.2	532.4	-	586.5	675.0	800.1
AlAs [357]	83.5	-	-	52.1	56.8	61.2	1347.0	-	-	675.0	804.1	898.5
GaAs [357]	84.9	55.1	55.8	59.6	57.1	65.0	1334.0	604.0	781.9	766.2	787.2	934.9
ZnTe [358]	76.5	61.7	-	64.8	59.3	67.3	1359.3	797.8	-	981.1	964.3	1131.8
CdTe [355]	76.6	73.9	-	76.5	63.6	71.3	1740.2	1091.2	-	1273.6	1337.0	1539.8
InP [357]	91.0	-	-	61.5	64.0	75.9	1507.9	-	-	808.1	937.3	1169.2
AlSb [357]	98.7	-	-	70.7	68.6	75.9	1850.8	-	-	1088.4	1135.9	1320.9
GaSb [357]	99.8	-	-	80.8	68.1	79.2	1825.7	-	-	1215.5	1098.9	1353.4
InAs [357]	95.3	-	-	74.2	67.8	80.1	1682.9	-	-	1026.0	1063.5	1325.1
Sn [351]	107.8	-	-	98.6	77.5	91.6	2282.0	-	-	1739.7	1456.0	1835.6
InSb [357]	110.4	-	-	94.4	79.2	95.1	2235.6	-	-	1550.1	1426.7	1823.4

**Table A.3:** The isotropic static polarizability,  $\alpha(0)$  (in bohr<sup>3</sup>), and van der Waals  $C_6$  coefficient (in hartree·bohr<sup>6</sup>) for molecules calculated using linear response CCSD method. The experimental values for isotropic static polarizabilities are taken from Ref. [250]. The values for  $C_6^{\text{DOSD}}$  coefficient are taken from experimental dipole oscillator strength distributions (DOSD) data. [252–264]

	$\alpha^{\text{Exp}}(0)$	$\alpha^{\text{LRCCSD}}(0)$	$C_6^{\text{DOSD}}$	$C_6^{\text{LRCCSD}}$
SO <sub>2</sub>	25.1	32.9	293.9	369.5
SiH <sub>4</sub>	36.7	32.0	343.9	335.2
NH <sub>3</sub>	14.2	14.6	89.0	86.1
N <sub>2</sub> O	20.7	24.2	184.9	231.6
N <sub>2</sub>	11.5	11.8	73.3	71.4
HF	5.4	5.8	19.0	19.7
HCl	17.7	16.4	130.4	116.7
HBr	24.4	22.5	216.6	198.1
H <sub>2</sub> S	25.5	26.4	216.8	230.0
H <sub>2</sub> O	9.8	9.9	45.3	46.2
H <sub>2</sub>	5.4	5.2	12.1	11.1
H <sub>2</sub> CO	18.9	18.2	165.2	143.4
CS <sub>2</sub>	59.0	58.4	871.1	955.4
COS	35.1	35.8	402.2	446.6
CO	13.2	13.3	81.4	79.4
CO <sub>2</sub>	19.6	18.3	158.7	161.0
Cl <sub>2</sub>	31.1	29.2	389.2	361.2
CH <sub>4</sub>	17.5	16.8	129.6	120.5
CH <sub>3</sub> OH	21.9	21.6	222.0	212.1
CH <sub>3</sub> OCH <sub>3</sub>	35.7	34.1	534.1	511.3
CH <sub>3</sub> NHCH <sub>3</sub>	43.0	38.7	647.8	627.9
CH <sub>3</sub> NH <sub>2</sub>	27.1	26.2	303.7	290.5
CH <sub>3</sub> COCH <sub>3</sub>	42.7	42.6	794.3	772.4
CH <sub>3</sub> CHO	31.0	30.8	401.7	400.7
CH <sub>3</sub> CH <sub>3</sub> CH <sub>3</sub> N	55.0	51.8	1063.1	1100.9
CH <sub>3</sub> CH <sub>2</sub> OCH <sub>2</sub> CH <sub>3</sub>	68.8	59.2	1563.4	1508.2
CCl <sub>4</sub>	70.9	69.7	2024.1	1959.3
C <sub>6</sub> H <sub>6</sub>	67.5	69.8	1722.7	1716.7
C <sub>5</sub> H <sub>12</sub>	67.4	65.6	1905.0	1827.2
C <sub>4</sub> H <sub>8</sub>	-	48.6	1130.2	1000.7
C <sub>4</sub> H <sub>10</sub> O	-	58.6	1566.8	1487.2
C <sub>4</sub> H <sub>10</sub>	55.3	53.2	1268.2	1205.6
C <sub>3</sub> H <sub>8</sub>	42.4	40.9	768.1	714.9
C <sub>3</sub> H <sub>7</sub> OH	47.0	46.0	973.8	923.6
C <sub>3</sub> H <sub>6</sub>	38.2	36.7	662.1	567.0
C <sub>2</sub> H <sub>6</sub>	29.9	28.8	381.9	354.4
C <sub>2</sub> H <sub>5</sub> OH	34.5	33.8	535.2	507.1
C <sub>2</sub> H <sub>4</sub>	28.7	27.5	300.2	285.2
C <sub>2</sub> H <sub>2</sub>	22.5	22.8	204.1	195.7
C <sub>6</sub> H <sub>14</sub>	80.3	78.1	2649.9	2540.5

**Table A.4:** The isotropic polarizability  $\alpha_{\text{iso}}$  for a dataset of 238 molecule calculated using various methods (in bohr<sup>3</sup>). The experimental values for isotropic static polarizabilities are taken from Ref. [250].

Molecule	Exp.	HF	LDA	PBE	PBEO	TS	CARMA
H <sub>2</sub>	5.3	4.6	5.0	5.3	5.6	4.6	4.0
N <sub>2</sub>	11.9	11.1	11.7	12.2	11.9	12.6	11.3
O <sub>2</sub>	10.8	9.7	0.0	10.9	10.3	10.1	9.2
CO	13.2	11.9	13.0	13.6	13.2	14.6	12.9
Dimethylether	35.4	31.0	35.1	36.0	34.5	39.2	32.3
Formaldehyde	16.5	16.1	17.7	18.8	18.1	19.0	15.9
Acetonitrile	30.2	27.7	29.9	30.7	30.0	32.5	28.8
(CH <sub>3</sub> ) <sub>3</sub> CCN	64.7	62.0	68.2	68.7	66.7	79.2	67.9
H <sub>2</sub> O	10.1	7.8	9.2	10.6	10.1	10.3	8.5
Methane	17.5	15.5	16.9	17.4	17.1	18.9	14.8
Acetylene	22.5	21.2	21.5	23.5	23.6	24.8	21.0
Ethylene	28.7	26.5	26.9	28.3	28.1	29.4	24.3
Ethane	30.2	27.0	29.4	29.8	29.2	33.7	27.2
Propyne	41.7	33.8	35.9	37.8	37.3	39.2	35.3
Propene	42.2	38.2	40.2	41.5	40.7	44.3	37.5
Cyclopropane	38.2	34.4	36.9	37.6	36.8	43.7	35.6
Propane	42.4	38.5	42.4	42.7	41.6	49.1	40.0
1-butyne	50.0	45.8	49.4	51.1	50.0	54.4	48.9
1,3-butadiene	58.3	55.4	56.5	58.4	57.6	54.8	49.1
1-butene	53.8	50.5	54.1	55.1	53.9	59.6	51.1
Trans-2-butene	57.3	50.8	54.9	55.7	54.3	59.2	51.9
2-methylpropene	55.9	50.3	54.1	55.0	53.7	59.7	50.7
Butane	55.3	50.0	55.4	55.6	54.1	64.5	53.7
Isobutane	54.9	49.9	55.5	55.6	53.9	65.1	53.0
1,3-cyclopentasiene	58.3	54.9	57.7	59.6	58.4	64.7	53.4
1-pentyne	61.5	57.7	62.9	64.5	63.0	69.8	63.4
Trans-1,3-cyclopentadiene	67.5	69.1	72.9	74.5	72.8	69.6	64.4
Isoprene	67.4	65.8	68.6	70.2	68.8	70.2	61.6
Cyclopentane	61.7	55.9	61.1	61.6	60.0	74.0	59.4
1-pentene	65.1	62.3	67.5	68.4	66.6	75.0	65.4
2-pentene	66.4	62.9	68.7	69.4	67.4	74.4	66.0
Penetane	67.4	61.6	68.5	68.7	66.7	79.8	68.0
Neopentane	68.8	61.1	68.3	68.3	66.1	81.2	65.8
Benzene	67.5	65.9	68.3	70.2	69.4	74.4	62.2
1-hexyne	73.6	69.5	76.4	77.9	75.8	85.1	78.0
2-ethyl-1,3-butadiene	79.6	74.4	79.5	80.8	78.8	85.3	75.1
3-methyl-1,3-pentadiene	79.6	79.2	84.5	85.9	83.7	85.2	76.4
2-methyl-1,3-pentadiene	81.7	79.3	84.7	86.0	83.8	85.0	77.2
2,3-dimethyl-1,3-butadiene	79.6	76.0	80.4	81.7	79.9	85.6	74.4
Cyclohexene	72.2	67.0	72.4	73.2	71.3	85.1	69.7
Cyclohexane	74.2	67.2	74.3	74.4	72.2	90.6	72.7
1-hexene	78.6	74.1	81.0	81.8	79.5	90.3	80.0
Hexane	80.3	73.4	81.8	81.9	79.4	95.2	82.7
Toluene	79.6	78.4	83.0	84.8	83.2	89.6	77.4
1-heptyne	86.4	81.5	89.9	91.4	88.7	100.5	93.2
Methylcyclohexane	88.4	78.8	87.8	87.8	85.0	106.5	87.1
1-heptene	91.2	86.0	94.4	95.2	92.5	105.7	95.2
Heptane	91.8	85.2	95.1	95.1	92.2	110.6	97.8
Styrene	101.2	95.3	100.6	103.1	100.9	100.0	89.8
Ethylbenzene	95.8	90.0	96.1	97.7	95.7	104.8	91.7
<i>o</i> -xylene	100.6	90.3	96.9	98.5	96.3	105.0	91.5
<i>p</i> -xylene	92.5	91.2	98.3	99.7	97.4	104.6	93.6
<i>m</i> -xylene	95.8	90.9	97.8	99.3	97.0	104.7	93.1
Ethylcyclohexane	107.3	90.2	100.6	100.4	97.2	121.9	101.2
n-octane	107.3	97.0	108.6	108.5	105.1	125.9	113.3
3-methylheptane	104.2	95.9	107.5	107.3	103.9	126.7	110.2
2,2,4-trimethylpentane	104.2	94.7	106.4	106.0	102.4	128.4	105.8
$\alpha$ -methylstyrene	108.3	104.9	111.9	113.9	111.2	115.4	103.2
Isopropylbenzene	108.0	101.6	109.3	110.7	108.1	120.9	105.1
1,3,5-trimethylbenzene	104.6	103.5	112.8	114.0	111.0	119.8	109.1
Isopropylcyclohexane	116.1	101.3	113.2	112.9	109.3	138.0	114.6
Nonane	117.2	108.9	122.0	122.0	118.1	141.3	128.9
Naphthalene	111.3	114.3	120.4	123.0	120.7	119.9	106.5
Durene	116.7	115.5	126.9	127.9	124.3	135.5	123.1
Tert-butylbenzene	116.1	112.7	122.0	123.2	120.1	137.1	117.9
Tert-butylcyclohexane	133.6	111.9	125.2	124.8	120.7	154.4	126.7
Decane	128.9	120.8	135.6	135.4	131.1	156.7	144.7
$\alpha$ -methylnaphthalene	130.6	126.6	134.6	136.9	134.1	135.3	121.3
$\beta$ -methylnaphthalene	131.7	128.1	137.3	139.5	136.4	135.0	123.7
$\alpha, \beta$ -trimethylstyrene	132.5	127.6	137.9	139.5	135.8	145.7	131.5
Pentamethylbenzene	128.9	126.6	139.7	140.5	136.5	151.1	136.4
Undecane	141.9	132.8	149.1	148.9	144.1	172.0	160.7
Acenaphthacene	139.1	133.6	142.4	144.7	141.4	144.8	129.2
$\alpha$ -ethylnaphthalene	143.0	138.3	148.0	150.1	146.8	150.7	136.7
$\beta$ -ethylnaphthalene	144.1	140.6	151.7	153.8	149.9	150.4	138.6
Hexamethylbenzene	141.0	138.2	153.0	153.8	149.2	166.8	150.2
Dodecane	153.5	144.7	162.7	162.5	157.1	187.4	176.7
Fluorene	146.3	146.2	157.5	160.3	156.2	154.9	143.6
Anthracene	171.4	173.2	184.9	188.0	183.6	165.4	156.5
Phenanthrene	248.3	163.6	175.6	178.8	174.5	165.5	153.4
<i>p</i> -di-tert-butylbenzene	165.3	160.8	178.1	178.3	172.8	199.8	177.9
pyrene	190.4	190.9	202.6	205.9	201.5	185.6	171.7
2,3-benfluorene	203.9	203.6	223.3	226.6	219.4	200.4	196.1
Naphthacene	217.8	242.6	262.1	265.6	258.1	210.8	210.8
1,2-benzanthracene	221.8	225.1	246.2	249.8	242.2	210.9	206.2
Chrysene	223.1	218.6	238.4	242.2	235.2	211.0	204.3
Triphenylene	209.7	209.5	227.5	231.3	225.0	211.1	200.5

Continued on next page

Table A.4 – continued from previous page

Molecule	EXP	HF	LDA	PBE	PBE0	TS	CARMA
1,3-tri-tert-butylbenzene	214.6	206.2	230.1	229.6	222.1	262.7	233.0
Coronene	286.8	285.4	312.1	315.9	307.1	271.4	260.5
Tetranitromethane	103.2	77.0	87.3	88.5	83.1	76.9	71.3
Formaldehyde	18.9	16.1	17.7	18.8	18.1	19.1	15.9
Formic acid	22.9	19.9	23.5	24.8	23.1	24.8	21.1
Formamide	28.3	24.1	28.4	30.1	28.2	29.0	25.0
Nitromethane	49.7	30.3	32.9	34.0	32.7	33.5	29.1
Methanol	21.8	19.2	21.4	22.6	21.7	24.4	19.9
Methylamine	27.1	23.3	25.9	27.4	26.3	28.9	23.7
Cyrogen	53.9	31.6	33.3	34.5	33.8	31.4	30.6
Ketene	29.7	26.4	28.0	29.6	29.0	29.3	25.6
Acetonitrile	29.7	27.7	29.9	30.7	30.0	32.5	28.8
Acetaldehyde	31.0	27.7	31.6	32.4	30.9	34.1	28.7
Ethylene oxide	29.9	26.5	28.9	29.9	29.0	33.7	27.8
Acetic acid	34.4	30.7	35.4	36.4	34.6	39.5	33.8
Methyl formate	34.1	27.7	31.6	32.4	30.9	34.1	28.7
Acetamide	38.3	35.1	40.5	42.1	39.8	43.9	37.7
N-methyl formamide	39.9	35.5	40.9	42.4	40.2	43.4	37.0
Nitroethane	65.0	41.2	45.5	46.3	44.7	48.6	41.7
Ethylnitrite	47.2	40.9	46.5	47.3	45.3	48.8	41.4
Ethanol	34.5	30.7	34.7	35.5	34.0	39.7	32.6
Methyl ether	34.8	30.9	35.2	36.1	34.5	39.4	32.4
Ethylene glycol	38.5	34.3	38.9	40.5	38.6	45.5	38.5
Dimethyl sulfone	49.3	48.6	55.5	56.5	54.1	62.4	54.8
Ethanethiol	50.0	46.2	49.8	51.3	50.1	53.7	48.1
Ethyl amine	47.9	35.1	39.8	40.9	38.9	44.2	36.4
Dimethyl amine	39.8	35.1	39.8	40.9	39.1	44.0	36.3
Ethylene diamine	48.6	42.9	48.6	50.5	48.0	54.5	46.3
Malononitrile	39.1	40.4	43.3	44.6	43.4	46.2	44.1
Acrylonitrile	54.3	41.2	42.7	44.1	43.3	42.6	39.3
Pyrazole	48.8	45.5	48.2	50.2	49.0	53.2	44.8
Propenal	43.1	39.5	42.4	43.9	42.6	44.1	38.3
Propionitrile	42.3	39.3	42.7	43.5	42.4	47.6	42.0
Acetone	42.7	38.8	44.0	44.8	42.8	49.1	41.5
Allyl alcohol	51.6	42.5	46.0	47.7	46.1	50.1	43.5
Propionaldehyde	43.9	39.1	44.0	44.8	43.0	49.2	41.6
Propionic acid	46.6	41.8	47.8	48.7	46.6	54.7	46.8
Ethyl formate	46.4	41.9	47.8	48.7	46.6	54.7	46.9
Methyl acetate	46.8	42.2	48.4	49.2	47.1	53.7	46.4
Dimethyl carbonate	52.0	45.7	52.7	53.6	51.2	58.8	51.4
N-methyl acetamide	52.8	46.7	53.8	54.9	52.4	58.3	50.6
N,N-dimethyl formamide	52.7	47.3	54.4	55.4	52.9	58.4	49.8
Nitropropane	57.4	52.8	58.5	59.4	57.2	63.8	55.1
2-propanol	47.0	42.1	47.7	48.4	46.4	55.4	45.7
1-propanol	45.5	42.1	47.2	48.1	46.3	55.0	46.0
ethyl methyl ether	53.5	42.7	48.5	49.3	47.2	54.6	46.0
dimethoxy methane	52.0	46.8	54.0	55.2	52.5	59.9	51.7
2-Methoxyethanol	50.2	46.3	52.7	54.2	51.7	60.2	51.9
Propylamine	52.0	46.5	52.4	53.4	51.2	59.5	49.8
Isopropylamine	52.4	46.4	52.7	53.5	51.2	60.1	49.6
Trimethylamine	52.5	47.0	54.3	55.0	52.3	60.0	49.3
Fumaronitrile	79.6	59.4	63.6	65.0	63.1	56.1	56.7
Succinonitrile	54.7	52.5	57.1	58.3	56.6	61.5	58.3
Pyrimidine	57.6	54.9	58.2	59.7	58.3	62.5	52.6
Pyridazine	62.6	55.9	58.8	60.4	59.0	62.4	52.6
Diketene	54.0	50.7	55.6	57.1	55.1	58.8	53.8
Thiophene	65.3	60.5	63.0	65.3	64.3	68.6	59.5
Methacrylonitrile	54.0	52.6	55.8	56.9	55.6	57.8	52.7
Trans-crotononitrile	55.3	54.2	58.3	59.4	57.8	57.5	54.3
N-methylpyrazole	60.7	58.3	62.6	64.4	62.7	68.0	58.8
Crotonaldehyde	57.4	52.6	58.3	59.5	57.4	59.0	52.9
Methacrylaldehyde	56.0	52.1	56.3	57.5	55.8	59.5	51.8
Biacyl	55.3	50.7	57.4	58.3	55.8	64.0	55.8
Acetic anhydride	60.1	54.2	62.8	63.8	60.7	68.5	61.2
Divinyl sulfide	73.6	74.3	79.8	82.0	79.8	73.8	71.7
Butyronitrile	56.7	51.1	56.1	56.7	55.1	62.9	56.0
Isobutyronitrile	54.3	50.7	55.6	56.2	54.6	63.2	55.1
Butanal	55.3	49.9	56.2	56.8	54.6	64.5	53.9
Methylethylketone	54.9	49.9	56.3	57.0	54.7	64.3	54.3
Trans-2,3-epoxy butane	55.5	49.8	55.6	56.3	54.3	64.2	55.4
Ethyl acetate	58.2	53.8	61.4	62.2	59.7	69.0	60.4
1,4-dioxane	58.0	52.1	59.8	60.8	57.7	70.5	57.5
2-methyl-1,3-dioxolane	63.7	51.6	58.4	59.3	56.8	69.7	57.4
Butyric acid	57.9	53.0	60.3	61.1	58.5	70.0	59.2
Methyl propionate	60.5	53.4	60.6	61.4	58.9	69.0	59.7
1-nitrobutane	70.2	64.4	71.5	72.3	69.8	79.2	69.5
2-methyl-2-nitropropane	69.5	62.9	70.0	70.6	68.1	80.0	66.7
Ethylether	58.9	54.4	61.8	62.5	60.0	69.8	60.0
1-butanol	59.9	53.7	60.2	61.1	58.8	70.3	60.0
2-methylpropanol	60.2	53.1	60.0	60.5	58.2	70.9	58.4
Methyl propyl ether	59.8	54.2	61.3	62.0	59.5	69.8	59.8
2-ethoxyethanol	62.6	58.0	66.6	67.7	64.6	75.5	65.9
Ethyl sulfide	72.9	70.4	77.5	78.7	76.4	84.3	76.4
Butylamine	91.1	58.0	65.2	66.2	63.7	74.9	64.1
Diethylamine	64.9	58.6	66.7	67.5	64.6	74.6	64.1
Pyridine	64.1	60.6	63.4	65.2	64.0	68.4	57.3
4-cyno-1,3-butadiene	70.9	75.0	79.0	80.8	78.8	67.9	66.8
1,5-dimethylpyrazole	72.3	69.9	75.9	77.5	75.3	82.9	72.9
Acetyl acetone	70.9	61.4	72.2	72.9	68.6	79.4	68.3
Valeronitrile	70.2	62.8	69.4	70.0	67.9	78.2	70.4
22-DMPN	64.7	62.0	68.2	68.7	66.7	79.2	67.9
Diethylketone	67.0	61.1	68.8	69.2	66.7	79.3	68.6
Methyl propyl ketone	67.0	61.5	69.5	70.0	67.3	79.5	69.1
Ethyl propionate	70.3	65.2	74.2	74.9	71.9	84.1	74.4

Continued on next page

Table A.4 – continued from previous page

Molecule	EXP	HF	LDA	PBE	PBE0	TS	CARMA
Methyl butanoate	70.3	65.1	74.2	74.8	71.9	84.3	74.6
Diethyl carbonate	76.3	69.5	79.8	80.6	77.2	89.0	80.3
Ethyl propyl ether	72.1	66.0	74.8	75.4	72.5	85.0	74.3
Tetramethyl orthocarbonate	87.7	75.2	86.4	87.4	83.4	99.9	85.3
<i>p</i> -dinitrobenzene	124.2	100.0	109.9	111.9	107.7	103.0	95.1
<i>p</i> -benzoquinone	97.9	74.5	78.5	80.3	78.3	79.0	69.5
Bitrobenzene	87.2	82.7	88.8	90.6	88.2	88.5	78.2
Phenol	74.9	70.0	74.8	76.9	75.1	80.1	68.5
Aniline	81.7	75.5	81.3	83.9	81.8	84.6	73.1
Phenylenediamine	93.1	84.9	94.3	97.5	93.8	94.5	84.4
Phenyldrazine	87.1	84.5	92.4	95.0	92.0	94.3	82.6
1-ethyl-5-methylpyrazole	84.4	81.3	88.8	90.3	87.6	98.3	86.0
Ethyl acetoacetate	87.1	77.2	90.2	91.0	86.2	99.3	88.4
Dimethylketazine	105.3	91.9	103.6	104.3	99.9	102.9	93.4
Cyclohexanol	78.0	70.9	79.7	80.2	77.1	96.8	78.8
Amyl formate	95.8	77.6	88.3	89.0	85.5	100.1	89.7
Paraldehyde	120.8	79.5	91.6	92.2	87.9	106.4	94.4
Propyl ether	84.4	76.6	86.6	86.9	83.7	100.3	85.9
1,1-diethoxyethane	89.1	81.3	93.5	94.1	89.9	105.7	92.8
1,2-diethoxyethane	76.3	81.1	92.9	93.6	89.5	105.6	92.3
Triethylamine	90.3	81.2	94.1	94.5	89.8	106.2	89.6
Dipropylamine	89.7	80.7	91.8	92.2	88.4	105.3	89.5
<i>p</i> -cynonitrobenzene	128.2	101.1	111.1	112.9	108.7	102.0	97.7
bezonitrile	84.4	82.7	87.4	89.2	87.4	87.7	80.6
Nitroanisole	105.9	101.4	115.4	117.0	111.8	108.9	99.4
Anisole	88.4	82.5	89.5	91.5	89.0	94.9	82.5
<i>o</i> -anisidine	95.8	91.9	101.7	104.5	100.9	105.0	92.9
1,1-methylphenylhydrazine	99.9	97.1	107.5	110.0	106.2	109.7	96.5
Cyclohexyl methyl ether	90.4	82.7	93.1	93.4	90.0	111.5	92.5
2,4-dimethyl-3-pentene	91.1	83.3	94.0	94.1	90.7	110.9	94.1
Pentyl acetate	100.6	89.1	101.5	102.1	98.1	114.9	104.6
<i>p</i> -dicynobenzene	129.6	101.9	110.2	112.1	108.6	101.2	100.6
Quinoxaline	102.1	104.8	110.9	113.1	110.5	107.8	96.3
Acetophenone	101.2	92.0	100.1	101.9	98.9	104.5	93.0
2,5-dimethyl-1,4-benzoquinone	126.9	98.3	107.3	108.5	105.1	109.3	99.6
Phenetole	100.6	95.0	103.9	105.8	102.7	110.1	98.0
N-dimethylaniline	109.3	98.2	106.8	108.6	105.3	114.9	100.1
1,1-ethylphenylhydrazine	112.2	109.3	122.5	124.9	119.9	124.9	111.3
Ethyl sorbate	116.1	115.2	130.0	131.1	125.6	119.2	116.7
Tetramethyl cyclobutane-1,3-dione	125.5	92.0	104.3	105.1	100.8	120.8	104.1
Diethyl succinate	113.4	104.5	121.3	122.1	116.5	134.4	126.4
Butyl ether	116.1	101.4	114.8	115.2	110.9	131.1	119.3
Quinoline	105.9	108.8	115.3	117.7	115.2	113.8	101.4
Isoquinoline	110.9	108.0	114.3	116.7	114.2	113.8	101.0
Ethyl bezoate	114.0	107.8	119.2	120.9	116.9	124.4	112.9
Tripropyl amine	127.3	116.3	133.3	133.2	127.5	152.0	133.6
$\alpha$ -naphthylamine	131.6	123.9	133.2	136.5	133.0	130.2	117.1
$\beta$ -naphthylamine	133.1	125.5	136.8	140.1	135.8	130.0	118.9
2-methylquinoline	125.9	122.5	132.3	134.4	130.9	128.9	118.7
1-methylisoquinoline	123.4	123.2	135.6	138.4	133.5	131.1	120.6
2,3-dimethylquinoxaline	126.2	131.9	144.4	146.2	141.5	138.3	129.1
1-naphthaldehyde	133.3	130.0	139.8	142.2	138.5	134.8	122.4
2-naphthaldehyde	135.4	132.9	145.1	147.5	143.0	134.8	125.6
Phenazine	158.1	164.7	175.4	178.2	173.7	153.2	145.6
4-nitrodiphenyl ether	166.7	155.9	174.3	176.8	169.7	164.1	153.3
Anthraquinone	165.1	160.9	178.0	180.4	174.1	169.2	159.5
Di- <i>p</i> -tolyl ether	168.0	160.8	174.9	177.2	172.2	180.2	168.0

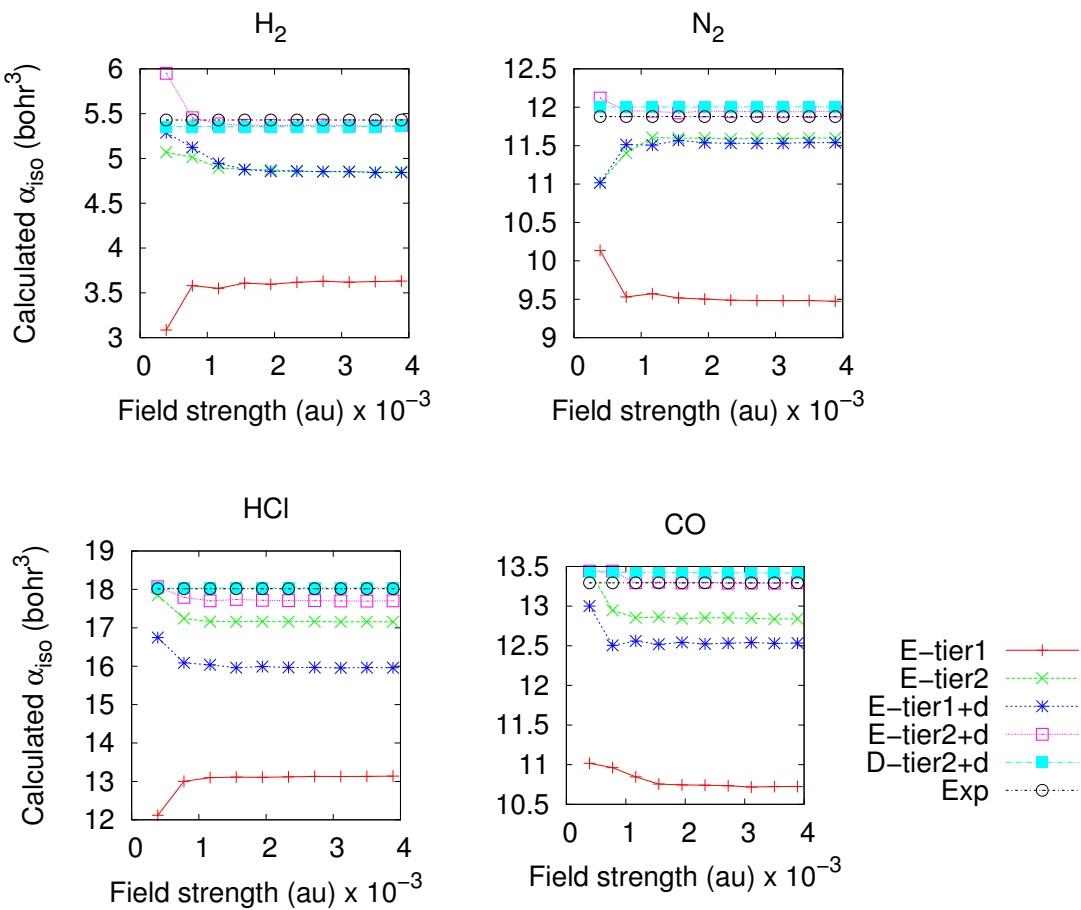


## Extra technical details

### B.1 Technical details about finite-difference approach

The static polarizabilities for H<sub>2</sub>, N<sub>2</sub>, HCl and CO molecules are calculated based on a finite-difference approach (as discussed in Section (3.2)). We here test the numerical convergence of static polarizabilities for the parameters that include basis sets and effect of varying external perturbing electric field. In general, it is well known that a large basis set is required for an accurate calculation of the polarizability and the effect of additional polarization and diffuse functions in the basis set is quite considerable. The molecular static polarizabilities are calculated using two procedures : 1) First as second derivative of total electronic energy with external electric field, 2) as first derivative of induce dipole moment with external electric field. The isotropic static polarizability calculated with PBE0 functional for H<sub>2</sub>, N<sub>2</sub>, HCl and CO molecules are shown in Figure (B.1). All calculations were carried out with the FHI-aims package [265], employing numeric atom-centered (NAO) basis functions and also including additional diffuse functions from augmented basis sets for respective elements. These convergence tests show that the first derivative of the induced dipole moment with external electric field provides well converged values for isotropic static polarizability.

**Figure B.1:** Convergence of the (isotropic) static polarizability (y-axis) for H<sub>2</sub>, N<sub>2</sub>, HCl and CO molecules calculated based on finite-differences with varying external perturbing field (x-axis). The prefix "E" in legends indicate finite-differences derivative with the total electronic energy and "D" with the induce dipole moment. Whereas, *tier1* and *tier2* are NAO basis functions and "d" indicate diffuse function from d-aug-cc-pVQZ basis set. The experimental values for isotropic polarizabilities are taken from Ref. [250].



---

## Symbols

$\hat{\mathcal{H}}$	Hamilton operator
$\nabla^2$	Laplacian operator
$n_0$	Ground-state electron density
$\psi$	Wave function
$\mathcal{E}$	Electric field
$\chi_e$	Electric susceptibility
$L$	Lorentz factor
$\epsilon$	Fermi energy
$\mathbf{P}$	Polarization
$\alpha$	Polarizability
$\omega$	Frequency
$V$	Volume
$f_{\text{damp}}$	Damping function
$s_R$	Scaling parameter in the TS method



---

## Abbreviations

<b>ACFDT</b>	Adiabatic-connection fluctuation-dissipation theorem
<b>ARF</b>	Atomic response function
<b>BOA</b>	Born-Oppenheimer approximation
<b>CARMA</b>	Coupled atomic response in matter
<b>CC</b>	Coupled cluster
<b>CCSD</b>	Coupled cluster singles, doubles
<b>DFA</b>	Density-functional approximation
<b>DFT</b>	Density-functional theory
<b>DOSD</b>	Dipole oscillator strength distribution
<b>GGA</b>	Generalized gradient approximation
<b>HF</b>	Hartree-Fock
<b>HK</b>	Hohenberg-Kohn
<b>KS-DFT</b>	Kohn-Sham density-functional theory
<b>LDA</b>	Local-density approximation
<b>MAE</b>	Mean absolute error
<b>MARE</b>	Mean absolute relative error
<b>MBPT</b>	Many-body perturbation theory
<b>MBD</b>	Many-body dispersion
<b>ME</b>	Mean error
<b>MP2</b>	Möller-Plesset second-order perturbation theory
<b>MRE</b>	Mean relative error
<b>PBC</b>	Periodic boundary condition
<b>PBE</b>	Perdew-Burke-Enzerhof
<b>QMC</b>	Quantum Monte Carlo
<b>QHO</b>	Quantum harmonic oscillator
<b>RPA</b>	Random-phase approximation
<b>SE</b>	Schrödinger equation
<b>SO</b>	Single oscillator
<b>TDDFT</b>	Time-dependent density-functional theory
<b>TF</b>	Thomas Fermi
<b>TS</b>	Tkatchenko-Scheffler
<b>vdW</b>	van der Waals
<b>XC</b>	Exchange-correlation
<b>XDM</b>	Exchange-dipole moment



---

## Acknowledgements

I would like to thank Prof. Matthias Scheffler for giving me the opportunity to carry out my Ph.D. studies in the very interesting atmosphere of the Fritz Haber Institute. I had the chance to meet and discuss with many experts of the field, not to mention the easy access to computational facilities and time. I would like to express my deepest gratitude to my advisor, Prof. Alexandre Tkatchenko, who has supported me throughout my thesis with patience and guided me by his immense knowledge. I thank him for allowing and giving me opportunity to work independently and add value to the research work. A big thank goes to Prof. Robert A. DiStasio Jr. for sharing your valuable insights in science throughout the last six years. I have learned many things and I am grateful for your ideas and support. I must acknowledge Prof. Shridhar P. Gejji for introducing me to quantum chemistry and computational chemistry. I would also like to record my sincere gratitude to department of chemistry at University of Pune where I took my first lesson of research. I would also like to acknowledge all my present and former colleagues from the Theory Department. I would also like to thank Julia, Birgit, Carmen, and Steffen for your support with all administrative help. A special thanks goes to the van der Waals group for many fruitful discussions and feedback. I must thank Guo-xu, Nicola, Victor, Jan, Johannes, Alberto, Mausami and Fairoja thank you for your patience and explanations during my PhD work. A special thanks goes to Gionni, for being a good friend, for proofreading, and also for sharing your valuable insights into the English language. Finally, I would like to thank my family and my friends outside the Institute, especially Rinata, Anshuman, Neloy, Biswajit, Biswadip, Moumita and many others. Finally, I am grateful to my parents and many close family members who have been beside me in every circumstances and this thesis is dedicated to them.



---

## Bibliography

### Bibliography

- [1] Tkatchenko, A. & Scheffler, M. [Accurate molecular van der Waals interactions from ground-state electron density and free-atom reference data](#). *Phys. Rev. Lett.* **102**, 073005 (2009).
- [2] DeVoe, H. [Optical properties of molecular aggregates. II. Classical theory of the refraction, absorption, and optical activity of solutions and crystals](#). *J. Chem. Phys.* **43**, 3199–3208 (1965).
- [3] Felderhof, B. U. [On the propagation and scattering of light in fluids](#). *Physica* **76**, 486–502 (1974).
- [4] Applequist, J., Carl, J. R. & Fung, K.-K. [Atom dipole interaction model for molecular polarizability. application to polyatomic molecules and determination of atom polarizabilities](#). *J. Am. Chem. Soc.* **94**, 2952–2960 (1972).
- [5] Thole, B. T. [Molecular polarizabilities calculated with a modified dipole interaction](#). *Chem. Phys.* **59**, 341–350 (1981).
- [6] Mayer, A. [Formulation in terms of normalized propagators of a charge-dipole model enabling the calculation of the polarization properties of fullerenes and carbon nanotubes](#). *Phys. Rev. B* **75**, 045407 (2007).
- [7] Tkatchenko, A., DiStasio, R. A., Jr., Car, R. & Scheffler, M. [Accurate and efficient method for many-body van der Waals interactions](#). *Phys. Rev. Lett.* **108**, 236402 (2012).
- [8] Berne, B. J. & Pecora, R. *Dynamic light scattering: with applications to Chemistry, Biology, and Physics* (Courier Corporation, 2000).
- [9] Feynman, R. P. & Zee, A. *QED: The strange theory of light and matter* (Princeton University Press, 2006).

- [10] Bruus, H. & Flensberg, K. *Many-body quantum theory in condensed matter physics: an introduction* (OUP Oxford, 2004).
- [11] Lu, W. & Lieber, C. M. **Nanoelectronics from the bottom up**. *Nat. Mater.* **6**, 841–850 (2007).
- [12] Ohno, Y., Maehashi, K., Yamashiro, Y. & Matsumoto, K. **Electrolyte-gated graphene field-effect transistors for detecting pH and protein adsorption**. *Nano Lett.* **9**, 3318–3322 (2009).
- [13] Schedin, F. *et al.* **Detection of individual gas molecules adsorbed on graphene**. *Nat. Mater.* **6**, 652–655 (2007).
- [14] Marković, N. & Ross, P. N. **Surface science studies of model fuel cell electrocatalysts**. *Surface Science Reports* **45**, 117–229 (2002).
- [15] Stockman, M. I. **Nanoplasmonics: past, present, and glimpse into future**. *Opt. express* **19**, 22029–22106 (2011).
- [16] Novoselov, K. S. *et al.* **Two-dimensional gas of massless dirac fermions in graphene**. *Nature* **438**, 197–200 (2005).
- [17] Daniel, M.-C. & Astruc, D. **Gold nanoparticles: assembly, supramolecular chemistry, quantum-size-related properties, and applications toward biology, catalysis, and nanotechnology**. *Chem. Rev.* **104**, 293–346 (2004).
- [18] Landau, L. D. *et al.* *Electrodynamics of continuous media*, vol. 8 (elsevier, 1984).
- [19] Jackson, J. D. & Jackson, J. D. *Classical electrodynamics*, vol. 3 (Wiley New York etc., 1962).
- [20] Scheel, S. & Buhmann, S. Y. **Macroscopic quantum electrodynamics—concepts and applications**. *Acta Phys. Slovaca* **58**, 675–809 (2008).
- [21] Buckingham, A. **Permanent and induced molecular moments and long-range intermolecular forces**. *Adv. Chem. Phys.* **12**, 107–142 (1967).
- [22] Kaplan, I. G. *Intermolecular interactions: Physical Picture, Computational Methods and Model Potentials* (John Wiley & Sons, 2006).
- [23] Stone, A. *The theory of intermolecular forces* (Oxford University Press, 2013).
- [24] Joh, N. H., Oberai, A., Yang, D., Whitelegge, J. P. & Bowie, J. U. **Similar energetic contributions of packing in the core of membrane and water-soluble proteins**. *J. Am. Chem. Soc.* **131**, 10846–10847 (2009).

- [25] Lalatonne, Y., Richardi, J. & Pilani, M. **Van der Waals versus dipolar forces controlling mesoscopic organizations of magnetic nanocrystals.** *Nat. Mater.* **3**, 121–125 (2004).
- [26] Atwood, J. L., Barbour, L. J. & Jerga, A. **Storage of methane and freon by interstitial van der Waals confinement.** *Science* **296**, 2367–2369 (2002).
- [27] Ruoff, R. S., Tersoff, J., Lorents, D. C., Subramoney, S. & Chan, B. **Radial deformation of carbon nanotubes by van der Waals forces.** *Nature* **364**, 514–516 (1993).
- [28] Koski, W., Kaufman, J. & Wilson, K. **Physicochemical aspects of the action of general anaesthetics.** *Nature* **242**, 65–66 (1973).
- [29] Autumn, K. *et al.* **Evidence for van der Waals adhesion in gecko setae.** *Proc. Natl. Acad. Sci. USA* **99**, 12252–12256 (2002).
- [30] Hansen, W. & Autumn, K. **Evidence for self-cleaning in gecko setae.** *Proc. Natl. Acad. Sci. USA* **102**, 385–389 (2005).
- [31] Kesel, A. B., Martin, A. & Seidl, T. **Getting a grip on spider attachment: an AFM approach to microstructure adhesion in arthropods.** *Smart Mater. Struct.* **13**, 512 (2004).
- [32] Scheeres, D., Hartzell, C., Sánchez, P. & Swift, M. **Scaling forces to asteroid surfaces: The role of cohesion.** *Icarus* **210**, 968–984 (2010).
- [33] Parsegian, V. A. *Van der Waals forces: A Handbook for Biologists, Chemists, Engineers and Physicists.* (Cambridge University Press, 2005).
- [34] Šiber, A. *et al.* **Dispersion interactions between optically anisotropic cylinders at all separations: Retardation effects for insulating and semiconducting single-wall carbon nanotubes.** *Phys. Rev. B* **80**, 165414 (2009).
- [35] Rajter, R. & French, R. **New perspectives on van der Waals–London interactions of materials. From planar interfaces to carbon nanotubes.** In *Journal of Physics: Conference Series*, vol. 94, 012001 (IOP Publishing, 2008).
- [36] Rahi, S. J., Emig, T., Graham, N., Jaffe, R. L. & Kardar, M. **Scattering theory approach to electrodynamic casimir forces.** *Phys. Rev. D* **80**, 085021 (2009).
- [37] Brooks, B. R. *et al.* **CHARMM: A program for macromolecular energy, minimization, and dynamics calculations.** *J. Comp. Chem.* **4**, 187–217 (1983).

- [38] Cornell, W. D. *et al.* A second generation force field for the simulation of proteins, nucleic acids, and organic molecules. *J. Am. Chem. Soc.* **117**, 5179–5197 (1995).
- [39] Draine, B. T. & Flatau, P. J. Discrete-dipole approximation for scattering calculations. *JOSA A* **11**, 1491–1499 (1994).
- [40] Schrödinger, E. An undulatory theory of the mechanics of atoms and molecules. *Phys. Rev.* **28**, 1049–1070 (1926).
- [41] Hohenberg, P. & Kohn, W. Inhomogeneous electron gas. *Phys. Rev.* **136**, B864–B871 (1964).
- [42] Kohn, W. & Sham, L. J. Self-consistent equations including exchange and correlation effects. *Phys. Rev.* **140**, A1133–A1138 (1965).
- [43] Runge, E. & Gross, E. K. U. Density-functional theory for time-dependent systems. *Phys. Rev. Lett.* **52**, 997–1000 (1984).
- [44] Olsen, T. & Thygesen, K. S. Accurate ground-state energies of solids and molecules from time-dependent density-functional theory. *Phys. Rev. Lett.* **112**, 203001 (2014).
- [45] Heßelmann, A. & Jansen, G. Intermolecular dispersion energies from time-dependent density functional theory. *Chem. Phys. Lett.* **367**, 778–784 (2003).
- [46] Misquitta, A. J., Jeziorski, B. & Szalewicz, K. Dispersion energy from density-functional theory description of monomers. *Phys. Rev. Lett.* **91**, 033201 (2003).
- [47] Fuchs, M. & Gonze, X. Accurate density functionals: Approaches using the adiabatic-connection fluctuation-dissipation theorem. *Phys. Rev. B* **65**, 235109 (2002).
- [48] Furche, F. & Van Voorhis, T. Fluctuation-dissipation theorem density-functional theory. *J. Chem. Phys.* **122**, 164106 (2005).
- [49] Toulouse, J., Gerber, I. C., Jansen, G., Savin, A. & Angyán, J. G. Adiabatic-connection fluctuation-dissipation density-functional theory based on range separation. *Phys. Rev. Lett.* **102**, 096404 (2009).
- [50] Nguyen, H.-V., Pham, T. A., Rocca, D. & Galli, G. Improving accuracy and efficiency of calculations of photoemission spectra within the many-body perturbation theory. *Phys. Rev. B* **85**, 081101 (2012).

- [51] Pham, T. A., Nguyen, H.-V., Rocca, D. & Galli, G. **GW calculations using the spectral decomposition of the dielectric matrix: Verification, validation, and comparison of methods.** *Phys. Rev. B* **87**, 155148 (2013).
- [52] Caruso, F., Rinke, P., Ren, X., Rubio, A. & Scheffler, M. **Self-consistent GW: All-electron implementation with localized basis functions.** *Phys. Rev. B* **88**, 075105 (2013).
- [53] Dobson, J. F. & Wang, J. **Successful test of a seamless van der Waals density functional.** *Phys. Rev. Lett.* **82**, 2123 (1999).
- [54] Dion, M., Rydberg, H., Schröder, E., Langreth, D. C. & Lundqvist, B. I. **van der Waals density functional for general geometries.** *Phys. Rev. Lett.* **92**, 246401 (2004).
- [55] Dobson, J. F. & Gould, T. **Calculation of dispersion energies.** *J. Phys.: Condens. Matter* **24**, 073201 (2012).
- [56] Tkatchenko, A., Ambrosetti, A. & DiStasio Jr, R. A. **Interatomic methods for the dispersion energy derived from the adiabatic connection fluctuation-dissipation theorem.** *J. Chem. Phys.* **138**, 074106 (2013).
- [57] Ambrosetti, A., Reilly, A. M., DiStasio Jr, R. A. & Tkatchenko, A. **Long-range correlation energy calculated from coupled atomic response functions.** *J. Chem. Phys.* **140**, 18A508 (2014).
- [58] Furche, F. **Molecular tests of the random phase approximation to the exchange-correlation energy functional.** *Phys. Rev. B* **64**, 195120 (2001).
- [59] Furche, F. **Developing the random phase approximation into a practical post-Kohn–Sham correlation model.** *J. Chem. Phys.* **129**, 114105 (2008).
- [60] Ren, X. *et al.* **Resolution-of-identity approach to Hartree–Fock, hybrid density functionals, RPA, MP2 and GW with numeric atom-centered orbital basis functions.** *New J. Phys.* **14**, 053020 (2012).
- [61] Ren, X., Rinke, P., Scuseria, G. E. & Scheffler, M. **Renormalized second-order perturbation theory for the electron correlation energy: Concept, implementation, and benchmarks.** *Phys. Rev. B* **88**, 035120 (2013).
- [62] Bates, J. E. & Furche, F. **Communication: Random phase approximation renormalized many-body perturbation theory.** *J. Chem. Phys.* **139**, 171103 (2013).

- [63] Nguyen, N. L., Colonna, N. & De Gironcoli, S. **Ab initio self-consistent total-energy calculations within the EXX/RPA formalism.** *Phys. Rev. B* **90**, 045138 (2014).
- [64] Langreth, D. C. & Perdew, J. P. **The exchange-correlation energy of a metallic surface.** *Solid State Comm.* **17**, 1425–1429 (1975).
- [65] Langreth, D. C. & Perdew, J. P. **Exchange-correlation energy of a metallic surface: Wave-vector analysis.** *Phys. Rev. B* **15**, 2884 (1977).
- [66] Yabana, K. & Bertsch, G. **Application of the time-dependent local density approximation to optical activity.** *Phys. Rev. A* **60**, 1271 (1999).
- [67] Sternheimer, R. **On nuclear quadrupole moments.** *Phys. Rev.* **84**, 244 (1951).
- [68] CASIDA, M. E. Time-dependent density functional response theory for molecules. *Recent Advances in Density Functional Methods* **1**, 155 (1995).
- [69] Dobson, J. F. Quasi-local-density approximation for a van der Waals energy functional. *arXiv preprint cond-mat/0311371* (2003).
- [70] Scherrer, A., Dreßler, C., Ahlert, P. & Sebastiani, D. **Generalization of the electronic susceptibility for arbitrary molecular geometries.** *J. Chem. Phys.* **144**, 144111 (2016).
- [71] Scherrer, A. & Sebastiani, D. **Moment expansion of the linear density-density response function.** *J. Comp. Chem.* **37**, 665–674 (2016).
- [72] Scherrer, A., Verschinin, V. & Sebastiani, D. **Eigensystem representation of the electronic susceptibility tensor for intermolecular interactions within density functional theory.** *J. Chem. Theory Comput.* **8**, 106–111 (2011).
- [73] London, F. Über einige eigenschaften und anwendungen der molekularkräfte. *Z. phys. Chem* **11**, 222–251 (1930).
- [74] Israelachvili, J. N. *Intermolecular and surface forces: revised third edition* (Academic press, 2011).
- [75] London, F. **The general theory of molecular forces.** *Trans. Faraday Soc.* **33**, 8b–26 (1937).
- [76] Mahanty, J. & Ninham, B. W. *Dispersion forces*, vol. 5 (IMA, 1976).

- [77] Casimir, H. B. G. & Polder, D. [The influence of retardation on the London-van der Waals forces](#). *Phys. Rev.* **73**, 360–372 (1948).
- [78] Milton, K. A., Parashar, P. & Wagner, J. [Exact results for casimir interactions between dielectric bodies: The weak-coupling or van der Waals limit](#). *Phys. Rev. Lett.* **101**, 160402 (2008).
- [79] Gunnarsson, O. & Lundqvist, B. I. [Exchange and correlation in atoms, molecules, and solids by the spin-density-functional formalism](#). *Phys. Rev. B* **13**, 4274–4298 (1976).
- [80] Oxtoby, D. W. & Gelbart, W. M. [Collisional polarizability anisotropies of the noble gases](#). *Mol. Phys.* **29**, 1569–1576 (1975).
- [81] DiStasio Jr, R. A., Gobre, V. V. & Tkatchenko, A. [Many-body van der Waals interactions in molecules and condensed matter](#). *J. Phys.: Condens. Matter* **26**, 213202 (2014).
- [82] Szabo, A. & Ostlund, N. S. *Modern Quantum Chemistry: Introduction to Advanced Electronic Structure Theory* (McGraw-Hill, New York, 1989).
- [83] Fiolhais, C., Nogueira, F. & Marques, M. A. *A Primer in Density Functional Theory*, vol. 620 (Springer, 2003).
- [84] Born, M. & Oppenheimer, R. [Zur Quantentheorie der Moleküle](#). *Ann. Phys.* **389**, 457–484 (1927).
- [85] Behler, J., Delley, B., Lorenz, S., Reuter, K. & Scheffler, M. [Dissociation of O<sub>2</sub> at Al \(111\): The role of spin selection rules](#). *Phys. Rev. Lett.* **94**, 036104 (2005).
- [86] Behler, J., Reuter, K. & Scheffler, M. [Nonadiabatic effects in the dissociation of oxygen molecules at the Al \(111\) surface](#). *Phys. Rev. B* **77**, 115421 (2008).
- [87] Wodtke, A. M., Tully, J. C. & Auerbach, D. J. [Electronically non-adiabatic interactions of molecules at metal surfaces: Can we trust the Born–Oppenheimer approximation for surface chemistry?](#) *Int. Rev. Phys. Chem.* **23**, 513–539 (2004).
- [88] Luntz, A., Persson, M. & Sitz, G. O. [Theoretical evidence for nonadiabatic vibrational deexcitation in H<sub>2</sub> \(D<sub>2</sub>\) state-to-state scattering from cu \(100\)](#). *J. Chem. Phys.* **124**, 91101–91101 (2006).
- [89] Hartree, D. R. [The wave mechanics of an atom with a non-coulomb central field. Part I. Theory and methods](#). In *Mathematical Proceedings of the Cambridge Philosophical Society*, vol. 24, 89–110 (Cambridge Univ Press, 1928).

- [90] Fock, V. Näherungsmethode zur lösung des quantenmechanischen mehrkörperproblems. *Zeitschrift für Physik* **61**, 126–148 (1930).
- [91] Koopmans, T. Über die zuordnung von wellenfunktionen und eigenwerten zu den einzelnen elektronen eines atoms. *Physica* **1**, 104–113 (1934).
- [92] Taylor, D. P., Hess, W. P. & McCarthy, M. I. Structure and energetics of the water/NaCl (100) interface. *J. Phys. Chem. B* **101**, 7455–7463 (1997).
- [93] Baranek, P., Pinarello, G., Pisani, C. & Dovesi, R. Ab initio study of the cation vacancy at the surface and in bulk MgO. *Phys. Chem. Chem. Phys.* **2**, 3893–3901 (2000).
- [94] Casassa, S., Ferrari, A., Busso, M. & Pisani, C. Structural, magnetic, and electronic properties of the NiO monolayer epitaxially grown on the (001) Ag surface: an ab initio density functional study. *J. Phys. Chem. B* **106**, 12978–12985 (2002).
- [95] Löwdin, P.-O. Correlation problem in many-electron quantum mechanics I. Review of different approaches and discussion of some current ideas. *Adv. Chem. Phys.* **2**, 207–322 (2007).
- [96] Bartlett, R. J. Many-body perturbation theory and coupled cluster theory for electron correlation in molecules. *Annual Review of Physical Chemistry* **32**, 359–401 (1981).
- [97] Møller, C. & Plesset, M. S. Note on an approximation treatment for many-electron systems. *Phys. Rev.* **46**, 618 (1934).
- [98] Scott, A. P. & Radom, L. Harmonic vibrational frequencies: an evaluation of Hartree-Fock, Møller-Plesset, Quadratic configuration interaction, Density functional theory, and Semiempirical scale factors. *J. Phys. Chem.* **100**, 16502–16513 (1996).
- [99] Rablen, P. R., Lockman, J. W. & Jorgensen, W. L. Ab initio study of hydrogen-bonded complexes of small organic molecules with water. *J. Phys. Chem. A* **102**, 3782–3797 (1998).
- [100] Curtiss, L. A., Redfern, P. C., Raghavachari, K. & Pople, J. A. Gaussian-3X (G3X) theory: Use of improved geometries, zero-point energies, and Hartree–Fock basis sets. *J. Chem. Phys.* **114**, 108–117 (2001).
- [101] Leininger, M. L., Allen, W. D., Schaefer III, H. F. & Sherrill, C. D. Is Møller–Plesset perturbation theory a convergent *ab initio* method? *J. Chem. Phys.* **112**, 9213–9222 (2000).

- [102] Coester, F. & Kümmel, H. **Short-range correlations in nuclear wave functions.** *Nucl. Phys.* **17**, 477–485 (1960).
- [103] Bartlett, R. J. & Musiał, M. **Coupled-cluster theory in quantum chemistry.** *Rev. Mod. Phys.* **79**, 291 (2007).
- [104] Becke, A. D. **Perspective: Fifty years of density-functional theory in chemical physics.** *J. Chem. Phys.* **140**, 18A301 (2014).
- [105] Burke, K. **Perspective on density functional theory.** *J. Chem. Phys.* **136**, – (2012).
- [106] Cohen, A. J., Mori-Sánchez, P. & Yang, W. **Challenges for density functional theory.** *Chem. Rev.* **112**, 289–320 (2011).
- [107] Cohen, A. J., Mori-Sánchez, P. & Yang, W. **Insights into current limitations of density functional theory.** *Science* **321**, 792–794 (2008).
- [108] Perdew, J. P. *et al.* **Prescription for the design and selection of density functional approximations: More constraint satisfaction with fewer fits.** *J. Chem. Phys.* **123**, 062201 (2005).
- [109] Thomas, L. H. **The calculation of atomic fields.** In *Math. Proc. Cambridge*, vol. 23, 542–548 (Cambridge Univ Press, 1927).
- [110] Fermi, E. Un metodo statistico per la determinazione di alcune proprietà dell’atomo. *Rend. Accad. Naz. Lincei* **6**, 602–607 (1927).
- [111] Slater, J. C. **A simplification of the Hartree-Fock method.** *Physical Review* **81**, 385 (1951).
- [112] Burke, K. *The ABC of DFT* (2007).
- [113] Levy, M. Universal variational functionals of electron densities, first-order density matrices, and natural spin-orbitals and solution of the  $\nu$ -representability problem. *Proc. Natl. Acad. Sci. USA* **76**, 6062–6065 (1979).
- [114] Kohn, W.  **$\nu$ -representability and density functional theory.** *Phys. Rev. Lett.* **51**, 1596 (1983).
- [115] Chayes, J., Chayes, L. & Ruskai, M. B. **Density functional approach to quantum lattice systems.** *J. Stat. Phys.* **38**, 497–518 (1985).
- [116] Perdew, J. P. & Schmidt, K. **Jacob’s ladder of density functional approximations for the exchange-correlation energy.** In *AIP Conference Proceedings*, 1–20 (2001).

- [117] Marques, M. A., Oliveira, M. J. & Burnus, T. [Libxc: A library of exchange and correlation functionals for density functional theory](#). *Comput. Phys. Comm.* **183**, 2272–2281 (2012).
- [118] Perdew, J. P. & Wang, Y. [Accurate and simple analytic representation of the electron-gas correlation energy](#). *Phys. Rev. B* **45**, 13244 (1992).
- [119] Langreth, D. C. & Mehl, M. [Beyond the local-density approximation in calculations of ground-state electronic properties](#). *Phys. Rev. B* **28**, 1809 (1983).
- [120] Becke, A. D. [A new inhomogeneity parameter in density-functional theory](#). *J. Chem. Phys.* **109**, 2092–2098 (1998).
- [121] Becke, A. D. [A new mixing of Hartree–Fock and local density-functional theories](#). *J. Chem. Phys.* **98**, 1372–1377 (1993).
- [122] Perdew, J. P. & Zunger, A. [Self-interaction correction to density-functional approximations for many-electron systems](#). *Phys. Rev. B* **23**, 5048 (1981).
- [123] Kümmel, S. & Kronik, L. [Orbital-dependent density functionals: Theory and applications](#). *Rev. Mod. Phys.* **80**, 3 (2008).
- [124] Gell-Mann, M. & Brueckner, K. A. [Correlation energy of an electron gas at high density](#). *Phys. Rev.* **106**, 364 (1957).
- [125] Ceperley, D. M. & Alder, B. [Ground state of the electron gas by a stochastic method](#). *Phys. Rev. Lett.* **45**, 566 (1980).
- [126] Perdew, J., McMullen, E. & Zunger, A. [Density-functional theory of the correlation energy in atoms and ions: a simple analytic model and a challenge](#). *Phys. Rev. A* **23**, 2785 (1981).
- [127] Vosko, S., Wilk, L. & Nusair, M. [Accurate spin-dependent electron liquid correlation energies for local spin density calculations: a critical analysis](#). *Can. J. Phys.* **58**, 1200–1211 (1980).
- [128] Csonka, G. I. *et al.* [Assessing the performance of recent density functionals for bulk solids](#). *Phys. Rev. B* **79**, 155107 (2009).
- [129] Harl, J., Schimka, L. & Kresse, G. [Assessing the quality of the random phase approximation for lattice constants and atomization energies of solids](#). *Phys. Rev. B* **81**, 115126 (2010).
- [130] Haas, P., Tran, F. & Blaha, P. [Calculation of the lattice constant of solids with semilocal functionals](#). *Phys. Rev. B* **79**, 085104 (2009).

- [131] Haas, P., Tran, F., Blaha, P., Schwarz, K. & Laskowski, R. **Insight into the performance of GGA functionals for solid-state calculations.** *Phys. Rev. B* **80**, 195109 (2009).
- [132] Perdew, J. P., Ruzsinszky, A., Csonka, G. I., Constantin, L. A. & Sun, J. **Erratum: Workhorse semilocal density functional for condensed matter physics and quantum chemistry [phys. rev. lett. 103, 026403 (2009)].** *Phys. Rev. Lett.* **106**, 179902 (2011).
- [133] Zhang, Y. & Yang, W. **Comment on “Generalized Gradient Approximation Made Simple”.** *Phys. Rev. Lett.* **80**, 890–890 (1998).
- [134] Hammer, B., Hansen, L. B. & Nørskov, J. K. **Improved adsorption energetics within density-functional theory using revised Perdew-Burke-Ernzerhof functionals.** *Phys. Rev. B* **59**, 7413–7421 (1999).
- [135] Perdew, J. P. *et al.* **Restoring the density-gradient expansion for exchange in solids and surfaces.** *Phys. Rev. Lett.* **100**, 136406 (2008).
- [136] Becke, A. D. **Density functional calculations of molecular bond energies.** *J. Chem. Phys.* **84**, 4524–4529 (1986).
- [137] Becke, A. D. **Correlation energy of an inhomogeneous electron gas: A coordinate–space model.** *J. Chem. Phys.* **88**, 1053–1062 (1988).
- [138] Lee, C., Yang, W. & Parr, R. G. **Development of the colle-salvetti correlation-energy formula into a functional of the electron density.** *Phys. Rev. B* **37**, 785–789 (1988).
- [139] Tao, J., Perdew, J. P., Staroverov, V. N. & Scuseria, G. E. **Climbing the density functional ladder: Nonempirical meta-generalized gradient approximation designed for molecules and solids.** *Phys. Rev. Lett.* **91**, 146401 (2003).
- [140] Ghosh, S. K. & Parr, R. G. **Phase-space approach to the exchange-energy functional of density-functional theory.** *Phys. Rev. A* **34**, 785 (1986).
- [141] Becke, A. & Roussel, M. **Exchange holes in inhomogeneous systems: A coordinate-space model.** *Phys. Rev. A* **39**, 3761 (1989).
- [142] Arbuznikov, A. V. & Kaupp, M. **The self-consistent implementation of exchange-correlation functionals depending on the local kinetic energy density.** *Chem. Phys. Lett.* **381**, 495–504 (2003).

- [143] Perdew, J. P. & Constantin, L. A. Laplacian-level density functionals for the kinetic energy density and exchange-correlation energy. *Phys. Rev. B* **75**, 155109 (2007).
- [144] Adamo, C., Ernzerhof, M. & Scuseria, G. E. The meta-GGA functional: Thermochemistry with a kinetic energy density dependent exchange-correlation functional. *J. Chem. Phys.* **112**, 2643–2649 (2000).
- [145] Perdew, J. P., Kurth, S., Zupan, A. c. v. & Blaha, P. Accurate density functional with correct formal properties: A step beyond the generalized gradient approximation. *Phys. Rev. Lett.* **82**, 2544–2547 (1999).
- [146] Zhao, Y., Schultz, N. E. & Truhlar, D. Exchange-correlation functional with broad accuracy for metallic and nonmetallic compounds, kinetics, and noncovalent interactions. *J. Chem. Phys.* **123**, 161103 (2005).
- [147] Zhao, Y. & Truhlar, D. G. A new local density functional for main-group thermochemistry, transition metal bonding, thermochemical kinetics, and noncovalent interactions. *J. Chem. Phys.* **125**, 194101 (2006).
- [148] Zhao, Y. & Truhlar, D. G. The M06 suite of density functionals for main group thermochemistry, thermochemical kinetics, noncovalent interactions, excited states, and transition elements: two new functionals and systematic testing of four M06-class functionals and 12 other functionals. *Theor. Chim. Acta* **120**, 215–241 (2008).
- [149] Zhao, Y. & Truhlar, D. G. Exploring the limit of accuracy of the global hybrid meta density functional for main-group thermochemistry, kinetics, and noncovalent interactions. *J. Chem. Theory Comput.* **4**, 1849–1868 (2008).
- [150] Becke, A. D. Density-functional thermochemistry. III. The role of exact exchange. *J. Chem. Phys.* **98**, 5648 (1993).
- [151] Ernzerhof, M. & Scuseria, G. E. Assessment of the Perdew-Burke-Ernzerhof exchange-correlation functional. *J. Chem. Phys.* **110**, 5029–5036 (1999).
- [152] Adamo, C. & Barone, V. Toward reliable density functional methods without adjustable parameters: The PBE0 model. *J. Chem. Phys.* **110**, 6158–6170 (1999).
- [153] Perdew, J. P., Ernzerhof, M. & Burke, K. Rationale for mixing exact exchange with density functional approximations. *J. Chem. Phys.* **105**, 9982–9985 (1996).

- [154] Stephens, P., Devlin, F., Chabalowski, C. & Frisch, M. J. **Ab initio calculation of vibrational absorption and circular dichroism spectra using density functional force fields.** *J. Phys. Chem.* **98**, 11623–11627 (1994).
- [155] M. J. Frisch et al. Computer code Gaussian 03, Revision B.05 (2003).
- [156] Bohm, D. & Pines, D. **A collective description of electron interactions. I. Magnetic interactions.** *Phys. Rev.* **82**, 625–634 (1951).
- [157] Pines, D. & Bohm, D. **A collective description of electron interactions: II. Collective vs individual particle aspects of the interactions.** *Phys. Rev.* **85**, 338–353 (1952).
- [158] Bohm, D. & Pines, D. **A collective description of electron interactions: III. Coulomb interactions in a degenerate electron gas.** *Phys. Rev.* **92**, 609–625 (1953).
- [159] Marini, A., García-González, P. & Rubio, A. **First-principles description of correlation effects in layered materials.** *Phys. Rev. Lett.* **96**, 136404 (2006).
- [160] Harl, J. & Kresse, G. **Cohesive energy curves for noble gas solids calculated by adiabatic connection fluctuation-dissipation theory.** *Phys. Rev. B* **77**, 045136 (2008).
- [161] Harl, J. & Kresse, G. **Accurate bulk properties from approximate many-body techniques.** *Phys. Rev. Lett.* **103**, 056401 (2009).
- [162] Jiang, H. & Engel, E. **Random-phase-approximation-based correlation energy functionals: Benchmark results for atoms.** *J. Chem. Phys.* **127**, 184108 (2007).
- [163] Ren, X., Rinke, P., Joas, C. & Scheffler, M. **Random-phase approximation and its applications in computational chemistry and materials science.** *J. Mater. Sci.* **47**, 7447–7471 (2012).
- [164] Eshuis, H., Bates, J. E. & Furche, F. **Electron correlation methods based on the random phase approximation.** *Theor. Chim. Acta* **131**, 1–18 (2012).
- [165] Ren, X., Tkatchenko, A., Rinke, P. & Scheffler, M. **Beyond the random-phase approximation for the electron correlation energy: The importance of single excitations.** *Phys. Rev. Lett.* **106**, 153003 (2011).
- [166] Adler, S. L. **Quantum theory of the dielectric constant in real solids.** *Phys. Rev.* **126**, 413–420 (1962).

- [167] Wiser, N. [Dielectric constant with local field effects included.](#) *Phys. Rev.* **129**, 62–69 (1963).
- [168] Lein, M., Gross, E. & Perdew, J. P. [Electron correlation energies from scaled exchange-correlation kernels: Importance of spatial versus temporal nonlocality.](#) *Phys. Rev. B* **61**, 13431 (2000).
- [169] Dobson, J. F. & Wang, J. [Energy-optimized local exchange-correlation kernel for the electron gas: Application to van der Waals forces.](#) *Phys. Rev. B* **62**, 10038 (2000).
- [170] London, F. [Zur theorie und systematik der molekularkräfte.](#) *Zeitschrift für Physik* **63**, 245–279 (1930).
- [171] van Mourik, T. & Gdanitz, R. J. [A critical note on density functional theory studies on rare-gas dimers.](#) *J. Chem. Phys.* **116**, 9620–9623 (2002).
- [172] Lee, K., Murray, E. D., Kong, L., Lundqvist, B. I. & Langreth, D. C. [Higher-accuracy van der Waals density functional.](#) *Phys. Rev. B* **82**, 081101 (2010).
- [173] Vydrov, O. A. & Van Voorhis, T. [Nonlocal van der Waals density functional made simple.](#) *Phys. Rev. Lett.* **103**, 063004 (2009).
- [174] Vydrov, O. A. & Van Voorhis, T. [Nonlocal van der Waals density functional: The simpler the better.](#) *J. Chem. Phys.* **133**, 244103 (2010).
- [175] Langreth, D. *et al.* [A density functional for sparse matter.](#) *J. Phys.: Condens. Matter* **21**, 084203 (2009).
- [176] Klimeš, J., Bowler, D. R. & Michaelides, A. [Van der Waals density functionals applied to solids.](#) *Phys. Rev. B* **83**, 195131 (2011).
- [177] Wellendorff, J. & Bligaard, T. [On the importance of gradient-corrected correlation for van der Waals density functionals.](#) *Top. Catal.* **54**, 1143–1150 (2011).
- [178] Tang, K. T. [Dynamic polarizabilities and van der Waals coefficients.](#) *Phys. Rev.* **177**, 108–114 (1969).
- [179] Grimme, S. [Density functional theory with London dispersion corrections.](#) *Comput. Mol. Sci.* **1**, 211–228 (2011).
- [180] Hepburn, J., Scoles, G. & Penco, R. [A simple but reliable method for the prediction of intermolecular potentials.](#) *Chem. Phys. Lett.* **36**, 451–456 (1975).
- [181] Wu, Q. & Yang, W. [Empirical correction to density functional theory for van der Waals interactions.](#) *J. Chem. Phys.* **116**, 515–524 (2002).

- [182] Elstner, M., Hobza, P., Frauenheim, T., Suhai, S. & Kaxiras, E. Hydrogen bonding and stacking interactions of nucleic acid base pairs: A density-functional-theory based treatment. *J. Chem. Phys.* **114**, 5149–5155 (2001).
- [183] Grimme, S. Accurate description of van der Waals complexes by density functional theory including empirical corrections. *J. Comp. Chem.* **25**, 1463–1473 (2004).
- [184] Grimme, S. Semiempirical GGA-type density functional constructed with a long-range dispersion correction. *J. Comp. Chem.* **27**, 1787–1799 (2006).
- [185] Jurečka, P., Černý, J., Hobza, P. & Salahub, D. R. Density functional theory augmented with an empirical dispersion term. interaction energies and geometries of 80 noncovalent complexes compared with *ab initio* quantum mechanics calculations. *J. Comp. Chem.* **28**, 555–569 (2007).
- [186] Ortmann, F., Bechstedt, F. & Schmidt, W. G. Semiempirical van der Waals correction to the density functional description of solids and molecular structures. *Phys. Rev. B* **73**, 205101 (2006).
- [187] Becke, A. D. & Johnson, E. R. A density-functional model of the dispersion interaction. *J. Chem. Phys.* **123**, 154101 (2005).
- [188] Kannemann, F. O. & Becke, A. D. van der Waals interactions in density-functional theory: intermolecular complexes. *J. Chem. Theory Comput.* **6**, 1081–1088 (2010).
- [189] Becke, A. D. & Johnson, E. R. Exchange-hole dipole moment and the dispersion interaction: High-order dispersion coefficients. *J. Chem. Phys.* **124**, 014104 (2006).
- [190] Tkatchenko, A. *et al.* Van der Waals interactions between organic adsorbates and at organic/inorganic interfaces. *MRS bulletin* **35**, 435–442 (2010).
- [191] Klimeš, J. & Michaelides, A. Perspective: Advances and challenges in treating van der Waals dispersion forces in density functional theory. *J. Chem. Phys.* **137**, 120901 (2012).
- [192] Grimme, S., Antony, J., Ehrlich, S. & Krieg, H. A consistent and accurate *ab initio* parametrization of density functional dispersion correction (DFT-D) for the 94 elements H-Pu. *J. Chem. Phys.* **132**, 154104 (2010).
- [193] Hirshfeld, F. L. Bonded-atom fragments for describing molecular charge densities. *Theor. Chim. Acta* **44**, 129–138 (1977).

- [194] Dobson, J. F., White, A. & Rubio, A. [Asymptotics of the dispersion interaction: analytic benchmarks for van der Waals energy functionals](#). *Phys. Rev. Lett.* **96**, 073201 (2006).
- [195] Chu, X. & Dalgarno, A. [Linear response time-dependent density functional theory for van der Waals coefficients](#). *J. Chem. Phys.* **121**, 4083 (2004).
- [196] Bondi, A. [van der Waals volumes and radii](#). *J. Chem. Phys.* **68**, 441–451 (1964).
- [197] Jurečka, P., Šponer, J., Černý, J. & Hobza, P. [Benchmark database of accurate \(MP2 and CCSD\(T\) complete basis set limit\) interaction energies of small model complexes, DNA base pairs, and amino acid pairs](#). *Phys. Chem. Chem. Phys.* **8**, 1985–1993 (2006).
- [198] Marom, N. *et al.* [Dispersion interactions with density-functional theory: benchmarking semiempirical and interatomic pairwise corrected density functionals](#). *J. Chem. Theory Comput.* **7**, 3944–3951 (2011).
- [199] Steinmann, S. N. & Corminboeuf, C. [Comprehensive benchmarking of a density-dependent dispersion correction](#). *J. Chem. Theory Comput.* **7**, 3567–3577 (2011).
- [200] von Lilienfeld, O. A. & Tkatchenko, A. [Two-and three-body interatomic dispersion energy contributions to binding in molecules and solids](#). *J. Chem. Phys.* **132**, 234109 (2010).
- [201] Grimme, S. [Supramolecular binding thermodynamics by dispersion-corrected density functional theory](#). *Chem. Eur. J.* **18**, 9955–9964 (2012).
- [202] Zhang, G.-X., Tkatchenko, A., Paier, J., Appel, H. & Scheffler, M. [van der Waals interactions in ionic and semiconductor solids](#). *Phys. Rev. Lett.* **107**, 245501 (2011).
- [203] Ruiz, V. G., Liu, W., Zojer, E., Scheffler, M. & Tkatchenko, A. [Density-functional theory with screened van der Waals interactions for the modeling of hybrid inorganic-organic systems](#). *Phys. Rev. Lett.* **108**, 146103 (2012).
- [204] DiStasio, R. A., von Lilienfeld, O. A. & Tkatchenko, A. [Collective many-body van der Waals interactions in molecular systems](#). *Proc. Natl. Acad. Sci. USA* **109**, 14791–14795 (2012).
- [205] Donchev, A. G. [Many-body effects of dispersion interaction](#). *J. Chem. Phys.* **125**, 074713 (2006).

- [206] Harris, J. [Adiabatic-connection approach to kohn-sham theory](#). *Phys. Rev. A* **29**, 1648 (1984).
- [207] Kubo, R. [The fluctuation-dissipation theorem](#). *Rep. Prog. Phys.* **29**, 255 (1966).
- [208] Marom, N. *et al.* [Many-body dispersion interactions in molecular crystal polymorphism](#). *Angew. Chem. Int. Ed.* **52**, 6629–6632 (2013).
- [209] Reilly, A. M. & Tkatchenko, A. [Role of dispersion interactions in the polymorphism and entropic stabilization of the aspirin crystal](#). *Phys. Rev. Lett.* **113**, 055701 (2014).
- [210] Reilly, A. M. & Tkatchenko, A. [van der Waals dispersion interactions in molecular materials: Beyond pairwise additivity](#). *Chem. Sci.* **6**, 3289–3301 (2015).
- [211] Bernard, W. & Callen, H. B. [Irreversible thermodynamics of nonlinear processes and noise in driven systems](#). *Rev. Mod. Phys.* **31**, 1017 (1959).
- [212] Peterson, R. L. [Formal theory of nonlinear response](#). *Rev. Mod. Phys.* **39**, 69 (1967).
- [213] Hellmann, H. *Einführung in die Quantenchemie* (Leipzig: Franz Deuticke) (1937).
- [214] Feynman, R. P. [Forces in molecules](#). *Phys. Rev.* **56**, 340–343 (1939).
- [215] Cohen, H. D. & Roothaan, C. [Electric dipole polarizability of atoms by the Hartree—Fock method. I. Theory for closed-shell systems](#). *J. Chem. Phys.* **43**, S34–S39 (1965).
- [216] Abramowitz, M., Stegun, I. A. *et al.* *Handbook of mathematical functions*, vol. 1046 (Dover New York, 1965).
- [217] Bishop, D. M. [Molecular vibrational and rotational motion in static and dynamic electric fields](#) **62**, 343 (1990).
- [218] Monkhorst, H. J. [Calculation of properties with the coupled-cluster method](#). *Int. J. Quantum Chem.* **12**, 421–432 (1977).
- [219] Koch, H., Jo, P. *et al.* [Coupled cluster response functions](#). *J. Chem. Phys.* **93**, 3333–3344 (1990).
- [220] Christiansen, O., Jørgensen, P. & Hättig, C. [Response functions from fourier component variational perturbation theory applied to a time-averaged quasienergy](#). *Int. J. Quantum Chem.* **68**, 1–52 (1998).

- [221] Kobayashi, R., Koch, H. & Jørgensen, P. Calculation of frequency-dependent polarizabilities using coupled-cluster response theory. *Chem. Phys. Lett.* **219**, 30–35 (1994).
- [222] Hättig, C., Christiansen, O., Koch, H. & Jørgensen, P. Frequency-dependent first hyperpolarizabilities using coupled cluster quadratic response theory. *Chem. Phys. Lett.* **269**, 428–434 (1997).
- [223] Hättig, C., Christiansen, O. & Jørgensen, P. Frequency-dependent second hyperpolarizabilities using coupled cluster cubic response theory. *Chem. Phys. Lett.* **282**, 139–146 (1998).
- [224] Kállay, M. & Gauss, J. Calculation of frequency-dependent polarizabilities using general coupled-cluster models. *J. Mol. Struct. (THEOCHEM)* **768**, 71–77 (2006).
- [225] Hammond, J. R., Kowalski, K. et al. Dynamic polarizabilities of polyaromatic hydrocarbons using coupled-cluster linear response theory. *J. Phys. Chem. A* **127**, 144105 (2007).
- [226] Hammond, J. R., De Jong, W. A. & Kowalski, K. Coupled-cluster dynamic polarizabilities including triple excitations. *J. Chem. Phys.* **128**, 224102 (2008).
- [227] HAMMOND, J. R. COUPLED-CLUSTER RESPONSE THEORY: PARALLEL ALGORITHMS AND NOVEL APPLICATIONS. Ph.D. thesis, The University of Chicago, CHICAGO, USA (2009).
- [228] E. J. Bylaska et al. NWChem, A Computational Chemistry Package for Parallel Computers, Version 5.1 (2007), Pacific Northwest National Laboratory, Richland, Washington 99352-0999, USA.
- [229] Fiolhais, C., Nogueira, F. & Marques, M. A. *A primer in density functional theory*, vol. 620 (Springer, 2003).
- [230] Marques, M. *Time-dependent density functional theory*, vol. 706 (Springer, 2006).
- [231] Marques, M., Castro, A. & Rubio, A. Assessment of exchange-correlation functionals for the calculation of dynamical properties of small clusters in time-dependent density functional theory. *J. Chem. Phys.* **115**, 3006–3014 (2001).
- [232] Castro, A. et al. Can optical spectroscopy directly elucidate the ground state of  $C_{20}$ ? *J. Chem. Phys.* **116**, 1930–1933 (2002).
- [233] Castro, A., Marques, M. A., Alonso, J. A. & Rubio, A. Optical properties of nanostructures from time-dependent density functional theory. *J. Comp. Theor. Nanosci.* **1**, 231–255 (2004).

- [234] Botti, S. & Marques, M. A. L. Identification of fullerene-like CdSe nanoparticles from optical spectroscopy calculations. *Phys. Rev. B* **75**, 035311 (2007).
- [235] Yabana, K. & Bertsch, G. Time-dependent local-density approximation in real time: Application to conjugated molecules. *Int. J. Quantum Chem.* **75**, 55–66 (1999).
- [236] Mallocci, G., Mulas, G. & Joblin, C. Electronic absorption spectra of PAHs up to vacuum UV. Towards a detailed model of interstellar PAH photophysics. *Astron. Astrophys.* **426**, 105–117 (2004).
- [237] Mallocci, G., Mulas, G., Cappellini, G., Fiorentini, V. & Porceddu, I. Theoretical electron affinities of PAHs and electronic absorption spectra of their mono-anions. *Astron. Astrophys.* **432**, 585–594 (2005).
- [238] Marques, M. A. L., López, X., Varsano, D., Castro, A. & Rubio, A. Time-dependent density-functional approach for biological chromophores: The case of the green fluorescent protein. *Phys. Rev. Lett.* **90**, 258101 (2003).
- [239] Lopez, X., Marques, M. A., Castro, A. & Rubio, A. Optical absorption of the blue fluorescent protein: A first-principles study. *J. Am. Chem. Soc.* **127**, 12329–12337 (2005).
- [240] Grossa, E., Dobsonb, J. & Petersilkaa, M. Density functional theory of time-dependent phenomena. *Top. Curr. Chem.* **181**, 81.
- [241] van Leeuwen, R. Causality and symmetry in time-dependent density-functional theory. *Phys. Rev. Lett.* **80**, 1280 (1998).
- [242] Petersilka, M., Gossmann, U. & Gross, E. Excitation energies from time-dependent density-functional theory. *Phys. Rev. Lett.* **76**, 1212 (1996).
- [243] Olsen, J., Jørgensen, P. & Yarkony, D. *Modern electronic structure theory* (World Scientific, 1995).
- [244] Rice, J. E. & Handy, N. C. The calculation of frequency-dependent polarizabilities as pseudo-energy derivatives. *J. Chem. Phys.* **94**, 4959–4971 (1991).
- [245] Aiga, F. & Itoh, R. Calculation of frequency-dependent polarizabilities and hyperpolarizabilities by the second-order møller-plesset perturbation theory. *Chem. Phys. Lett.* **251**, 372–380 (1996).

- [246] Hättig, C. & Hess, B. A. Correlated frequency-dependent polarizabilities and dispersion coefficients in the time-dependent second-order möller-plesset approximation. *Chem. Phys. Lett.* **233**, 359–370 (1995).
- [247] Hättig, C. & Hess, B. A. TDMP2 calculation of dynamic multipole polarizabilities and dispersion coefficients of the triplebonded molecules CO, N<sub>2</sub>, CN<sup>−</sup>, and NO<sup>+</sup>. *J. Chem. Phys.* **105**, 9948–9965 (1996).
- [248] Sekino, H. & Bartlett, R. J. Frequency-dependent hyperpolarizabilities in the coupled-cluster method: The Kerr effect for molecules. *Chem. Phys. Lett.* **234**, 87–93 (1995).
- [249] Dalskov, E. K. & Sauer, S. P. Correlated, static and dynamic polarizabilities of small molecules. comparison of four “black box” methods. *J. Phys. Chem. A* **102**, 5269–5274 (1998).
- [250] Lide, D. R. & Bruno, T. J. CRC Handbook of Chemistry and Physics (2012).
- [251] Zeiss, G., Meath, W. J., MacDonald, J. & Dawson, D. Dipole oscillator strength distributions, sums, and some related properties for Li, N, O, H<sub>2</sub>, N<sub>2</sub>, O<sub>2</sub>, NH<sub>3</sub>, H<sub>2</sub>O, NO, and N<sub>2</sub>O. *Can. J. Phys.* **55**, 2080–2100 (1977).
- [252] Jhanwar, B. & Meath, W. J. Pseudo-spectral dipole oscillator strength distributions for the normal alkanes through octane and the evaluation of some related dipole-dipole and triple-dipole dispersion interaction energy coefficients. *Mol. Phys.* **41**, 1061–1070 (1980).
- [253] Kumar, A. & Meath, W. J. Pseudo-spectral dipole oscillator strengths and dipole-dipole and triple-dipole dispersion energy coefficients for HF, HCl, HBr, He, Ne, Ar, Kr and Xe. *Mol. Phys.* **54**, 823–833 (1985).
- [254] Kumar, A. & Meath, W. J. Dipole oscillator strength properties and dispersion energies for acetylene and benzene. *Mol. Phys.* **75**, 311–324 (1992).
- [255] Kumar, M., Kumar, A. & Meath, W. J. Dipole oscillator strength properties and dispersion energies for Cl<sub>2</sub>. *Mol. Phys.* **100**, 3271–3279 (2002).
- [256] Kumar, A., Kumar, M. & Meath, W. J. Dipole oscillator strengths, dipole properties and dispersion energies for SiF<sub>4</sub>. *Mol. Phys.* **101**, 1535–1543 (2003).

- [257] Kumar, A. & Meath, W. J. Dipole oscillator strength distributions, properties and dispersion energies for the dimethyl, diethyl and methyl-propyl ethers. *Mol. Phys.* **106**, 1531–1544 (2008).
- [258] Kumar, A., Jhanwar, B. & Meath, W. J. Dipole oscillator strength distributions and properties for methanol, ethanol and propan-1-ol and related dispersion energies. *Collect. Czech. Chem. Commun.* **70**, 1196–1224 (2005).
- [259] Kumar, A. Reliable isotropic dipole properties and dispersion energy coefficients for  $\text{CCl}_4$ . *J. Mol. Struct. (THEOCHEM)* **591**, 91–99 (2002").
- [260] Kumar, A., Jhanwar, B. & Meath, W. Dipole oscillator strength distributions, properties, and dispersion energies for ethylene, propene, and 1-butene. *Can. J. Chem.* **85**, 724–737 (2007).
- [261] Pazur, R., Kumar, A., Thuraisingham, R. & Meath, W. J. Dipole oscillator strength properties and dispersion energy coefficients for  $\text{H}_2\text{S}$ . *Can. J. Chem.* **66**, 615–619 (1988).
- [262] Johnson, R. E., Epstein, S. T. & Meath, W. J. Evaluation of long-range retarded interaction energies. *J. Chem. Phys.* **47**, 1271–1274 (2004).
- [263] Kumar, A. & Meath, W. J. Pseudo-spectral dipole oscillator-strength distributions for  $\text{SO}_2$ ,  $\text{CS}_2$  and OCS and values of some related dipole-dipole and triple-dipole dispersion energy constants. *Chem. Phys.* **91**, 411–418 (1984).
- [264] Kumar, A., Kumar, M. & Meath, W. J. Dipole oscillator strength properties and dispersion energies for  $\text{SiH}_4$ . *Chem. Phys.* **286**, 227–236 (2003).
- [265] Blum, V. et al. Ab initio molecular simulations with numeric atom-centered orbitals. *Comput. Phys. Comm.* **180**, 2175–2196 (2009).
- [266] Kronig, R. d. On the theory of dispersion of X-rays. *JOSA* **12**, 547–556 (1926).
- [267] Kramers, H. A. *La diffusion de la lumiere par les atomes* (1927).
- [268] Alms, G., Burnham, A. & Flygare, W. Measurement of the dispersion in polarizability anisotropies. *J. Chem. Phys.* **63**, 3321–3326 (1975).
- [269] Okruss, M., Müller, R. & Hese, A. High-resolution ultraviolet laser spectroscopy on jet-cooled benzene molecules: Ground and excited electronic state polarizabilities determined from static stark effect measurements. *J. Chem. Phys.* **110**, 10393–10402 (1999).

- [270] Ritchie, G. L. & Watson, J. N. Temperature dependence of electric field-gradient induced birefringence (The Buckingham effect) in C<sub>6</sub>H<sub>6</sub> and C<sub>6</sub>F<sub>6</sub>: comparison of electric and magnetic properties of C<sub>6</sub>H<sub>6</sub> and C<sub>6</sub>F<sub>6</sub>. *Chem. Phys. Lett.* **322**, 143–148 (2000).
- [271] Rizzo, A. *et al.* Density-functional and electron correlated study of five linear birefringences—Kerr, Cotton–Mouton, Buckingham, Jones, and magnetoelectric—in gaseous benzene. *J. Chem. Phys.* **121**, 8814–8830 (2004).
- [272] Blum, L. C. & Reymond, J.-L. 970 million druglike small molecules for virtual screening in the chemical universe database GDB-13. *J. Am. Chem. Soc.* **131**, 8732–8733 (2009).
- [273] Thompson, M. A. Arguslab 4.0. 1. *Planaria Software LLC, Seattle, WA* (2004).
- [274] Adamo, C., Cossi, M., Scalmani, G. & Barone, V. Accurate static polarizabilities by density functional theory: Assessment of the PBE0 model. *Chem. Phys. Lett.* **307**, 265–271 (1999).
- [275] Weininger, D. SMILES, a chemical language and information system. 1. introduction to methodology and encoding rules. *J. Chem. Inf. Comp. Sci.* **28**, 31–36 (1988).
- [276] Weininger, D., Weininger, A. & Weininger, J. L. SMILES. 2. algorithm for generation of unique smiles notation. *J. Chem. Inf. Comp. Sci.* **29**, 97–101 (1989).
- [277] Perdew, J. P., Burke, K. & Ernzerhof, M. Generalized gradient approximation made simple. *Phys. Rev. Lett.* **77**, 3865–3868 (1996).
- [278] Kato, T. & Frechet, J. M. A new approach to mesophase stabilization through hydrogen bonding molecular interactions in binary mixtures. *J. Am. Chem. Soc.* **111**, 8533–8534 (1989).
- [279] Braga, D. & Grepioni, F. Intermolecular interactions in nonorganic crystal engineering. *Accounts Chem. Res.* **33**, 601–608 (2000).
- [280] Mann, S. Self-assembly and transformation of hybrid nano-objects and nanostructures under equilibrium and non-equilibrium conditions. *Nat. Mater.* **8**, 781–792 (2009).
- [281] Li, X. *et al.* Two-dimensional GaSe/MoSe<sub>2</sub> misfit bilayer heterojunctions by van der Waals epitaxy. *Sci. Adv.* **2**, e1501882 (2016).
- [282] Hamel, S. *et al.* First-principles calculations of the dielectric properties of silicon nanostructures. *Appl. Phys. Lett.* **92**, 3115 (2008).

- [283] Lu, D., Gygi, F. & Galli, G. Dielectric properties of ice and liquid water from first-principles calculations. *Phys. Rev. Lett.* **100**, 147601 (2008).
- [284] Bade, W. L. Drude-model calculation of dispersion forces.I. General theory. *J. Chem. Phys.* **27**, 1280–1284 (1957).
- [285] Cole, M. W., Velegol, D., Kim, H.-Y. & Lucas, A. A. Nanoscale van der Waals interactions. *Mol. Simul.* **35**, 849–866 (2009).
- [286] Liu, R.-F., Ángyán, J. G. & Dobson, J. F. Dispersion interaction in hydrogen-chain models. *J. Chem. Phys.* **134**, 114106 (2011).
- [287] Shtogun, Y. V. & Woods, L. M. Many-body van der Waals interactions between graphitic nanostructures. *J. Phys. Chem. Lett.* **1**, 1356–1362 (2010).
- [288] Lamoureux, G., MacKerell Jr, A. D. & Roux, B. A simple polarizable model of water based on classical drude oscillators. *J. Chem. Phys.* **119**, 5185–5197 (2003).
- [289] Rick, S. W., Stuart, S. J. & Berne, B. J. Dynamical fluctuating charge force fields: Application to liquid water. *J. Chem. Phys.* **101**, 6141–6156 (1994).
- [290] Lieb, E. H. & Thirring, W. E. Universal nature of van der waals forces for coulomb systems. *Phys. Rev. A* **34**, 40 (1986).
- [291] Taylor, T., Schmollngruber, M., Schröder, C. & Steinhauser, O. The effect of thole functions on the simulation of ionic liquids with point induced dipoles at various densities. *J. Chem. Phys.* **138**, 204119 (2013).
- [292] Baker Jr, G. A. The theory and application of the padé approximant method. In *Advances in Theoretical Physics, Volume 1*, vol. 1, 1 (1965).
- [293] Applequist, J. A multipole interaction theory of electric polarization of atomic and molecular assemblies. *J. Chem. Phys.* **83**, 809–826 (1985).
- [294] Flügge, S. *Practical quantum mechanics*, vol. 177 (Springer, 1994).
- [295] Jones, A. *Quantum Drude Oscillators for Accurate Many-body Intermolecular Forces*. Ph.D. thesis, University of Edinburgh (2010).
- [296] Jones, A. P., Crain, J., Sokhan, V. P., Whitfield, T. W. & Martyna, G. J. Quantum drude oscillator model of atoms and molecules: Many-body polarization and dispersion interactions for atomistic simulation. *Phys. Rev. B* **87**, 144103 (2013).

- [297] Tabor, D. *Gases, liquids and solids: and other states of matter* (Cambridge University Press, 1991).
- [298] Brinck, T., Murray, J. S. & Politzer, P. *Polarizability and volume*. *J. Chem. Phys.* **98**, 4305–4306 (1993).
- [299] Politzer, P., Jin, P. & Murray, J. S. *Atomic polarizability, volume and ionization energy*. *J. Chem. Phys.* **117**, 8197–8202 (2002).
- [300] Marshalek, E. R. & da Providência, J. *Sum rules, random-phase-approximation, and constrained self-consistent fields*. *Phys. Rev. C* **7**, 2281 (1973).
- [301] Applequist, J. *An atom dipole interaction model for molecular optical properties*. *Accounts Chem. Res.* **10**, 79–85 (1977).
- [302] Helgaker, T., Jorgensen, P. & Olsen, J. *Molecular electronic-structure theory* (John Wiley & Sons, 2014).
- [303] Brandt, W. & Lundqvist, S. *Collective effects in atomic spectra*. *J. Quant. Spectrosc. Radiat. Transfer* **4**, 679–689 (1964).
- [304] Brandt, W., Eder, L. & Lundqvist, S. *Atomic photoabsorption cross sections*. *J. Quant. Spectrosc. Radiat. Transfer* **7**, 185–202 (1967).
- [305] Becke, A. D. & Johnson, E. R. *Exchange-hole dipole moment and the dispersion interaction revisited*. *J. Chem. Phys.* **127**, 154108 (2007).
- [306] Becke, A. D. *A multicenter numerical integration scheme for polyatomic molecules*. *J. Chem. Phys.* **88**, 2547–2553 (1988).
- [307] Johnson, E. R. & Becke, A. D. *A post-hartree–fock model of intermolecular interactions*. *J. Chem. Phys.* **123**, 024101 (2005).
- [308] Johnson, E. R. & Becke, A. D. *A post-hartree-fock model of intermolecular interactions: inclusion of higher-order corrections*. *J. Chem. Phys.* **124**, 174104–174104 (2006).
- [309] Olasz, A. *et al.* *The use of atomic intrinsic polarizabilities in the evaluation of the dispersion energy*. *J. Chem. Phys.* **127**, 224105 (2007).
- [310] Proft, F. D., Vivas-Reyes, R., Peeters, A., Van Alsenoy, C. & Geerlings, P. *Hirshfeld partitioning of the electron density: atomic dipoles and their relation with functional group properties*. *J. Comp. Chem.* **24**, 463–470 (2003).
- [311] Becke, A. D. & Johnson, E. R. *A unified density-functional treatment of dynamical, nondynamical, and dispersion correlations*. *J. Chem. Phys.* **127**, 124108 (2007).

- [312] Kumar, A. & Meath, W. J. **Integrated dipole oscillator strengths and dipole properties for Ne, Ar, Kr, Xe, HF, HCl, and HBr.** *Canadian journal of chemistry* **63**, 1616–1630 (1985).
- [313] Parkinson, W. A., Sauer, S. P., Oddershede, J. & Bishop, D. M. **Calculation of the verdet constants for H<sub>2</sub>, N<sub>2</sub>, CO, and FH.** *J. Chem. Phys.* **98**, 487–495 (1993).
- [314] Jamieson, M. **A time-dependent Hartree–Fock study of dispersion in the Cotton–Mouton effect for the helium isoelectronic sequence.** *Chem. Phys. Lett.* **183**, 9–15 (1991).
- [315] Yabana, K. & Bertsch, G. **Time-dependent local-density approximation in real time.** *Phys. Rev. B* **54**, 4484 (1996).
- [316] Maeder, F. & Kutzelnigg, W. **Natural states of interacting systems and their use for the calculation of intermolecular forces: IV. calculation of van der Waals coefficients between one-and two-valence-electron atoms in their ground states, as well as of polarizabilities, oscillator strength sums and related quantities, including correlation effects.** *Chem. Phys.* **42**, 95–112 (1979).
- [317] Thouless, D. **Vibrational states of nuclei in the random phase approximation.** *Nucl. Phys.* **22**, 78–95 (1961).
- [318] Castro, A. *et al.* **octopus: a tool for the application of time-dependent density functional theory.** *physica status solidi (b)* **243**, 2465–2488 (2006).
- [319] Troullier, N. & Martins, J. L. **Efficient pseudopotentials for plane-wave calculations.** *Phys. Rev. B* **43**, 1993 (1991).
- [320] Wemple, S. H. & DiDomenico, M. **Behavior of the electronic dielectric constant in covalent and ionic materials.** *Phys. Rev. B* **3**, 1338–1351 (1971).
- [321] Zhang, G.-X. **Understanding the role of van der Waals forces in solids from first principles.** Ph.D. thesis, Freie Universität Berlin (2009).
- [322] Kroto, H. W., Heath, J. R., O'Brien, S. C., Curl, R. F. & Smalley, R. E. **C<sub>60</sub>: buckminsterfullerene.** *Nature* **318**, 162–163 (1985).
- [323] Iijima, S. **Helical microtubules of graphitic carbon.** *Nature* **354**, 56–58 (1991).
- [324] Geim, A. K. & Novoselov, K. S. **The rise of graphene.** *Nat. Mater.* **6**, 183–191 (2007).
- [325] Nair, R. R. *et al.* **Fine structure constant defines visual transparency of graphene.** *Science* **320**, 1308–1308 (2008).

- [326] Ruzsinszky, A., Perdew, J. P., Tao, J., Csonka, G. I. & Pitarke, J. M. **Van der Waals coefficients for nanostructures: Fullerenes defy conventional wisdom.** *Phys. Rev. Lett.* **109**, 233203 (2012).
- [327] Ghosh, S. *et al.* **Dimensional crossover of thermal transport in few-layer graphene.** *Nat. Mater.* **9**, 555–558 (2010).
- [328] Gobre, V. V. & Tkatchenko, A. **Scaling laws for van der Waals interactions in nanostructured materials.** *Nat. Commun.* **4**, 2341 (2013).
- [329] Kumar, A. & Meath, W. J. **Dipole oscillator strength properties and dispersion energies for acetylene and benzene.** *Mol. Phys.* **75**, 311–324 (1992).
- [330] Antoine, R. *et al.* **Direct measurement of the electric polarizability of isolated C<sub>60</sub> molecules.** *J. Chem. Phys.* **110**, 9771–9772 (1999).
- [331] Jiemchooroj, A., Norman, P. & Sernelius, B. E. **Complex polarization propagator method for calculation of dispersion coefficients of extended π-conjugated systems: The C<sub>6</sub> coefficients of polyacenes and C<sub>60</sub>.** *J. Chem. Phys.* **123**, 124312 (2005).
- [332] Kauczor, J., Norman, P. & Saidi, W. A. **Non-additivity of polarizabilities and van der Waals C<sub>6</sub> coefficients of fullerenes.** *J. Chem. Phys.* **138**, 114107 (2013).
- [333] Bruch, L. W. **Evaluation of the van der Waals force for atomic force microscopy.** *Phys. Rev. B* **72**, 033410 (2005).
- [334] Rajter, R. F., French, R. H., Ching, W., Podgornik, R. & Parsegian, V. A. **Chirality-dependent properties of carbon nanotubes: Electronic structure, optical dispersion properties, hamaker coefficients and van der Waals - london dispersion interactions.** *RSC Adv.* **3**, 823–842 (2013).
- [335] Liu, Z. *et al.* **Interlayer binding energy of graphite: A mesoscopic determination from deformation.** *Phys. Rev. B* **85**, 205418 (2012).
- [336] Zacharia, R., Ulbricht, H. & Hertel, T. **Interlayer cohesive energy of graphite from thermal desorption of polyaromatic hydrocarbons.** *Phys. Rev. B* **69**, 155406 (2004).
- [337] Lebegue, S. *et al.* **Cohesive properties and asymptotics of the dispersion interaction in graphite by the random phase approximation.** *Phys. Rev. Lett.* **105**, 196401 (2010).

- [338] Spanu, L., Sorella, S. & Galli, G. [Nature and strength of interlayer binding in graphite](#). *Phys. Rev. Lett.* **103**, 196401 (2009).
- [339] Axilrod, B. M. & Teller, E. [Interaction of the van der Waals type between three atoms](#). *J. Chem. Phys.* **11**, 299–300 (1943).
- [340] Zwanzig, R. [Two assumptions in the theory of attractive forces between long saturated chains](#). *J. Chem. Phys.* **39**, 2251–2258 (1963).
- [341] Bučko, T., Lebègue, S., Hafner, J. & Ángyán, J. G. [Tkatchenko-Scheffler van der Waals correction method with and without self-consistent screening applied to solids](#). *Phys. Rev. B* **87**, 064110 (2013).
- [342] Misquitta, A. J., Spencer, J., Stone, A. J. & Alavi, A. [Dispersion interactions between semiconducting wires](#). *Phys. Rev. B* **82**, 075312 (2010).
- [343] Rance, G. A., Marsh, D. H., Bourne, S. J., Reade, T. J. & Khlobystov, A. N. [van der Waals interactions between nanotubes and nanoparticles for controlled assembly of composite nanostructures](#). *ACS Nano* **4**, 4920–4928 (2010).
- [344] Loskill, P. *et al.* [Is adhesion superficial silicon wafers as a model system to study van der Waals interactions](#). *Adv. Coll. Interf. Sci.* **179**, 107–113 (2012).
- [345] Auckenthaler, T. *et al.* [Parallel solution of partial symmetric eigenvalue problems from electronic structure calculations](#). *Parallel Computing* **37**, 783–794 (2011).
- [346] Mitroy, J., Safranova, M. & Clark, C. W. [Theory and applications of atomic and ionic polarizabilities](#). *J. Phys. B: At. Mol. Opt. Phys.* **43**, 202001 (2010).
- [347] Dzuba, V., Kozlov, A. & Flambaum, V. [Scalar static polarizabilities of lanthanides and actinides](#). *Phys. Rev. A* **89**, 042507 (2014).
- [348] Stoupin, S. & Shvyd'ko, Y. V. [Thermal expansion of diamond at low temperatures](#). *Phys. Rev. Lett.* **104**, 085901 (2010).
- [349] Aguado, F. & Baonza, V. G. [Prediction of bulk modulus at high temperatures from longitudinal phonon frequencies: Application to diamond, c-BN, and 3c-SiC](#). *Phys. Rev. B* **73**, 024111 (2006).
- [350] Wettling, W. & Windscheif, J. [Elastic constants and refractive index of boron phosphide](#). *Solid State Commun.* **50**, 33–34 (1984).

- [351] Schimka, L., Harl, J. & Kresse, G. **Improved hybrid functional for solids: The HSEsol functional.** *J. Chem. Phys.* **134**, 024116 (2011).
- [352] Greene, R. G., Luo, H., Ruoff, A. L., Trail, S. S. & DiSalvo, F. J. **Pressure induced metastable amorphization of BAs: Evidence for a kinetically frustrated phase transformation.** *Phys. Rev. Lett.* **73**, 2476–2479 (1994).
- [353] Reeber, R. R. **Thermal expansion of some group IV elements and ZnS.** *phys. status solidi (a)* **32**, 321–331 (1975).
- [354] Reeber, R. R. & Wang, K. **Thermal expansion and lattice parameters of group IV semiconductors.** *Mater. Chem. Phys.* **46**, 259–264 (1996).
- [355] Sarkar, S., Pal, S., Sarkar, P., Rosa, A. & Frauenheim, T. **Self-consistent-charge density-functional tight-binding parameters for Cd-X (X= S, Se, Te) compounds and their interaction with H, O, C, and N.** *J. Chem. Theory Comput.* **7**, 2262–2276 (2011).
- [356] Lee, G.-D., Lee, M. H. & Ihm, J. **Role of d electrons in the zinc-blende semiconductors ZnS, ZnSe, and ZnTe.** *Phys. Rev. B* **52**, 1459–1462 (1995).
- [357] Vurgaftman, I., Meyer, J. & Ram-Mohan, L. **Band parameters for III–V compound semiconductors and their alloys.** *J. Appl. Phys.* **89**, 5815–5875 (2001).
- [358] Ley, L., Pollak, R., McFeely, F., Kowalczyk, S. & Shirley, D. **Total valence-band densities of states of III-V and II-VI compounds from X-ray photoemission spectroscopy.** *Phys. Rev. B* **9**, 600 (1974).